IDENTIFICATION OF NEW CATALYTIC MOTIFS IN FLAVOENZYMES AND MECHANISTIC STUDIES OF A COFACTOR INDEPENDENT OXYGENASE

A Dissertation

by

SANJOY ADAK

Submitted to the Office of Graduate and Professional Studies of
Texas A&M University
in partial fulfillment of the requirements for the degree of

DOCTOR OF PHILOSOPHY

Chair of Committee,	Tadhg Begley
Committee Members,	Frank Raushel
	David Barondeau
	Paul Straight
Head of Department,	Simon North

December 2019

Major Subject: Chemistry

ABSTRACT

In this dissertation we discuss function identification and detailed mechanistic studies of the enzymes involved in the bacterial xenobiotic, amino acid, and vitamin catabolic pathways. The studies are mainly focused on 1) Identification of flavin-N5-oxide intermediates in bacterial dibenzothiophene, uracil and hexachlorobenzene catabolic pathway; 2) Identification of bacterial folate and lumichrome catabolic pathways; 3) Mechanistic studies on the flavoenzyme (IifA) involved in the bacterial tetramethyl pyrazine catabolic pathway; 4) Mechanistic studies on the cofactor independent oxygenase in the bacterial indole catabolic pathway.

Our mechanistic studies on the DszA catalyzed reaction in the bacterial dibenzothiophene catabolic pathway revealed that the reaction proceeds via the flavin-N5-oxide intermediate, a newly discovered flavin oxidation state. DszA is the second enzyme which has been characterized as flavin-N5-oxide utilizing enzyme. Guided by the similar mechanistic hypothesis that we had on the DszA catalyzed reaction, we were able to discover flavin-N5-oxide in the RutA-catalyzed oxidative amide bond cleavage reaction in the uracil catabolic pathway reaction and in the HcbA1-catalyzed dehalogenation reaction in the hexachlorobenzene catabolic pathway.

Unlike the vitamin biosynthesis, the vitamin catabolism is an unwritten chapter in fundamental biochemistry. In an effort to broaden our knowledge on vitamin catabolism we have identified bacterial folate and lumichrome catabolic pathways. Detailed biochemical studies on the folate catabolic pathway in *Mesorhizobium loti* revealed a

unique flavoenzyme mediated Baeyer-Villiger type rearrangement. We have identified a similar Baeyer-villiger type rearrangement in the bacterial tetramethyl pyrazine catabolic pathway. We have also identified a lumichrome catabolic pathway in *Pimelobacter simplex* and the initial three enzyme catalyzed reactions have been reconstituted *in vitro.*

We have studied the mechanism of a cofactor-independent oxygenase (IifA) involved in the bacterial indole catabolic pathway. IifA catalyzes the transformation of 3-hydroxy-oxindole to anthranilic acid. Our mechanistic studies on the IifA catalyzed reaction support a Baeyer-Villiger type rearrangement, first of its kind, in a cofactor-independent enzyme. We have shown that the reaction goes via the isatoic anhydride intermediate, identified bicarbonate as the reaction product, labeling experiments with O-18 labeled water and molecular oxygen showed that the oxygen atom from water molecule incorporated into anthranilic acid product while oxygen atom from molecular oxygen incorporated into carbon dioxide.

DEDICATION

To Baba and Maa

ACKNOWLEDGEMENTS

First of all, I would like to thank Prof. Tadhg P. Begley for his continuous guidance and support throughout the course of my research in his laboratory. Thank you Tadhg for introducing me into the wonderful world of enzyme chemistry. Thank you Tadhg for providing me all the opportunities and freedom to explore my thoughts and ideas. I am intrigued by his work ethic and dedication towards science.

I will take this opportunity to acknowledge my committee members, Dr. Frank Raushel, Dr. David Barondeau and Dr. Paul Straight for their valuable advice and insights during all the committee meetings and seminar presentations.

I would like to thank all the Begley group members for being wonderful colleagues and providing me with the learning environment. Thanks to Dr. Angad Mehta for training me during my initial days in the lab. I would like thank Dr. Nitai Giri for all the discussion on the metalloenzymes. Thanks to Dr. Yindrila Chakrabarty, Dr. Brateen Shome, Dr. Prem Chanani, Dr. Dhananjay Bhandary for their valuable discussion. I am thankful to Dr. Xiaohong Jian for teaching me molecular biology techniques and identifying the lumichrome catabolic strain which laid the foundation of catabolic gene cluster identification. Thank you Isita Jhulki for all the discussion on flavoenzymes. Thank you Dr. Yuanyou Wang for all the critical discussion that we had on radical chemistry. Thank you Dr. Sameh Abdelwahed and Dr. Dmytro Fedoseyenko for the guidance on organic synthesis. Thank you, Dr. Lina Xie, and Sumedh Joshi for the enthusiasm in science. I

would also like to thank the new energetic members of the lab, Avick, Indranil, Anushree, Saad, Sohan, Hannah, Vishav and Sreyashi.

I am extremely thankful to Dr. Baoyu Zhao and Prof. Pingwei Li for teaching me protein crystallography and helping me in solving the structure of the flavin oxygenase involved in the folate catabolic pathway. I would like to thank Seth Cory (Barondeau lab) for his assistance in collecting the X-ray data from Stanford Synchrotron Radiation Light source (SSRL).

I would like to thank all my friends at College Station for making my life a memorable one. Special thanks to Arghya, Srobona, RajatDa and AnanyaDi for their help during my initial days at College Station. Thank you Sayan for being an awesome roommate.

My journey would not have been possible without the support from my family. It's my parents' hard work that brought me here. I am fortunate to have a sister who is always in my side with her love and support. Credit goes to my cousin, Swadesh Ranjan Adak for bringing a learning atmosphere in my family and giving me the guidance for the higher studies.

CONTRIBUTORS AND FUNDING SOURCES

This work was supervised by a dissertation committee consisting of Professor Tadhg P. Begley (advisor), Professor Frank M. Raushel and Professor David P. Barondeau of the Department of Chemistry and Professor Paul D. Straight of the Department of Biochemistry and Biophysics.

Dr. Xiaohong Jian identified the lumichrome catabolic strain which laid the foundation for catabolic gene cluster identification.

Dr. Baoyu Zhao and Prof. Pingwei Li solved the crystal structure of the flavin oxygenase involved in the folate catabolic pathway.

All other work conducted for the dissertation was completed by the student independently.

Graduate study was supported by Teaching Assistantship from the Department of Chemistry at Texas A&M University. This work was made possible by funding from the Robert A. Welch Foundation grant A-0034 and National Institute of Health (NIH) grant DK44083

NOMENCLATURE

BLAST	Basic Local Alignment Search Tool
CTP	Cytidine triphosphate
DTT	Dithiothreitol
EIC	Extracted Ion chromatogram
FMN	Flavin Mononucleotide
FAD	Flavin Adenine Dinucleotide
HPLC	High Performance Liquid Chromatography
kDa	kilodalton
LC-MS	Liquid Chromatography-Mass Spectrometry
NAD^+	Nicotinamide Adenine Dinucleotide (oxidized form)
NADH	Nicotinamide Adenine Dinucleotide (reduced form)
NMR	Nuclear Magnetic Resonance
OD_{600}	Optical density at 600 nm
PFBHA	o-(2,3,4,5,6-pentafluorobenzyl)-hydroxylamine
RT	Room Temperature

TABLE OF CONTENTS

Page

LIST OF FIGURES

Page

CHAPTER I

INTRODUCTION

1.1 Flavoenzymes

Flavoenzymes are ubiquitous in all forms of life and extensive studies in this area demonstrate that the isoalloxazine heterocycle is the most chemically versatile heterocycle in biology.[1-3] Flavin can undergo 1 and 2- electron reversible redox chemistry to form the flavin semiquinone and dihydroflavin respectively (Figure 1.1). The ability of flavins to undergo single electron transfer chemistry underlies much of the catalytic versatility of this cofactor. Flavin is one of the few cofactors (Heme, Non-heme iron, copper, and pterin being the rest) used by living systems to activate molecular oxygen. Extensive mechanistic studies on the flavin dependent oxygenases over the last several decades have provided the basis of our current understanding of how these enzymes work. During the reaction with molecular oxygen N5-C4a locus of the isoalloxazine ring plays the key role in stabilizing the flavin semiquinone species before it recombines with superoxide radical to

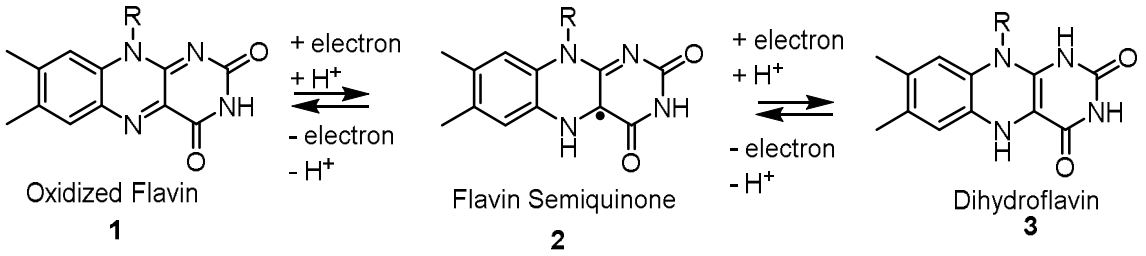

Figure 1.1: Known oxidation states of flavin.

form the flavin-C4a-hydroperoxide.[4] It is the flavin-C4a-hydroperoxide which is the key oxygenating species during flavoenzyme catalyzed hydroxylation, epoxidation, sulfoxidation, Baeyer-Villiger oxidation reaction etc.[5] (Figure 1.2) and thus, can be considered as biological equivalent of m-chloroperbenzoic acid. After years of extensive studies, the field of flavoenzymology was considered to be a saturated field. However, the last decade has seen a radical shift in flavoenzymology with the identification of two new catalytic motifs: prenylated flavin and flavin-N5-oxide (Figure 1.3). Prenylated flavin was first discovered in ubiquinone biosynthesis and since then has been implicated in

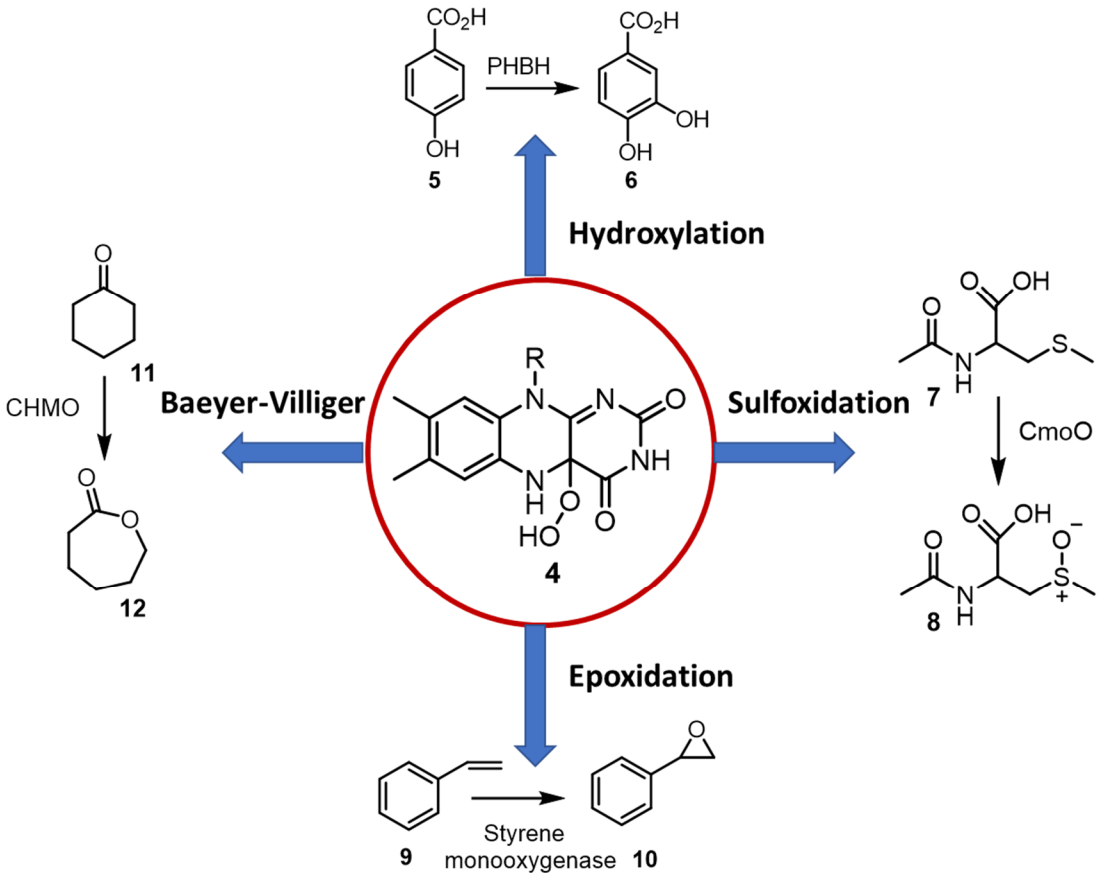

Figure 1.2 Diverse reactions mediated by Flavin hydroperoxide.

decarboxylation reactions in many enzymatic systems.[6-8] Flavin-N5-oxide was first identified in the EncM catalyzed reaction in the enterocin biosynthesis by Bradley Moore's group.[9, 10] We have been able to identify Flavin-N5-oxide species in three more enzymatic systems: DszA-catalyzed oxidative C-S bond cleavage reaction in dibenzothiophene catabolic pathway, RutA-catalyzed amide bond cleavage reaction in uracil catabolic pathway, and HcbA1-catalyzed dehalogenation reaction in the hexachlorobenzene degradation pathway. Details are outlined in Chapter 1, 2 and 3.

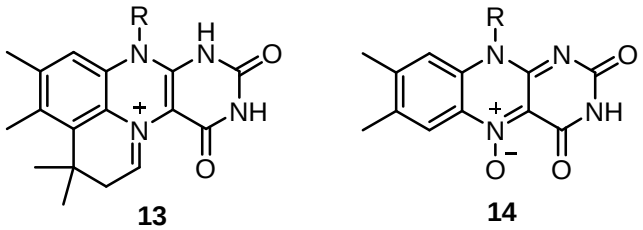

Figure 1.3: Newly discovered flavin intermediates: prenylated flavin and flavin-N5-oxide.

1.2 Cofactor catabolism

In contrast to our understanding of the biosynthesis of cofactors, there is a dearth of information about their degradation pathways. Although there are reports of bacterial strains which can degrade cofactors, very little is known about the genes involved in the degradation pathway. As of now the best studied catabolic pathways are that of PLP and NAD. Landmark studies by Snell using selective culture technique resulted in the identification of several bacterial strains which are able to grow on PLP as a sole source

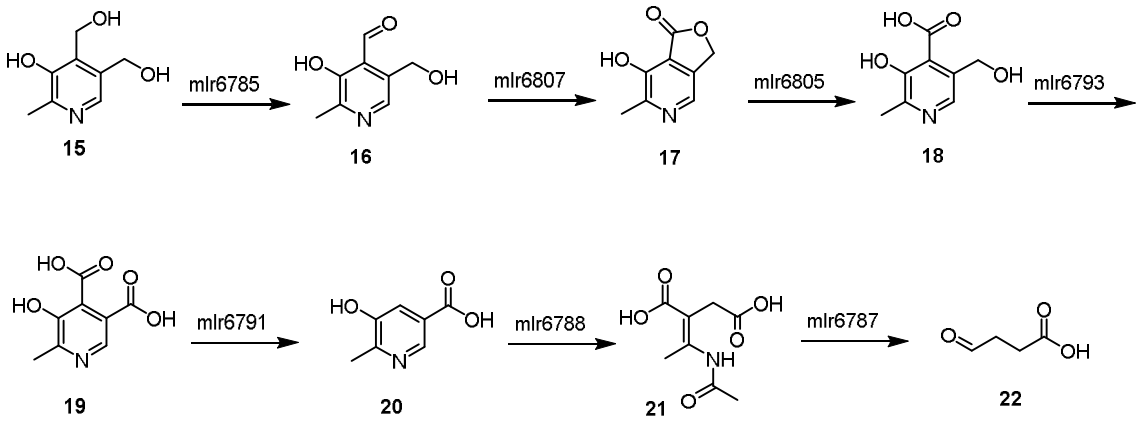

Figure 1.4: PLP catabolic pathway in *Mesorhizobium loti* MAFF303099.

of carbon and nitrogen.[11-13] Based on the work from the same group several catabolic intermediates were characterized from the growth medium. Later, Yagi and Begley groups identified pyridoxin catabolic genes in *Mesorhizobium loti* MAFF303099. Detailed biochemical studies by the Begley group on the enzymes involved in the PLP catabolic pathway further advanced our understanding (Figure 1.4).[14] NAD

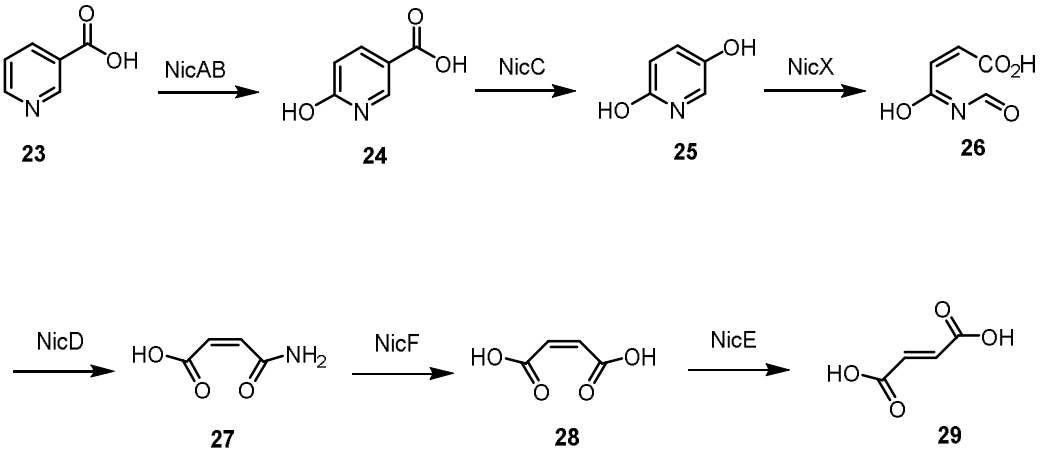

Figure 1.5: Aerobic NAD catabolic pathway.

catabolic pathway has been reported in bacteria, plants and animals. The catabolic pathway proceeds via the intermediate nicotinic acid **23** (Figure 1.5). The catabolic pathways of the rest of the cofactors are largely unexplored. Thiamin, folate, riboflavin, and biotin-degrading bacteria were once isolated, but samples have not been preserved. In an effort to broaden our knowledge on cofactor catabolism, we have successfully identified the folate and lumichrome catabolic pathways as detailed out in Chapter V and Chapter VIII.

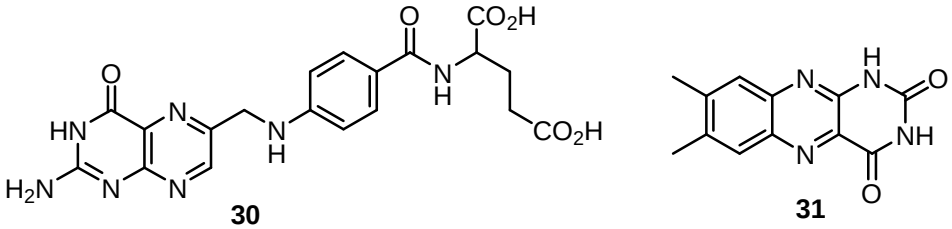

Figure 1.6: The structures of folic acid and lumichrome. Catabolic pathways of these two molecules will be discussed in Chapter V and Chapter VIII.

1.3 Baeyer-Villiger rearrangement

Baeyer-Villiger rearrangement is the transformation of ketones to esters or of cyclic ketones into lactones by peracids. The first example of Baeyer-Villiger rearrangement is the lactonization of menthone with potassium monopersulfate reported by Adolf von Baeyer and Victor Villiger in 1899.[15] According to the current mechanistic understanding, the reaction proceeds via nucleophilic addition of peracid to the electrophilic carbonyl center to form tetrahedral intermediate which is also known as Criegee intermediate[16]

(Figure 1.7). This is followed by the concerted migration of one of the adjacent carbons to the oxygen to yield the rearranged product. Enzyme catalyzed Baeyer-Villiger rearrangements are widely distributed in nature.[17] The first biological example of Baeyer-Villiger reaction was discovered in the microbial degradation of steroids in 1948.[18] Majority of biological Baeyer-Villiger rearrangements are catalyzed by flavoenzymes. The prototype of flavin-dependent Baeyer-Villiger oxygenase is cyclohexanone monooxygenase (CHMO) which was first purified to homogeneity from *Acinetobacter sp.*

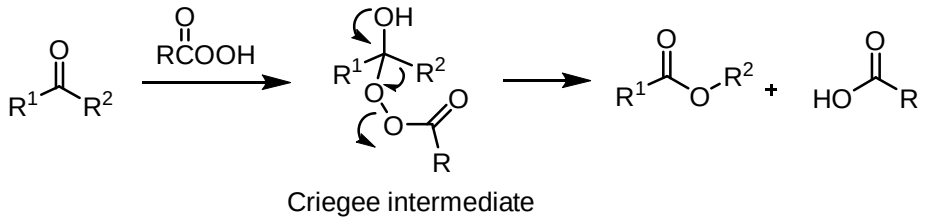

Figure 1.7: Baeyer-Villiger reaction proceeds via Criegee intermediate.

strain NCIB 9871.[19] CHMO catalyzed reaction has been proposed to proceed via Criegee intermediate in the same manner as that of non-enzymatic Baeyer-Villiger reaction; the only difference being flavin hydroperoxide acts as a nucleophile instead of a peracid. Apart from CHMO, several other flavin dependent Baeyer-Villiger monooxygenases (BVMO) have been identified in the biosynthetic pathways of polyketides, aminoglycosides, cofactors and many other secondary natural products. Example of P450 dependent Baeyer-Villiger oxidation is the AflN catalyzed reaction during Aflatoxin biosynthesis.[20, 21] Toxoflavin lyase (TflA) utilizes manganese to carry out Baeyer-Villiger reaction during the degradation of toxoflavin,[22] a plant toxin (Figure 1.8). We have

identified a new catalytic motif in flavin dependent Baeyer-Villiger oxygenases where flavin hydroperoxide adds to an imine instead of a carbonyl center and involved in the degradation of a pyrazine ring. The studies of these unique enzymes are reported in Chapter V and Chapter VI. We have also characterized a cofactor independent Baeyer-Villiger oxygenases, first of its kind, in a bacterial indole catabolic pathway. Details are described in Chapter VII.

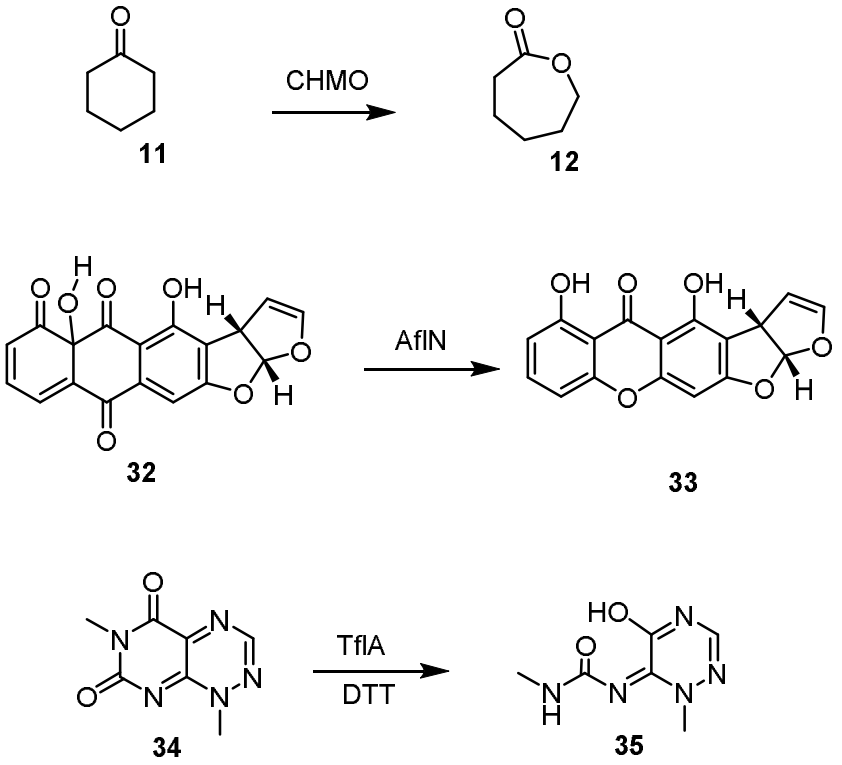

Figure 1.8: Examples of enzymatic Baeyer-Villiger reactions which use either flavin, heme or manganese as cofactor.

CHAPTER II

MECHANISTIC STUDIES ON DSZA CATALYZED REACTION IN BACTERIAL DIBENZOTHIOPHENE CATABOLIC PATHWAY

2.1 Introduction

Acid rain is formed from sulfur dioxide generated during fossil fuel combustion and the removal of sulfur from these fuels is an important step in pollution control. The widely used metal-catalyzed hydrodesulfurization is only partially successful because it is inefficient with sulfur-containing heterocyclic compounds. Dibenzothiophene is the major sulfur-containing heterocycle in crude petroleum[23] and the possibility of removing this compound by microbial degradation has led to the discovery of its catabolic pathway in *Rhodococcus erythropolis* (Figure 2.1).[24] The first two steps of this pathway involve well-precedented flavin-hydroperoxide mediated thioether oxidation[25] to sulfone **38** via sulfoxide **37**, and the last step most[26] likely involves bisulfite loss in an ipso substitution reaction. The mechanism of the third step, involving conversion of sulfone **38** to sulfinic acid **39**, is not obvious and does not conform to any of the well-established motifs in flavoenzymology.

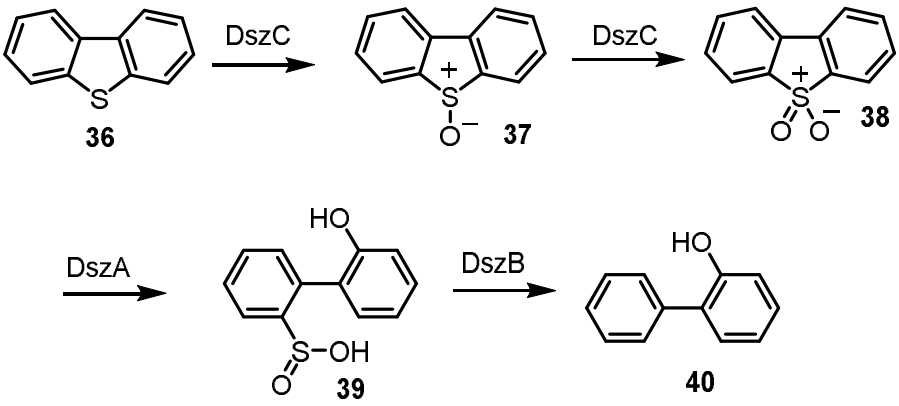

Figure 2.1: Four-step dibenzothiophene catabolic pathway in *Rhodococcus erythropolis*.

The two flavoenzymes which are known to cleave C-S bond are SsuD and YtnJ and both the enzymes act on aliphatic substrates (Figure 2.2). SsuD acts on alkanesulfonates **41** and converts it to corresponding aldehyde **42** and sulfite.[27] The enzyme allows *Escherichia coli* to use a wide range of alkanesulfonates as sulfur sources for growth under sulfate or cysteine deprived condition. YtnJ involves in cysteine salvage pathway in *Bacillus subtilis* where it converts sulfoxide **43** to sulfenic acid **44**. In this Chapter, we describe studies to elucidate the mechanism of DszA catalyzed reaction.

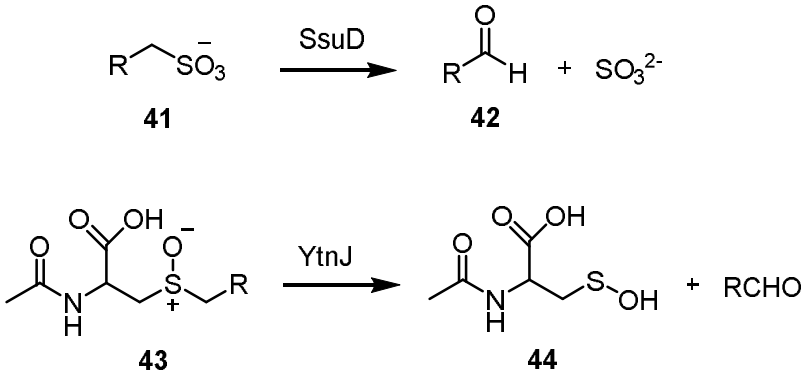

Figure 2.2: Flavoenzyme catalyzed C-S bond cleavage reactions.

2.2 Results and Discussion

2.2.1 Overexpression and purification of DszA

DszA and DszB were overexpressed in *E. coli* BL21(DE3) and purified by Ni-affinity chromatography.

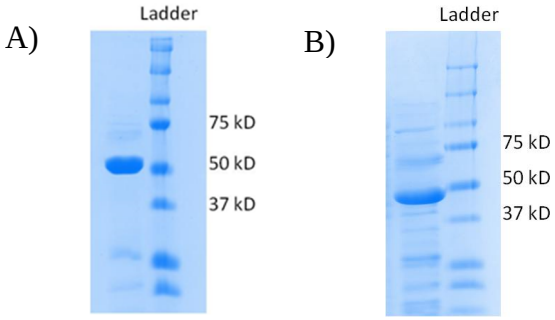

Figure 2.3: SDS-PAGE of purified DszA (A) and DszB (B). Molecular weights of DszA

2.2.2 Reconstitution of DszA activity

The DszA-catalyzed reaction was reconstituted by incubating sulfone (**38**), DszA, *E. coli* flavin reductase (to replace DszD), NADH, and FMN at 25 °C. The formation of sulfinic acid **39** was monitored by HPLC analysis (Figure 2.4).

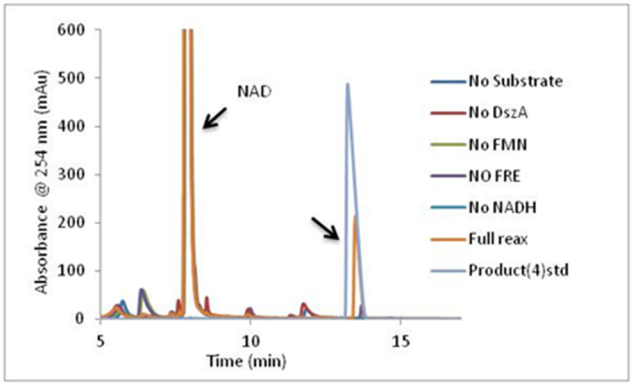

Figure 2.4: Analysis of the DszA enzymatic reaction with the native substrate dibenzothiophene sulfone (**38**). HPLC analysis of the reaction mixture @ 254 nm revealed

formation of sulfinic acid product (**39**) only when all the components were present. In this HPLC condition, dibenzothiophene elutes at 20.5 min.

2.2.3 Mechanistic proposal for DszA catalyzed reaction.

The previously reported $S_{RN}1$ reaction of dibenzothiophene sulfone **38** with alkoxides to form the corresponding alkylated biphenyl **45** served as our first model for the enzymatic reaction[28, 29] (Figure 2.5), and the corresponding $S_{RN}1$ proposal for DszA is shown in Figure 2.6. In this proposal, electron transfer from FlH^- to the electron-deficient sulfone **38** gives the sulfone radical anion **46**. Fragmentation of the C−S bond gives **47**. Ring closure and electron transfer to the flavin semiquinone gives **49**. Hydrolysis of **49** completes the reaction. While the initial electron transfer to form **46** is likely to be unfavorable, rapid rearrangement of **46** to **48** could drive the reaction.

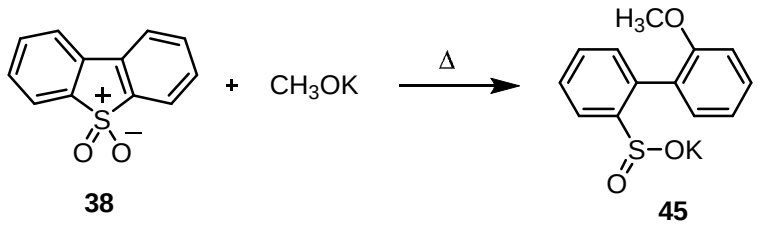

Figure 2.5: Literature reported model reaction on dibenzothiophene sulfone.

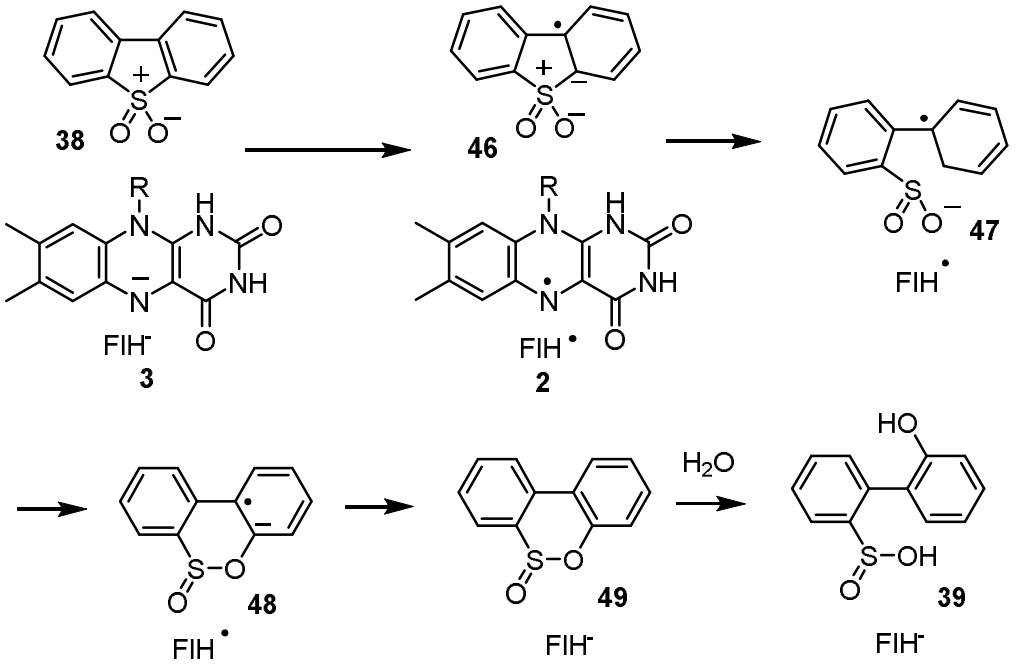

Figure 2.6: $S_{RN}1$ mechanistic proposal of DszA catalyzed reaction.

2.2.4 DszA catalyzed reaction under anaerobic condition

According the proposed mechanism discussed above there is no requirement of molecular oxygen in the DszA catalyzed reaction. To test this hypothesis, DszA catalyzed reaction was carried out in anaerobic environment. Under this condition no product formation was observed.

2.2.5 DszA reaction in the presence of $H_2{}^{18}O$ and $^{18}O_2$

The DszA reaction was also run in [18O]-H_2O/$^{16}O_2$ buffer to look for the oxygen incorporation expected for the hydrolysis of **49** to **39**. No oxygen incorporation was detected (Figure 2.7A). In contrast, when the enzymatic assay was carried out in the

presence of $^{18}O_2$, a 2 Da increase in the mass of the product was observed consistent with the incorporation of a single oxygen atom from molecular oxygen (Figure 2.7B).

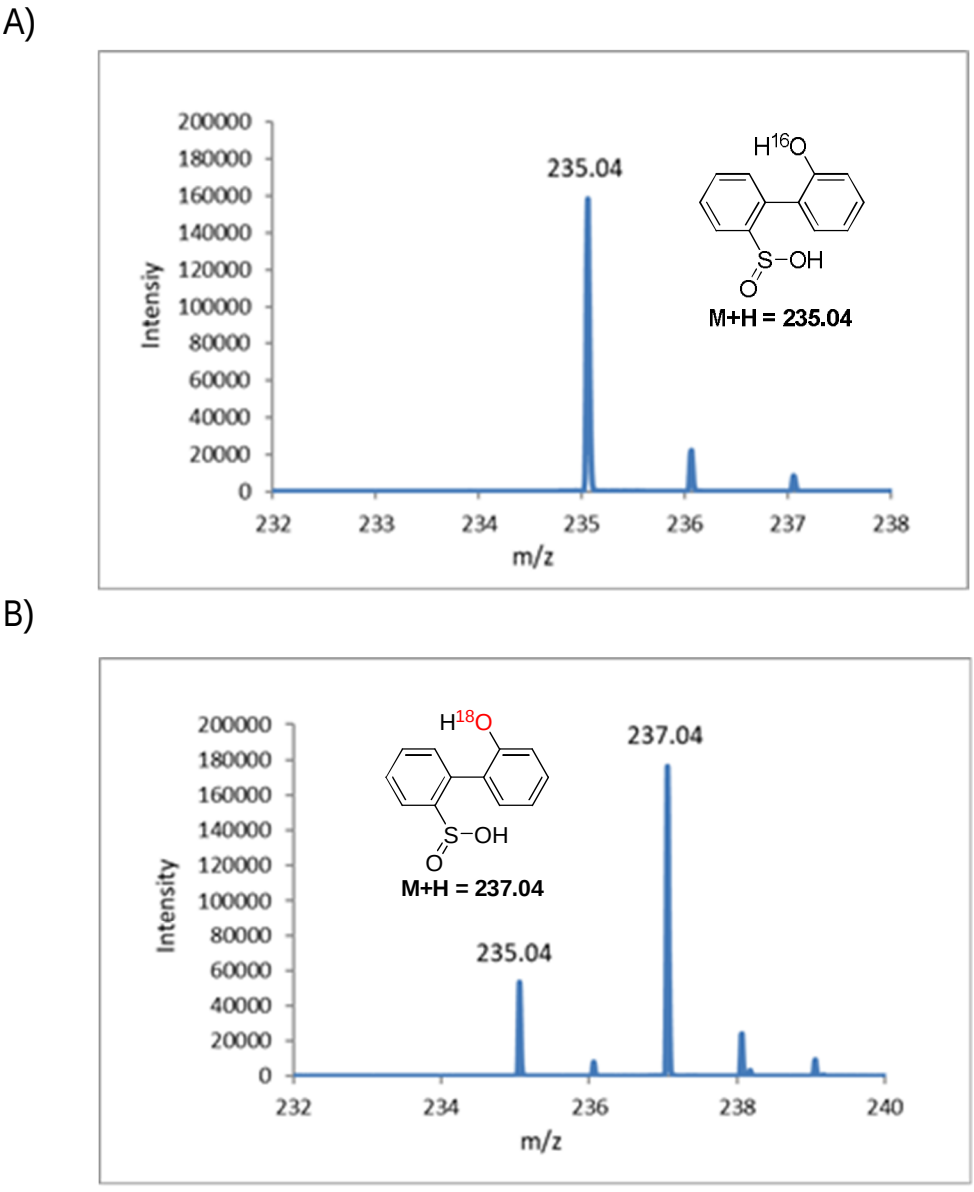

Figure 2.7: LC-MS analysis of the DszA reaction run in [18O]-H_2O/$^{16}O_2$ buffer or H_2O/$^{18}O_2$. Panel A shows that oxygen from the buffer is not incorporated into the reaction product **39**. Panel B shows the incorporation of a single oxygen atom from molecular oxygen. m/z for **39** and [18O1]-**39** are 235 Da and 237 Da respectively**.**

2.2.6 Determination of oxygen incorporation site

There are two possible sites for oxygen incorporation in the final product: phenolic oxygen or sulfinic oxygen. Oxygen incorporation into the phenol rather than the sulfinate was established by demonstrating retention of label when [18O1]-**39** was converted to **40** using DszB (Figure 2.8). These experiments eliminate the possibility that the DszA reaction proceeds by an $S_{RN}1$ mechanism.

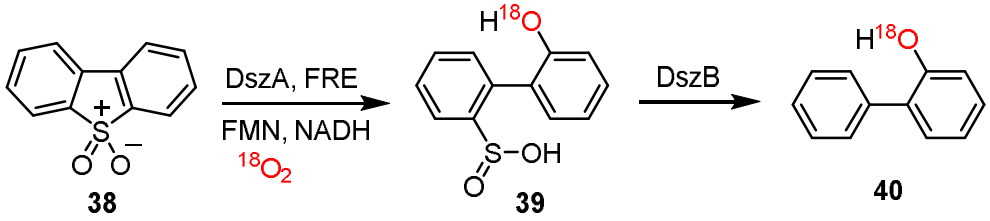

A)

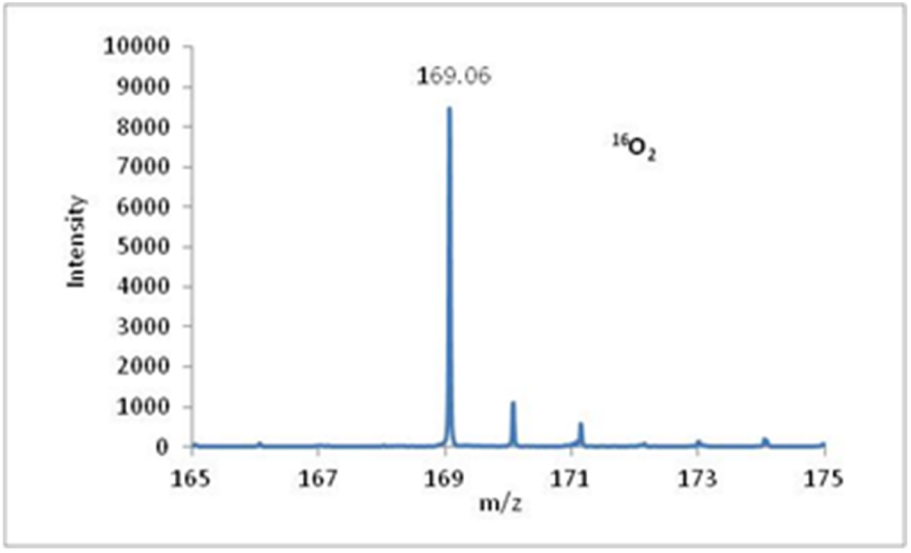

B)

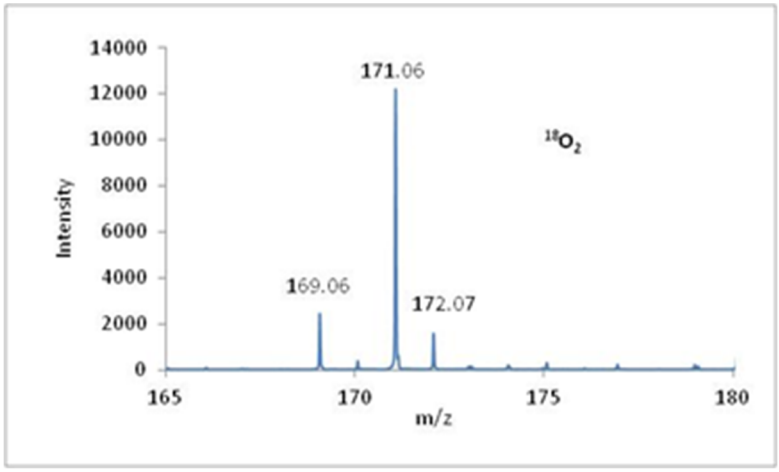

Figure 2.8: LC-MS analysis of the coupled assay (DszA+DszB) run in presence of $^{16}O_2$ or $^{18}O_2$. Panel A shows that mass of the coupled assay product (M-H) is 169.06 which is consistent with the structure of 2-hydroxybiphenyl (**40**). Panel B shows the incorporation of a single oxygen atom from molecular oxygen into the coupled assay product resulting a 2 Da increase in mass (M-H= 171.06).

2.2.7 Revised mechanistic proposal for DszA catalyzed reaction.

We next considered the possibility of a nucleophilic addition of flavin hydroperoxide **4** to **38**. The nucleophilicity of **4** is well established in the flavoenzyme-mediated Baeyer−Villiger oxidation of ketones[30] and the RutA-catalyzed uracil ring opening reaction.[31] In this proposal (Figure 2.9), addition of the flavin hydroperoxide to dibenzothiophene sulfone gives the sulfone-stabilized carbanion **50**. Protonation, followed by flavin elimination, gives hydroperoxide **51**. NADH-mediated reduction of this hydroperoxide, as previously observed for the RutA system, gives **52**, which is converted to product by a ring opening/tautomerization/bond rotation sequence (A Baeyer−Villiger-like mechanism, involving flavin peroxide attack on the sulfone sulfur, results in the formation of a sulfonic rather than a sulfinic acid and is therefore not possible). The normal

mechanism of flavoenzyme-mediated peroxide cleavage[32] is also not possible because DszA is cysteine free.

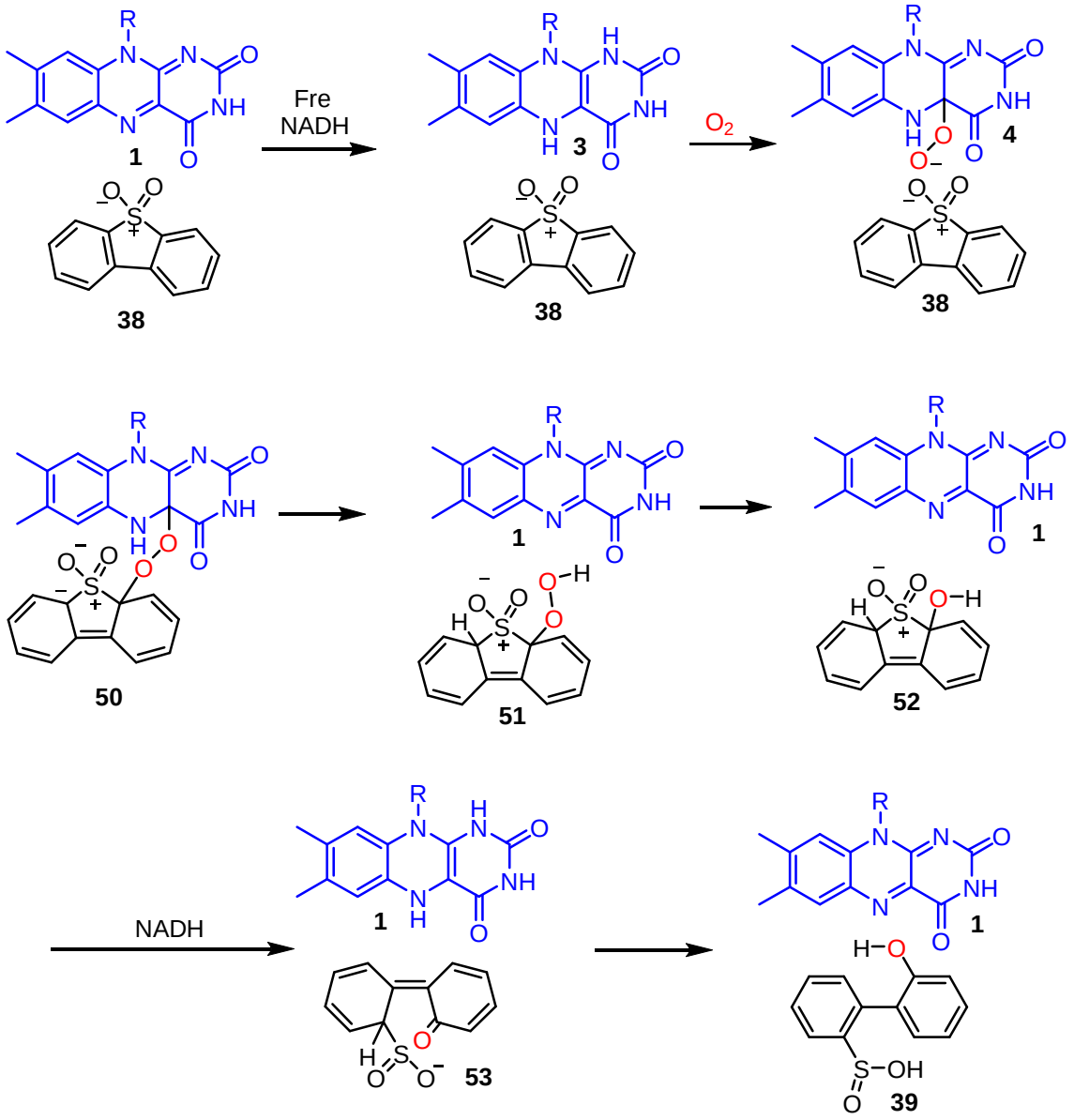

Figure 2.9: Revised mechanistic proposal of DszA catalyzed reaction.

This mechanism predicts that it should be possible to trap hydroperoxide **51** if the DszA reaction is run in the absence of excess reducing agent. These reaction conditions were

achieved by initial photoreduction of the flavin using EDTA and by running the reaction in phosphate buffer using stoichiometric amounts of photoreduced FMN, DszA, and dibenzothiophene sulfone. The reaction mixture did not contain DTT, protein thiol, free FMN, or NADH, and the photogenerated glyoxylic acid was not consumed. It was prepared under anaerobic conditions in a glovebox and then exposed to air to allow formation of the enzyme bound flavin hydroperoxide. Under these reaction conditions, sulfinic acid **39** was the major reaction product, and peroxide **51** was not detected raising the question as to how peroxide **51** is reduced.

In the absence of any obvious reducing agent in the reaction buffer, the possibility of a flavin-N5-oxide was considered. This new flavin oxidation state was recently identified in the EncM-catalyzed Favorskii rearrangement involved in enterocin biosynthesis.[9, 10, 33] HPLC analysis of the DszA reaction mixture (containing stoichiometric amounts of photoreduced FMN, DszA, and dibenzothiophene sulfone) demonstrated the consumption of FMN and the formation of a new species eluting after 20.3 min (Figure 2.10A). This species comigrates with and has an identical UV−vis spectrum to a synthetic sample of FMN-N5-oxide (Figure 2.10 B, C). MS analysis of I20.3 is also consistent with the FMN-N5-oxide structure (Figure 2.10 D, E), and running the DszA reaction in the presence of $^{18}O_2$ showed the expected 2 Da mass increase (Figure 2.10F). Finally, the ratio of FMN consumed to sulfinic acid formed in a reaction containing stoichiometric amounts of photoreduced FMN, DszA, and dibenzothiophene sulfone was 1:0.9 consistent with the stoichiometric conversion of FMN to FMN-N5-oxide during the course of the DszA-catalyzed reaction

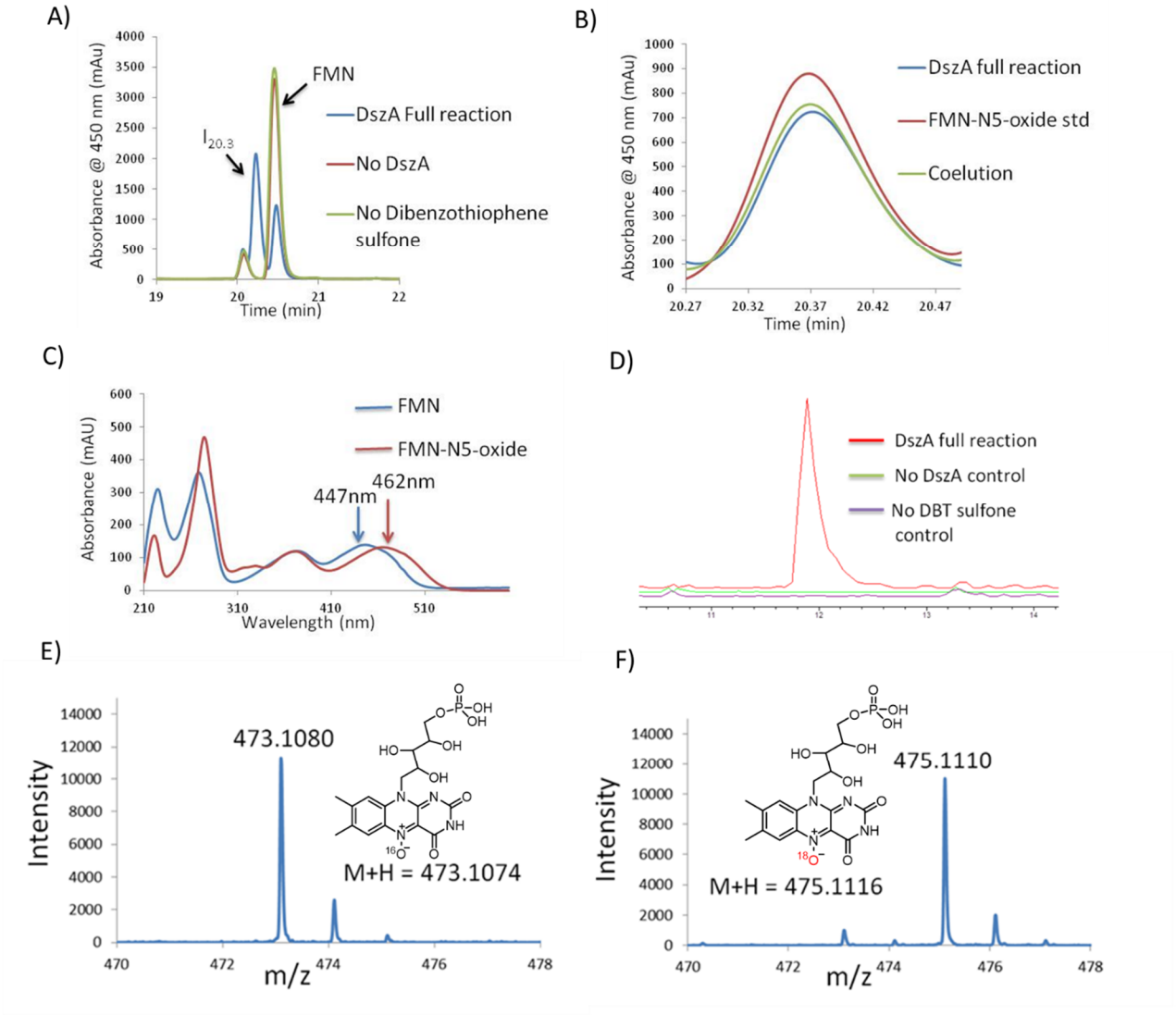

Figure 2.10: Characterization of a new intermediate in the DszA-catalyzed reaction. (A) Partial HPLC chromatogram of the DszA/photoreduced FMN reaction mixture showing the new intermediate (I20.3) eluting at 20.3 min. The peak eluting at 20.1 min corresponds to an impurity present in commercial FMN. (B) Co-elution of I20.3 with synthesized FMN-N5-oxide. (C) UV−vis spectra of FMN and FMN-N5-oxide. The I20.3 spectrum was identical to that of FMN-N5-oxide. (D) Extracted ion chromatograms for [M + H] = 473.1 Da demonstrate that I20.3 is present only in the full reaction mixture. (E) Exact mass of I20.3 consistent with the mass expected for FMN-N5-oxide ([M + H] = 473.11 Da). (F) Exact mass of I20.3 generated using $^{18}O_2$ consistent with the mass expected for [18O1]-FMN-N5-oxide ([M + H] = 475.11 Da).

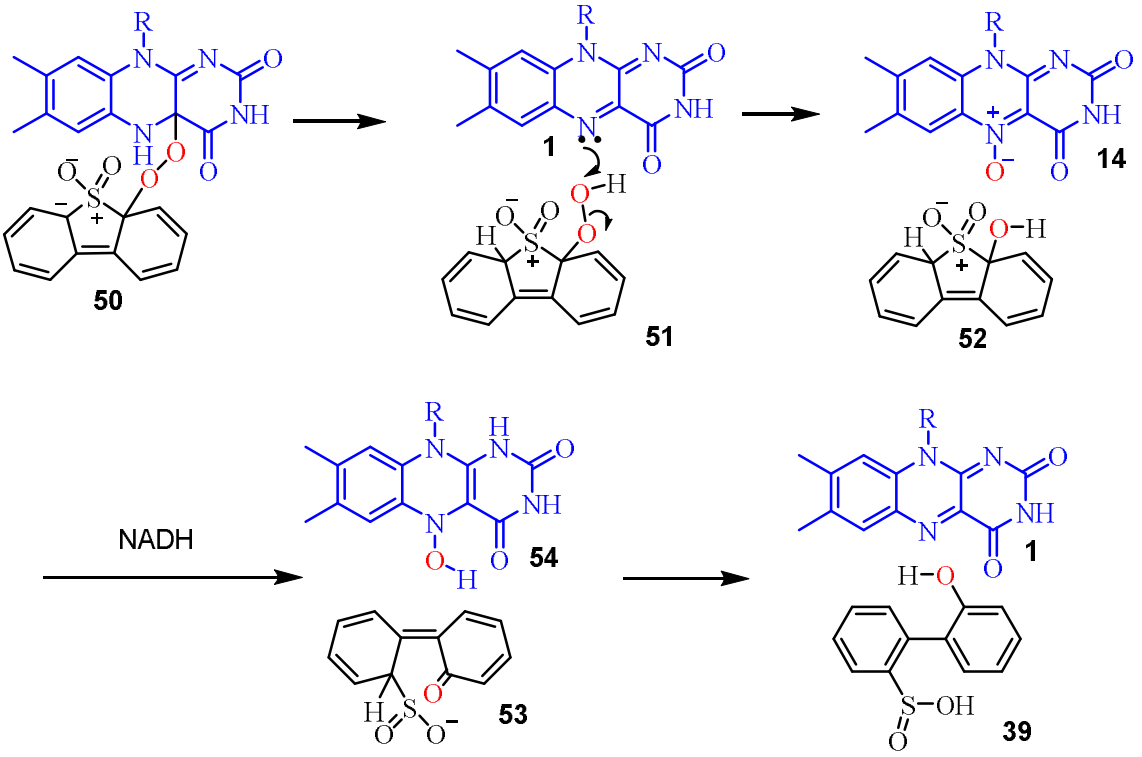

Figure 2.11: Mechanistic rationale for the formation of flavin-N5-oxide.

2.3 Conclusion

Our studies on DszA suggest a mechanism involving initial formation of flavin hydroperoxide from reduced flavin. This adds to **38** to form the sulfone-stabilized carbanion **50**. Protonation followed by flavin elimination gives **51** and **1**. Flavin-mediated peroxide cleavage[34, 35] would form **52** and **14**. The catalytic cycle is then completed by the conversion of **52** to **39** and **14** to **1**.

Decades ago, flavin-N5-oxide **14** was considered as an intermediate in flavin-dependent oxygenase chemistry but was almost entirely replaced by the flavin

hydroperoxide mecha- nistic paradigm. Since FMN-N5-oxide and organic peroxides are easily reduced by widely used biochemical reducing agents, (DTT, TCEP, NADH etc.),[36] it is easy to miss this intermediate, and a systematic search for other FMN-N5-oxide-mediated reactions is merited.

2.4 Experimental Procedure

Materials

All chemicals were purchased from Sigma-Aldrich unless mentioned otherwise. A dehydrated form of LB broth was purchased from EMB Millipore. Kanamycin and IPTG were obtained from Lab Scientific Inc. $H_2{}^{18}O$ was purchased from Cambridge Isotope Laboratories Inc. Amicon Ultra centrifugal filter devices (10,000 MWCO) were obtained from Millipore. Histrap column was obtained from GE Healthcare. Econo-Pack 10DG desalting columns were purchased from Bio-Rad. 2.5 L baffled ultra yield flasks for protein overexpression were obtained from Thomson Instrument Company. ZORBAX Eclipse XDB-C18 column (15 cm x 4.6 mm, 5 μm particles) was purchased from Agilent Technologies. PFP column (150 x 4.6 mm, 2.6 μm particles) was purchased from phenomenex.

Over-expression and purification of DszA and DszB

The DszA gene cloned in pTHT vector (derivative of pET28b vector with TEV protease cleavage site after the N-terminal His-tag) was purchased from GenScript. The plasmid was transformed into *Escherichia coli* BL21 (DE3). A starter culture was grown overnight in 90 ml of LB media containing 40 μg/ml of Kanamycin at 37 °C with overnight agitation. 9 liters of LB medium (20 g/L) in 6×1.5 L flasks, containing 40 μg/ml of Kanamycin, was

inoculated with this starter culture. The cells were grown at 37 °C with shaking (220 rpm) until the culture reached an OD_{600} of 0.6. The flasks were then incubated at 4°C for ~1h without shaking. Then the cultures were induced by adding IPTG to a final concentration of 0.4 mM, the temperature was lowered to 15 °C and the cells were allowed to grow with shaking (180 rpm) for a further 15 hours. The cells were then harvested by centrifugation at 10,000g for 10 min at 4 °C. Typical yields were 20-25 g cell pellet (wet weight) from 9 L culture.

Cells from 9 liters of culture were re-suspended in 30 ml of binding buffer (50 mM KH_2PO_4, 150 mM NaCl, 10 mM imidazole, pH 8.0) and approximately 5 mg of lysozyme was added. The cells were then lysed by sonication (Misonix Sonicator 3000, pulse 'on' time 1.0 sec, pulse 'off' time 1.0 sec, output level 0.8, 30x6 cycles) on ice. The cell debris was removed by centrifugation at 39,000g for 40 minutes at 4 °C. The clarified supernatant was loaded onto a 5 mL Ni-NTA-affinity column pre-equilibrated with binding buffer kept at 4°C. The Ni-NTA-affinity column was then washed with 50 ml wash buffer (50 mM KH_2PO_4, 150 mM NaCl, 20 mM imidazole, pH 8.0). The protein was eluted from the column with elution buffer (50 mM KH_2PO_4, 150 mM NaCl, 200 mM imidazole, pH 8.0) at 4°C. The fractions containing protein were pooled and concentrated using YM-10 Amicon ultracentrifugal filters at 5000g to a final volume of 3 mL. The concentrated sample was buffer exchanged into 100 mM phosphate buffer at pH 7.5 containing 100 mM NaCl and glycerol to a final concentration of 15% using an Econo-Pac 10DG desalting column. Protein concentration was determined from the absorbance at 280 nm

(A280) with an Extinction coefficient calculated using the ProtParam tool of the ExPASy proteomics Server. A typical yield was 6 mg/liter.

The DszB gene was cloned in pTHT vector. The plasmid was transformed into *Escherichia coli* BL21(DE3). The overexpression and purification procedure were the same as that for DszA. For DszB, a typical yield was 5 mg/liter.

HPLC parameters

An Agilent 1260 HPLC equipped with a quaternary pump was used. The system included a diode array UV-Vis detector and products were detected using absorbance at 254 nm, and 450 nm. Analysis was performed either on a ZORBAX Eclipse XDB-C18 column (15 cm x 4.6 mm, 5 μm particles, Agilent Technologies) or PFP column (150 x 4.6 mm, 2.6 μm particles, Kinetex).

HPLC conditions (for C18 column):

A-Water

B-10mM ammonium acetate buffer, pH 6.6

C-Methanol

HPLC method:

0 min-90% A 10% B, 2 min- 90% A 10% B, 22 min-20%A 10%B 70% C, 27 min-20%A 10%B 70% C, 28 min-90% A 10% B, 36 min-90% A 10% B

HPLC conditions (for PFP column):

A-Water

B-100 mM potassium phosphate buffer, pH 6.6

C-Methanol

HPLC method:

0 min-90% A 10% B, 2 min- 90% A 10% B, 22 min-20%A 10%B 70% C, 27 min-20%A 10%B 70% C, 28 min-90% A 10% B, 36 min-90% A 10% B

LC-MS parameters

LC-ESI-TOF-MS was performed using an Agilent 1260 HPLC system which is equipped with a binary pump and a 1200 series diode array detector followed by a MicroToF-Q II mass spectrometer (Bruker Daltonics) using an ESI source either in negative mode or positive mode. Analysis was performed on an LC-18-T column (15 cm x 3 mm, 3 μm particles, Supelco).

LC conditions:

A-5 mM Ammonium acetate buffer, pH 6.6

B-75% Methanol and 25 % Water.

LC method: (for positive and negative mode on MS) 0 min-100% A, 2 min-100% A, 12 min-30% A 70% B, 17 min-30% A 70% B, 18 min-100% A, 30 min-100%A

Enzymatic assay conditions for DszA using FRE-NADH as reducing system

The DszA assay was performed in 100 mM phosphate buffer, pH 7.5 containing DszA (50 μM), dibenzothiophene sulfone (**38**, 500 μM), FMN (20 μM), *E. coli* flavin reductase (200 nM) and NADH (1 mM). The enzymatic reaction mixture was incubated at RT for 2 hr. The protein was heat-denatured and the remaining solution was filtered (10kda cut-off). Finally, the samples were analyzed by HPLC (C-18 column)

DszA reaction in the presence of $H_2{}^{18}O$ and $^{18}O_2$

Two identical solutions were made; each 200 μL solution contained 500 μM dibenzothiophene sulfone **38**, 50 μM DszA, 20 μM FMN, 200 nM Fre and 1mM NADH. One of the samples had a final concentration of 90% $H_2{}^{18}O$. The other sample was used as a 'control' and contained 100% $H_2{}^{16}O$. The caps of the eppendorf tubes were left open for atmospheric oxygen to dissolve. The reaction mixture was incubated at room temperature for 1 hour after which both the samples were analyzed by LC-MS.

Two identical assay mixtures were made in a glove box; each 200 μL solution contains 500 μM dibenzothiophene sulfone **38**, 50 μM DszA, 20 μM FMN, 200 nM Fre and 1mM NADH. One of the assay mixtures was exposed to $^{18}O_2$ while the other assay mixture was used as a 'control' and exposed to $^{16}O_2$. Samples were analyzed by LC-MS.

Coupled (DszA+DszB) assay to identify the oxygen incorporation site

The DszA assay was carried out using 500 μM dibenzothiophene sulfone **38**, 50 μM DszA, 20 μM FMN, 200 nM FRE and 1mM NADH under an $^{18}O_2$ atmosphere. After 2 hr, the protein was heat-denatured and the solution was passed through a10kda cut-off filter. To the resulting solution DszB (final concentration 50 μM) was added and incubated at RT under atmospheric oxygen for 1 hr. The DszB protein was heat-denatured and the remaining solution was filtered (10kda cut-off). Finally, the samples were analyzed by LC-MS.

Enzymatic assay condition for DszA using photoreduced FMN

A solution containing FMN (500 μM) and EDTA (10 mM) was irradiated with a A21 LED light bulb (100-W, white light) for 5 min under anaerobic conditions in a glove box. Once FMN was photo-reduced, dibenzothiophene sulfone **38** and DszA were added. Final

concentrations of reduced FMN, dibenzothiophene sulfone and DszA were 50 μM. The resulting mixture was incubated in a glove-box for 0.5 hr. and then exposed to oxygen and incubated for an additional 0.5 hr at 25 ˚C. The protein was heat-denatured and the remaining solution was filtered (10kda cut-off). Finally, the samples were analyzed by HPLC (PFP column) and LC-MS.

DszA reaction in the presence of $^{18}O_2$ using photoreduced FMN

FMN was photo-reduced in a glove-box using EDTA as discussed above. Substrate and enzyme were added. Final concentrations of reduced FMN, dibenzothiophene sulfone and DszA were 50 μM. The resulting mixture was incubated in a glove-box for 0.5 hr and exposed to $^{18}O_2$ and incubated for an additional 0.5 hr at 25 ˚C. The protein was heat-denatured and the remaining solution was filtered (10kda cut-off). Finally, the samples were analyzed by LC-MS.

Quantification of FMN-N5-oxide formed in DszA catalysed reaction

DszA assay using photoreduced FMN was carried out using the above-mentioned protocol. Final concentrations of reduced FMN, dibenzothiophene sulfone and DszA were 50 μM. Based on the calculation of the area under the peak it was determined that 34 μM FMN is consumed in the full reaction. Amount of sulfinic acid product **39** formed was 30 μM. (Calculated using reference compound **39**). Thus, the ratio of FMN consumed to sulfinic acid formed was 1:0.9 consistent with the stoichiometric conversion of FMN to FMN-N5-oxide during the course of the DszA catalyzed reaction.

A)

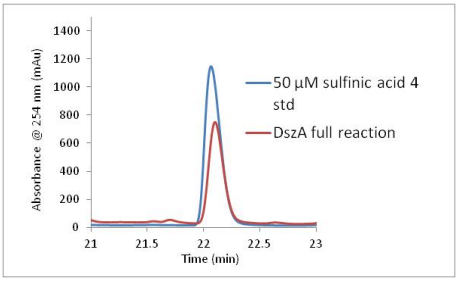

B)

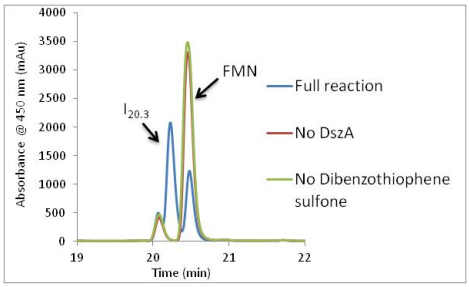

Figure 2.12: Quantification of FMN-N5-oxide by calculating the amount of FMN consumed and the amount of sulfinic acid product **39** formed. Panel A shows the consumption of FMN in the full reaction (34 µM FMN is consumed). Panel B shows formation of sulfinic acid product **39** in the full reaction (30 µM sulfinic acid product **39** is formed).

Derivatization of glyoxylic acid formed during photoreduction of FMN using EDTA

DszA assay was carried out (using photoreduced FMN) following the procedure described above. Final concentrations of reduced FMN, dibenzothiophene sulfone and DszA were 50 µM. Once the assay was over, the assay solution was made acidic (pH=1) by adding HCl. Then, o-phenylenediamine was added (final concentration was 1mM). The assay mixture was kept at room temperature for 2hr. Finally, the samples were analyzed by HPLC (C-18 column).

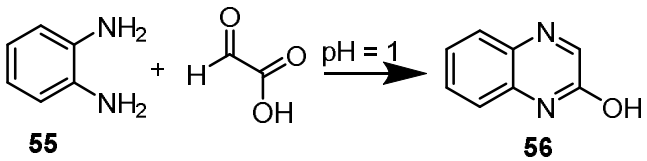

55 **56**

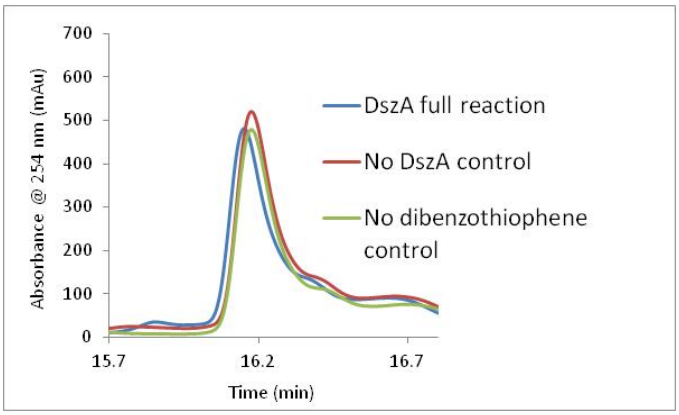

Figure 2.13: HPLC analysis of the derivatization of glyoxylic acid using o-phenylenediamine. Amount of o-phenylenediamine glyoxylic acid adduct formed is the same in full reaction, in the no DszA control and in the no dibenzothiophene control. This demonstrates that the glyoxylic acid produced during the flavin reduction is not used to reduce hydroperoxide **51**.

Synthesis of 2-(2-hydroxyphenyl)-benzenesulfinic acid (39)

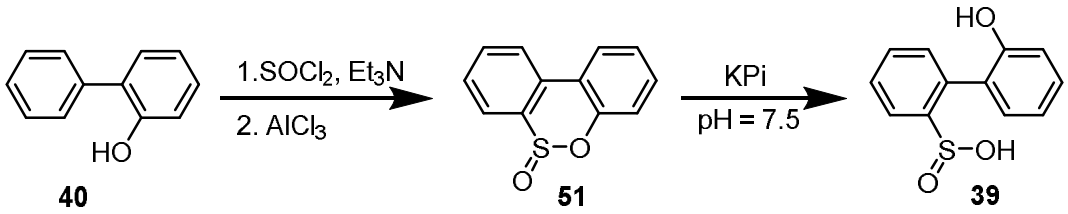

Figure 2.14: Synthetic scheme for 2-(2-hydroxyphenyl)-benzenesulfinic acid (**39**)

Synthesis of **51** was carried out following the known literature protocol. A solution of 2-hydroxybiphenyl (0.5 g, 2.94 mmol) in dichloromethane (2.5 mL) was added to thionyl chloride (0.23 mL, 3.23 mmol) in dichloromethane (2.5 mL) at 0 ˚C under inert atmosphere (dry argon). Then, triethylamine (0.41 mL, 2.94 mmol) was added to that solution dropwise over a period of 5 min. This mixture was stirred at 0 ˚C for 15 min and at 25 ˚C for an additional 15 min before filtering by suction and subsequent dropwise

addition over a 15-min period to a vigorously stirred suspension of aluminum chloride (0.8 g, 6 mmol) in dichloromethane (25 mL at 0 ˚C under dry argon). The resulting dark green solution was stirred at 0 ˚C for 1 h and at 25 ˚C for 12 h. Addition of water (25 mL), filtration, acid wash (15 mL, 3 N), collection of organic layer, drying (Na_2SO_4), and solvent evaporation led to a red-orange oil which was purified using silica gel column chromatography (hexane:ethyl acetate = 9:1) to yield compound **51** in 40% yield.

1H NMR (400 MHz, $CDCl_3$): δ 7.96 (d, 1H), 7.93 (d, 1H), 7.67-7.60 (m, 2H), 7.47(dt, 1H), 7.42 (dt, 1H), 7.35-7.27 (m, 2H)

13C NMR (100 MHz, $CDCl_3$): δ 144.7, 136.9, 132.8, 130.5, 128.3, 126.3, 125.5, 125.3, 124.4, 124.3, 121.2, 120.3

When the compound **51** was dissolved in KPi buffer (pH=7.5), it was converted to **39** as reported in literature.

Synthesis of FMN-N5-Oxide (14)

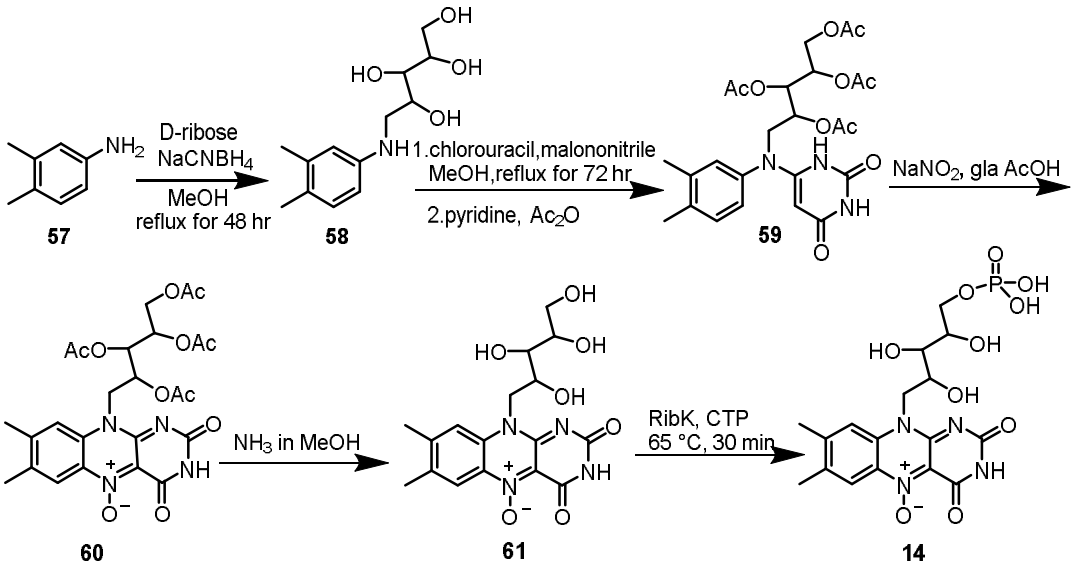

Figure 2.15: Synthetic scheme for FMN-N5-oxide (**14**)

Compound **57** (1g, 8.24 mmol), $NaCNBH_3$ (1g, 16.48 mmol) and D-ribose (3.7g, 24.73 mmol) were dissolved in anhydrous MeOH (50 mL). The resulting mixture was stirred under reflux (80 ˚C) for 48 hr. Then the solvent was removed under reduced pressure, and the remaining material was diluted in 1M HCl (20 mL) to quench any residual $NaCNBH_3$. The resulting acidic solution was neutralized using a saturated $NaHCO_3$ solution, and extracted into EtOAc (3 x 20mL), dried over Na_2SO_4, and concentrated. Silica gel column chromatography was carried out to purify compound **58** as a white solid, eluting with DCM – MeOH (90:5 → 90:10). The yield was 80%.

1H NMR (400 MHz, CD_3OD): δ 6.86 (d, 1H), 6.54 (d, 1H), 6.46 (dd, 1H), 3.93-3.87 (m, 1H), 3.80-3.71 (m, 2H), 3.66-3.59 (m, 2H), 3.42 (dd, 1H), 3.09 (dd, 1H), 2.16 (s, 3H), 2.11 (s, 3H)

13C NMR (100 MHz, CD_3OD): δ 148.1, 137.9, 131.1, 126.7, 116.7, 112.5, 74.9, 74.4, 72.2, 64.7, 48.1, 20.0, 18.7

Ribosylated aniline **58** (250mg, 0.97 mmol), 6-chlorouracil (171 mg, 1.17 mmol), and malononitrile (58mg, 0.87 mmol) were suspended in anhydrous methanol (25 mL) and stirred at reflux (80 ˚C) for 3 days. Then, solvent was removed under reduced pressure. Crude product was dissolved in pyridine (4.0 mL). To that solution, acetic anhydride (1.0 mL) was added, and the resulting mixture was stirred at RT overnight. The solvent was removed under reduced pressure, and the resulting residue was dissolved in DCM (60 mL) and washed with water (3 x 20 mL) and brine (20 mL). The organic extracts were dried with $MgSO_4$, filtered, and the solvent was removed under reduced pressure. Column chromatography on silica gel, eluting with DCM –MeOH (5%) produced **59** (yield was 40 % after two steps).

1H NMR (400 MHz, $CDCl_3$): δ 7.22 (d, 1H), 6.95-6.85 (m, 2H), 5.36-5.24 (m, 2H), 5.14-5.09 (m, 1H), 4.91 (s, 1H), 4.27 (dd, 1H), 4.10-4.00 (m, 2H), 3.73 (dd, 1H), 2.29 (s, 3H), 2.27 (s, 3H), 2.10 (s, 3H), 2.02 (s, 3H), 2.01 (s, 3H), 1.90 (s, 3H)

13C NMR (100 MHz, $CDCl_3$): δ 170.4, 169.8, 169.5, 169.4, 164.7, 153.5, 150.4, 139.6, 138.3, 136.9, 131.7, 128.9, 125.2, 77.1, 70.1, 69.3, 69.2, 61.6, 51.7, 20.8, 20.6, 20.5, 20.4, 19.7, 19.3

To a solution of **59** (60mg, 0.11mmol) in acetic acid (1mL) in the dark, $NaNO_2$ (39mg, 0.56mmol) was added. The resulting mixture was stirred for 3h. After that, water (1mL) was added and the resulting solution was stirred for additional 3h. Then, the solvents were removed under reduced pressure to get a crude orange solid. Silica gel column

chromatography (MeOH:DCM=0.5:9.5) was carried out to get pure compound **60** in 80% yield.

1H NMR (400 MHz, $CDCl_3$): δ 8.21 (s, 1H), 7.81 (s, 1H), 5.68-5.62 (m, 1H), 5.53-5.49 (m, 1H), 5.44-5.38 (m, 1H), 5.15-4.93 (m, 2H), 4.49 (dd, 1H), 4.24 (dd, 1H), 2.56 (s, 3H), 2.45 (s, 3H), 2.18 (s, 3H), 2.17 (s, 3H), 2.01 (s, 3H), 1.97 (s, 3H)

13C NMR (100 MHz, $CDCl_3$): δ 172.3, 171.8, 171.5, 171.3, 158.9, 157.3, 155.0, 149.1, 138.6, 131.7, 125.9, 121.7, 118.7, 71.7, 71.4, 70.7, 63.0, 45.9, 20.9, 20.8, 20.7, 20.6, 20.4, 19.5

Compound **60** was converted to compound **61** using NH_3 in MeOH. Compound **61** was phosphorylated by treating compound **61** with Cytidine triphosphate (CTP) and Ribokinase (RibK) @ 60 ˚C for 30 min. Due to the scale of the reactions the identity of compound **61** and **14** was established by UV-visible spectra and LC-MS analysis.

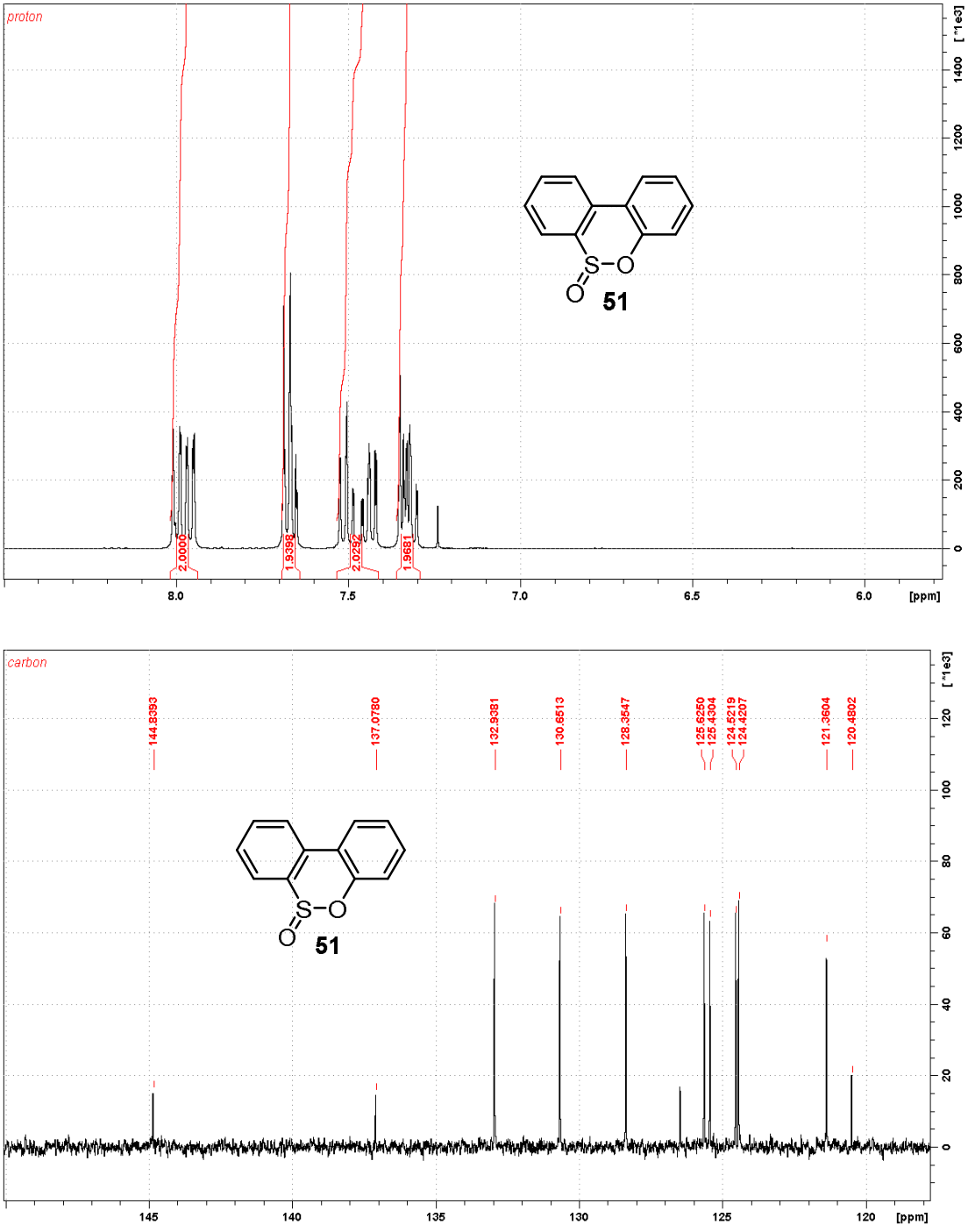

Figure 2.16: 1H NMR and 13C NMR spectrum of compound **51**.

.

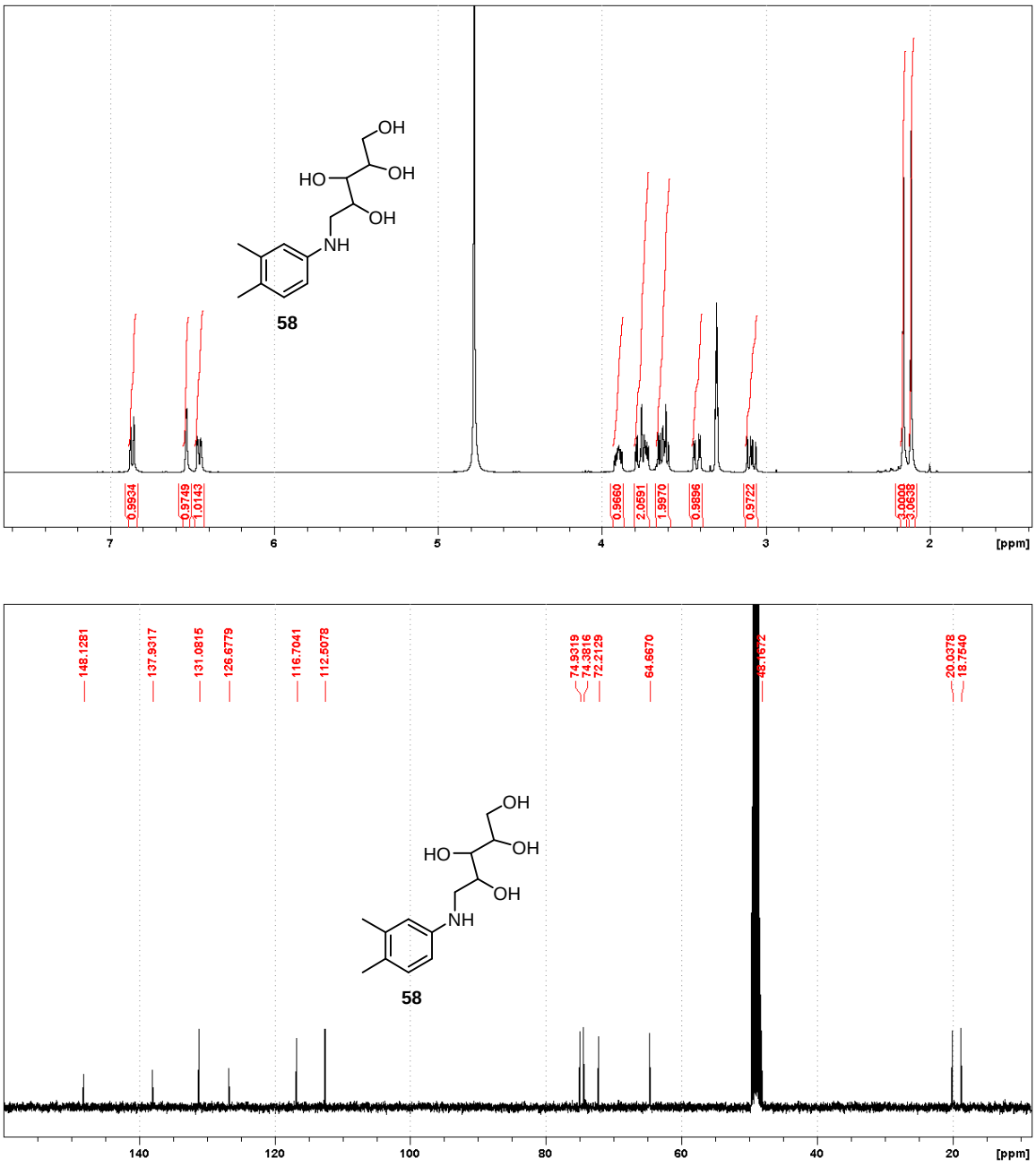

Figure 2.17: 1H NMR and 13C NMR spectrum of compound **58**.

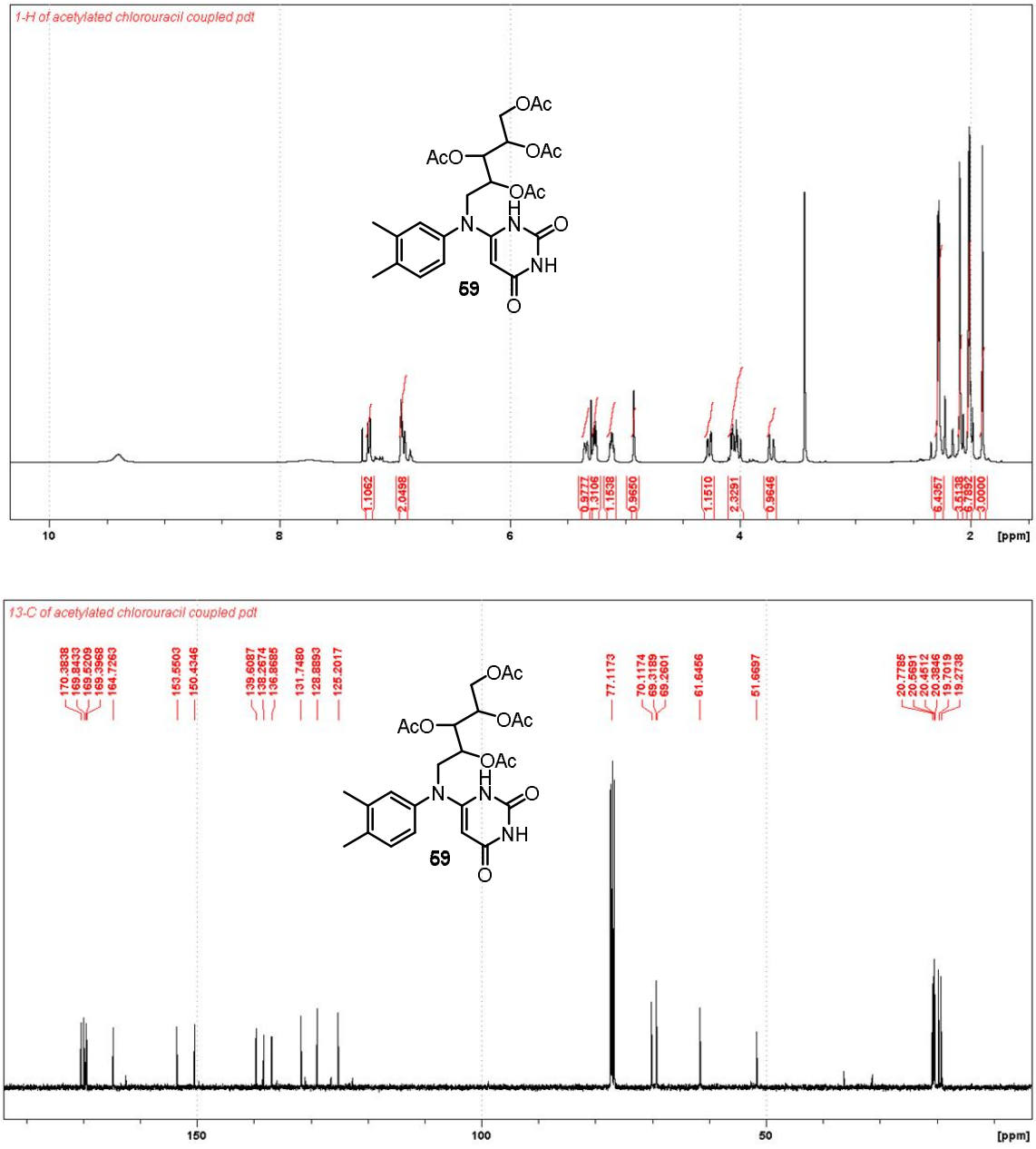

Figure 2.18: 1H NMR and 13C NMR spectrum of compound **59**.

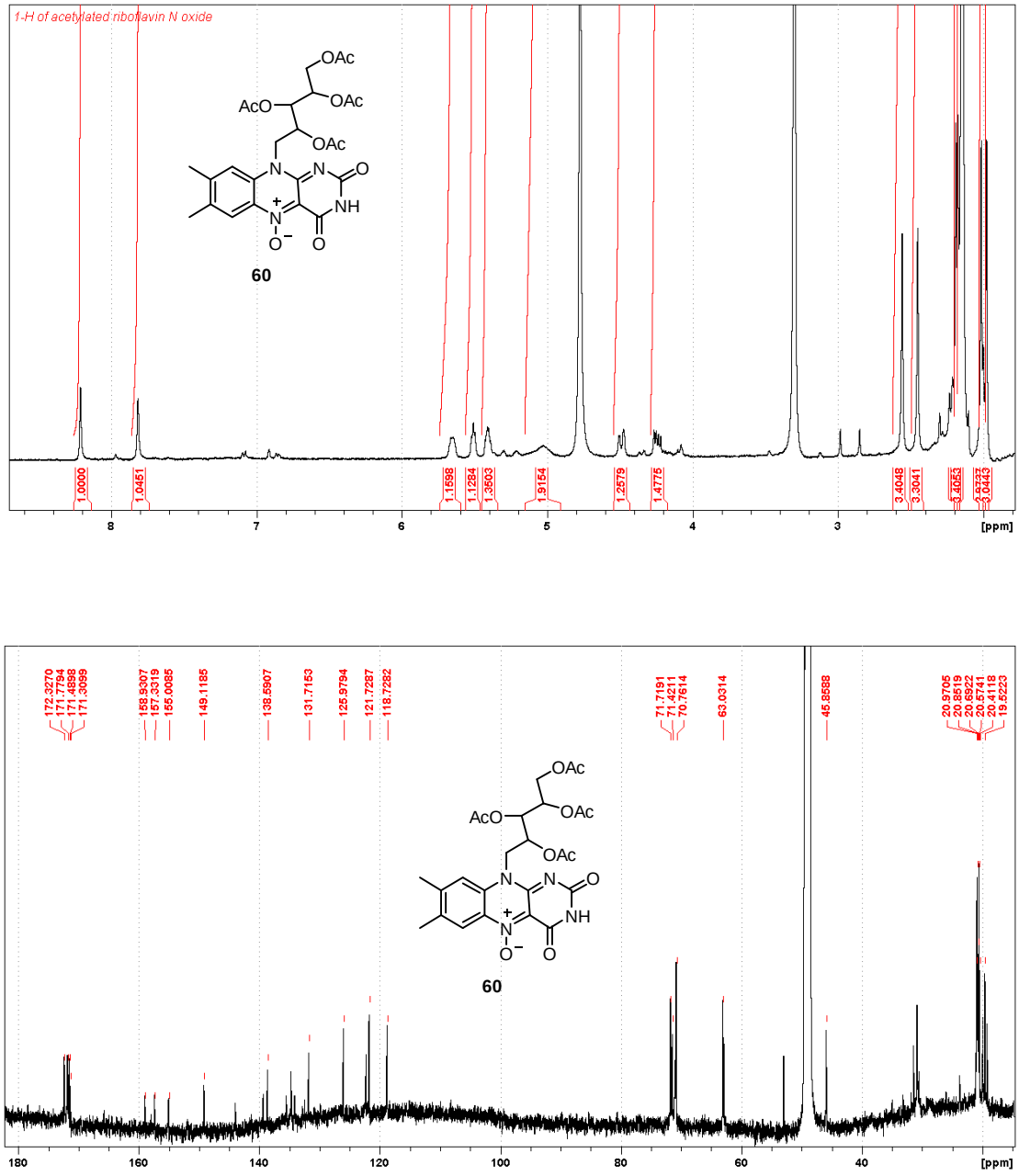

Figure 2.19: 1H NMR and 13C NMR spectrum of compound **60**.

A)

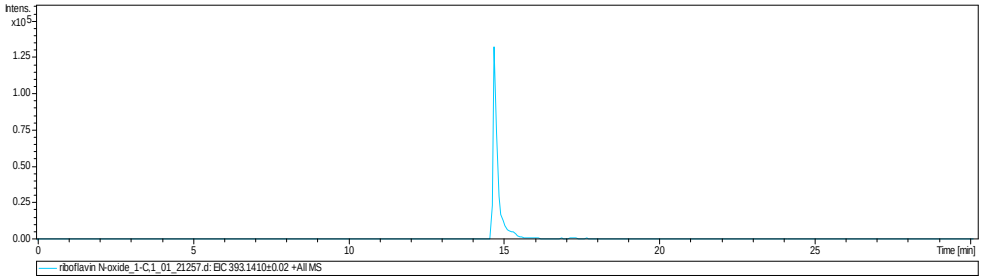

B)

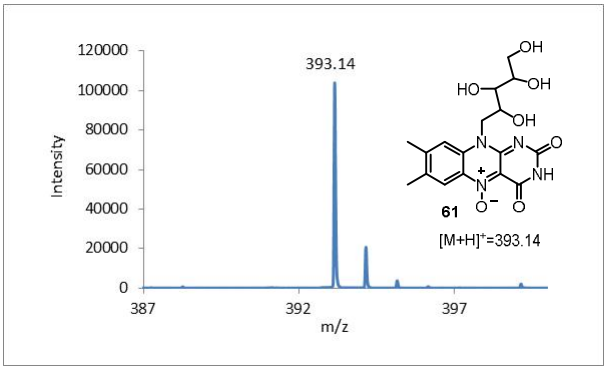

Figure 2.20: LC-MS analysis of synthesized Riboflavin-N5-oxide (**61**). (A) Extracted ion chromatogram (EIC) for $[M+H]^+$= 393.14 Da indicating formation of **61**. (B) Exact mass is consistent with the expected mass of Riboflavin-N5-oxide ($[M+H]^+$= 393.14 Da).

A)

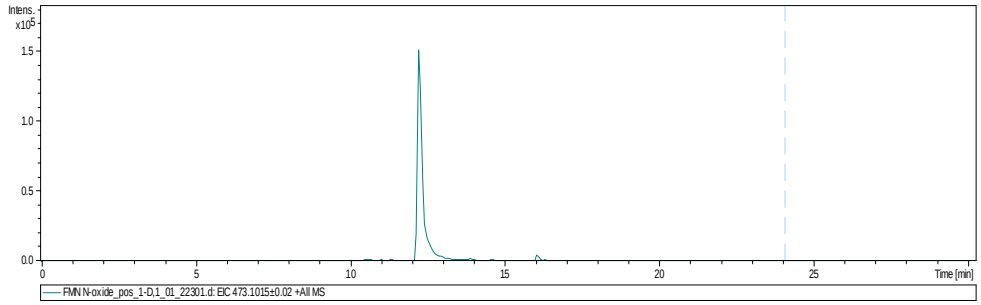

B)

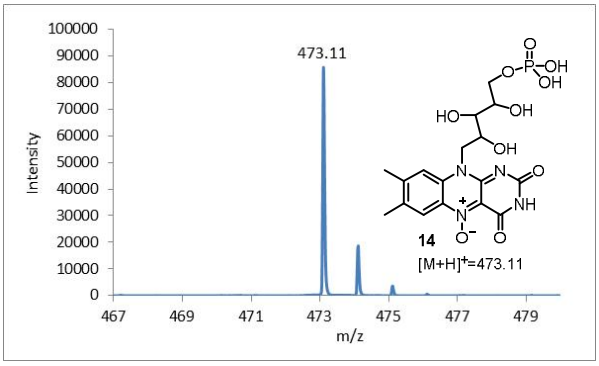

Figure 2.21: LC-MS analysis of synthesized FMN-N5-oxide (**14**). (A) Extracted ion chromatogram (EIC) for $[M+H]^+$= 473.11 Da indicating formation of **14**. (B) Exact mass is consistent with the expected mass of FMN-N5-oxide ($[M+H]^+$= 473.11 Da).

CHAPTER III

IDENTIFICATION OF FLAVIN-N5-OXIDE IN THE RUTA-CATALYZED OXIDATIVE CLEAVAGE OF URACIL AMIDE

3.1 Introduction

There are two major degradation pathways of uracil: one is reductive pathway[37] while the other is oxidative pathway[38] (Figure 3.1). The reductive pathway is more widespread: present in bacteria, archaea and human. Less studied oxidative pathway has been found only in a variety of bacteria. In the reductive pathway, uracil is at first reduced to dihydrouracil which then undergoes two successive hydrolysis reactions to give ammonia, carbon dioxide and β-alanine as end products. While in the oxidative pathway, uracil undergoes oxidation to give barbituric acid which upon hydrolysis reactions produce urea and malonic acid.

Recently, Sydney Kustu group discovered the third uracil catabolic pathway in *Escherichia coli* K-12, which is known as Rut pathway.[39] In the Rut pathway, uracil **62** is converted to 3- hydroxypropionate **70**, ammonia, and carbon dioxide (Figure 3.2). RutA catalyzes the first step of this pathway in which uracil is converted to 3-ureidoacrylic acid

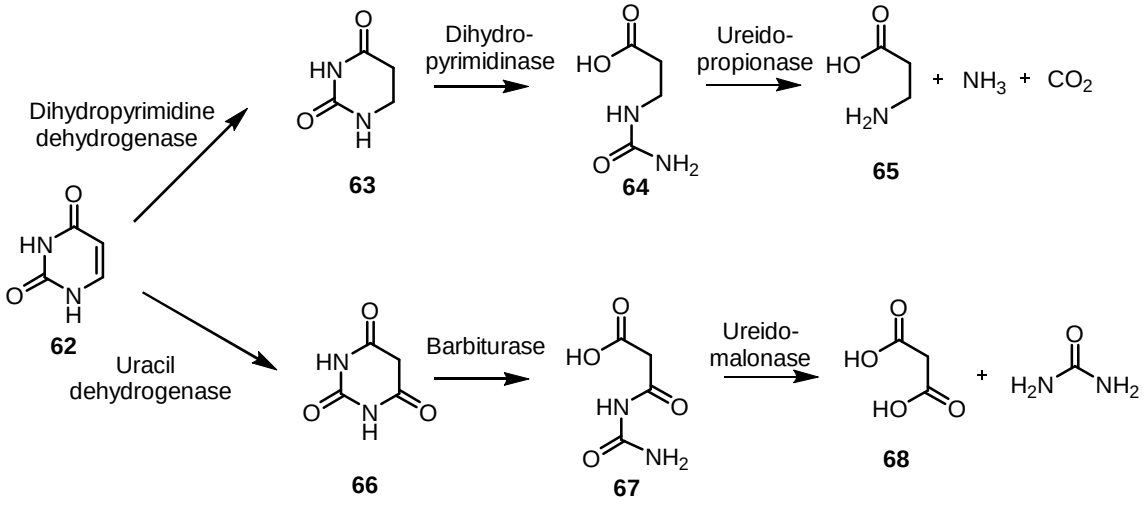

Figure 3.1: Two well-known uracil catabolic pathways.

69. Although this reaction seems like a simple amide hydrolysis, a labeling experiment showed that molecular oxygen is the source of one of the carboxylate oxygens of **69**; thus, RutA catalyzes an oxidative amide bond cleavage reaction[31] instead of an amide hydrolysis. Previous mechanistic studies of this reaction identified RutA as the first example of a flavin hydroperoxide-mediated amide cleavage reaction (conversion of **62** to **69** in Figure 3.3). The mechanism of hydroperoxide reduction (**73** to **69**) remained unclear. The observation that chemically synthesized peracid **69** was readily reduced by NADH or DTT initially suggested that this reduction was not enzyme-catalyzed. This was further supported by the absence of a suitable cysteine residue at the active site of RutA that can participate in peroxide reduction by the well-characterized peroxiredoxin mechanism.[32]

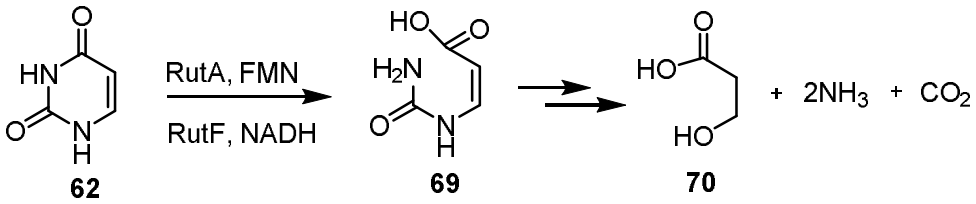

Figure 3.2: RutA catalyzes the first step in uracil catabolism.

Flavin-N5-oxide **14** has recently been identified as a new flavin oxidation state in the EncM- and DszA-catalyzed reactions[9, 10, 40] (Figure 3.4). EncM catalyzes 1,3-diketone oxidation during the biosynthesis of polyketide antibiotic enterocin. Detailed mechanistic studies of this system revealed the formation of flavin-N5-oxide upon reaction of reduced flavin with molecular oxygen. Flavin-N5-oxide, thus formed, acts as an oxidizing agent

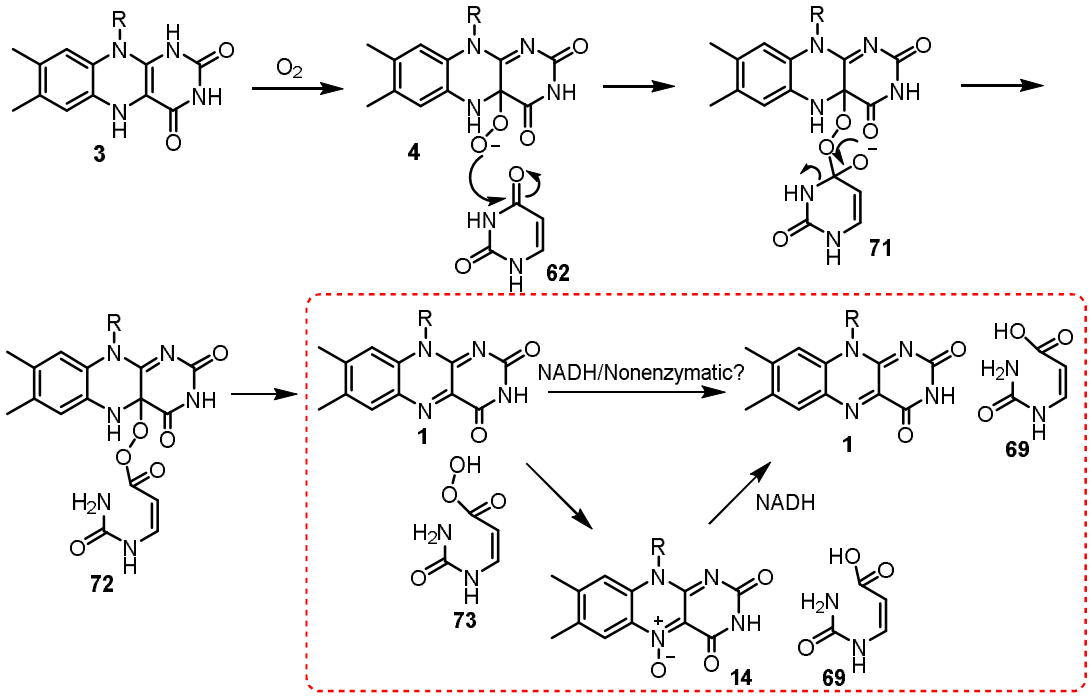

Figure 3.3: Mechanistic proposal for the RutA catalyzed reaction.

to convert 1,3-diketone **74** to 1,2,3- triketone product **75**. DszA catalyzes a novel oxidative C−S bond cleavage reaction in the dibenzothiophene catabolic pathway. In this reaction, flavin-N5-oxide is formed by the transfer of oxygen from the substrate hydroperoxide to oxidized flavin. This suggested the possibility that acyl hydroperoxide **73** might also undergo a similar reduction (Figure 3.3). In this chapter, we describe the experimental validation of this hypothesis.

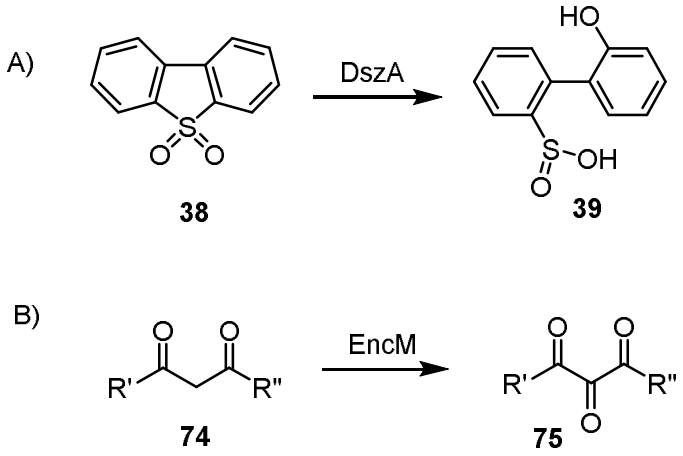

Figure 3.4: Two newly discovered flavin-N5-oxide utilizing enzymes.

3.2 Results and discussion

3.2.1 Reconstitution of RutA activity

RutA was overexpressed in *Escherichia coli* BL21(DE3) and purified by Ni-affinity chromatography. The normal RutA activity was confirmed by incubating uracil in the presence of RutA, FMN, NADH, and E. coli flavin reductase (Fre)[41] (to substitute for the RutF flavin reductase).

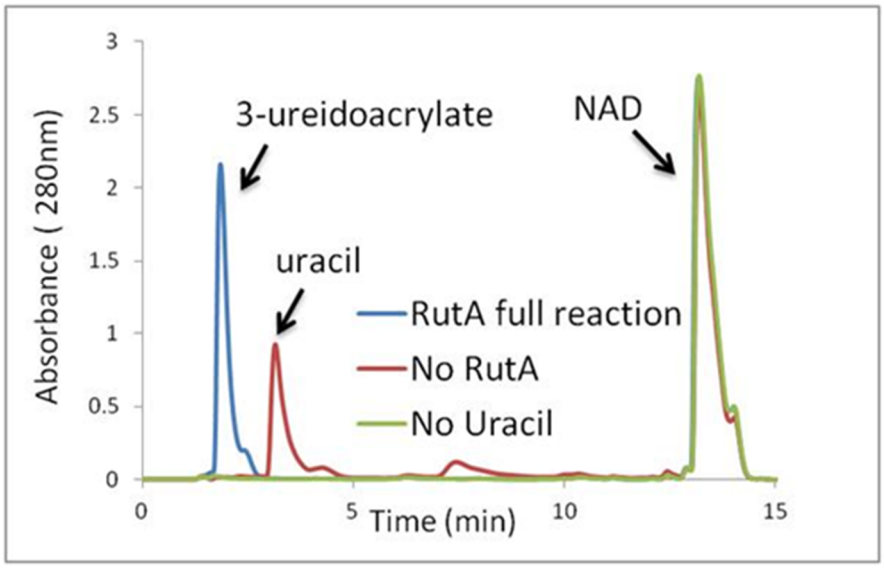

Figure 3.5: HPLC chromatogram of RutA catalyzed reaction using NADH-Fre.

3.2.2 RutA catalyzed reaction using photoreduced FMN

To test for the formation of the FMN-N5-oxide, the RutA assay had to be performed in the absence of NADH. The flavin reductase/ NADH was therefore replaced by the photochemical reduction of the flavin by EDTA.[42] In this reaction mixture, FMN was photoreduced using EDTA under anaerobic conditions; stoichiometric amounts of uracil and RutA were added, and the resulting mixture was incubated in a glovebox for 30 min. The mixture was then exposed to air to initiate formation of the flavin hydroperoxide. After 1 h, the reaction was heat-quenched. High-performance liquid chromatography (HPLC) analysis demonstrated the consumption of FMN and uracil in a 1:1 ratio and the formation of a new FMN derivative at 20.3 min (Figure 3.6).

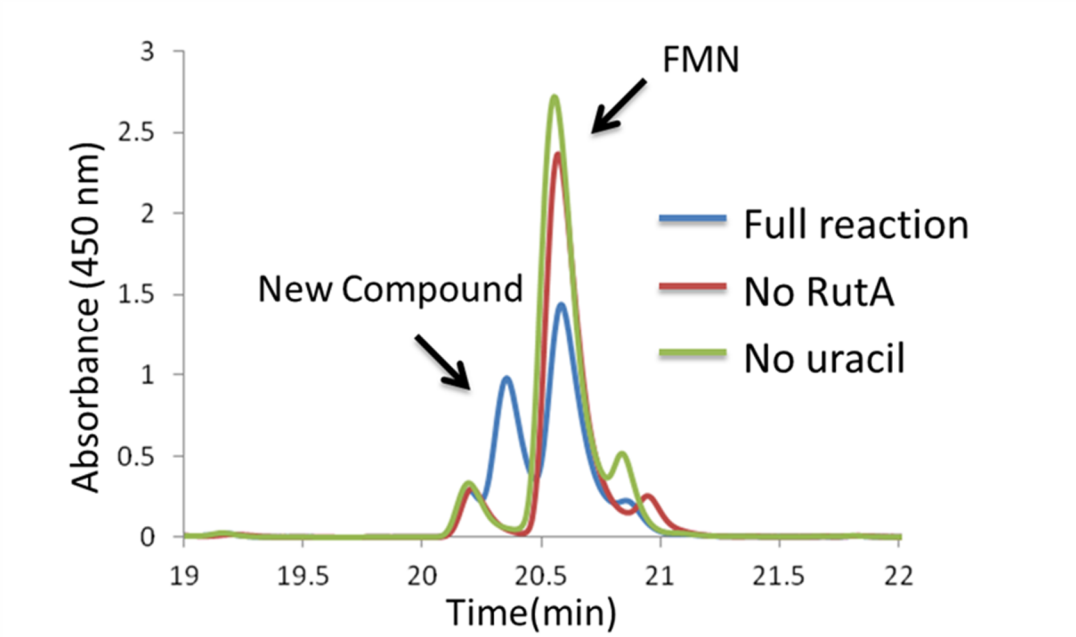

Figure 3.6: HPLC chromatogram of RutA catalyzed reaction using photoreduced FMN.

3.2.3 Characterization of flavin-N5-oxide

The new compound co-eluted with an authentic standard of chemically synthesized FMN-N5-oxide, and its ultraviolet−visible (UV−vis) spectrum was identical to that of the standard (Figure 3.7A, B). Liquid chromatography−mass spectrometry (LC−MS) analysis revealed that the mass corresponding to FMN-N5-oxide is present only in the full reaction (Figure 3.7C, D). When the reaction was performed in the presence of $^{18}O_2$, the expected 2 Da mass increase was observed (Figure 3.7E). These data unequivocally establish formation of FMN-N5-oxide in the RutA-catalyzed reaction.

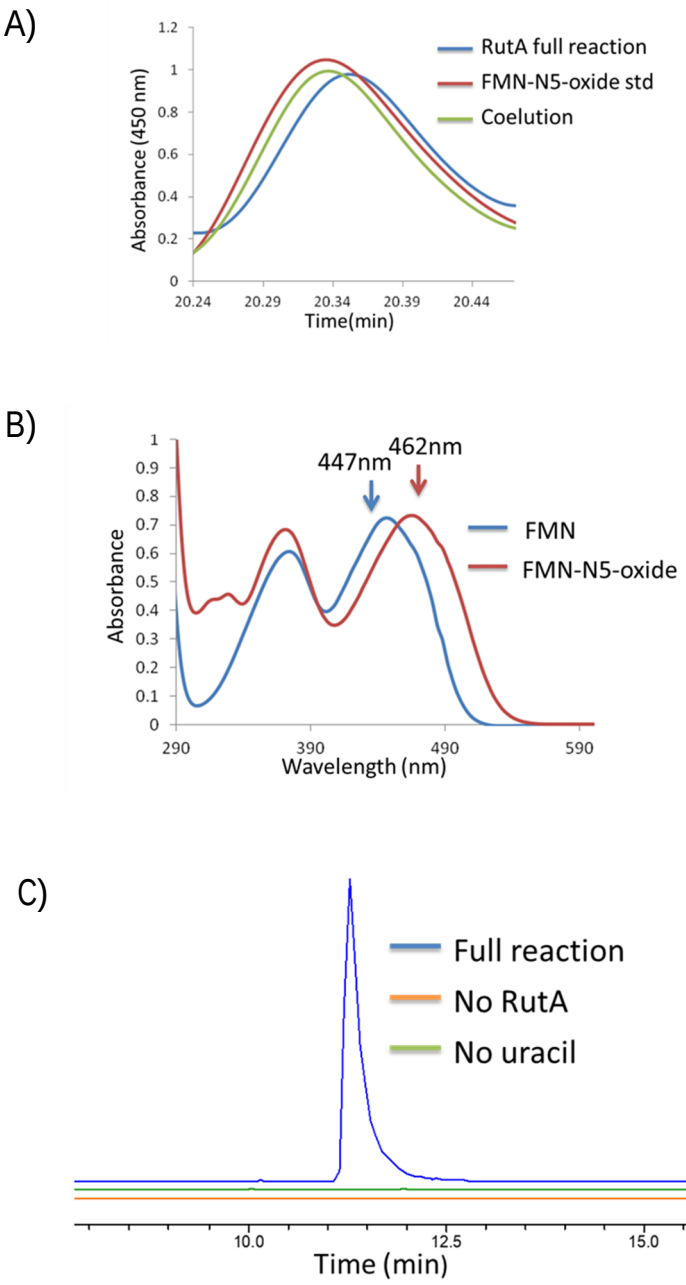

Figure 3.7: Characterization of flavin-N5-oxide in the RutA catalyzed reaction. (A) Co-elution of the new compound with synthetically prepared FMNN5- oxide. (B) Comparison of the UV−vis spectra of FMN and FMNN5- oxide formed in the RutA full reaction. (C) Extracted ion chromatograms for $[M + H]^+$ = 473.1 Da demonstrate FMN-N5-oxide formation only in the full reaction mixture. (D) The exact mass of the new compound is

consistent with the mass expected for the FMN-N5-oxide ($[M + H]^+$ = 473.1 Da). (F) Exact mass of the new compound formed when the reaction is performed in the presence of $^{18}O_2$.

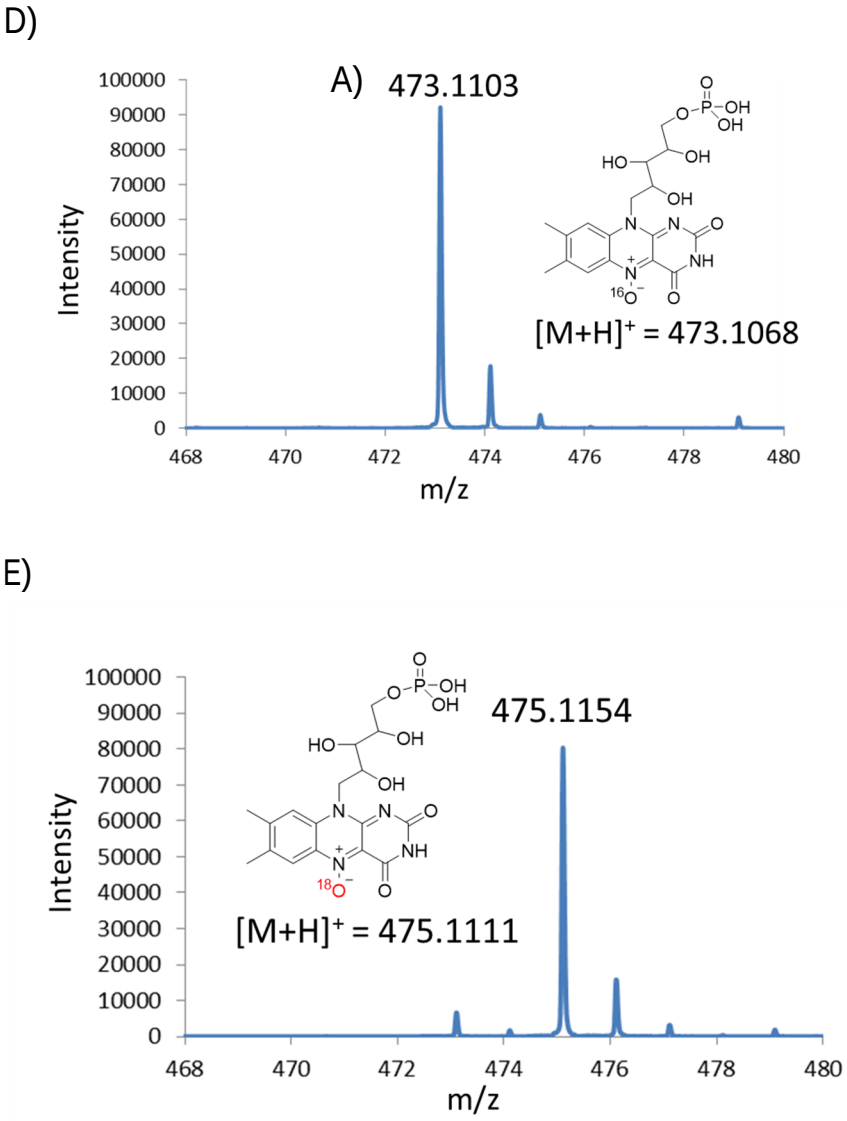

Figure 3.7: Continued

3.3 Conclusion

Flavin-N5-oxide was proposed as a possible oxidizing intermediate in the early days of flavoenzymology but was then dismissed in favor of the flavin hydroperoxide. The unequivocal identification of this new flavin oxidation state in the EncM-catalyzed (enolate oxidation), DszA-catalyzed (sulfone monooxygenase), and RutA-catalyzed (amide monooxygenase) reactions suggests that the use of this new flavin oxidation state may be more prevalent than previously thought. EncM may have evolved the use of flavin-N5-oxide because the Baeyer−Villiger oxidation using flavin hydroperoxide is likely to compete with ketone Cα hydroxylation. We would therefore expect to find other examples of the EncM motif in flavoenzymes involved in hydroxylation of sites adjacent to electrophilic centers. This expectation is further supported by the versatility of oxoammonium ions as oxidants in organic synthesis.[43-45] Our studies of DszA and RutA suggest that the reduction of substrate-derived hydroperoxide by oxidized flavin, is another catalytic motif likely to involve the formation of a flavin-N5-oxide.

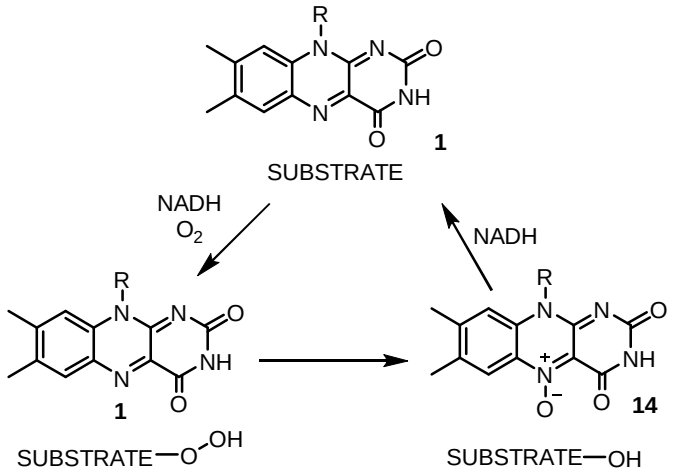

3.4 Experimental Procedure

Materials

All chemicals were purchased from Sigma-Aldrich unless mentioned otherwise. LB broth (Lennox) was purchased from EMB Millipore. Chloramphenicol and IPTG were obtained from Lab Scientific Inc. Amicon Ultra centrifugal filter devices (10,000 MWCO) were obtained from Millipore. Histrap column was obtained from GE Healthcare. Econo-Pack 10DG desalting columns were purchased from Bio-Rad. 2.5 L baffled ultra yield flasks for protein overexpression were obtained from Thomson Instrument Company. HPLC and LC-MS solvents were purchased from EMD and were used without further purification. ZORBAX Eclipse XDB-C18 column (15 cm x 4.6 mm, 5 μm particles) was purchased from Agilent Technologies. PFP column (150 x 4.6 mm, 2.6 μm particles) was purchased from phenomenex.

Over-expression and purification of RutA and Fre

The RutA gene containing overexpression plasmid (pCA24N)1 was transformed into *Escherichia coli* BL21 (DE3). For the overexpression of the protein, a starter culture was grown overnight in 15 ml of LB medium containing 20 μg/ml of chloramphenicol at 37 °C. 1.5 liter of LB medium (20 g/L) containing 20 μg/ml of chloramphenicol, was inoculated with this starter culture. The cells were grown at 37 °C with shaking (220 rpm) until the culture reached an OD_{600} of 0.6. The culture was then incubated at 4°C for ~45min without shaking. Then the culture was induced by adding IPTG to a final concentration of 0.4 mM, the temperature was lowered to 15 °C and the cells were grown

with shaking (180 rpm) for a further 15 hours. The cells were then harvested by centrifugation at 10,000g for 10 min at 4 °C and store at -80 ˚C.

The cell pellet was re-suspended in 30 ml of lysis buffer (50 mM KH_2PO_4, 150 mM NaCl, 10 mM imidazole, pH 8.0). Lysozyme (5 mg) was added and the cells were lysed by sonication on ice (Misonix Sonicator 3000, six cycles of 30 s duration during which 1.5 s sonicator pulses at output level 0.8 were followed by 1.5 s pauses). The resulting suspension was centrifuged (18,000 rpm, 30 min) and the supernatant was filtered through a sterile syringe filter (pore size 0.45 μm). The clarified supernatant was loaded onto a 5 mL Ni-NTA-affinity column pre-equilibrated with lysis buffer kept at 4°C. The Ni-NTA-affinity column was then washed with 50 ml wash buffer (50 mM KH_2PO_4, 150 mM NaCl, 20 mM imidazole, pH 8.0). The protein was eluted from the column with elution buffer (50 mM KH_2PO_4, 150 mM NaCl, 200 mM imidazole, pH 8.0) at 4°C. The fractions containing protein were pooled and concentrated using YM-10 Amicon ultracentrifugal filters at 5000g to a final volume of 3 mL. The concentrated sample was buffer exchanged, using an Econo-Pac 10DG desalting column, into 100 mM phosphate buffer at pH 7.5 containing 100 mM NaCl and glycerol to a final concentration of 15%. Protein concentration was determined from the absorbance at 280 nm (A280) with an Extinction coefficient calculated using the ProtParam tool of the ExPASy proteomics Server ($\epsilon 280 = 56380$). A typical yield was 20 mg/liter.

The *E. coli* Fre gene was cloned into pTHT vector (derivative of pET28b vector with TEV protease cleavage site after the N-terminal His-tag). The plasmid was transformed into *Escherichia coli* BL21 (DE3). A starter culture was grown overnight in 15 ml of LB

medium containing 40 μg/ml of Kanamycin at 37 ˚C. Next, 1.5 L of LB medium containing 40 μg/ml of Kanamycin was inoculated with this starting culture. The cells were grown at 37 ˚C till the OD_{600} reached a value of 0.6. The culture was then incubated at 4 ˚C for 45 min without shaking and induced with 0.5 mM IPTG followed by incubation at 15 ˚C for 15 hr with shaking (180 rpm). The cells were then harvested by centrifugation and stored at -80 ˚C until further use. The purification procedure was same as that for RutA.

HPLC parameters

An Agilent 1260 HPLC equipped with a quaternary pump was used. The system included a diode array UV-Vis detector and products were detected using absorbance at 280 nm, and 450 nm. Analysis was performed either on a ZORBAX Eclipse XDB-C18 column (15 cm x 4.6 mm, 5 μm particles, Agilent Technologies) or PFP column (150 x 4.6 mm, 2.6 μm particles, Kinetex).

HPLC conditions (for C18 column):

A-Water

B-100 mM potassium phosphate buffer, pH 6.6

C-Methanol

HPLC method:

0 min-100% B, 5 min- 10% A 90% B, 12 min-48%A 40%B 12% C, 14 min-50%A 30%B 20% C, 18 min-30% A 10% B 60% C, 20 min-100% B, 25 min-100% B

HPLC conditions (for PFP column):

A-Water

B-100 mM potassium phosphate buffer, pH 6.6

C-Methanol

HPLC method:

0 min-90% A 10% B, 2 min- 90% A 10% B, 22 min-20%A 10%B 70% C, 27 min-20%A 10%B 70% C, 28 min-90% A 10% B, 36 min-90% A 10% B

LC-MS parameters

LC-ESI-TOF-MS was performed using an Agilent 1260 HPLC system which is equipped with a binary pump and a 1200 series diode array detector followed by a MicroToF-Q II mass spectrometer (Bruker Daltonics) using an ESI source either in negative mode or positive mode. Analysis was performed on an LC-18-T column (15 cm x 3 mm, 3 μm particles, Supelco).

LC conditions:

A-5 mM Ammonium acetate buffer, pH 6.6

B-75% Methanol and 25 % Water.

LC method: (for positive and negative mode on MS) 0 min-100% A, 2 min-100% A, 12 min-30% A 70% B, 17 min-30% A 70% B, 18 min-100% A, 30 min-100%A

RutA catalyzed reaction using Fre-NADH as reducing system

The RutA catalyzed reaction was performed in 100 mM phosphate buffer, pH 7.5. A 200 μL aliquot of the reaction mixture containing RutA (50 μM), uracil (500 μM), FMN (20 μM), *E. coli* Fre (400 nM) and NADH (1 mM) was incubated at RT for 3 hr. The protein was heat-denatured and the resulting solution was filtered using an Amicon Ultra

centrifugal filter (10kda cut-off). The samples were analyzed by HPLC (using a C-18 column).

RutA catalyzed reaction using photoreduced FMN

In order to photoreduce FMN, a solution containing FMN (500 μM) and EDTA (10 mM) was irradiated, under anaerobic conditions, for 5 min in a glove box with an A21 LED light bulb (100-W, white light). Uracil (100 μM) and RutA (100 μM) were added to a solution containing photo-reduced FMN (100 μM). The resulting mixture was incubated in the glove-box for 0.5 hr. and then exposed to oxygen for an additional 1 hr at 25 ˚C. The protein was heat-denatured and the resulting solution was filtered using an Amicon Ultra centrifugal filter (10kda cut-off). The samples were analyzed by HPLC (using a PFP column) and LC-MS.

RutA reaction in the presence of $^{18}O_2$ using photoreduced FMN

FMN was photo-reduced in a glove-box using EDTA as described above. Substrate and enzyme were added. Final concentrations of reduced FMN, uracil and RutA were 100 μM each. The resulting mixture was incubated in a glove-box for 0.5 hr, exposed to 18O2 and incubated for an additional 1 hr at 25 ˚C. The protein was heat-denatured and the resulting solution was filtered using an Amicon Ultra centrifugal filter (10kda cut-off). Finally, the samples were analyzed by LC-MS.

Quantification of the FMN-N5-oxide formed in the RutA-catalysed reaction

The RutA-catalyzed reaction, using photoreduced FMN, was carried out as described above. Final concentrations of reduced FMN, uracil and RutA were 100 μM. Based on calculated peak areas, it was determined that 54 μM FMN was consumed in the full

reaction. Consumption of uracil was 52 μM. Thus, the ratio of FMN consumed to uracil consumed was 1:0.9 consistent with the stoichiometric conversion of FMN to FMN-N5-oxide during the course of the RutA catalyzed reaction.

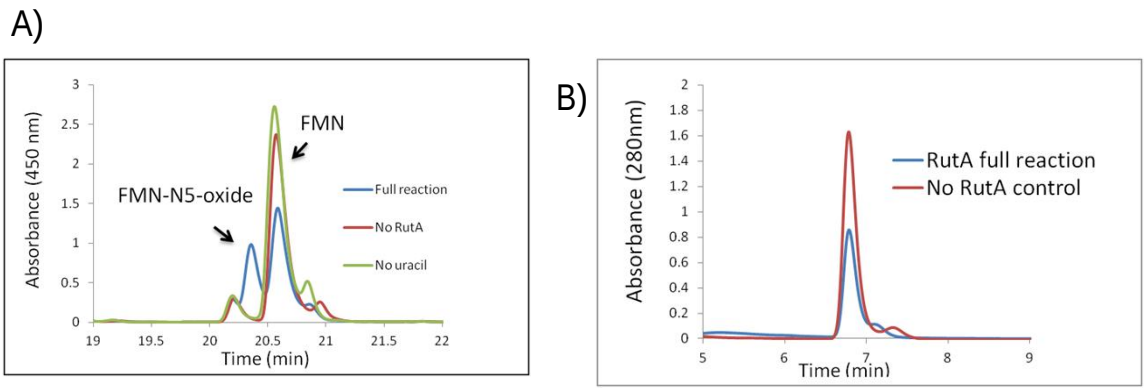

Figure 3.8: Estimation of FMN-N5-oxide formed by calculating the amount of FMN and uracil consumed in the RutA catalyzed reaction. Panel A shows the consumption of FMN (54 μM) in the full reaction. Panel B shows consumption of uracil (52 μM) in the full reaction.

CHAPTER IV

RECONSTITUTION AND MECHANISTIC STUDIES ON THE HCBA1 CATALYZED DEHALOGENATION REACTION IN HEXACHLOROBENZENE CATABOLIC PATHWAY

4.1 Introduction

Hexachlorobenzene (HCB, **76**) was widely used as a fungicide in agriculture until it was banned in 2001 under the Stockholm convention on persistent organic pollutants.[46] During the development of a bioremediation strategy for this compound, an HCB catabolizing strain of Nocardioides (strain PD653) was isolated and the catabolic operon involved in the conversion of HCB to pentachlorophenol (PCP, **80**) was cloned and sequenced.[47, 48] This gene cluster encoded three genes - a flavin monooxygenase (HcbA1), and two flavin reductases (HcbA2 and HcbA3). Cell lysate containing HcbA1 and HcbA3 catalyzed the conversion of HCB to PCP.

We have previously characterized the mechanism of dibenzothiophene sulfone mono-oxygenase (DszA).[40] For this enzyme, flavin hydroperoxide (**4**) adds to a substrate electrophilic carbon. This is followed by flavin elimination to give the substrate

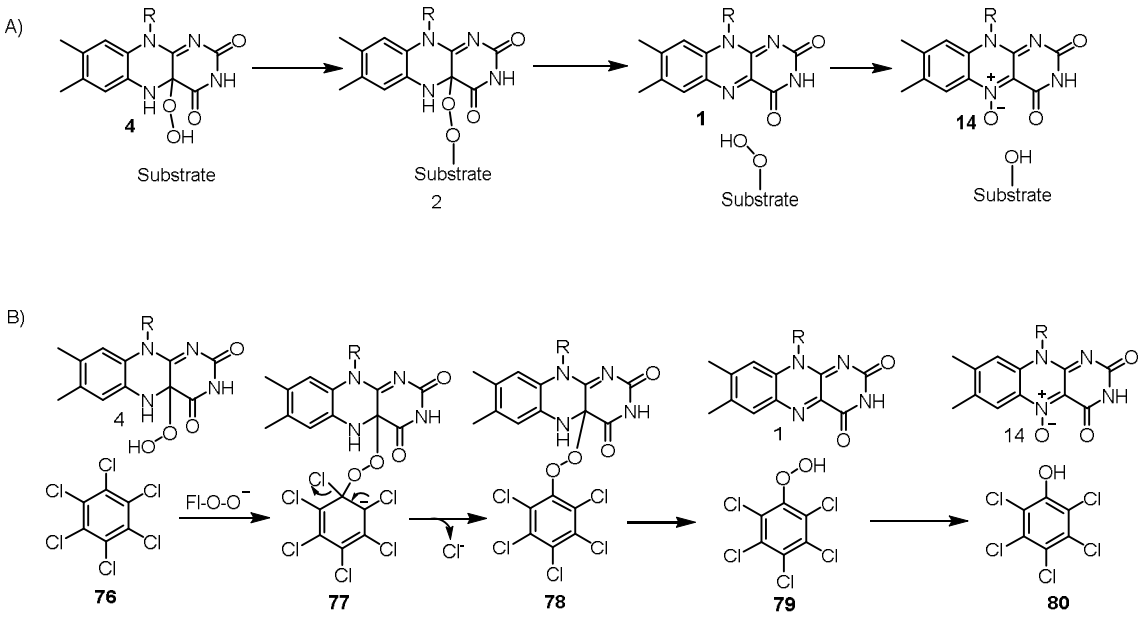

Figure 4.1: (A) A general model for the prediction of enzymes that generate flavin-N5-oxide as an intermediate. (B) Mechanistic proposal for the conversion of HCB **76** to PCP **80**.

hydroperoxide which then reacts with the eliminated flavin to give a flavin-N5-oxide (**14**) and the product. This mechanism represents a general reaction motif that can be used to predict flavin-N5-oxide utilizing enzymes (Figure 4.1A). Guided by this hypothesis, we have recently reported a second example of a flavin-N5-oxide-utilizing enzyme – uracil mono-oxygenase (RutA)[49, 50] involved in an oxidative amide cleavage in uracil catabolism. We, therefore, considered the mechanism shown in Figure 4.1B for hexachlorobenzene mono-oxygenase (HcbA1) as a possibility. In this proposal, flavin hydroperoxide adds to the highly electron depleted benzene ring to give the Meisenheimer intermediate **77**. Loss of chloride followed by flavin elimination gives the peroxide **79**. Cleavage of this peroxide by the eliminated flavin gives the final product **80** and flavin-N5-oxide. In this paper, a

mechanistic study that supports this proposal for the HcbA1-catalyzed reaction is described.

4.2 Results and discussion

4.2.1 Overexpression and purification of HcbA1

The HcbA1 sequence was optimized for expression in *E. coli* and inserted into the pTHT expression vector (derivative of pET28b vector with a TEV protease cleavage site after the N-terminal His-tag). The resulting plasmid was transformed into *E. coli* BL21(DE3). Overexpressed protein was purified using Ni-NTA-affinity chromatography.

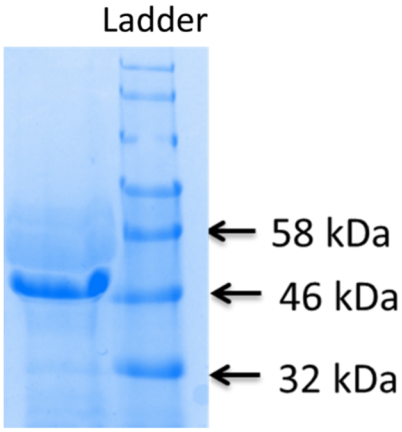

Figure 4.2: SDS-PAGE of purified HcbA1.

4.2.2 Reconstitution of HcbA1 activity

The HcbA1-catalyzed reaction was reconstituted by incubating HCB, HcbA1, *E. coli* flavin reductase (Fre), FMN (not FAD), and NADH at 25 °C for 3 h. Under these conditions, HCB was converted to a new product, which was identified as PCP by MS analysis and by HPLC comigration with an authentic sample (Figure 4.3).

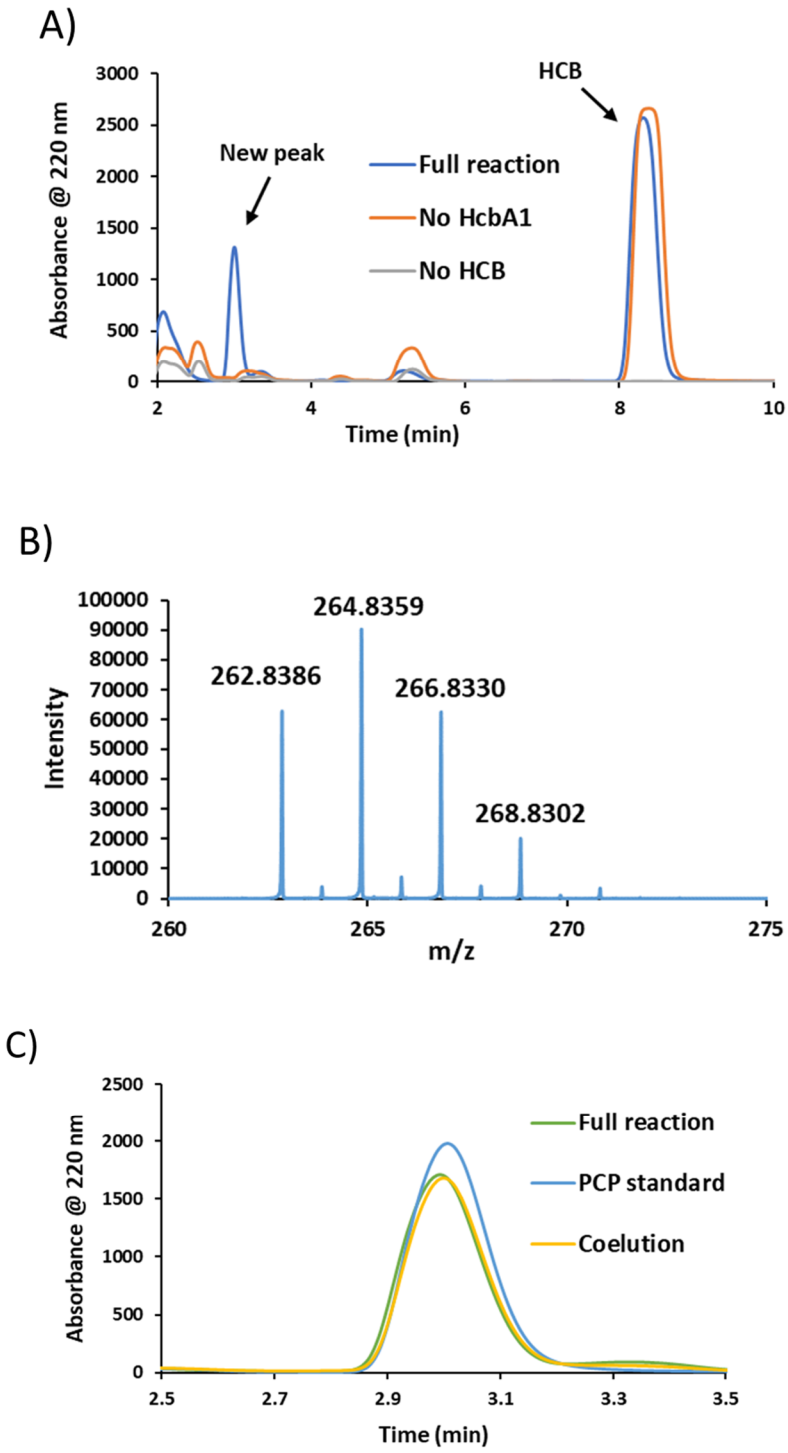

Figure 4.3: Reconstitution of HcbA1 activity. (A) HPLC chromatogram of the reaction mixture showing formation of a new peak eluting at 3.0 min. (B) MS data confirming PCP as the reaction product. (C) Coelution of the HcbA1 reaction product with an authentic PCP standard

4.2.3 Labeling experiments

The mechanistic proposal shown in Figure 4.1B predicts that the oxygen atom in PCP is derived from molecular oxygen. This was confirmed by MS analysis of the product formed when the reaction was run in the presence of $^{18}O_2$ (Figure 4.4 A). In a control reaction run in $H_2{}^{18}O$, 18O incorporation into PCP was not detected (Figure 4.4B).

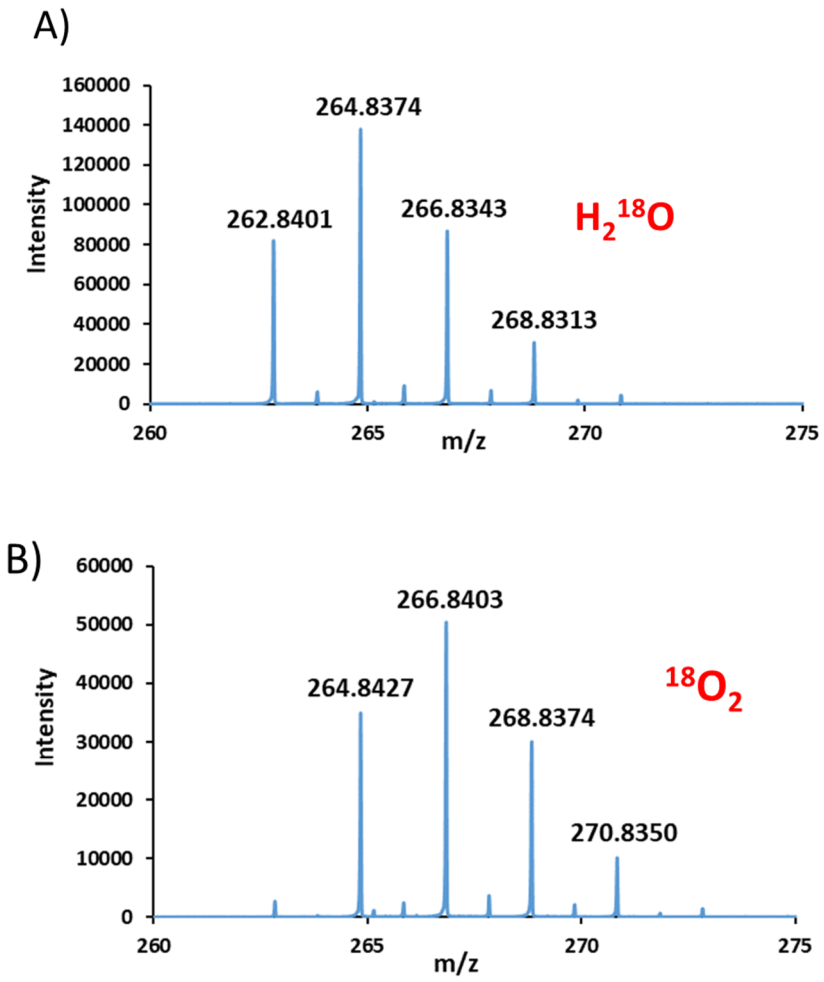

Figure 4.4: Labeling experiment of HcbA1 catalyzed reaction. A) ESI/MS analysis (in negative ion mode) of the PCP formed when the reaction was run in $H_2{}^{18}O$. (B) ESI/MS analysis (in negative ion mode) of the PCP formed when the reaction was run in $^{18}O_2$

4.2.4 HcbA1 reaction using photo reduced FMN

A similar strategy to that developed for the DszA and RutA systems was used to test for flavin-N5-oxide formation in the HcbA1-catalyzed reaction. To avoid reduction of the flavin- N5-oxide by excess NADH, the HcbA1-catalyzed reaction was carried out using photoreduced FMN. A typical reaction mixture containing stoichiometric amounts of HCB, HcbA1, and $FMNH_2$ was incubated for 30 min under anaerobic conditions before exposed to atmospheric oxygen for 1 h to allow the formation of the flavin-C4a-peroxide and the subsequent oxidation reaction to take place. LC−MS analysis of the resulting reaction mixture demonstrated the formation of a product with a mass corresponding to flavin-N5-oxide (Figure 4.5 A, B). When the reaction was carried out in the presence of $^{18}O_2$, the predicted 2 Da increase in the mass of flavin-N5-oxide was observed (Figure 4.5C).

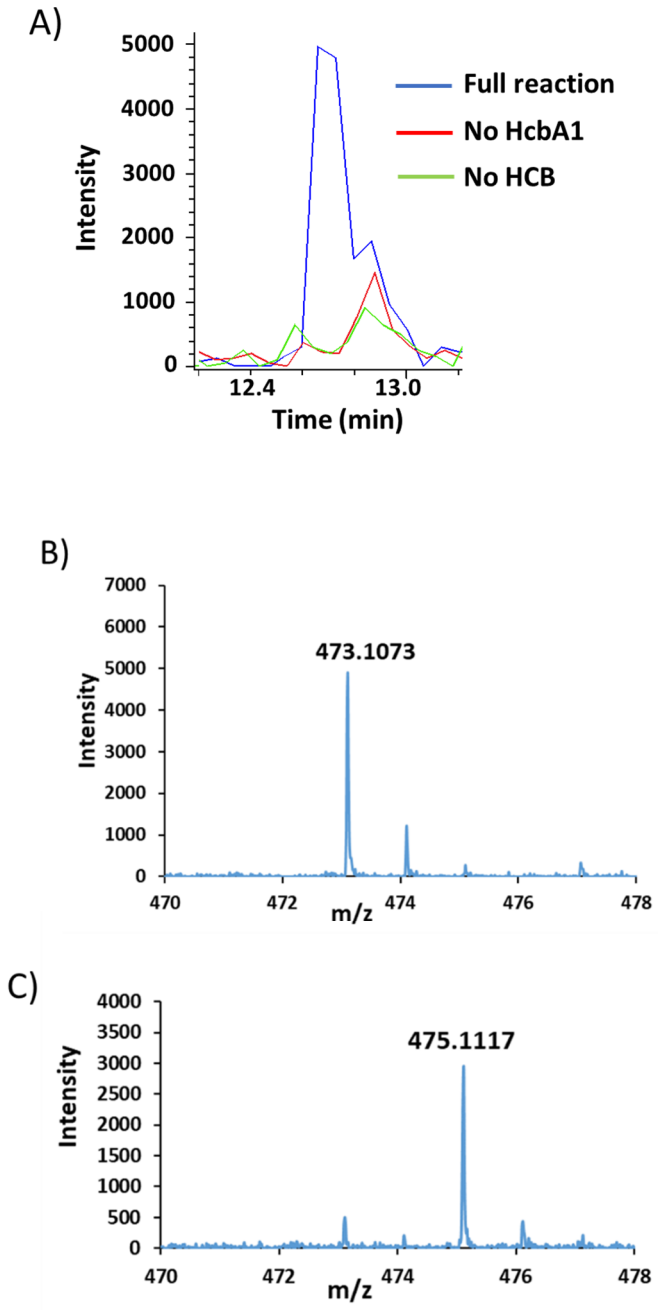

Figure 4.5: Characterization of flavin-N5-oxide in the HcbA1-catalyzed reaction. (A) EIC at m/z = 473.1 corresponding to $[M + H]^+$ for FMN-N5-oxide. (B) Exact mass of the FMN-N5-oxide formed when the reaction was carried out in the presence of $^{16}O_2$. (C) Exact mass of the FMN-N5-oxide formed when the reaction was carried out in the presence of $^{18}O_2$

4.3 Conclusion

Enzyme-mediated aryl ring dehalogenation reactions have been the focus of considerable study over the past several decades.[51-53] Two systems, relevant to the HCB dehalogenation, are shown in Figure 4.6. In the 4-chlorobenzoyl-CoA dehalogenase-catalyzed reaction[54-58] (panel A), an active site carboxylate adds to C4 of the substrate to give the Meisenheimer complex **82**. Loss of chloride followed by ester hydrolysis completes the reaction. Flavin hydroperoxide functions as an electrophile mediating the hydroxylation of the para position of **80** in the pentachlorophenol dehalogenase-catalyzed reaction[59-61] (panel B). Loss of chloride completes the reaction. The HCB dehalogenase-catalyzed reaction combines features of these two reactions in a novel way using flavin hydroperoxide to form a Meisenheimer complex and forming flavin- N5-oxide as a new intermediate in enzymatic dehalogenation reactions.

The identification of HcbA1 as a flavin-N5-oxide-utilizing enzyme further validates the proposal that flavin-N5-oxides are likely intermediates in flavoenzymes that form substrate hydroperoxides in the absence of an active site cysteine (Figure 4.1A). This model is consistent with three of the four known flavin- N5-oxide-utilizing enzymes. It does not include EncM, and the full scope of nature's use of this new flavin oxidation state has not yet been uncovered.

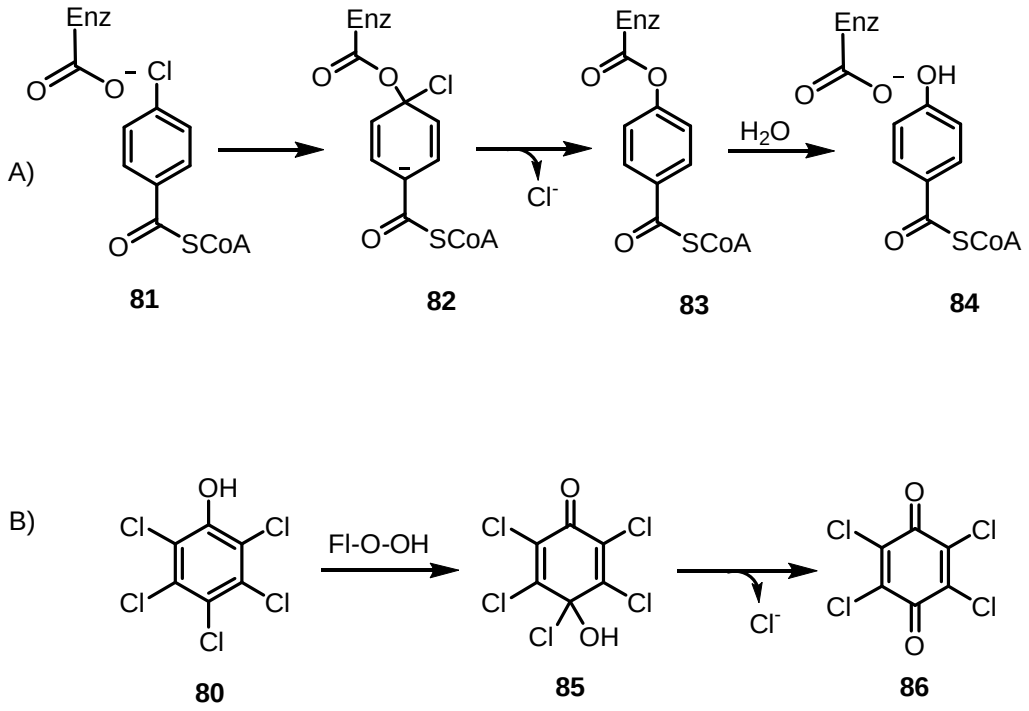

Figure 4.6: Relevant halobenzene dehalogenation reactions. (A) The 4-chlorobenzoyl-CoA dehalogenase-catalyzed reaction that proceeds via a Meisenheimer intermediate. (B) The PcpB-catalyzed conversion of pentachlorophenol to tetrachlorobenzoquinone.

4.4 Experimental Procedure

Materials

All chemicals were purchased from Sigma-Aldrich unless mentioned otherwise. LB broth (Lennox) was purchased from EMD Millipore. Kanamycin and IPTG were obtained from Lab Scientific Inc. Potassium phosphate salt was purchased from VWR. H218O was purchased from Cambridge Isotope Laboratories Inc. Ultra centrifugal filters (10,000 MWCO) were obtained from Millipore and Pall Life Sciences. Sterile syringe filters were obtained from VWR. Histrap column was obtained from GE Healthcare. Econo-Pack 10DG desalting columns were purchased from Bio-Rad. HPLC and LC-MS solvents were purchased from EMD and were used without further purification. ZORBAX Eclipse XDB-C18 column (15 cm x 4.6 mm, 5 μm particles) was purchased from Agilent Technologies. LC-18-T column (15 cm x 3 mm, 3 μm particles, Supelco) was obtained from Sigma.

Over-expression and purification of HcbA1

The HcbA1 gene containing overexpression plasmid (pTHT-HcbA1) was transformed into *Escherichia coli* BL21 (DE3). For the overexpression of the protein, a starter culture was grown overnight in 15 ml of LB medium containing 40 μg/ml of kanamycin at 37 °C. 1.5 liter of LB medium (20 g/L) containing 40 μg/ml of kanamycin, was inoculated with this starter culture. The cells were grown at 37 °C with shaking (220 rpm) until the culture reached an OD_{600} of 0.6 (3-3.5 hr). The culture was then incubated at 4°C for ~45min without shaking. Then the culture was induced by adding IPTG to a final concentration of 0.5 mM and the cells were grown with shaking (180 rpm) for a further 15 hours at 15 °C.

The cells were then harvested by centrifugation at 9000 rpm for 10 min at 4 °C and stored at -80 ˚C until protein purification.

For all the steps during the protein purification, the temperature was maintained at 4 ºC. At first, the cell pellet was re-suspended in 30 ml of lysis buffer (50 mM KH_2PO_4, 150 mM NaCl, 10 mM imidazole, pH 8.0). Lysozyme (5 mg) was added and the cells were lysed by sonication on ice (Misonix Sonicator 3000, each cycle takes 30 s, pulse 'on' time 1.0 s, pulse 'off' time 1.0 s, output level 0.8). The resulting suspension was centrifuged (18,000 rpm, 30 min) and the supernatant was filtered through a sterile syringe filter (pore size 0.45 μm). The clarified supernatant was loaded onto a 5 mL Ni-NTA-affinity column pre-equilibrated with lysis buffer at 1ml/min flow rate. The Ni-NTA-affinity column was then washed with 50 ml wash buffer (50 mM KH_2PO_4, 150 mM NaCl, 20 mM imidazole, pH 8.0) at 2ml/min flow rate. The protein was eluted from the column with elution buffer (50 mM KH_2PO_4, 150 mM NaCl, 200 mM imidazole, pH 8.0) at 1ml/min flow rate. The fractions containing protein were collected and concentrated using an Amicon ultracentrifugal filter (10,000 MWCO) at 5000 rpm to a final volume of 3 mL. The concentrated sample was buffer exchanged into 100 mM phosphate buffer at pH 7.5 containing 100 mM NaCl, 1mM TCEP and glycerol to a final concentration of 15% (using an Econo-Pac 10DG desalting column). A typical yield was 10 mg/liter.

HPLC parameters

An Agilent 1260 HPLC equipped with a quaternary pump was used. The system included a diode array UV-Vis detector and products were detected using absorbance at 220 nm. Analysis was performed on a ZORBAX Eclipse XDB-C18 column (15 cm x 4.6 mm, 5 μm particles, Agilent Technologies). Data were processed using Agilent ChemStation ver. B.04.03.

HPLC conditions for the analysis of the HcbA1 reaction mixture

A-Water with 0.1% formic acid, pH 2.65

B-Acetonitrile

HPLC method (flow rate 1 mL/min):

0 min-10% A 90% B, 30 min- 10% A 90%

LC-MS parameters

LC-ESI-TOF-MS was performed using an Agilent 1260 HPLC system which is equipped with a binary pump and a 1200 series diode array detector followed by a MicroToF-Q II mass spectrometer (Bruker Daltonics) using an ESI source either in negative mode or positive mode. Analysis was performed either on a ZORBAX Eclipse XDB-C18 column (15 cm x 4.6 mm, 5 μm particles, Agilent Technologies) or LC-18-T column (15 cm x 3 mm, 3 μm particles, Supelco). Data were processed with DataAnalysis ver. 4.0 (Bruker Daltonics).

LC conditions for the detection of PCP

A-Water with 0.1% formic acid, pH 2.65

B-Acetonitrile

LC method for the detection of PCP (negative mode on MS):

0 min-10% A 90% B, 30 min- 10% A 90%

LC conditions for the detection of flavin-N5-oxide:

A-5 mM Ammonium acetate buffer, pH 6.6

B-75% Methanol and 25 % Water.

LC method for the detection of flavin-N5-oxide (positive mode on MS):

0 min-100% A, 2 min-100% A, 12 min-30% A 70% B, 17 min-30% A 70% B, 18 min-100% A, 30 min-100%A

The mass spectrometer parameters: Capillary, 4500 V; end plate offset, 500V; nebulizer gas, 3.0 bar; Dry gas, 10.0 L/min; dry gas temperature, 200°C; funnel 1 RF, 200.0 Vpp; funnel 2 RF, 200.0 Vpp; ISCID, 0.0 eV; hexapole RF, 100 Vpp; quadrupole, Ion energy, 3.0 eV; low mass, 100 m/z; collision cell, collision energy, 8.0 eV; collision RF, 150.0 Vpp; transfer time, 80.0 μs; prepulse storage, 5.0 μs.

In vitro activity of HcbA1

Since HCB is insoluble in water, a 10mM stock solution of HCB in acetone was made. When 10 μL of this solution was added to the reaction buffer (final volume 200 μL), no visible precipitation was observed. We followed this solubilization procedure in all the HcbA1 catalyzed reactions discussed here.

The HcbA1 catalyzed reaction was performed in 100 mM phosphate buffer, pH 7.5. The final concentrations of all the reaction components were as follows: HcbA1 (50 μM), HCB (500 μM), FMN (20 μM), *E. coli* Fre (400 nM) and NADH (1 mM). The volume of the

reaction mixture was 200 µL and incubated at RT for 3 hr. The protein was heat-denatured and removed by centrifugal ultrafiltration through a 10 kDa MWCO membrane (Pall Life Sciences). The samples were analyzed by HPLC and LC-MS.

HcbA1-catalyzed reaction in the presence of $H_2{}^{18}O$

Two identical reactions were set up; each 200 µL solution contained 500 µM HCB, 50 µM HcbA1, 20 µM FMN, 400 nM Fre and 1mM NADH. One of the samples had a final concentration of 80% $H_2{}^{18}O$. The other sample was used as a 'control' and contained 100% $H_2{}^{16}O$. The reaction mixture was incubated at room temperature for 3 hours after which both the samples were analyzed by LC-MS.

HcbA1-catalyzed reaction in the presence of $^{18}O_2$

Two identical reaction mixtures were made in a glove box; each 200 µL solution contained 500 µM HCB, 50 µM HcbA1, 20 µM FMN, 400 nM Fre and 1mM NADH. One of the reaction mixtures was exposed to $^{18}O_2$ while the other reaction mixture was used as a 'control' and exposed to $^{16}O_2$. The reaction mixture was incubated at room temperature for 3 hours and then analyzed by LC-MS.

HcbA1-catalyzed reaction using photoreduced FMN

FMN (500 µM) was reduced by irradiating (A21 LED white light bulb, 100-W) for 5 min under anaerobic conditions in a glove box in the presence of EDTA (10 mM) as the reducing agent. Photoreduction of FMN can be observed visually by monitoring the change in color from intense yellow to pale yellow. Stoichiometric amounts of HCB (100 µM) and HcbA1 (100 µM) were added to a solution containing photo-reduced FMN (100 µM). The resulting mixture was incubated in the glove-box for 0.5 hr. and then exposed

to oxygen for an additional 1 hr at 25 ˚C. The protein was heat-denatured and removed by centrifugal ultrafiltration through a 10 kDa MWCO membrane (Pall Life Sciences). The samples were analyzed by LC-MS.

HcbA1 reaction in the presence of $^{18}O_2$ using photoreduced FMN

FMN was photo-reduced in a glove-box using EDTA as described above. Then stoichiometric amounts of substrate and enzyme were added. Final concentrations of reduced FMN, HCB and HcbA1 were 100 μM each. The resulting mixture was incubated in a glove-box for 0.5 hr, exposed to $^{18}O_2$ and incubated for an additional 1 hr at 25 ˚C. The protein was heat-denatured and the resulting solution was filtered using an ultra-centrifugal filter (10kda cut-off). Finally, the samples were analyzed by LC-MS.

CHAPTER V

RECONSTITUTION AND MECHANISTIC STUDIES ON THE BACTERIAL FOLATE CATABOLIC PATHWAY

5.1 Introduction

In contrary to our understanding of cofactor biosynthesis, little is known about their catabolic pathways. So far, the best-studied cofactor catabolic pathways are that of pyridoxal[14] and NAD[62]. Although there are several reports of catabolism of the rest of the cofactors, detailed understanding at the molecular level is still in its infancy. Since there are many diseases associated with cofactor depletion, elucidating the mechanism of cofactor catabolism is critical for understanding the relationship between cofactor metabolism and cofactor deficient diseases.

Folic acid (**30**) is an important cofactor which plays a key role in nucleic acid biosynthesis. It is made of 2-amino-4-hydroxypteridine moiety linked through a methylene carbon to p-amino-benzoylglutamate. It is the reduced tetrahydrofolates (THF)

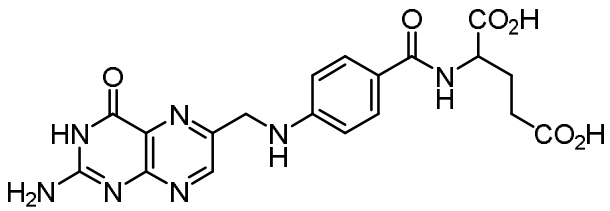

30

Figure 5.1: Structure of folic acid; consisting of pterin moiety and p-aminobenzoylglutamate

that actually serve as the cofactor. THF cofactors carry one-carbon units at three different oxidation states; from formate to methanol.[63]

Unlike most bacteria and yeast, mammals cannot synthesize folates de novo, therefore, folic acid has to be supplied through the diet to meet their daily requirements. Folate deficiency can result in many health problems. Pregnant women with folate deficiency are more likely to give birth to premature infants, and infants with neural tube defects.[64] Therefore, it is important to study folate catabolism at the molecular level. There are several literature reports describing the cleavage of amide bond by carboxypeptidases[65, 66] to give pteroic acid and glutamate. However, not much is known about how the pterin ring is further cleaved. While going through the literature, we came across a deaminase in *Agrobacterium radiobacter* identified by the Raushel group that can deaminate several 6-substituted pterins.[67] Analysis of the genomic context of the deaminase (Figure 5.2 and 5.3) revealed that there are putative flavin oxygenase, flavin reductase, and amidohydrolase encoding genes conserved across several organisms. We envisaged that along with deaminase, the rest the protein encoding genes in the operon will constitute a pterin catabolic pathway.

Figure 5.2: Genome neighborhood of the deaminase in Agrobacterium radiobacter

Gene ID	Annotated Function
Arad_3523	Amidohydrolase
Arad_3524	Transcriptional regulator
Arad_3525	ABC transporter
Arad_3527	ABC transporter
Arad_3528	ABC transporter
Arad_3529	Pterin deaminase
Arad_3530	Flavin oxygenase
Arad_3531	Flavin reductase

Figure 5.3: Proposed function of the gene products present in the cluster.

Initially, we came up with two proposals (Figure 4). According to the first proposal (Path A), flavin oxygenase catalyzes the oxidative cleavage of the amide bond of pyrimidine moiety of lumazine to give compound **89** which will be hydrolyzed by amidohydrolase to give compound **90**. There is a literature precedence of flavoenzyme mediated oxidative amide bond cleavage in RutA catalyzed reaction during the degradation of uracil.[31] Second proposal (Path B) involves the addition of flavin-C4a-peroxide at C4 followed by a Baeyer-Villiger type rearrangement to give **91** which upon amide hydrolysis will give compound **92**. Baeyer-Villiger rearrangement on pyrimidine moiety was previously observed in TflA catalyzed toxoflavin degradation reaction.[22] Although TflA does not contain flavin (instead contains Mn); flavoenzyme mediated Baeyer-Villiger rearrangement is well documented in the literature.

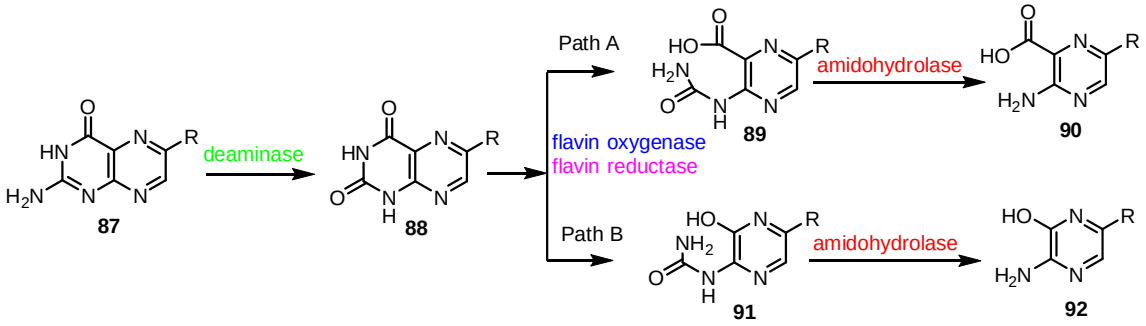

Figure 5.4: Initial working hypothesis for the bacterial pterin catabolic pathway

5.2: Results and discussion

5.2.1 Overexpression and purification of putative flavin oxygenase and amidohydrolase

In order to validate their roles, the putative flavin oxygenase and amidohydrolase from *Mesorhizobium loti* were heterologously expressed in *E. coli* BL21(DE3) and the N-terminally His6-tagged proteins were purified using a Ni-NTA column (Figure 5.5A). Purified putative flavin oxygenase protein was yellow and the UV-visible spectrum of the protein had maxima at 457 nm, 380 nm, and 280 nm, thereby, giving hints for enzyme bound flavin cofactor (Figure 5.5 B). This was confirmed by HPLC analysis of the heat-denatured protein and the flavin identified as the FAD (Figure 5.5C).

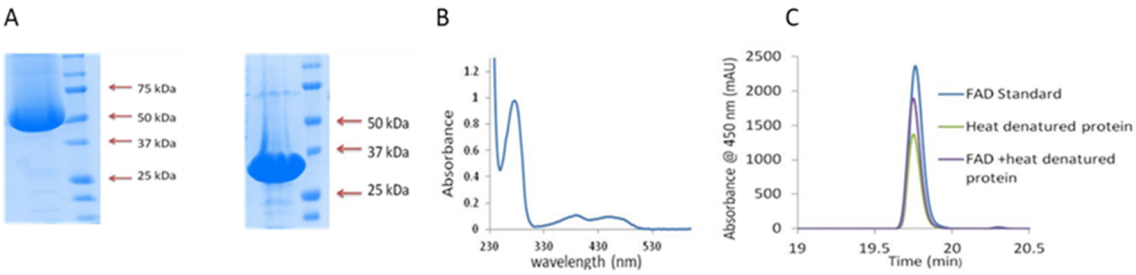

Figure 5.5: A) SDS-PAGE of the purified flavin oxygenase and amidohydrolase. The molecular weights are 51 kDa and 30 kDa respectively. B) UV-Visible spectrum of the

flavin oxygenase. C) HPLC chromatogram shows the flavin oxygenase contains a FAD cofactor.

5.2.2 Enzymatic activity of the putative flavin oxygenase

Having the purified flavin oxygenase in hand, we investigated its catalytic activity towards lumazine (**93**). Treatment of lumazine with the flavin oxygenase in the presence of NADH, *E. coli* Flavin reductase (Fre) and FAD resulted in the consumption of lumazine and formation of a new peak on the HPLC chromatogram (Figure 5.6A and 5.6B). However, characterization of this new product turned out to be difficult due to its instability.

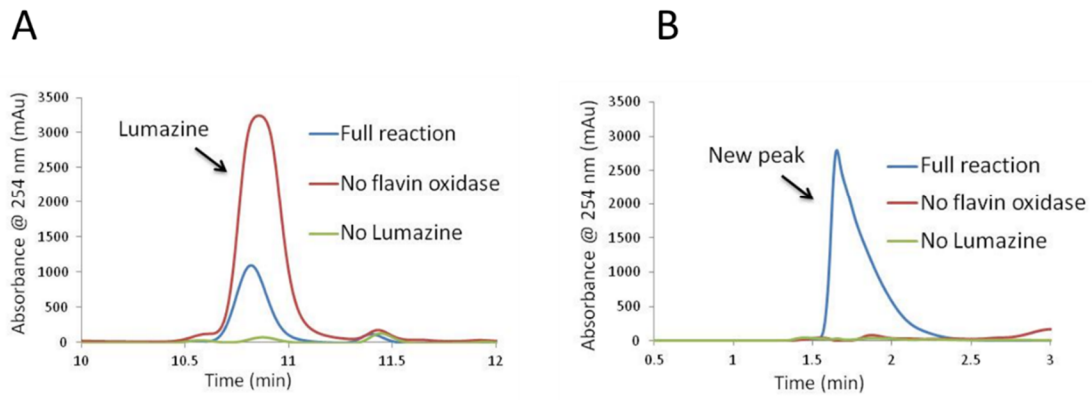

Figure 5.6: HPLC analysis of the flavin oxygenase catalyzed reaction A) HPLC chromatogram showing consumption of Lumazine in the full reaction. B) HPLC chromatogram showing formation of new peak at 2 min.

5.2.3 Enzymatic activity of the putative amidohydrolase

To check the activity of the putative amidohydrolase we carried out a sequential assay where we added the putative amidohydrolase after the flavin oxygenase catalyzed reaction. Under this condition we observed complete consumption of the product of the flavin oxygenase catalyzed reaction; suggesting that it is a substrate for the

amidohydrolase. The product of the amidohydrolase catalyzed reaction was characterized as xanthine based on LC-MS analysis and coelution experiment (Figure 5.7).

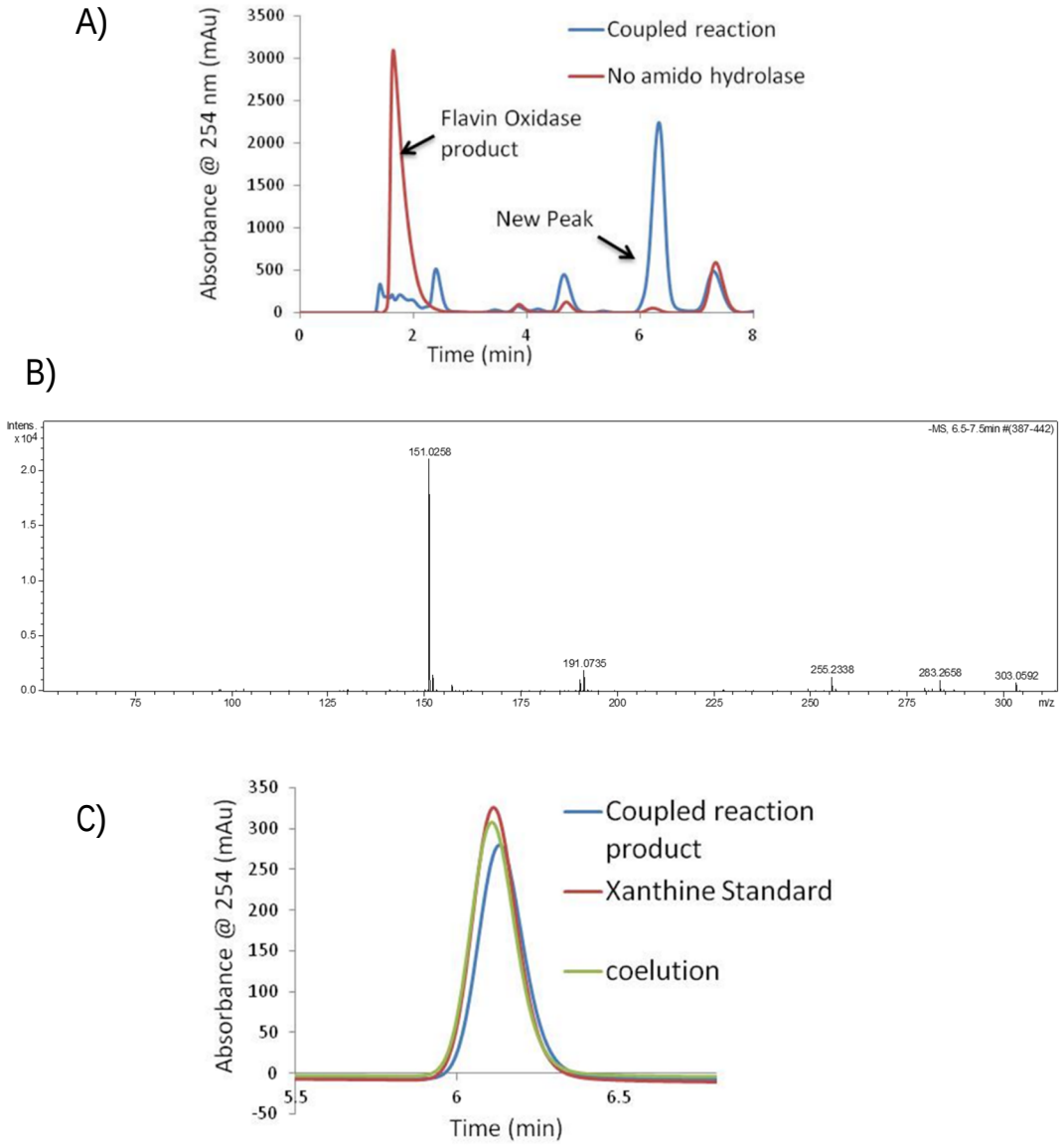

Figure 5.7: Characterization of amidohydrolase catalyzed reaction product A) Consumption of flavin oxygenase reaction product and formation of a new peak in the coupled reaction. B) Mass of the new product C) Coelution of coupled reaction product with xanthine stan

5.2.4 Mechanistic proposal for pyrazine ring contraction

Xanthine being identified as the final product; we came up with a mechanistic proposal for the formation of xanthine (Figure 5.8). According to this proposal, reduced flavin, at first, reacts with molecular oxygen to form flavin-C4a-peroxide which then attacks at C7 of lumazine to give intermediate **94**. Then a Baeyer-Villiger type rearrangement will lead to the oxadiazepine intermediate **95**. Addition of water followed by C-O bond cleavage gives compound **97**. Then the amidohydrolase cleaves the amide bond to give **98** with the release of formate. Cyclization followed the loss of water will give rise to xanthine **100** as the final product.

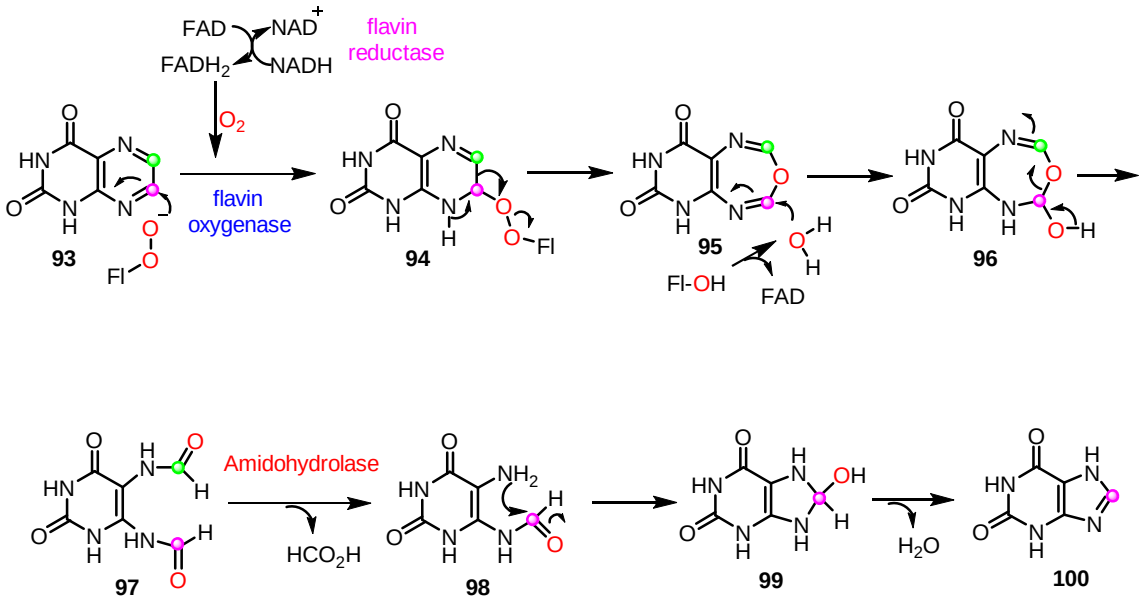

Figure 5.8: Mechanistic proposal for the flavin oxygenase and the amidohydrolase catalyzed reaction.

5.2.5 LC-MS analysis of the flavin oxygenase catalyzed reaction

According to our mechanistic proposal, compound **97** is the product of the flavin oxygenase catalyzed reaction. Indeed, LC-MS analysis of the flavin oxygenase catalyzed reaction showed the presence of the mass corresponding to compound **97** only in the full reaction and absent in other controls (Figure 5.9).

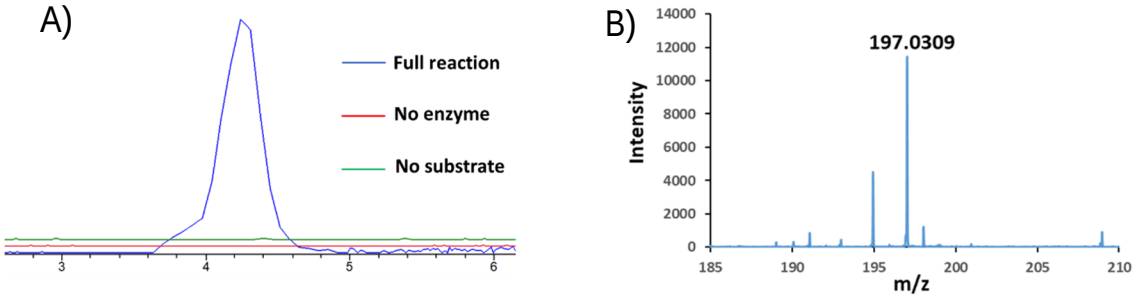

Figure 5.9: LC-MS analysis of the flavin oxygenase catalyzed reaction A) Extracted ion chromatogram at m/z = 197.0316, corresponding to $[M-H]^-$ for compound **97** B) Exact mass of the product of the flavin oxygenase catalyzed reaction matches with mass of compound **97**

5.2.6 Substrate scope of the flavin oxygenase catalyzed reaction

Several 6-substituted lumazines were tested as possible substrates for the flavin oxygenase and the amidohydrolase catalyzed coupled reaction and in all the cases xanthine was identified as the final product. However; none of the pterins tested are substrates for flavin oxygenase, implying the probable role of the oxygen atom at C2 in the binding of the substrate. Also, two substituents (methyl and hydroxy) at C-7 position tested are not accepted by the flavin oxygenase probably due to steric effect (Figure 5.10).

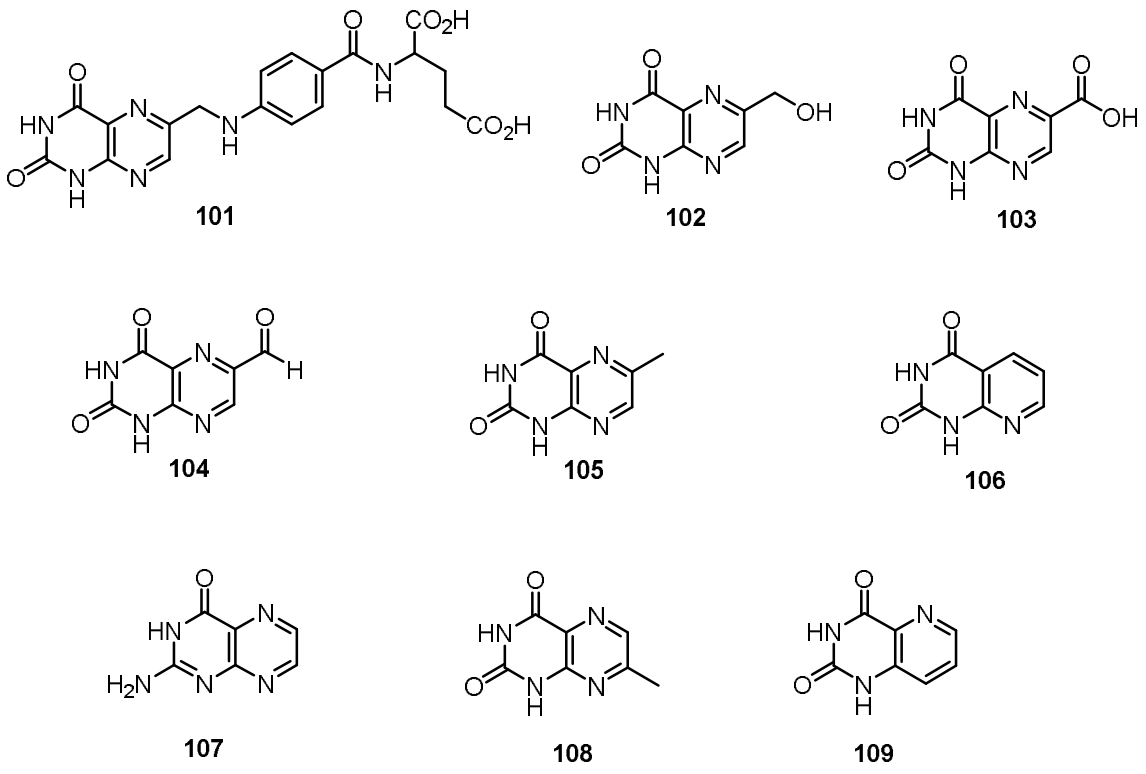

Figure 5.10: List of Substrates tested for flavin oxygenase catalyzed reaction.

5.2.7 Labeling experiment

Next, we carried out labeling experiments to provide evidence for our mechanistic proposal. The flavin oxygenase catalyzed reaction was carried out both in the presence of O-18 labeled water and O-18 labeled molecular oxygen. No O-18 label was incorporated into the product when the reaction was done in the presence of O-18 labeled water (Figure 5.11A). However, a 4 da increase in the mass of product was observed when the reaction was carried out in the presence of O-18 labeled molecular oxygen (Figure 5.11B). To account for the two oxygen atoms incorporation from the molecular oxygen we came up with the following rationale. We propose that the water molecule which adds to the

oxadiazepine intermediate **95** is derived from flavin hydroxide and is nonexchangeable. If this is the case, then, the two oxygen atoms have to be from a single oxygen molecule. To test this proposal, flavin oxygenase catalyzed reaction was carried out in the presence of O-16 and O-18 labeled oxygen gas mixture. Under this condition we only observe the masses corresponding to 197 and 201, implying that both the oxygen atoms are from a single oxygen molecule (Figure 5.11C). To the best of our knowledge, this is the first example of a flavin dependent oxygenase where both the oxygen atoms of molecular oxygen incorporated into the single product.

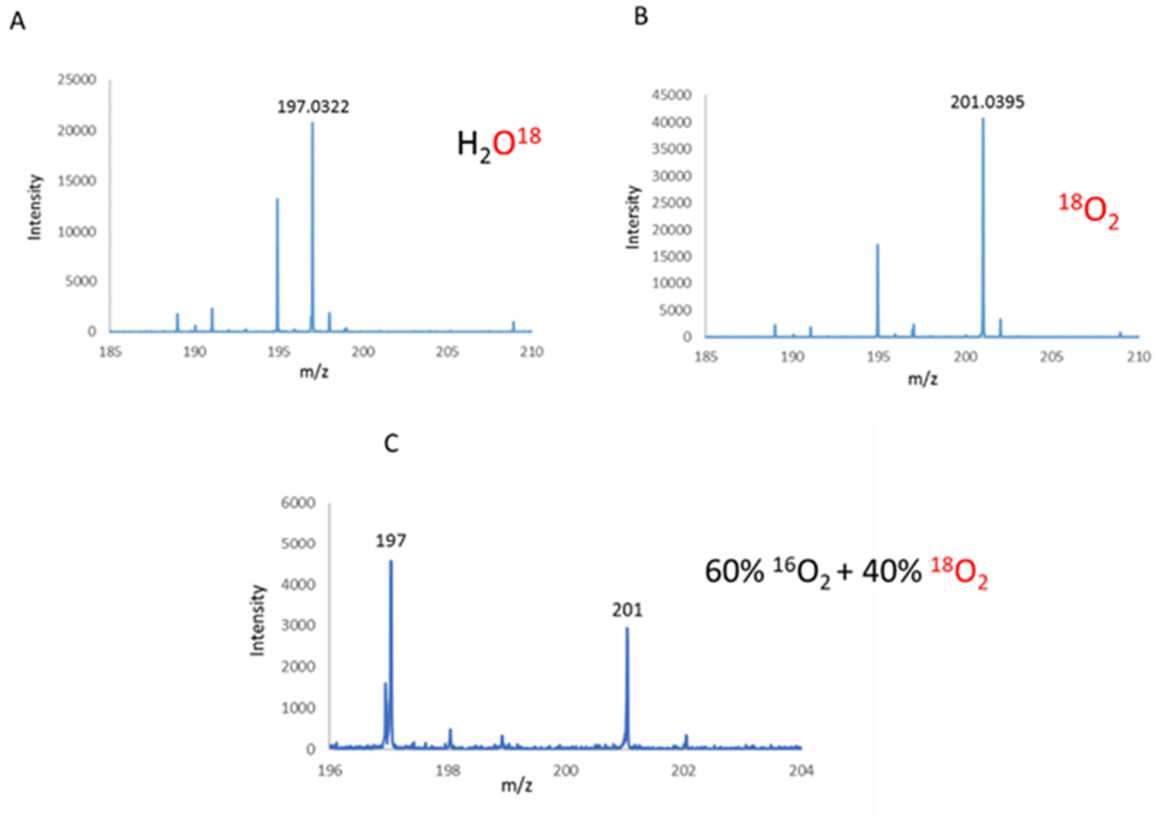

Figure 5.11: LC-MS analysis of the flavin oxygenase catalyzed reaction run in the presence of [18O]- H_2O or $^{18}O_2$ or $^{18}O_2$+$^{16}O_2$. Panel A shows that oxygen from the buffer is not incorporated into the reaction product. Panel B shows the incorporation of two

oxygen atoms from molecular oxygen into the reaction product. Panel C shows the masses 197 and 201 were obtained when the reaction was carried out in the presence of $^{18}O_2$+$^{16}O_2$.

5.2.8 Formate detection

According to our mechanistic proposal, formate is produced during the amidohydrolase catalyzed reaction. To confirm that, formate was trapped using nitrophenyl hydrazine[68] and mass of the corresponding adduct was observed after LC-MS analysis (Figure 5.12).

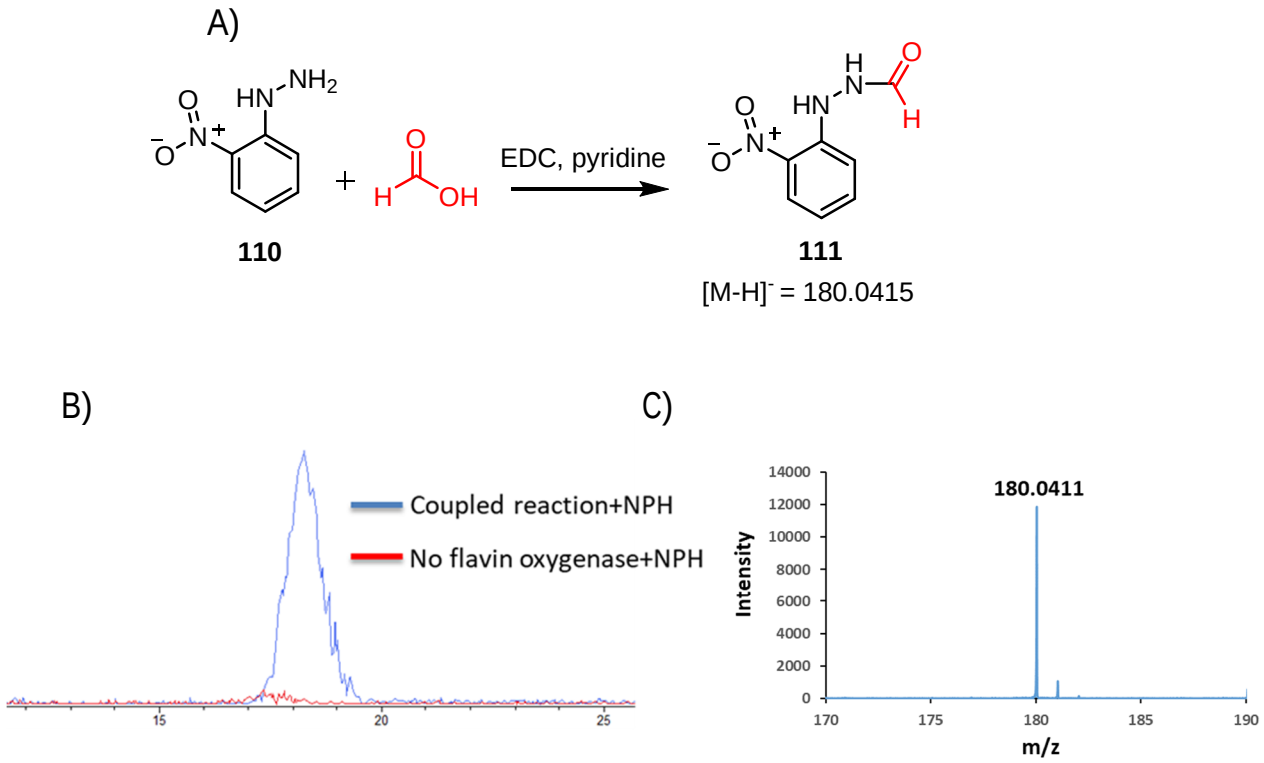

Figure 5.12: Characterization of formate byproduct A) The reaction used to trap formate using nitrophenylhydrazine **110** B) Extracted ion chromatogram at m/z = 180.0415, corresponding to $[M-H]^-$ for the adduct **111** C) Exact mass obtained for the adduct **111**

5.2.9 Non-enzymatic cyclization and dehydration steps

Next, we asked the question whether the late stage cyclization and dehydration steps are non-enzymatic in nature. The easiest way to test this proposal would be to synthesize compound **98** and check its stability in aqueous buffer. However, synthesis of compound **98** turned out to be difficult. So, we took an indirect approach. We designed 6-hydroxy lumazine **112** as a substrate analog to answer this question. If 6-hydroxy lumazine undergoes a similar enzymatic transformation, it will form the carbamic acid **116** as a product of the flavin oxygenase catalyzed reaction (Figure 5.13). The resulting carbamic acid will readily decarboxylate to form compound **117**. Thus, if the cyclization and dehydration steps are non-enzymatic, we expect xanthine to be the final product from 6-hydroxy lumazine. When flavin oxygenase catalyzed reaction was performed using 6-hydroxy lumazine, we indeed observed xanthine formation, thereby, confirming the non-enzymatic nature of the cyclization and dehydration steps. However, at this point, we cannot rule out the possibility of rate enhancement in the enzyme catalyzed reaction.

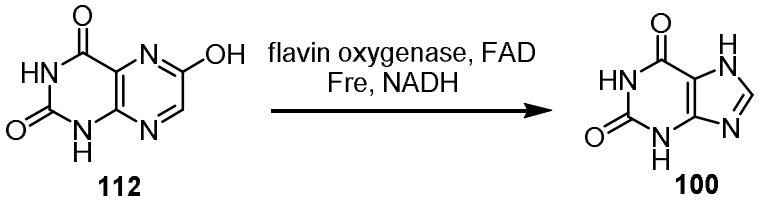

112 **100**

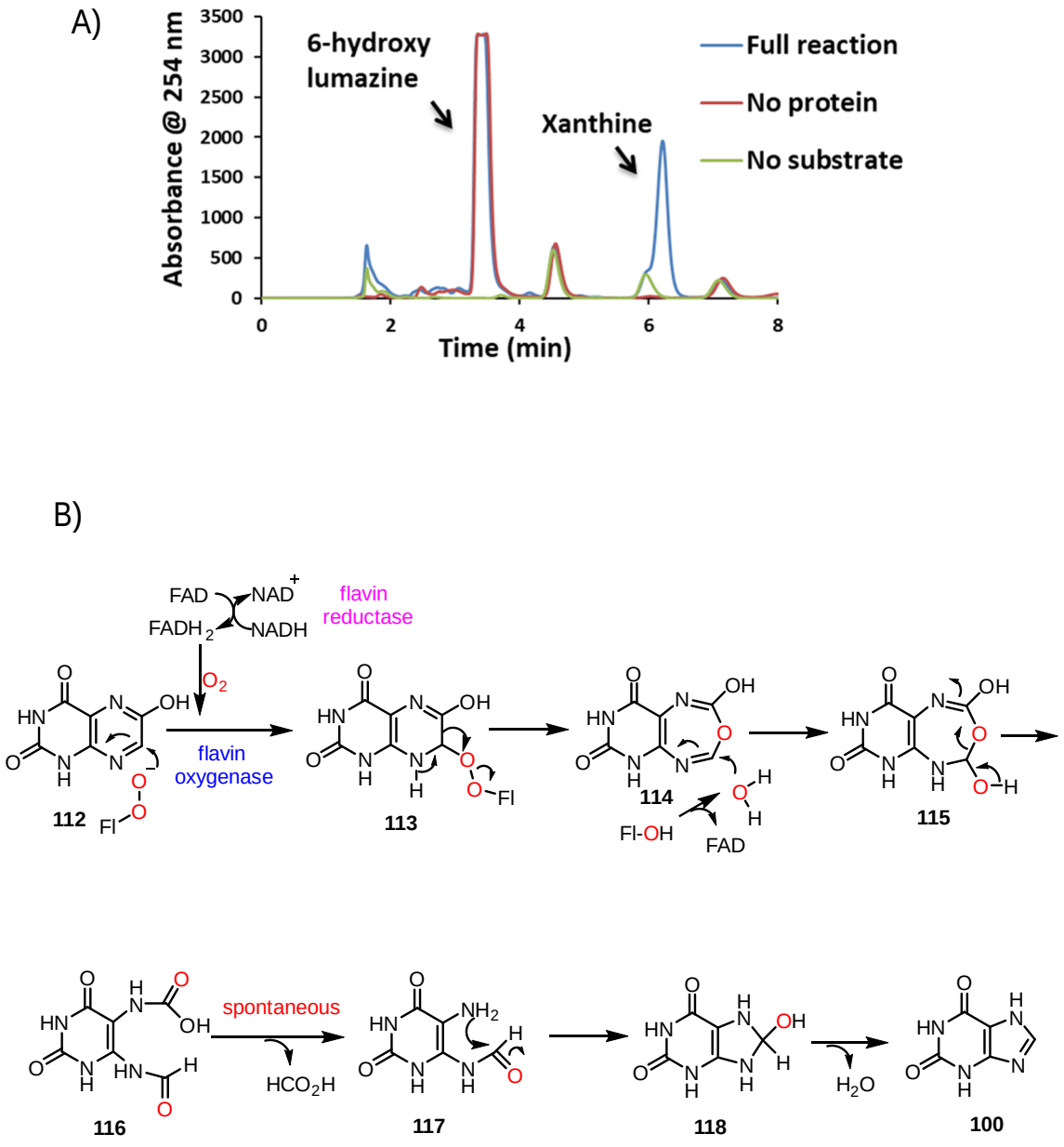

Figure 5.13: Flavin oxygenase catalyzed reaction with 6-hydroxy lumazine. A) HPLC analysis of the reaction mixture B) Mechanistic rationale for the production of xanthine

5.2.10 Amidohydrolase catalyzed reaction is metal dependent

ICP-MS analysis revealed zinc to be the bound metal in the amidohydrolase. Since the purified enzyme contained sub stoichiometric amount of bound metal, addition of external zinc increased the activity. Amongst the other first-row transition metals that have been tested for activity, cobalt also turned out to be an active one (Figure 5.14A). Amidohydrolase activity was inhibited in the presence of the chelating agent hydroxyquinoline sulfonic acid; the activity can be restored by adding external zinc (Figure 5.14B).

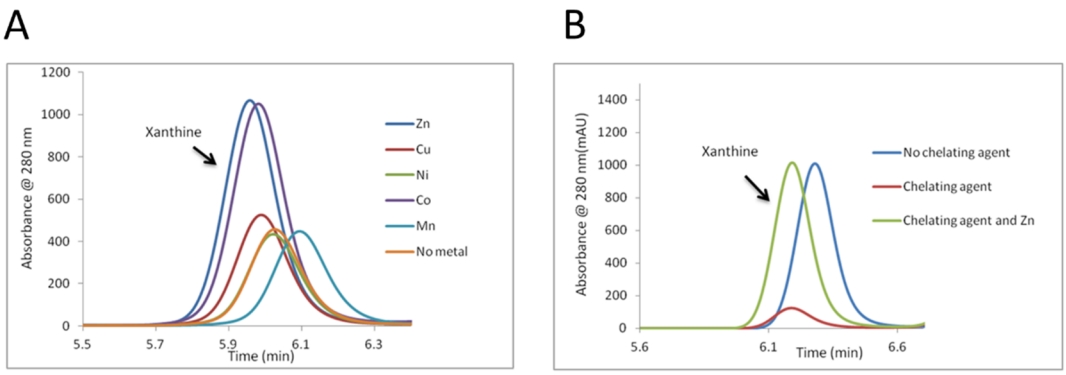

Figure 5.14: Amidohydrolase is metal dependent. A) HPLC chromatogram showing xanthine formation in the presence of different first row transition metals. B) HPLC chromatogram showing Inhibition of amidohydrolase activity in the presence of chelating agent hydroxyquinoline sulfonic acid.

5.2.11 X-ray crystal structure of the flavin oxygenase

In order to get further insights into the flavin oxygenase catalyzed reaction, we set out to obtain X-ray crystal structure of the flavin oxygenase. Despite the screening of large number of crystallizations conditions, we could not get the crystal of flavin oxygenase from *Mesorhizobium loti*. To get around of this problem we turned our attention to the orthologs of flavin oxygenase. The criterion for the selection of the orthologs were high sequence identity (>50%) and the presence of neighboring genes in the cluster. We overexpressed and purified the orthologs of flavin oxygenase from three different strains; 1) *Hoeflea phototrophica* 2) *Agrobacterium radiobacter* 3) *Dinoroseobacter shibae* (Figure 5.15). Activities of the three orthologs were confirmed by HPLC analysis.

A)

Organism	Query cover	Identity
Hoeflea phototrophica	99%	74%
Agrobacterium radiobacter	99%	66%
Dinoroseobacter shibae	95%	57%

B)

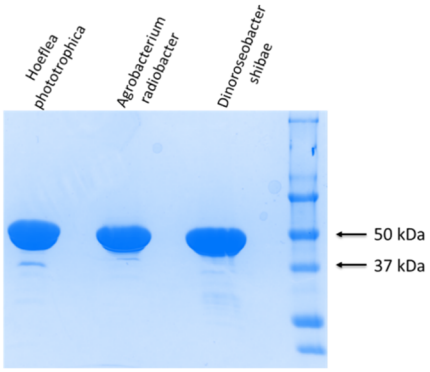

Figure 5.15: Purification of flavin oxygenase orthologs from *Hoeflea phototrophica*, *Agrobacterium radiobacter* and *Dinoroseobacter shibae.* A) Sequence identity of the orthologs compared with the *Mesorhizobium loti*. B) SDS-PAGE of the purified proteins.

After screening the three orthologs using commercially available crystallization solutions we could only get crystal of *Hoeflea phototrophica* ortholog in single condition and the corresponding diffraction data was collected (Figure 5.16). However, we could not solve the phase using molecular replacement method because of the unavailability of known structure of the protein with high sequence similarity to flavin oxygenase. To solve the phase problem, we decided to get the crystal of selenomethionine labeled protein. Using known procedure selenomethionine labeled protein was produced and verified by mass.

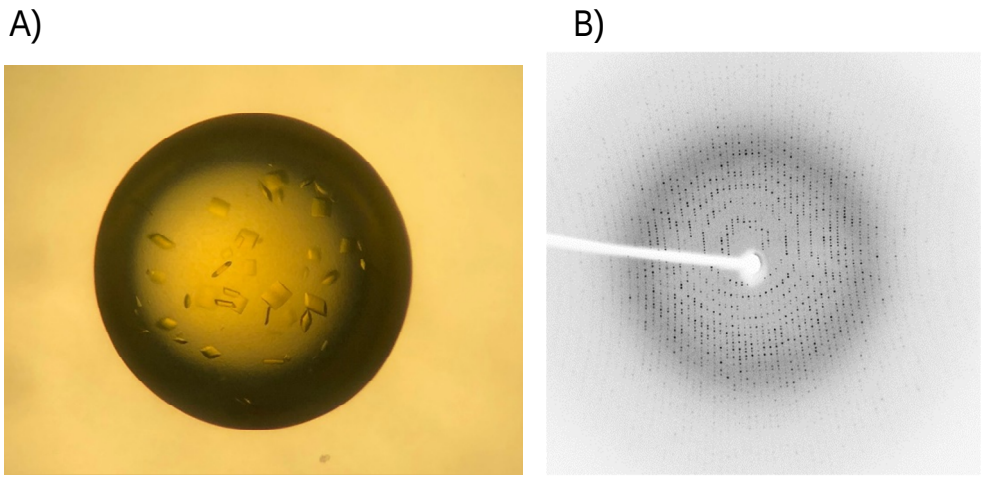

Figure 5.16: A) Crystal of Flavin oxygenase from *Hoeflea phototrophica* A) Diffraction data of the crystal

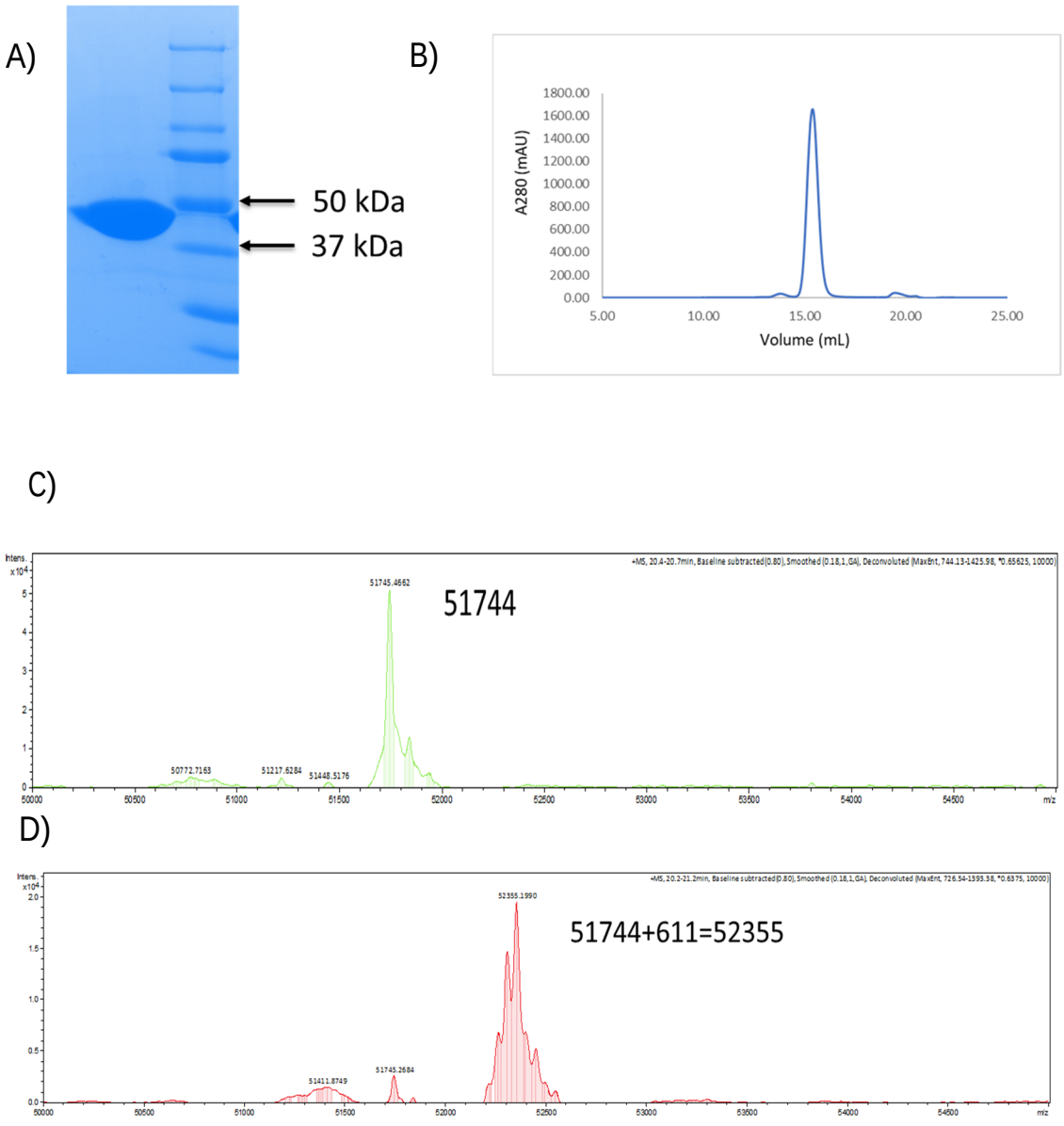

Figure 5.17: Production of selenomethionine labeled flavin oxygenase A) SDS-PAGE of the selenomethionine labeled protein B) Gel-filtration chromatogram of the purified protein C) Mass of the native protein D) Mass of the selenomethionine labeled protein

	Protein+FAD	Protein +FAD+lumazine
Data Collection		
Space group	P 21 21 21	P 21 21 21
Cell dimensions a, b, c (Å)	61.67 125.21 127.33	61.56 125.38 127.31
α, β, γ (º)	90, 90, 90	90, 90, 90
Resolution (Å)	62.6 - 1.35	61.56-1.77
R_{merge}	0.063 (0.637)*	0.190 (0.993)
$I/\sigma I$	14.1 (2.9)	6.1 (1.4)
Completeness (%)	99.6 (99.4)	94.8 (78.2)
Redundancy	6.7 (6.5)	6.4 (5.0)
Refinement		
Resolution (Å)	1.45	1.77
No. reflections	173850	90413
R_{work}/R_{free}	0.157/0.176	0.164/.197
Average B-factor	22.61	25.08
R.m.s deviations		
Bond length (Å)	0.008	0.008
Bond angles (º)	0.998	0.941

*Values presented in parentheses are for highest-resolution shell.

Figure 5.18: Data collection and refinement statistics for the flavin oxygenase.

Crystal of the selenomethionine labeled protein could be obtained using the same crystallization condition as that for native protein. With the diffraction data of the selenocysteine labelled protein we could solve the structure by SAD. The high-resolution crystal structure of the flavin oxygenase (1.45 Å) was obtained with FAD bound in it.

Surprisingly, the three-dimensional structure of the flavin oxygenase does not resemble to any known two component flavin oxygenase; instead, the structure shows similarity to D-lactate dehydrogenase (rmsd 2.9 and Z score 26.4), Alkylhydroxy acetone phosphate synthase (rmsd 3.6 and Z score 24.9), Cytokinin dehydrogenase 1 (rmsd 3.1 and Z score 25.6). To get the substrate bound structure flavin oxygenase was co-crystallized with lumazine and the structure was solved with high resolution (1.7 Å). Active site architecture revealed that the substrate sits on the si face of FAD (Figure 5.19). There is a conserved serine residue (Ser139) interacting with the N5 of the flavin; thereby stabilizing the flavin peroxy species. C7 of the substrate is perfectly positioned for the nucleophilic attack of flavin peroxy. There are extensive H-bonding interactions that hold the substrate in the substrate binding pocket. Backbone amide groups interact with the oxygen atom at C2, N3 and oxygen atom at C4; Asn82 takes part in H-bonding interaction with N1; Gln85 involves in H-bonding interaction with the oxygen atom at C2; Tyr 83 interacts with the N1, N3, and oxygen atom attached to C4 via H bonding; Ser154 participates in H-bonding interaction with the N5 and oxygen atom at C4; Asn 321 probably stabilizes the negative charge on the N8 (after the addition of flavin peroxy at C7).

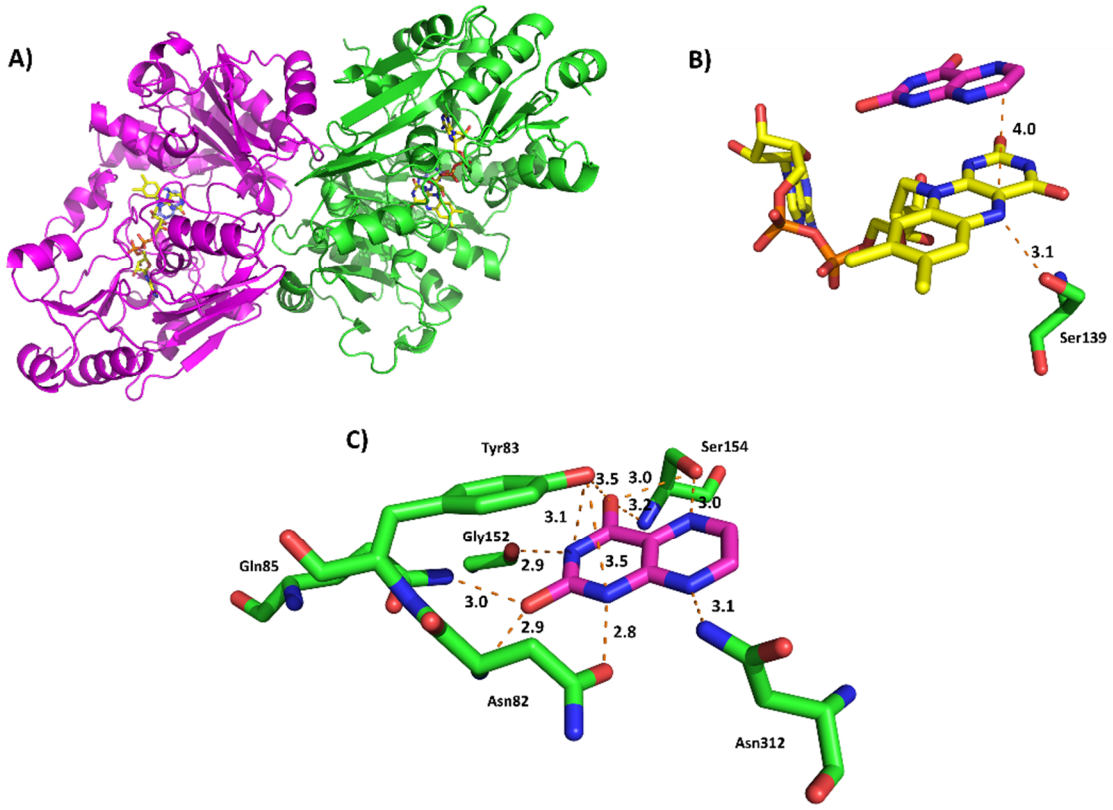

Figure 5.19: Crystal structure of the flavin oxygenase A) Ribbon diagram of the homodimer flavin oxygenase B) Orientation of lumazine, FAD and the Ser139 residue in the active site C) Interaction of the substrate with the active site residues.

5.3 Conclusion

To summarize, for the first time, we have presented detailed biochemical and structural studies on bacterial folate catabolic pathway. In the process, we have identified a novel flavin dependent Baeyer-Villiger type rearrangement which has been utilized to cleave a pyrazine ring. The enzyme is unique in so many ways: generally, Baeyer-Villiger rearrangement occurs via the addition of flavin-C4a-peroxide to a carbonyl center, however, in this case, flavin-C4a-peroxide adds to an imine. Also, as a rare example, the enzyme behaves as a flavin dependent dioxygenase instead of a typical monooxygenase. Structurally the enzyme is more similar to the flavin dependent oxidases while functionally the enzyme belongs to the flavin dependent oxygenase family. Since the gene cluster responsible for the folate catabolism is widespread amongst bacteria, it is important to examine its presence in the human gut microbiome and its connection to diseases like neural tube defects.

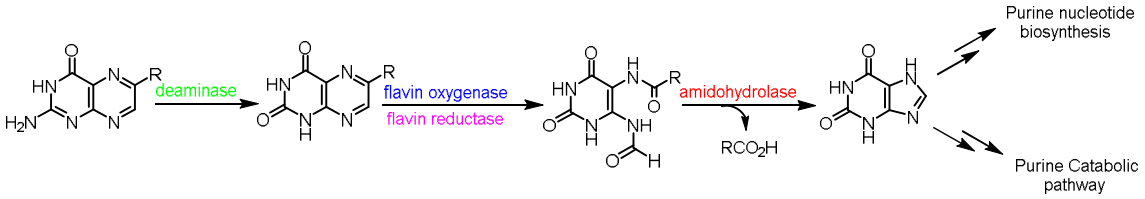

5.4 Experimental Procedure

Materials

All chemicals were purchased from Sigma-Aldrich unless mentioned otherwise. LB broth (Lennox) was purchased from EMD Millipore. Kanamycin and IPTG were obtained from Lab Scientific Inc. Potassium phosphate salt was purchased from VWR. H218O was purchased from Cambridge Isotope Laboratories Inc. Pterin was obtained from Schircks Laboratories. Ultra centrifugal filters (10,000 MWCO) were obtained from Millipore and Pall Life Sciences. Sterile syringe filters were obtained from VWR. Histrap column was obtained from GE Healthcare. Econo-Pack 10DG desalting columns were purchased from Bio-Rad. HPLC and LC-MS solvents were purchased from EMD and were used without further purification. ZORBAX Eclipse XDB-C18 column (15 cm x 4.6 mm, 5 μm particles) was purchased from Agilent Technologies. LC-18-T column (15 cm x 3 mm, 3 μm particles, Supelco) was obtained from Sigma.

Over-expression and purification of flavin oxygenase

The flavin oxygenase gene containing overexpression plasmid (flavin oxygenase gene in pTHT Vector) was transformed into *Escherichia coli* BL21 (DE3). For the overexpression of the protein, a starter culture was grown overnight in 15 ml of LB medium containing 40 μg/ml of kanamycin at 37 °C. 1.5 liter of LB medium (20 g/L) containing 40 μg/ml of kanamycin, was inoculated with this starter culture. The cells were grown at 37 °C with shaking (220 rpm) until the culture reached an OD_{600} of 0.6 (3-3.5 hr). The culture was then incubated at 4°C for ~45min without shaking. Then the culture was induced by adding IPTG to a final concentration of 0.5 mM and the cells were grown with shaking (180 rpm)

for a further 15 hours at 15 °C. The cells were then harvested by centrifugation at 9000 rpm for 10 min at 4 °C and stored at -80 ˚C until protein purification.

For all the steps during the protein purification, the temperature was maintained at 4 ºC. At first, the cell pellet was re-suspended in 30 ml of lysis buffer (50 mM KH_2PO_4, 150 mM NaCl, 10 mM imidazole, pH 8.0). Lysozyme (5 mg) was added and the cells were lysed by sonication on ice (Misonix Sonicator 3000, each cycle takes 30 s, pulse 'on' time 1.0 s, pulse 'off' time 1.0 s, output level 0.8). The resulting suspension was centrifuged (18,000 rpm, 30 min) and the supernatant was filtered through a sterile syringe filter (pore size 0.45 μm). The clarified supernatant was loaded onto a 5 mL Ni-NTA-affinity column pre-equilibrated with lysis buffer at 1ml/min flow rate. The Ni-NTA-affinity column was then washed with 50 ml wash buffer (50 mM KH_2PO_4, 150 mM NaCl, 20 mM imidazole, pH 8.0) at 2ml/min flow rate. The protein was eluted from the column with elution buffer (50 mM KH_2PO_4, 150 mM NaCl, 200 mM imidazole, pH 8.0) at 1ml/min flow rate. The fractions containing protein were collected and concentrated using an Amicon ultracentrifugal filter (10,000 MWCO) at 5000 rpm to a final volume of 3 mL. The concentrated sample was buffer exchanged into 100 mM phosphate buffer at pH 7.5 containing 100 mM NaCl, 1mM TCEP and glycerol to a final concentration of 15% (using an Econo-Pac 10DG desalting column). Flavin Oxygenase orthologs were overexpressed and purified using the same procedure as discussed above.

Over-expression and purification of amidohydrolase

The amidohydrolase encoding gene was cloned into pTHT vector (derivative of pET28b vector with TEV protease cleavage site after the N-terminal His-tag). The plasmid was

transformed into *Escherichia coli* BL21(DE3). Overexpression and purification of the amidohydrolase was same as that of flavin oxygenase.

HPLC parameters

An Agilent 1260 HPLC equipped with a quaternary pump was used. The system included a diode array UV-Vis detector and products were detected using absorbance at 280 nm, and 450 nm. Analysis was performed either on a ZORBAX Eclipse XDB-C18 column (15 cm x 4.6 mm, 5 μm particles, Agilent Technologies) or PFP column (150 x 4.6 mm, 2.6 μm particles, Kinetex).

HPLC conditions (for C18 column):

A-Water

B-100 mM potassium phosphate buffer, pH 6.6

C-Methanol

HPLC method:

0 min-100% B, 5 min- 10% A 90% B, 12 min-48%A 40%B 12% C, 14 min-50%A 30%B 20% C, 18 min-30% A 10% B 60% C, 20 min-100% B, 25 min-100% B

LC-MS parameters

LC-ESI-TOF-MS was performed using an Agilent 1260 HPLC system which is equipped with a binary pump and a 1200 series diode array detector followed by a MicroToF-Q II mass spectrometer (Bruker Daltonics) using an ESI source either in negative mode or positive mode. Analysis was performed on an LC-18-T column (15 cm x 3 mm, 3 μm particles, Supelco).

LC conditions:

A-5 mM Ammonium acetate buffer, pH 6.6

B-75% Methanol and 25 % Water.

LC method: (for positive and negative mode on MS) 0 min-100% A, 2 min-100% A, 12 min-30% A 70% B, 17 min-30% A 70% B, 18 min-100% A, 30 min-100%A

Activity assay of flavin oxygenase catalyzed reaction

The flavin catalyzed reaction was performed in 100 mM phosphate buffer, pH 7.5. The final concentrations of all the reaction components were as follows: flavin oxygenase (50 μM), lumazine (500 μM), FAD (20 μM), *E. coli* Fre (400 nM) and NADH (1 mM). The volume of the reaction mixture was 200 μL and incubated at RT for 3 hr. The protein was heat-denatured and removed by centrifugal ultrafiltration through a 10 kDa MWCO membrane (Pall Life Sciences). The samples were analyzed by HPLC and LC-MS.

Activity assay of amidohydrolase catalyzed reaction

To check the activity of the amidohydrolase catalyzed reaction we carried out a sequential assay. At first, flavin oxygenase catalyzed reaction was run following the protocol mentioned above. Once flavin oxygen catalyzed reaction is over, amidohydrolase was added and incubated for 3 hr. The samples were analyzed by HPLC and LC-MS.

Flavin oxygenase catalyzed reaction in the presence of $H_2{}^{18}O$

Two identical reactions were set up; each 200 μL solution contained 500 μM lumazine, 50 μM flavin oxygenase, 20 μM FAD, 400 nM Fre and 1mM NADH. One of the samples had a final concentration of 80% $H_2{}^{18}O$. The other sample was used as a ‘control’ and contained 100% $H_2{}^{16}O$. The reaction mixture was incubated at room temperature for 4 hours after which both the samples were analyzed by LC-MS.

Flavin oxygenase catalyzed reaction in the presence of $^{18}O_2$

Two identical reaction mixtures were made in a glove box; each 200 μL solution contained 500 μM lumazine, 50 μM flavin oxygenase, 20 μM FAD, 400 nM Fre and 1mM NADH. One of the reaction mixtures was exposed to $^{18}O_2$ while the other reaction mixture was used as a 'control' and exposed to $^{16}O_2$. The reaction mixture was incubated at room temperature for 3 hours and then analyzed by LC-MS.

Protocol for formate detection

Formate was detected following the literature reported procedure. To a 100 L of enzymatic reaction mixture 10 μL of 1:1 solution of pyridine: HCl. EDC (10 μL of a 0.29 M solution) was added. This was followed by addition of NPH (10 μL of a 0.12 mM solution in 250 mM HCl) and the resulting mixture was incubated at 60 C for 15 min. Precipitated protein was pelleted by centrifugation and the clear supernatant was analyzed by LC-MS.

Overexpression and purification of flavin oxygenase orthologs

Flavin oxygenase orthologs from *Hoeflea phototrophica, Agrobacterium radiobacter* and *Dinoroseobacter shibae* were overexpressed and purified following the same protocol as that of the flavin oxygenase from *Mesorhizobium loti*.

Crystallization condition

Crystallization trials were setup using commercially available Hampton research crystallization solution and hanging drop diffusion method. Protein concentration was in the range of 12-13 mg/mL in 10 mM Tris, 20 mM NaCl, pH 7.5. Since sub-stoichiometric amount of FAD copurify with the protein 1 mM of FAD was added to the protein before setting up the crystallization trials. Good quality yellow crystal was obtained within two

days at RT using the following condition: 0.1M TRIS hydrochloride pH 8.5, 2.0M ammonium sulfate. To get the lumazine bound crystal co-crystallization was setup using 1mM lumazine.

Collection of X-ray diffraction data

Crystals were harvested and cryoprotected by removing most of the liquor surrounding the crystal and gradually increasing the glycerol concentration in 5% (vol/vol) increments (30-s soaks) until the final con-centration reached 25% (vol/vol). Crystals were then removed from the mother liquor/cryoprotection mixture using 0.3–0.4-mm loops (Hampton Research) and plunged into liquid nitrogen. All data sets for SeMet was collected at SSRL at 100 K using a wavelength of 0.9776 Å. The selenium peak for the SeMet containing crystals was determined by an X-ray fluorescence scan. Diffraction data were integrated, scaled, and merged using HKL2000. All data sets for the native protein was collected in In-house facility in ILSB, Texas A&M University.

Incorporation of selenomethionine in the flavin oxygenase from Hoeflea phototrophica

Following protocol was used to get selenomethionine labeled protein.

-A 125 mL sterilized flask with 50 mL sterile LB was prepared. Kanamycin was added.

-Single colony of *E. coli* BL21(DE3) which harbor the flavin oxygenase encoding gene was transferred to the media.

-The cell culture was grown at 37 ºC with shaking at 220 rpm for 16-20 hrs.

-50 mL culture was pelleted by centrifugation at 4000g for 10 min at RT.

-The cell pellet was resuspended in 20 mL M9-kanamycin media, then spin down the cells.

-The above step was repeated to remove residual LB.

-The pellet was resuspended in 1L M9-kanamycin media.

-Cells were grown at 37 ºC with shaking until the OD600 0.6-1.0. decrease the temperature to 15 ºC and let equilibrate for 30 min.

-5 mL of Leu/Ile/Val 10mg/mL stock solution and 4 mL of Phe/Lys/Thr 25mg/mL stock solution were added to 1 litre culture.

-Incubation was continued for 30 min at 15 ºC and 220 rpm.

-4 mL of selenomethionine (15mg.mL stock solution) was added.

-400 µL of 1M IPTG solution was added.

-The induced culture was incubated at 15 ºC (220 rpm) for 20hrs.

-Cells were harvested and protein was purified using regular protocol.

CHAPTER VI

RECONSTITUTION AND MECHANISTIC STUDIES ON THE TPDA CATALYZED REACTION IN TETRAMETHYLPYRAZINE DEGRADATION

6.1 Introduction

Tetramethyl pyrazine (TTMP) **119** is a heterocyclic compound which is produced both chemically and biologically. It is the active ingredient in several Chinese medicinal herbs (*Ligusticum wallichii Franch, Ephedrae herba* etc)[69] which have traditionally been used to treat cardiovascular diseases in China. TTMP production has also been reported by the bacterium *Bacillus natto*[70] which ferments soybean to produce 'natto', a favorite food among Japanese people. While several bacteria strains, capable of using various alkyl-substituted pyrazines as a carbon and nitrogen source, have been isolated,[71] the genetics and biochemical details of the degradation pathways remained limited.

In 2013, Rolandas Meskys group identified the TTMP catabolic gene cluster in *Rhodococcus jostii* TMP1[72] (Figure 6.1). Based on experiments with cell-free extracts, it has been suggested that the initial aromatic ring opening of TTMP is catalyzed by TpdA and TpdB in the presence of a flavin reductase. Blast search predicted TpdA to be a flavin-dependent monooxygenase and TpdB to be a protein belonging to NTF2 superfamily. Flavoenzyme mediated pyridine ring cleavage reaction has been reported in MHPCO[73-75] catalyzed reaction during PLP catabolism. In MHPCO catalyzed reaction hydroxy moiety has been proposed to play key role by activating the ring for electrophilic aromatic substitution reaction. However, tetramethyl pyrazine molecule has no such activating

A)

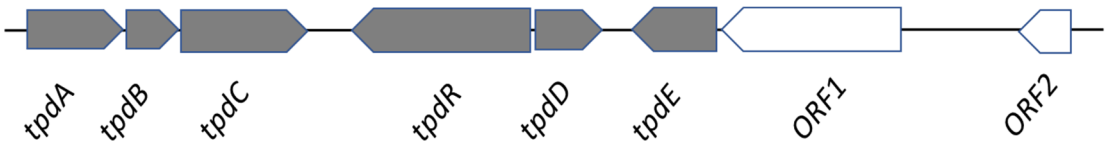

B)

Protein	Putative function
TpdA	Flavin oxygenase
TpdB	Unknown
TpdC	Amidase
TpdR	LuxR family regulator
TpdD	Flavin reductase
TpdE	Short-chain dehydrogenase
ORF1	N, N-dimethylformamidase
ORF2	Peptidase

C)

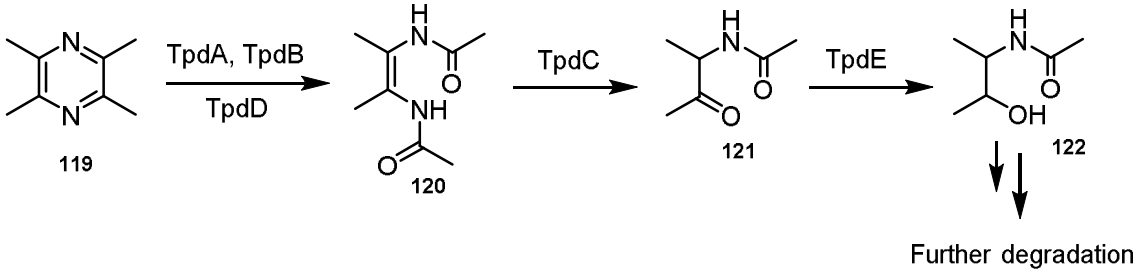

Figure 6.1: TTMP degradation by *Rhodococcus jostii* TMP1 A) TTMP catabolic gene cluster B) Putative function of the gene products C) Proposed TTMP catabolic pathway based on experiments using cell-free extracts**.**

group, thereby, requires different mechanism for the ring cleavage. In this chapter, we reconstituted the TpdA catalyzed reaction in tetramethylpyrazine catabolism and carried out detailed mechanistic studies to provide insights into the flavoenzyme mediated pyrazine ring cleavage reaction.

6.2 Results and discussion

6.2.1 Overexpression and purification of TpdA and TpdB

TpdA and TpdB genes were heterologously expressed in *E. Coli* BL21(DE3) and the N-terminally His6-tagged proteins were purified using Ni affinity chromatography

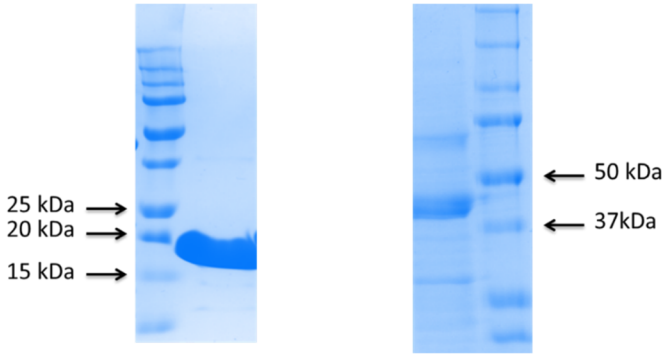

Figure 6.2: A) SDS-PAGE of the purified TpdA and TpdB. Molecular weights of TpdA and TpdB are 43 kDa and 16 kDa.

6.2.2 Reconstitution of TpdA activity

To check the catalytic activity, a reaction mixture containing TTMP, TpdA, *E. coli* Fre, FMN and NADH was incubated at room temperature for 4hr. HPLC analysis of the reaction mixture revealed consumption of TTMP and formation of a new peak (Figure 6.3 A). Initial LC-MS analysis suggested oxidative degradation of the pyrazine ring. Further NMR characterization confirmed the structure of the product as compound **120**. Thus, our

in vitro experiments suggest TpdA alone can cleave the pyrazine ring in the presence of reduced flavin and molecular oxygen.

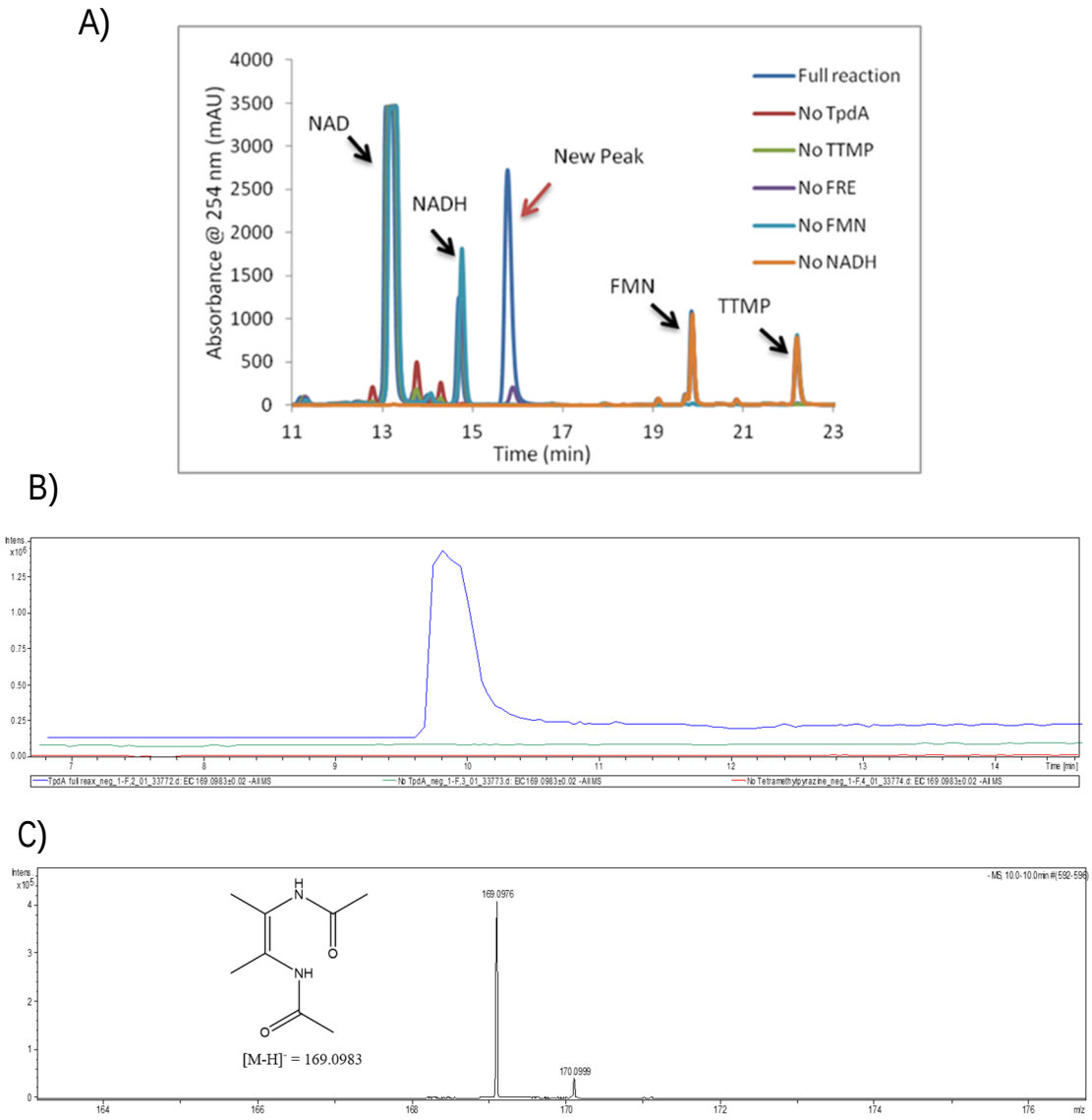

Figure 6.3: Reconstitution of TpdA activity. A) HPLC chromatogram shows formation of a new peak only in full reaction. B) Extracted ion chromatogram at m/z = 169.0983, corresponding to $[M-H]^-$ for the compound **120** C) Exact mass of the TpdA catalyzed reaction product

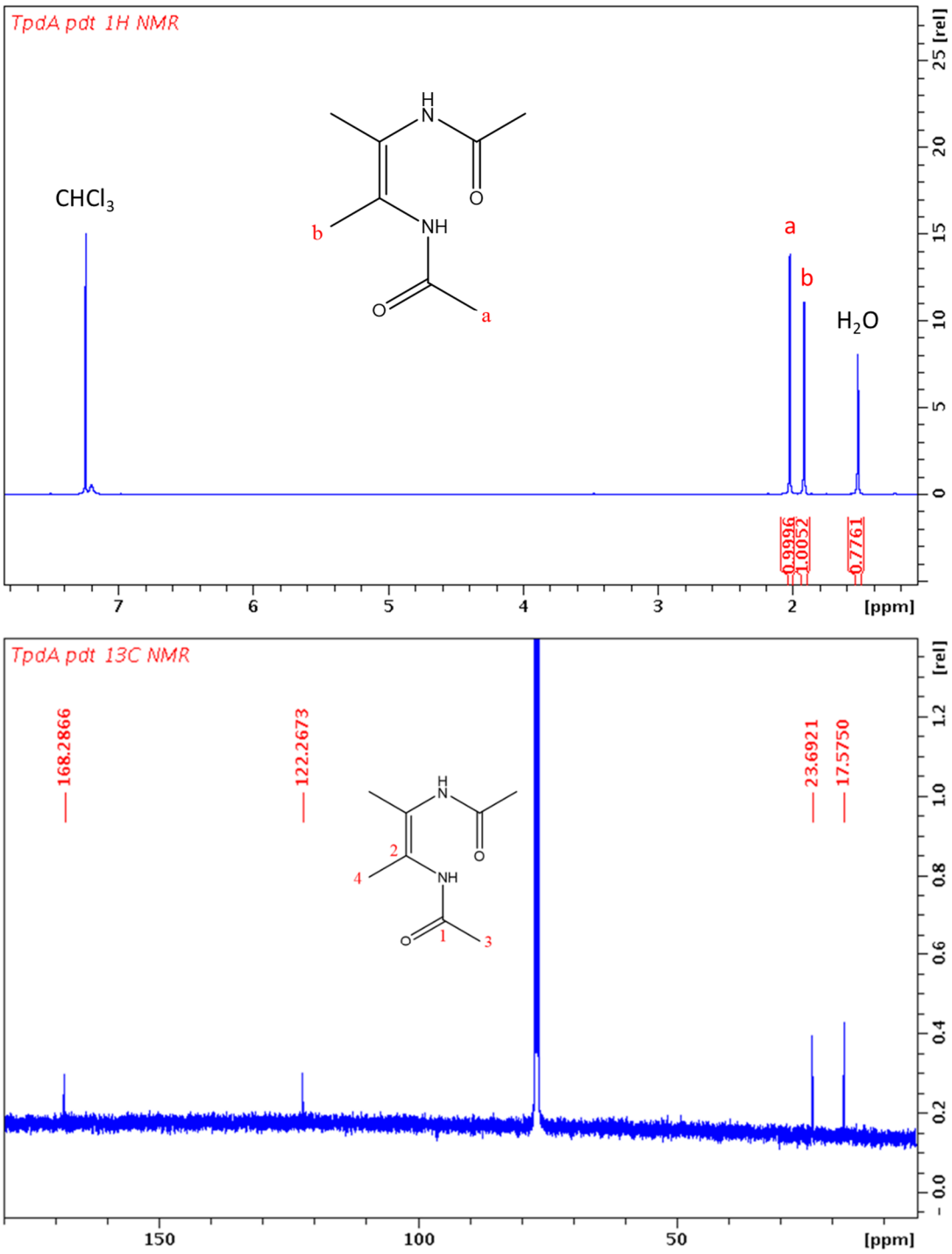

Figure 6.4: NMR characterization of TpdA catalyzed reaction product.

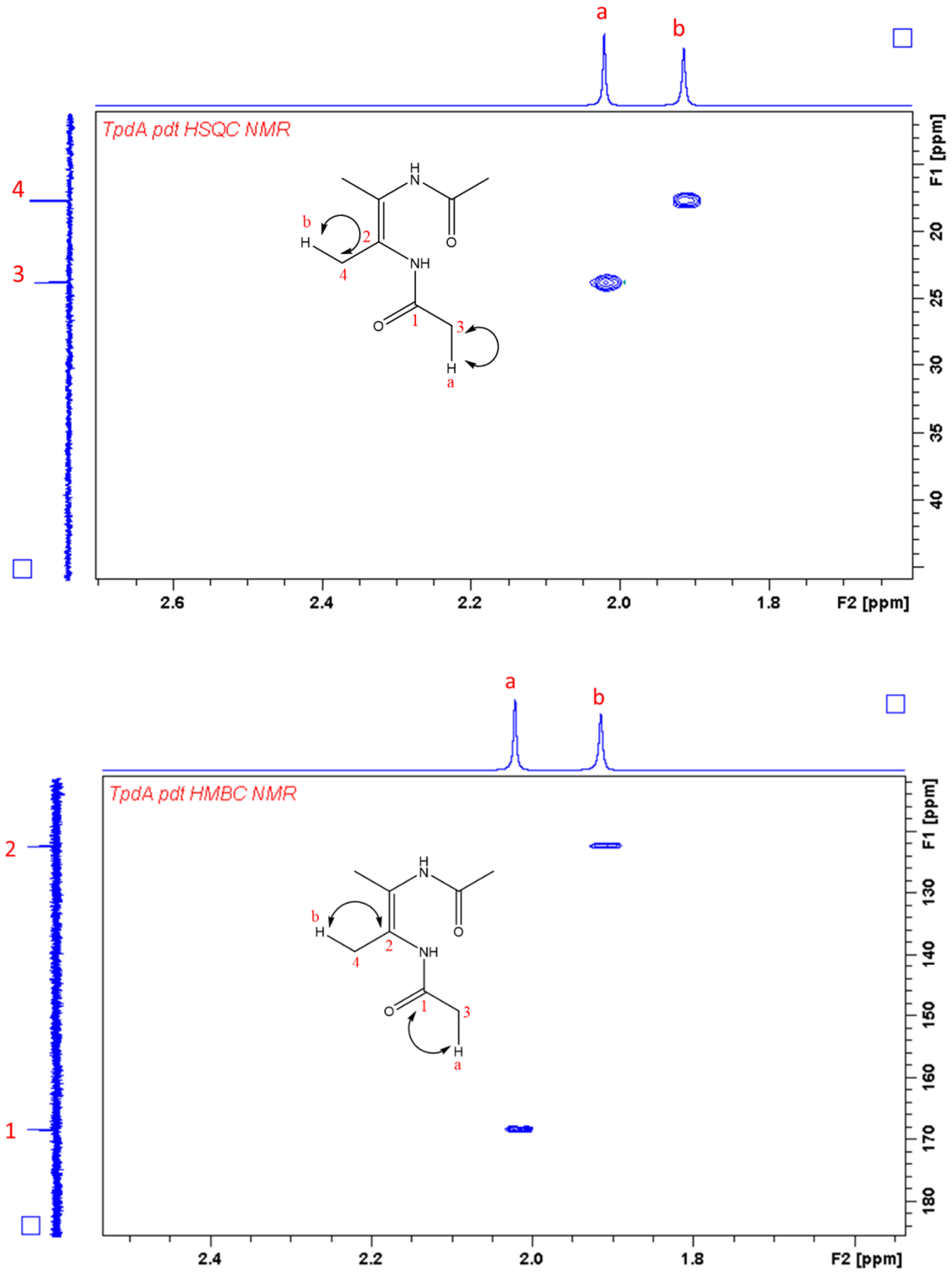

Figure 6.4: Continued

6.2.3 Mechanistic proposal for the TpdA catalyzed reaction

According to our proposal, reduced flavin (produced by *E. coli* flavin reductase) reacts with molecular oxygen to form flavin-C4a-peroxide which then adds the TTMP to give intermediate **123**. Then a Baeyer-Villiger type rearrangement will lead to oxadiazepine intermediate **124**. Water addition followed by C-O bond cleavage will give the final product **120**.

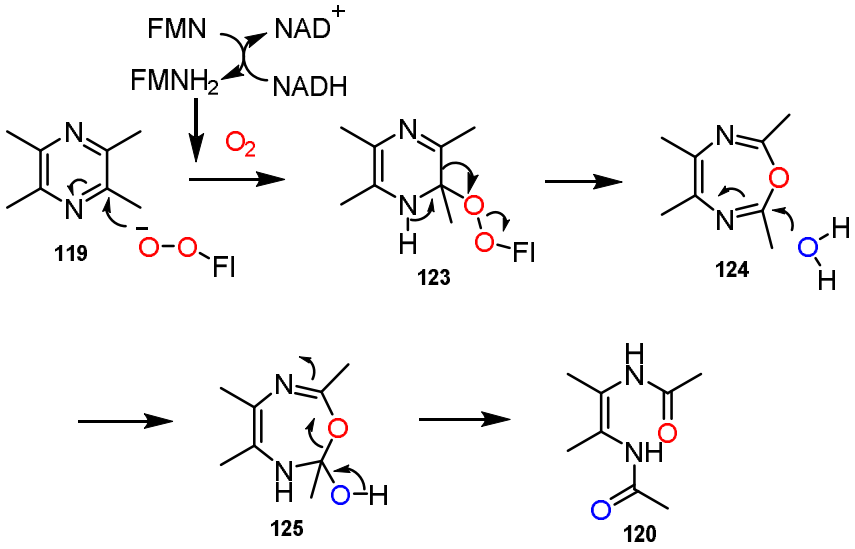

Figure 6.5: Mechanistic proposal for the TpdA catalyzed reaction.

6.2.4 Labeling experiments for the TpdA catalyzed reaction

According to this proposal, there is incorporation of one oxygen atom from water molecule and one from molecular oxygen in the final product. Labeling experiments were carried out to provide evidence to our mechanistic proposal. LC-MS analysis (Figure 6.6) of the reaction mixture using $H_2{}^{18}O$ revealed incorporation of one oxygen atom in the final

product. Similar analysis using $^{18}O_2$ resulted in the incorporation of one oxygen atom in the final product which is consistent with our mechanistic proposal.

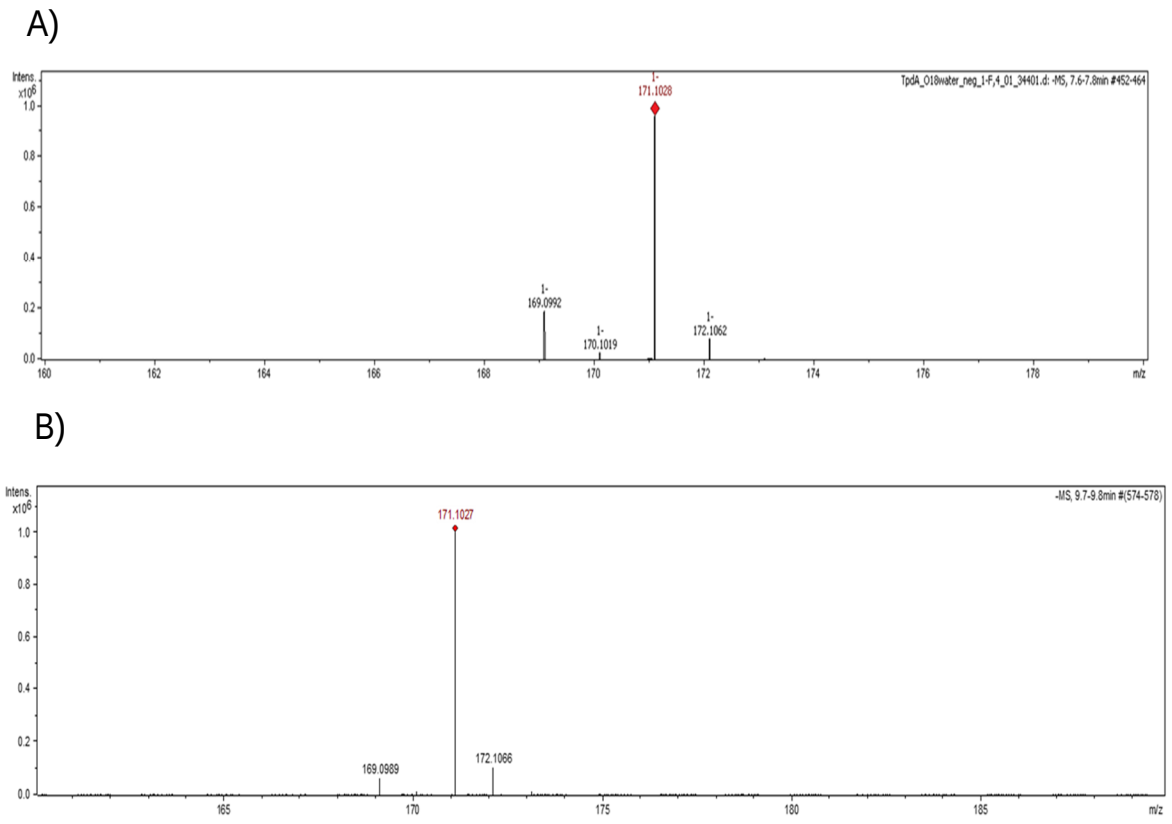

Figure 6.6: LC-MS analysis of the TpdA catalyzed reaction run in the presence of [18O]-H_2O or $^{18}O_2$. Panel A shows that one oxygen atom from the buffer is incorporated into the reaction product. Panel B shows the incorporation of one oxygen atom from molecular oxygen

6.2.5 Substrate analog studies

Substrate analog studies revealed that TpdA showed broad substrate specificity. All the di and tri methyl substituted pyrazines were substrates for TpdA. Several substituted pyridines were also turned out to be the substrates for TpdA. Interestingly, while 2,4,6-collidine was used as a substrate, apart from the native ring opened product **127**; a new

peak was observed in the HPLC chromatogram (Figure 3A). UV-visible spectrum of the new peak had a red shift in the λ_{max}. LC-MS analysis and NMR characterization identified the peak to be 3-hydroxy-2,4,6-collidine **128.** A formal C-H hydroxylation of an inactivated C-H bond is unprecedented in flavoenzymology (LadA[76] is the only known flavoenzyme to hydroxylate an inactivated C-H bond; however, detailed mechanistic studies yet to be done). Generally, such transformation is carried out by metalloenzymes.

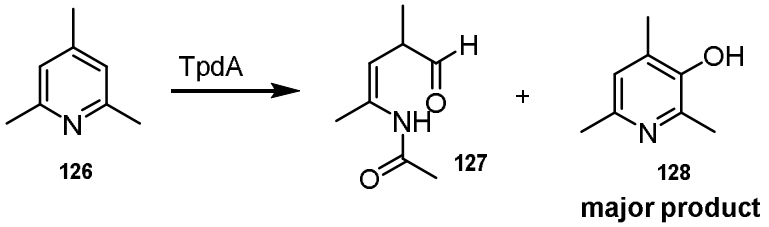

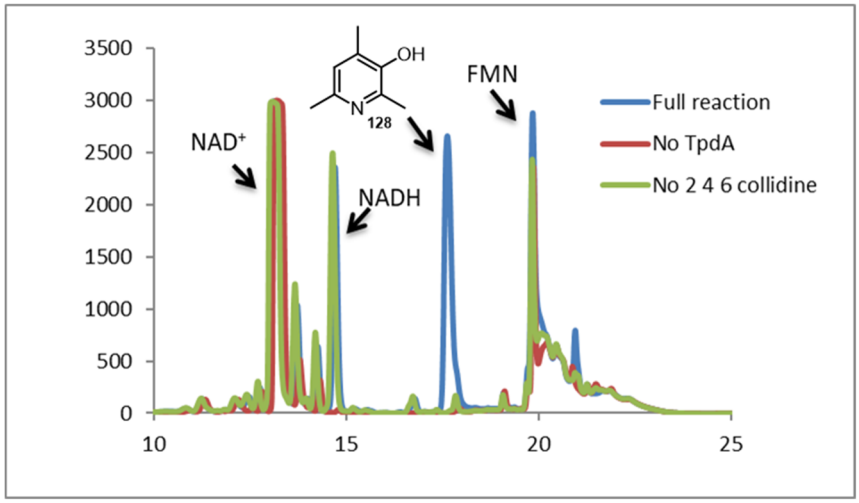

Figure 6.7: HPLC analysis of the TpdA catalyzed reaction in the presence of 2,4,6-collidine.

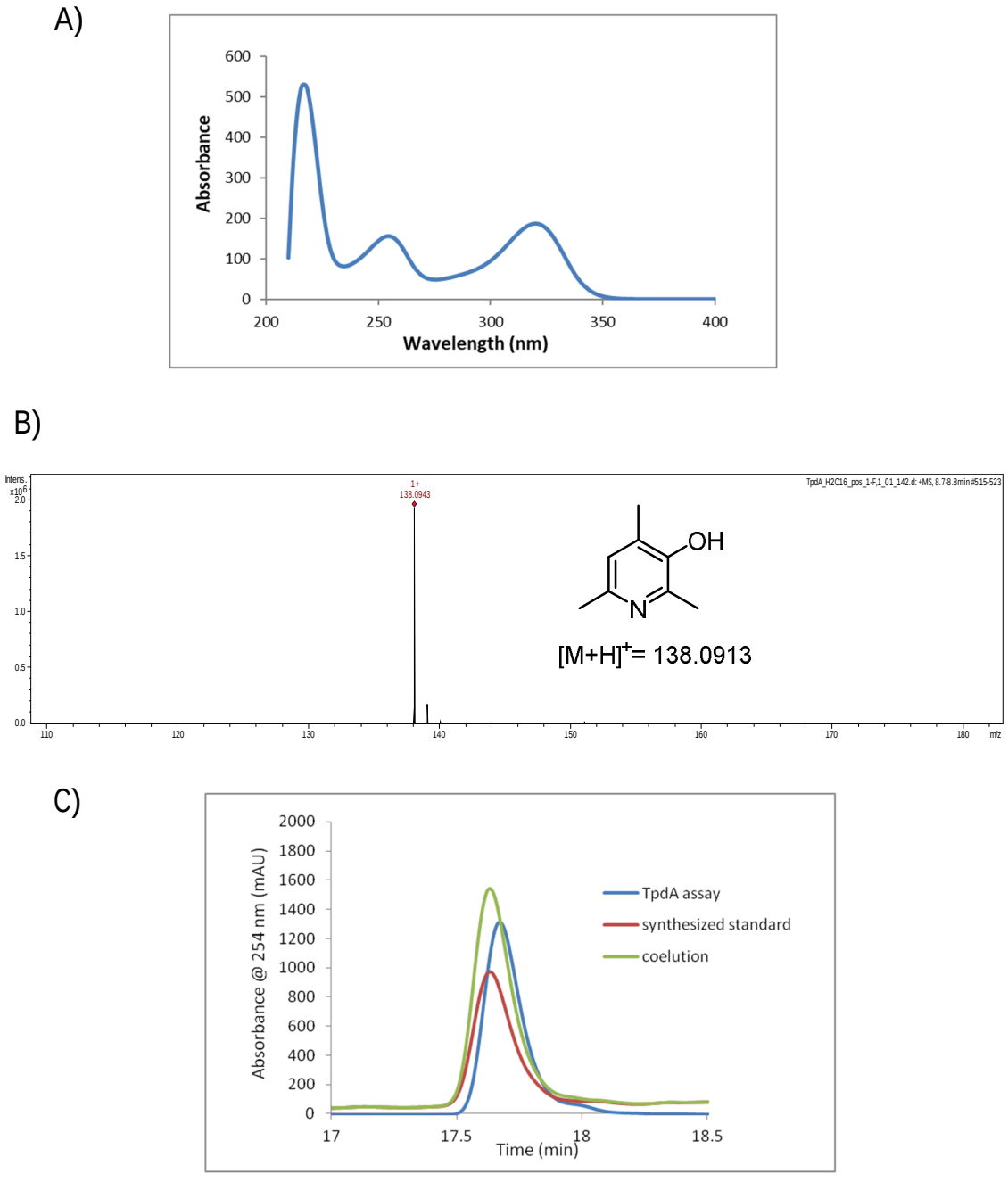

Figure 6.8: Characterization of the major product of TpdA catalyzed reaction with 2,4,6-collidine A) UV-vis spectrum of peak 2 shows red shift. B) Mass of the peak 2 matches with the 3-hydroxy-2,4,6-collidine. C) Coelution with a synthetic standard.

6.2.6 Mechanistic hypothesis for the unusual hydroxylation reaction

To rationalize the formation of this unusual hydroxylated product, we came up with the following proposal. According to this proposal, at first, flavin-C4a-peroxide adds to the C2 of 2,4,6-collidine to give intermediate **129** which upon a Baeyer-Villiger type rearrangement form oxazapine intermediate **130**. Now, there are two possible fates of this oxazapine intermediate: if water adds then it will lead to the native product **127**. However, if it undergoes a cyclization reaction then it will lead to epoxy compound **132** which will readily aromatize to give the final hydroxylated product **128.** There is literature precedence of such cyclization reactions in synthetic organic chemistry.[77]

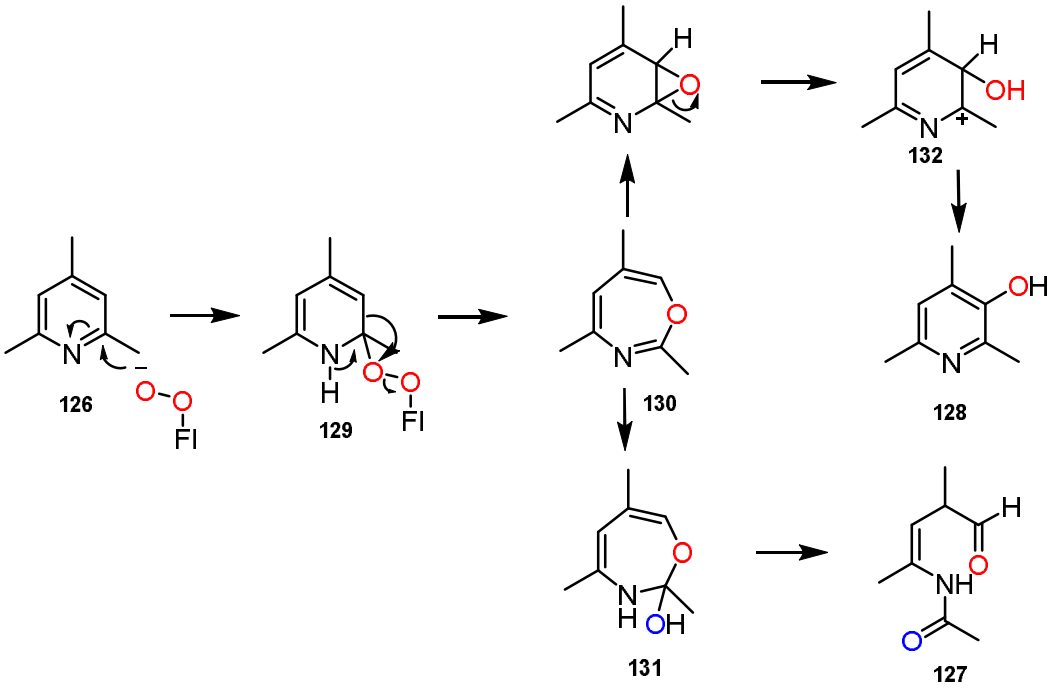

Figure 6.9: Mechanistic proposal for the TpdA catalyzed reaction in the presence of 2,4,6-collidine.

To provide evidence in favor of the proposal, we designed experiments using O-18 labeled H_2O, O-18 labeled O_2 and deuterated substrates. Reaction in the presence of O-18 labeled H_2O did not result in incorporation while reaction using O-18 labeled O_2 resulted in incorporation of one oxygen atom (Figure 6.10). These observations are in well agreement with our mechanistic proposal.

A)

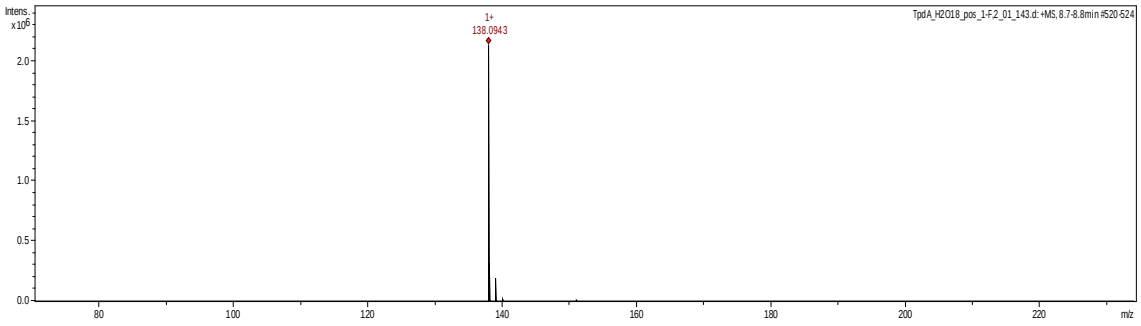

B)

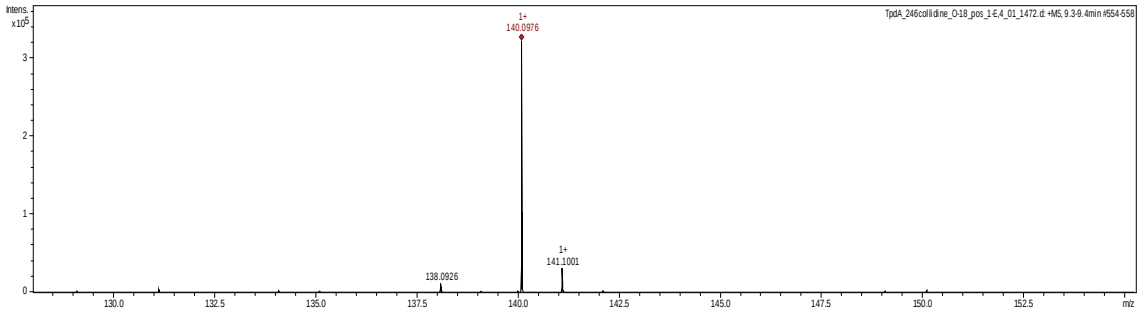

Figure 6.10: LC-MS analysis of the TpdA catalyzed reaction with 2,4,6-collidine run in the presence of [18O]- H_2O or $^{18}O_2$. Panel A shows that no oxygen atom from the buffer is incorporated into the reaction product. Panel B shows the incorporation of one oxygen atom from molecular oxygen.

In order to provide further evidence to our proposal, two deuterium labeled substrates were synthesized: D5-2,4,6-collidine **133** (ideally one would like to synthesize D2-2,4,6-collidine but because of the difficulties associated with the synthesis of D2-2,4,6-collidine we decided to synthesize D5-2,4,6-collidine which will serve our purpose equally well) and D9-2,4,6-collidine **135**. When the enzymatic reaction was carried out in the presence of D5-2,4,6-collidine, four deuteriums were retained in the final product and one is lost (Figure 6.11); While with D9-2,4,6-collidine, all the deuterium was retained, however, there was partial exchange of three protons (Figure 6.11). Observed exchange phenomenon can be rationalized based on the proposed cationic intermediate **132.** Now, if this is true, one should also observe similar exchange pattern when the reaction is carried out in the presence of unlabeled substrate in deuterated buffer. Indeed, when the reaction was carried out in the presence of D_2O, three protons were exchanged, thereby, validating our mechanistic proposal (Figure 6.11).

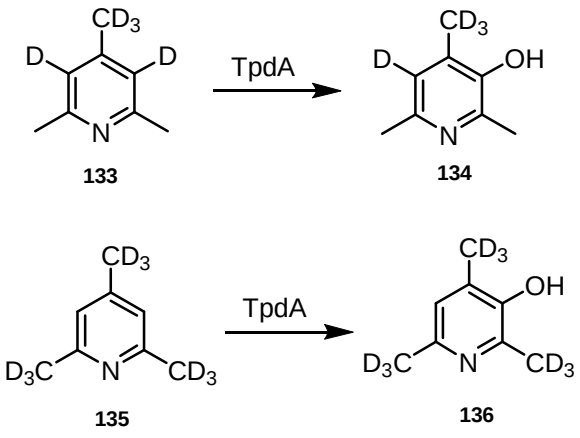

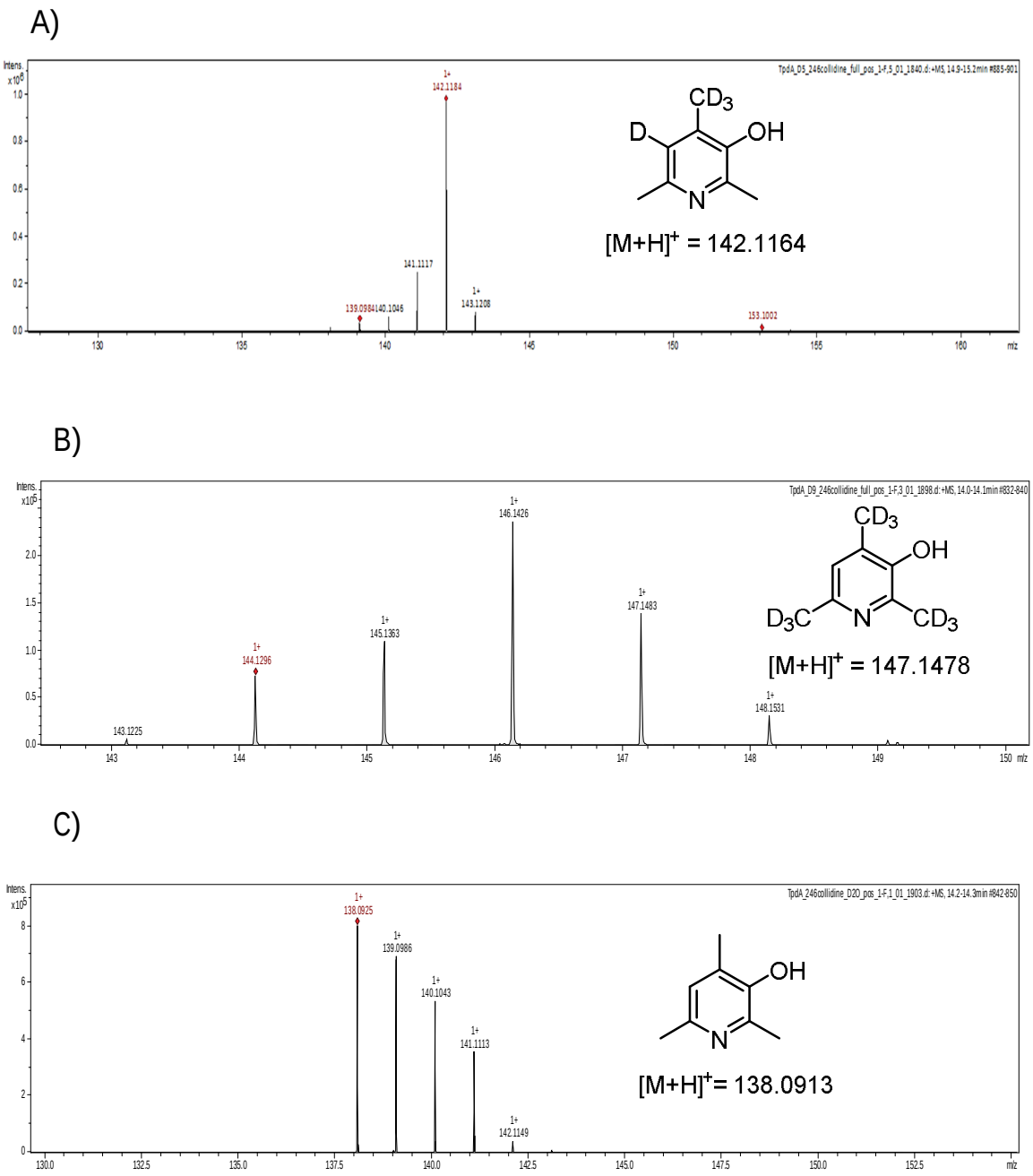

Figure 6.11: LC-MS analysis of the TpdA catalyzed reaction product in the presence of deuterium labeled 2,4,6-collidine. A) Mass of the reaction product when D5-2,4,6-collidine **133** was the substrate. B) Mass of the reaction product when D9-2,4,6-collidine **135** was the substrate. C) Mass of the reaction product when the reaction was carried out with unlabeled substrate in D_2O buffer

6.3 Conclusion

To summarize, we have reconstituted TpdA catalyzed oxidative ring opening of TTMP in vitro. Labeling experiments and substrate analog studies suggest a Baeyer-Villiger type rearrangement during the enzymatic conversion of TTMP **119** to **123**. Since, TpdB does not involve in the first step of the TTMP catabolism, we propose it might have a role in the downstream transformation. Generally, flavoenzyme catalyzed Baeyer-Villiger reactions proceed via the addition of flavin-C4a-peroxide to a carbonyl center. However, in this case, flavin-C4a-peroxide adds to the imine center which is unprecedented. Although, there were reports of oxepine during homogentisate formation[78] and phenylacetate catabolism[79], to the best of our knowledge, this is the first instance where we provide evidence of an oxadiazapine intermediate in an enzymatic reaction. Our studies on TpdA, once again, underscore the versatility of flavin cofactors in enzymology.

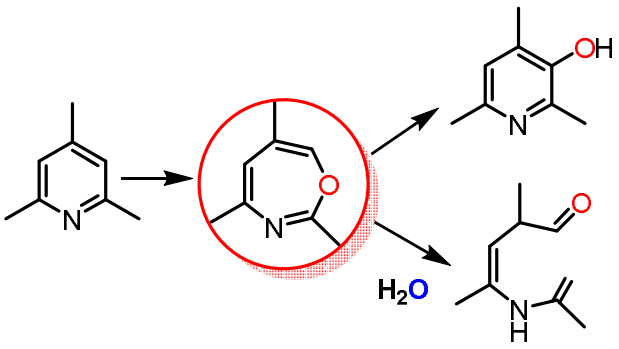

6.4 Experimental Procedure

Materials

All chemicals were purchased from Sigma-Aldrich unless mentioned otherwise. LB broth (Lennox) was purchased from EMB Millipore. kanamycin and IPTG were obtained from Lab Scientific Inc. Amicon Ultra centrifugal filter devices (10,000 MWCO) were obtained from Millipore. Histrap column was obtained from GE Healthcare. Econo-Pack 10DG desalting columns were purchased from Bio-Rad. 2.5 L baffled ultra yield flasks for protein overexpression were obtained from Thomson Instrument Company. HPLC and LC-MS solvents were purchased from EMD and were used without further purification. ZORBAX Eclipse XDB-C18 column (15 cm x 4.6 mm, 5 μm particles) was purchased from Agilent Technologies.

Over-expression and purification of TpdA and TpdB

The TpdA gene containing overexpression plasmid (pTHT-TpdA) was transformed into *Escherichia coli* BL21 (DE3). For the overexpression of the protein, a starter culture was grown overnight in 15 ml of LB medium containing 40 μg/ml of kanamycin at 37 °C. 1.5 liter of LB medium (20 g/L) containing 40 μg/ml of kanamycin, was inoculated with this starter culture. The cells were grown at 37 °C with shaking (220 rpm) until the culture reached an OD_{600} of 0.6. The culture was then incubated at 4°C for ~45min without shaking. Then the culture was induced by adding IPTG to a final concentration of 0.5 mM, the temperature was lowered to 15 °C and the cells were grown with shaking (180 rpm) for a further 15 hours. The cells were then harvested by centrifugation at 10,000g for 10 min at 4 °C and store at -80 ˚C.

The cell pellet was re-suspended in 30 ml of lysis buffer (50 mM KH_2PO_4, 150 mM NaCl, 10 mM imidazole, pH 8.0). Lysozyme (5 mg) was added and the cells were lysed by sonication on ice (Misonix Sonicator 3000, six cycles of 30 s duration during which 1.5 s sonicator pulses at output level 0.8 were followed by 1.5 s pauses). The resulting suspension was centrifuged (18,000 rpm, 30 min) and the supernatant was filtered through a sterile syringe filter (pore size 0.45 μm). The clarified supernatant was loaded onto a 5 mL Ni-NTA-affinity column pre-equilibrated with lysis buffer kept at 4°C. The Ni-NTA-affinity column was then washed with 50 ml wash buffer (50 mM KH_2PO_4, 150 mM NaCl, 20 mM imidazole, pH 8.0). The protein was eluted from the column with elution buffer (50 mM KH_2PO_4, 150 mM NaCl, 200 mM imidazole, pH 8.0) at 4°C. The fractions containing protein were pooled and concentrated using YM-10 Amicon ultracentrifugal filters at 5000g to a final volume of 3 mL. The concentrated sample was buffer exchanged, using an Econo-Pac 10DG desalting column, into 100 mM phosphate buffer at pH 7.5 containing 100 mM NaCl and glycerol to a final concentration of 15%. Protein concentration was determined from the absorbance at 280 nm (A280) with an Extinction coefficient calculated using the ProtParam tool of the ExPASy proteomics Server ($\epsilon 280$ = 56380). A typical yield was 20 mg/liter.

The TpdB encoding gene was cloned into pTHT vector (derivative of pET28b vector with TEV protease cleavage site after the N-terminal His-tag). The plasmid was transformed into *Escherichia coli* BL21 (DE3). A starter culture was grown overnight in 15 ml of LB medium containing 40 μg/ml of Kanamycin at 37 ˚C. Next, 1.5 L of LB

medium containing 40 μg/ml of Kanamycin was inoculated with this starting culture. The cells were grown at 37 ˚C till the OD_{600} reached a value of 0.6. The culture was then incubated at 4 ˚C for 45 min without shaking and induced with 0.5 mM IPTG followed by incubation at 15 ˚C for 15 hr with shaking (180 rpm). The cells were then harvested by centrifugation and stored at -80 ˚C until further use. The purification procedure was same as that for TpdA.

HPLC parameters and LC-MS parameters

Same as mentioned in Chapter V.

Activity assay of TpdA catalyzed reaction

The TpdA catalyzed reaction was performed in 100 mM phosphate buffer, pH 7.5. The final concentrations of all the reaction components were as follows: TpdA (50 μM), TTMP (500 μM), FMN (50 μM), *E. coli* Fre (400 nM) and NADH (1 mM). The volume of the reaction mixture was 200 μL and incubated at RT for 3 hr. The protein was heat-denatured and removed by centrifugal ultrafiltration through a 10 kDa MWCO membrane (Pall Life Sciences). The samples were analyzed by HPLC and LC-MS. To check the effect of TpdB, it was added to the reaction mixture such that the final concentration was 50 μM.

TpdA catalyzed reaction in the presence of $H_2{}^{18}O$

Two identical reactions were set up; each 200 μL solution contained 500 μM TTMP, 50 μM TpdA, 50 μM FMN, 400 nM Fre and 1mM NADH. One of the samples had a final concentration of 80% $H_2{}^{18}O$. The other sample was used as a 'control' and contained 100% $H_2{}^{16}O$. The reaction mixture was incubated at room temperature for 4 hours after which both the samples were analyzed by LC-MS.

TpdA catalyzed reaction in the presence of $^{18}O_2$

Two identical reaction mixtures were made in a glove box; each 200 µL solution contained 500 µM TTMP, 50 µM TpdA, 50 µM FMN, 400 nM Fre and 1mM NADH. One of the reaction mixtures was exposed to $^{18}O_2$ while the other reaction mixture was used as a 'control' and exposed to $^{16}O_2$. The reaction mixture was incubated at room temperature for 4 hours and then analyzed by LC-MS.

Synthesis of D5-2,4,6-collidine 133

D5-2,4,6-collidine **133** was synthesized following a literature reported protocol. A mixture of acetyl chloride (9.5 mL, 135 mmol) and A1C1$_3$ (5.3 g, 40.5 mmol) is treated with deuterated t-butanol (1 g, 13.5 mmol) for 0.5 h. at 35 ºC., and the crude reaction mixture poured into 100 mL of aqueous ammonia (34 %) with cooling. Solvent was evaporated under reduced pressure and the product was purified using HPLC.

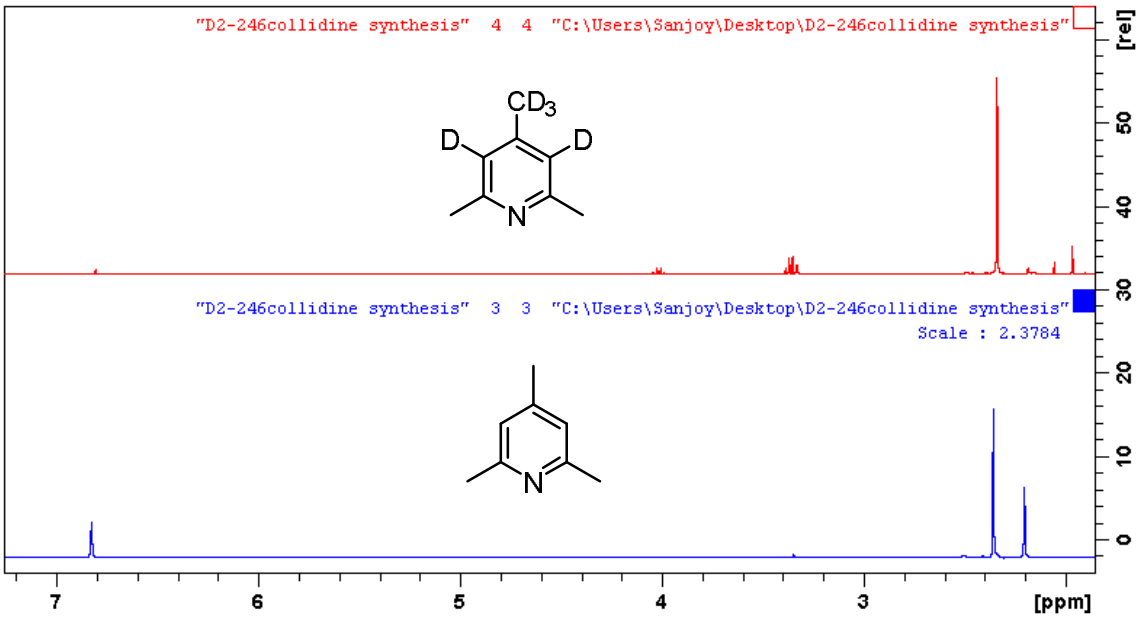

Figure 6.12: 1-H NMR of D5-2,4,6-collidine **133.**

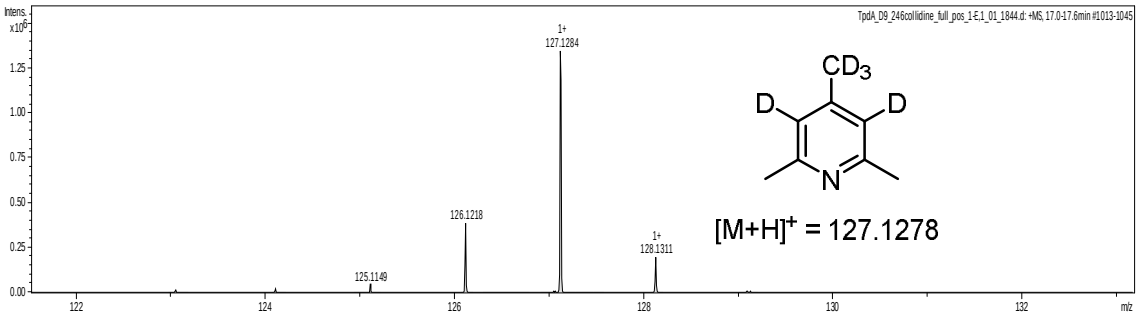

Figure 6.13: Mass of D5-2,4,6-collidine **133.**

Synthesis of D9-2,4,6-collidine 135

2,4,6-Trimethylpyrylium salt (5 g) was heated on the steam bath with deuterium oxide (ten fold) with a reflux condenser protected from atmospheric moisture. After two hours, the solution was cooled, the crystals were filtered off, dried, and the procedure was repeated thrice with fresh portions of deuterium oxide. Deuterated trimethylpyrylium thus produced was added into an excess (20 ml) of cold aqueous ammonia containing 20 mL of ether. After a few minutes' stirring, the two layers are separated, the ethereal layer is extracted with 20 ml of 10 % hydrochloric acid. The aqueous phase is extracted once more with ether, then it is made alkaline with sodium hydroxide solution, and the separated D9-2,4,6-collidine 135 is extracted with ether. The solvent was evaporated under reduced pressure to give the D9-2,4,6-collidine **135** (80% yield).

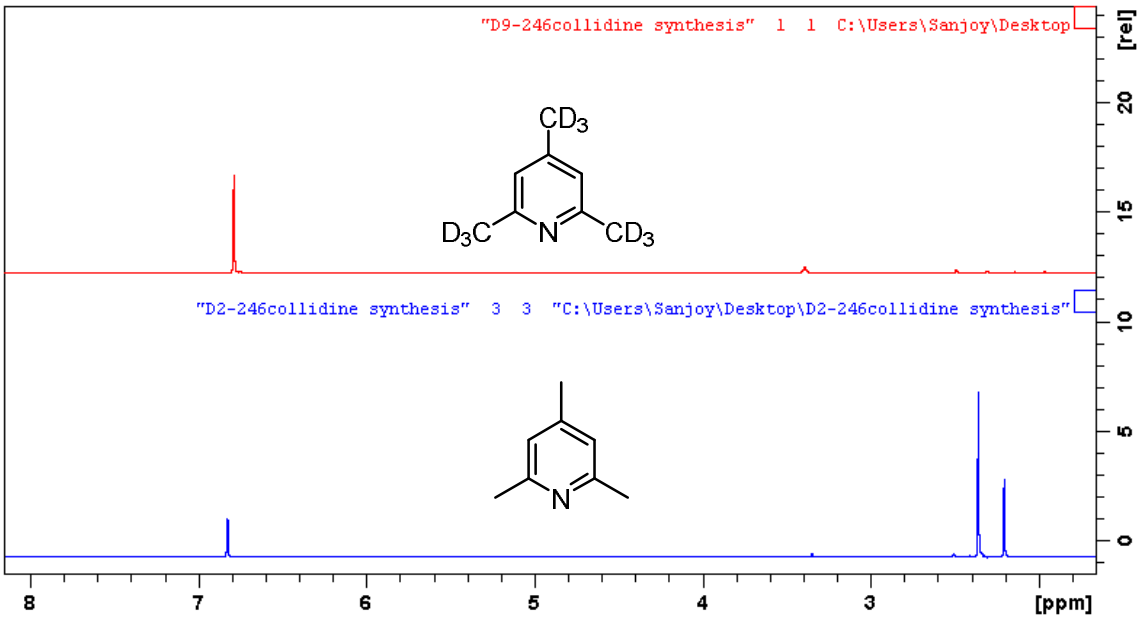

Figure 6.14: 1-H NMR of D9-2,4,6-collidine **135.**

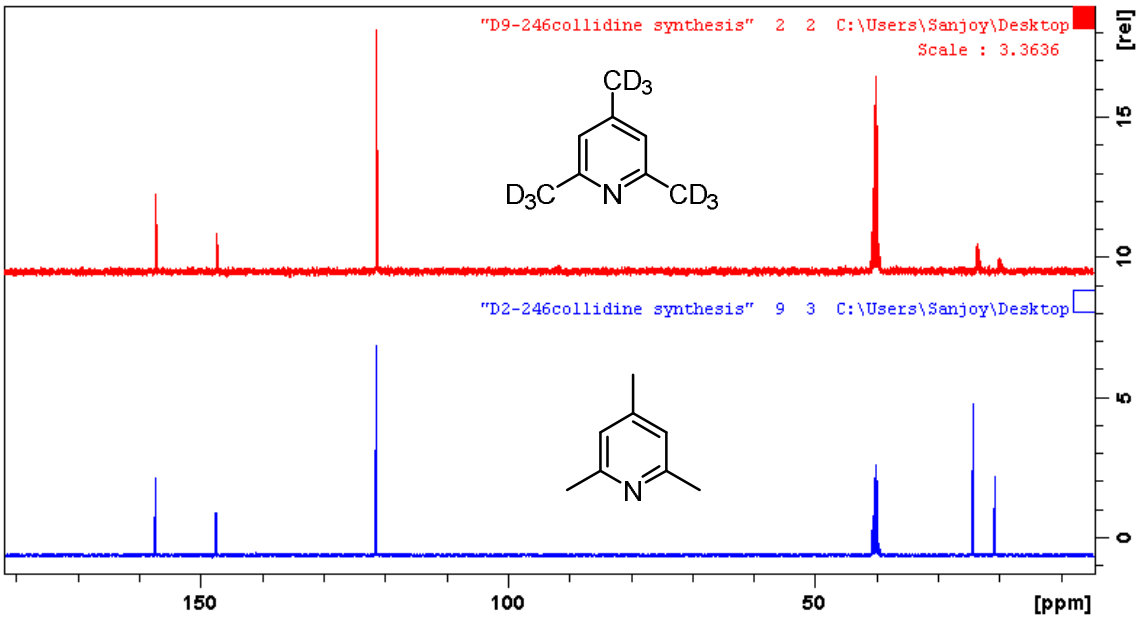

Figure 6.15: 13-C NMR of D9-2,4,6-collidine **135.**

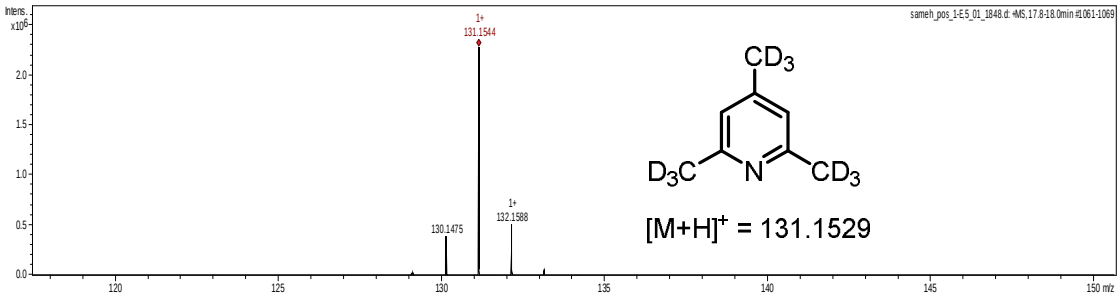

Figure 6.16: Mass of D9-2,4,6-collidine **135.**

CHAPTER VII

MECHANISTIC STUDIES OF A COFACTOR INDEPENDENT OXYGENASE INVOLVED IN BACTERIAL INDOLE CATABOLIC PATHWAY

7.1 Introduction

Molecular oxygen is a strong oxidant with a reduction potential of the O_2/H_2O couple of +0.82 V (at pH 7). However, it has a significant activation barrier to react with organic molecules. This kinetic inertness is the result of its electronic configuration. In ground state molecular oxygen has two unpaired electrons in a degenerate pair of π^* orbital, thus, having a total spin S=1, whereas most organic molecules in their ground state are spin-paired (S=0). To overcome this spin barrier nature employs cofactors (either metal or organic) in order to activate molecular oxygen.[80, 81] Iron and copper are the most widely used metal cofactors to activate molecular oxygen while flavin and pterin are known organic cofactors for the activation of dioxygen. Recently PLP has also been implicated in oxygen activation reaction.[82]

In contrast to these ubiquitous cofactor dependent oxygenases there are only a handful of enzymes which are known to activate molecular oxygen without employing any cofactors. These include ActVa-Orf6 catalyzed[83] oxidation of 6-deoxydihydrokalafungin **137** (6-DDHK) to dihydrokalafungin **138** (DHK), DpgC catalyzed[84] oxidation of 3,5-dihydroxyphenylacetyl coenzyme A **139** (DPA-CoA) to 3,5 dihydroxyphenylglyoxylate **140** (DPGX), RLuc-catalyzed[85] oxidation of coelenterazine **141**, an imidazolopyrazinone-

type luciferin, QDO[86] catalyzed ring cleavage of (2-alkyl)-3-hydroxy-4(1H)-quinolone **143** (Figure 7.1).

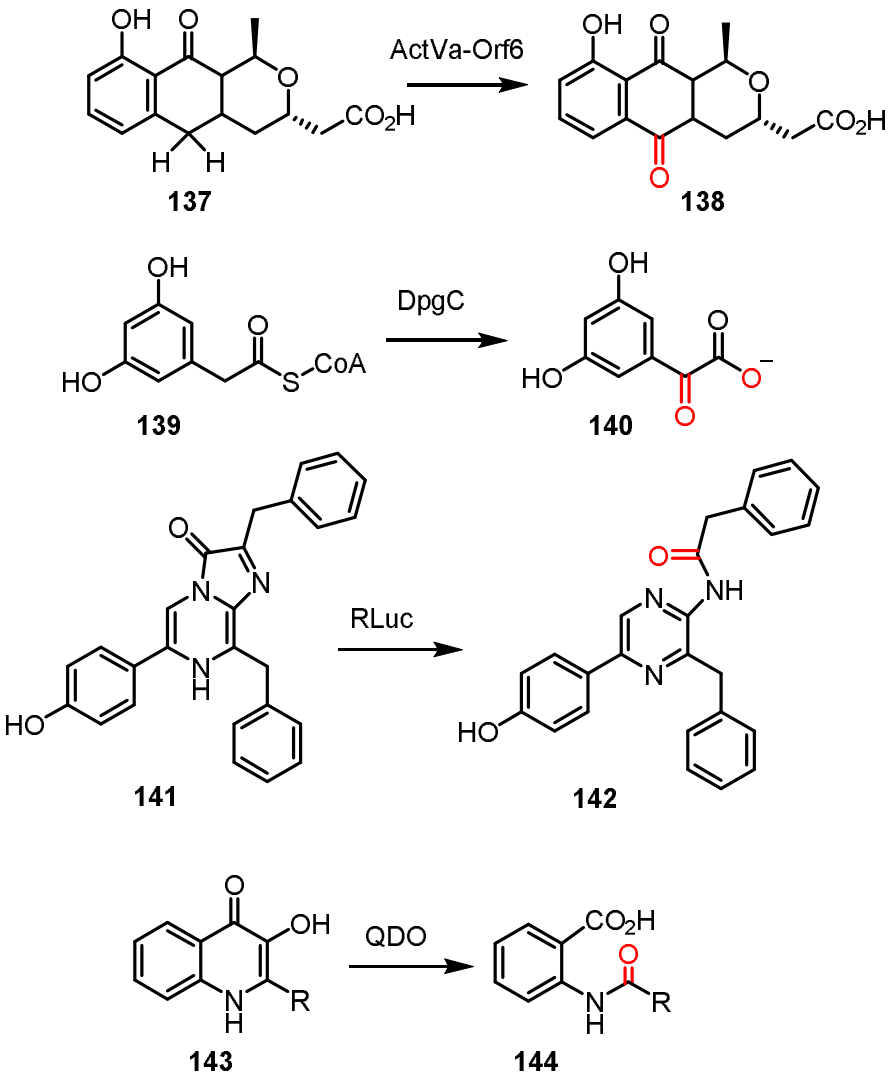

Figure 7.1: Representative examples of cofactor-independent oxygenases A) ActVa-Orf6 catalyzed reaction involved in actinorhodin biosynthesis B) DpgC catalyzed reaction during Vancomycin Biosynthesis C) The reaction catalyzed by Renilla luciferase monooxygenase (RLuc) D) QDO catalyzed degradation of quinolones

Recently a new cofactor-independent oxygenase (IifA) has been identified in the bacterial indole catabolic pathway.[87] Indole is a N-heterocyclic aromatic compound which is mainly produced by trytophanse activities.[88] Although indole is toxic in higher concentration[89], it has important functions as well: acts as cell-to-cell signaling molecule that regulates the expression of several virulence genes,[90] promotes biofilm formation,[91] and mediates complex predator-prey interactions.[92] In 2017, Rolandas Meškys group identified the indole catabolic gene cluster in Acinetobacter sp. strain O153[87] and proposed a catabolic pathway based on initial results (Figure 7.2). According to the proposal a flavin dependent oxygenase IifC carries out oxidation on indole to give indole-2,3-dihydrodiol; in the presence of a flavin reductase IifD. Then the reductase IifB converts the unstable intermediate indole-2,3-dihydrodiol to 3-hydroxyindolin-2-one; Finally, the cofactor independent oxygenase IifA catalyzes the transformation of 3-hydroxy- oxindole to anthranilic acid. In this section we have carried out detailed mechanistic studies on the IifA catalyzed reaction.

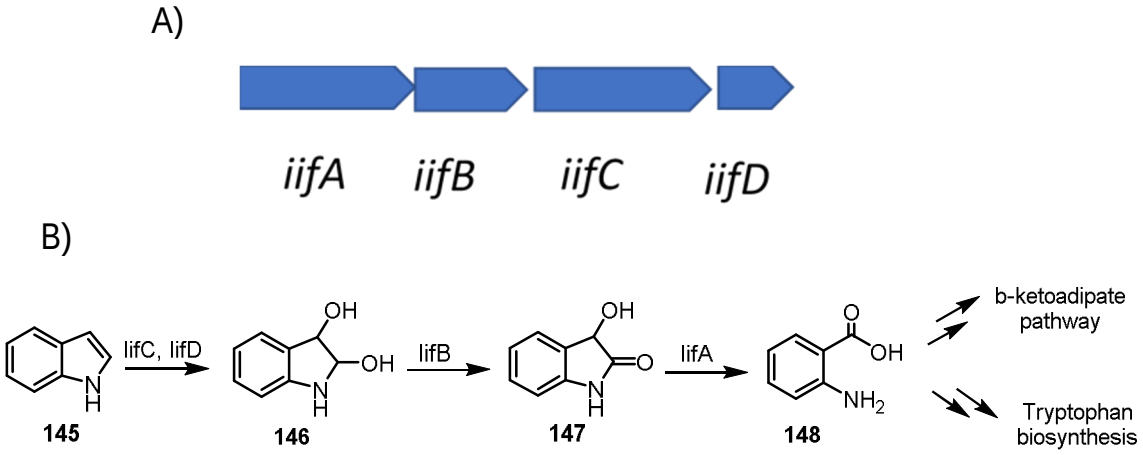

Figure 7.2: Indole catabolism by Acinetobacter sp. strain O153 A) Indole catabolic gene cluster B) Proposed pathway for indole degradation.

7.2 Results and discussion

7.2.1 Overexpression and purification of IifA

IifA gene was obtained from GenScript and was cloned into pTHT vector. IifA was overexpressed in *E. coli* BL21(DE3) and purified by Ni-affinity chromatography. The protein overexpressed well and was purified to homogeneity.

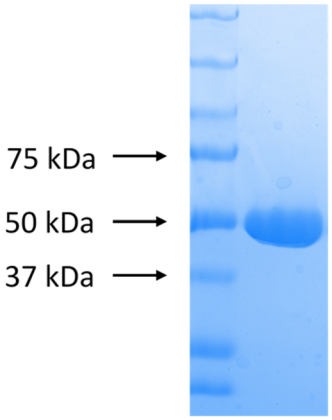

Figure 7.3: SDS-PAGE of purified IifA. Molecular weight of IifA is 48 kDa.

7.2.2 Reconstitution of IifA catalyzed reaction

With the purified protein in hand IifA was incubated with 3-hydroxyindolin-2-one **147** at room temperature for 3hr and the reaction mixture was analyzed by HPLC and LC-MS. Only in the full reaction a new peak was observed with the consumption of the starting material. LC-MS data and coelution experiment confirmed the new compound as anthranilic acid **148**.

A)

B)

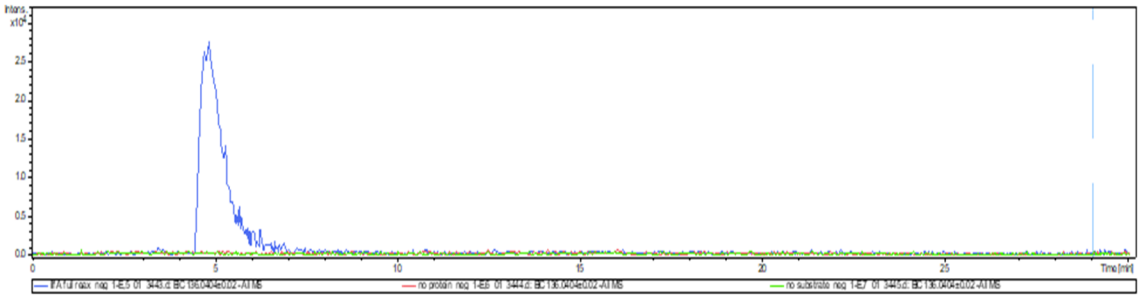

C)

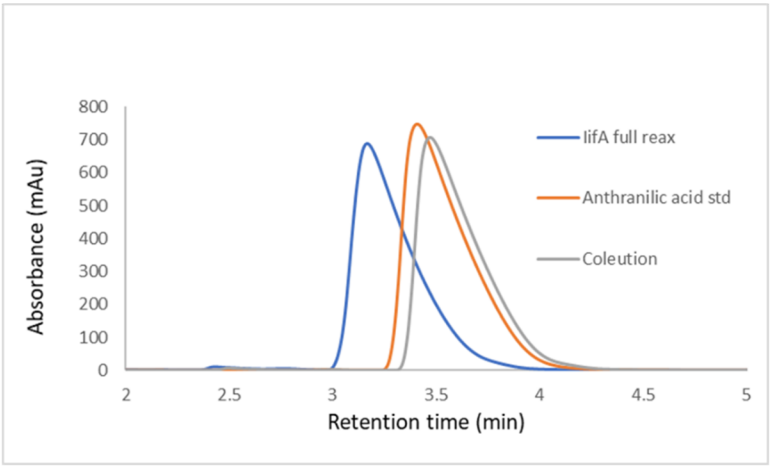

Figure 7.4: Characterization of IifA catalyzed reaction product. A) LC chromatogram showing consumption of the substrate and formation of a new peak only in full reaction. B) Extracted ion chromatogram at m/z = 136.0404, corresponding to $[M-H]^-$ for the anthranilic acid C) Coelution with an authentic anthranilic acid.

7.2.3 Mechanistic hypothesis for the IifA catalyzed reaction

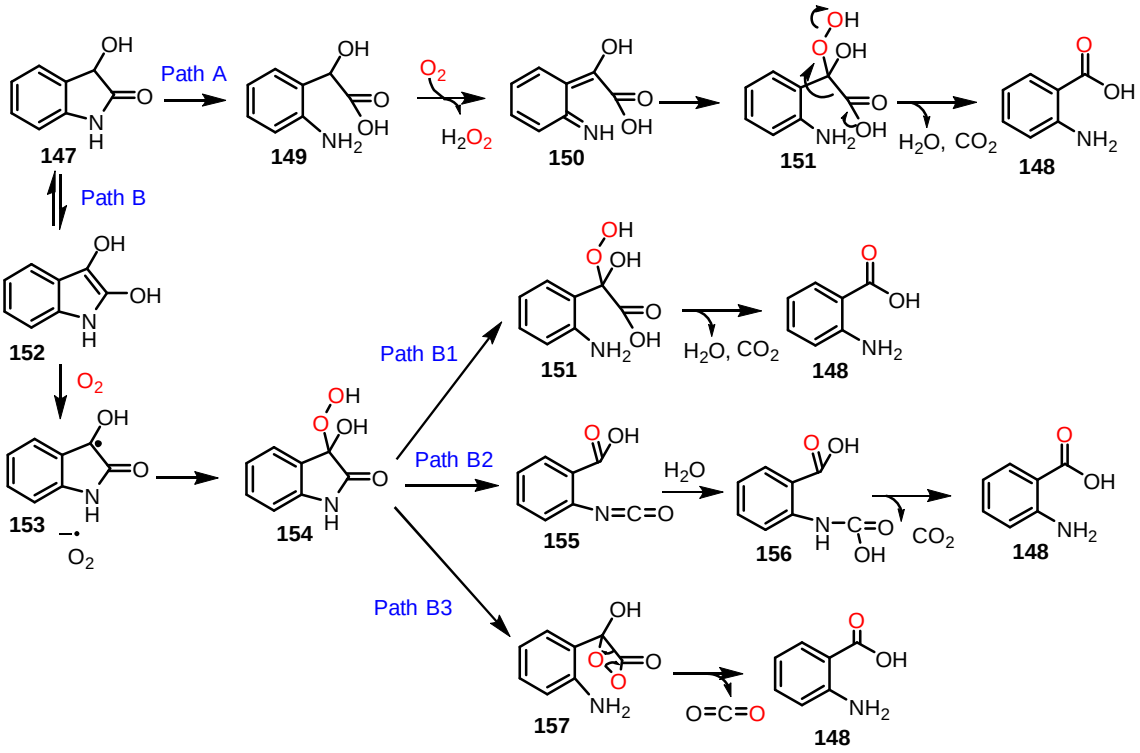

Figure 7.5: Mechanistic proposal for the IifA catalyzed reaction

Having reconstituted the IifA catalyzed reaction in vitro we consider several possible mechanisms for the conversion of **147** to **148**. According to the Path A, amide hydrolysis followed by reaction with molecular oxygen gives intermediate **150**. Addition of H_2O_2 yields compound **151** which readily loses water and carbon dioxide to give the final product. According to Path B, substrate **147** reacts with molecular oxygen via a single electron transfer to give **153** and superoxide radical which readily recombines to give hydroperoxide intermediate **154**. There are three possible pathways to convert **154** to anthranilic acid **148**: via amide hydrolyzed intermediate **151**, isocyanate intermediate **155**

and oxetane intermediate **157**. Although isocyanate is rare in biological systems there is a recent report of methyl isocyanate during biosynthesis of fungal alkaloid viridicatin.[93] Oxetane intermediates have been proposed in DpgC catalyzed reaction[84] during Vancomycin Biosynthesis and QDO[86] catalyzed degradation of quinolones.

7.2.4 $^{18}O_2$ labeling experiment for the IifA catalyzed reaction

According to all four mechanistic proposal there is a single oxygen incorporation from molecular oxygen to the final product. To test this IifA catalyzed reaction was carried out under $^{18}O_2$ atmosphere. However, there was no incorporation of labeled oxygen in the final product as the mass of the product remained same as it was when the reaction was carried out under $^{16}O_2$ atmosphere.

A)

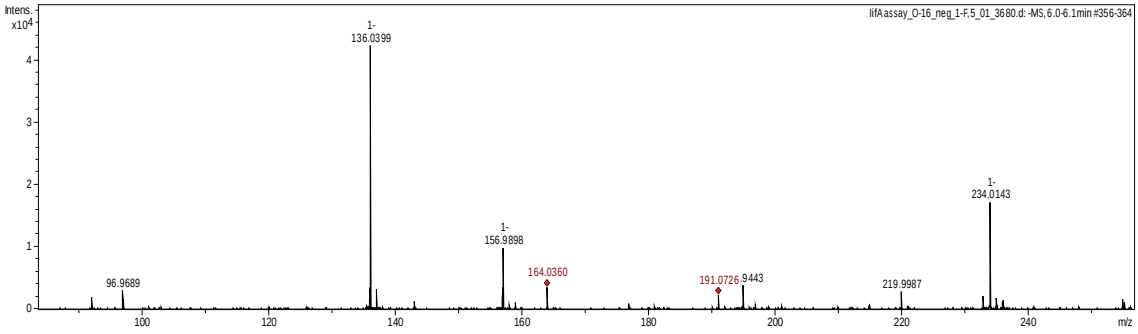

B)

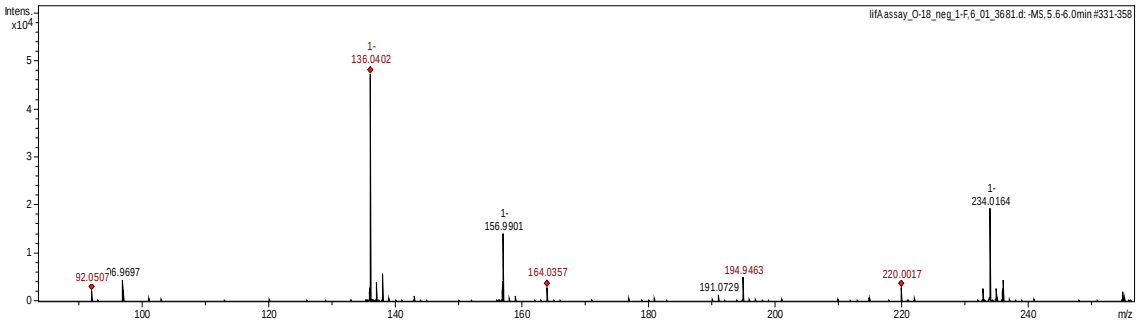

Figure 7.6: LC-MS analysis of IifA catalyzed reaction run either in the presence of $^{16}O_2$ (panel A) or $^{18}O_2$ (panel B)

Since there was no incorporation of oxygen atom from molecular oxygen in the final product, we considered whether water molecule is the source of oxygen atom. To test this hypothesis IifA catalyzed reaction was performed in 80% $H_2{}^{18}O$ containing buffer and the reaction mixture was analyzed by LC-MS. Under this condition there was 2 da increase in the mass of anthranilic acid product implying one of the oxygen atoms is from water molecule. The possibility of exchange of carboxy oxygen was ruled out since there was no change in mass was observed when anthranilic acid standard was incubated in the $H_2{}^{18}O$ containing buffer.

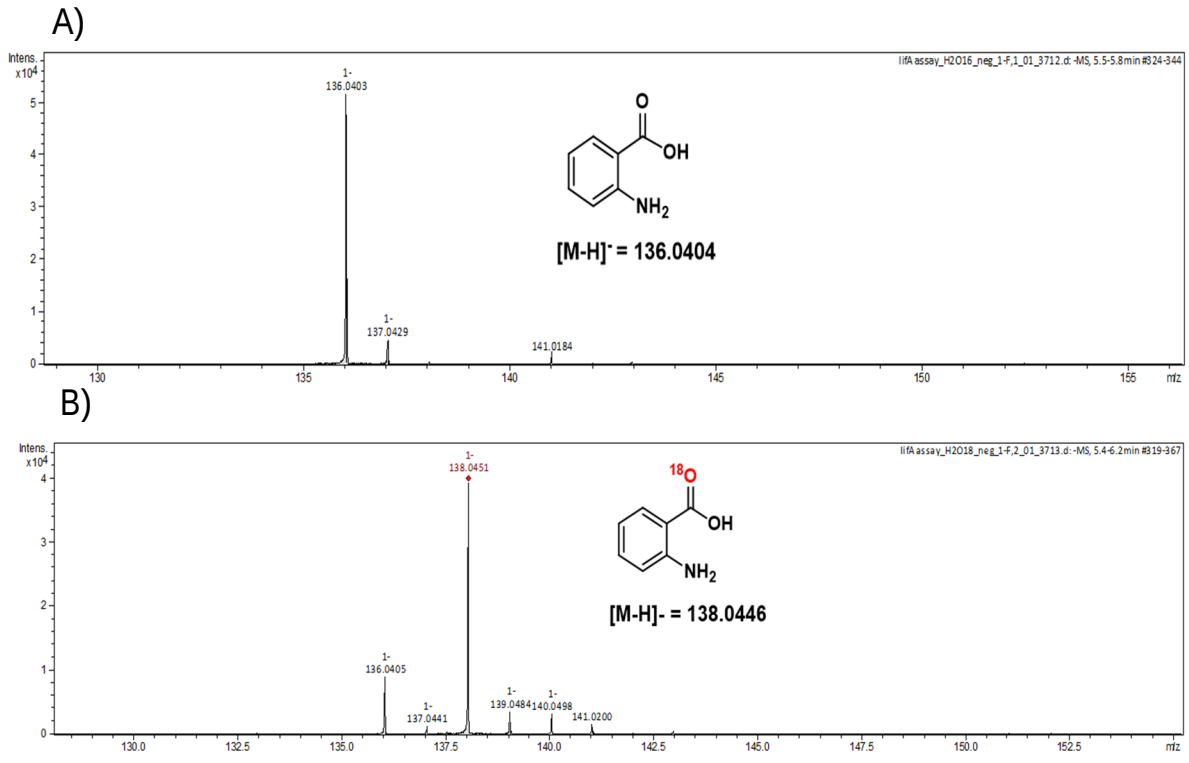

Figure 7.7: LC-MS analysis of IifA catalyzed reaction run either in the presence of $H_2{}^{16}O$ (panel A) or 80 % $H_2{}^{18}O$ (panel B)

7.2.6 New mechanistic hypothesis for the IifA catalyzed reaction

The fact that the source of oxygen atom in the final product is water molecule made us to come up with different mechanistic proposal. According to the new proposal the hydroperoxide intermediate **154** undergoes a Baeyer-Villiger type rearrangement to give isotoic anhydride **158**. Hydrolysis of the isotoic anhydride followed by decarboxylation yields the final product. Similar Baeyer-Villiger rearrangement has been reported during the oxidation of guanosine by singlet oxygen[94] and TflA catalyzed toxoflavin degradation reaction.[22]

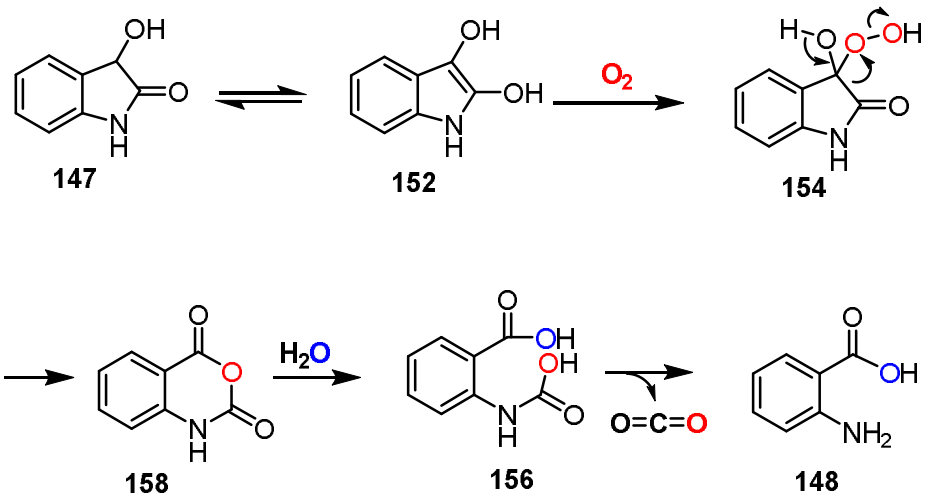

Figure 7.8: Mechanistic proposal for the IifA catalyzed reaction involving a Baeyer-Villiger type rearrangement.

7.2.7 C2 of substrate is lost during the IifA catalyzed formation of anthranilic acid

According to our mechanistic proposal C-2 carbon atom of the substrate is lost during the IifA catalyzed reaction. To test this proposal 13C labeled substrate at C-2 position was made. When IifA assay was carried out with this labeled substrate the mass of the

anthranilic acid product remained same implying that the labeled carbon is lost during the reaction.

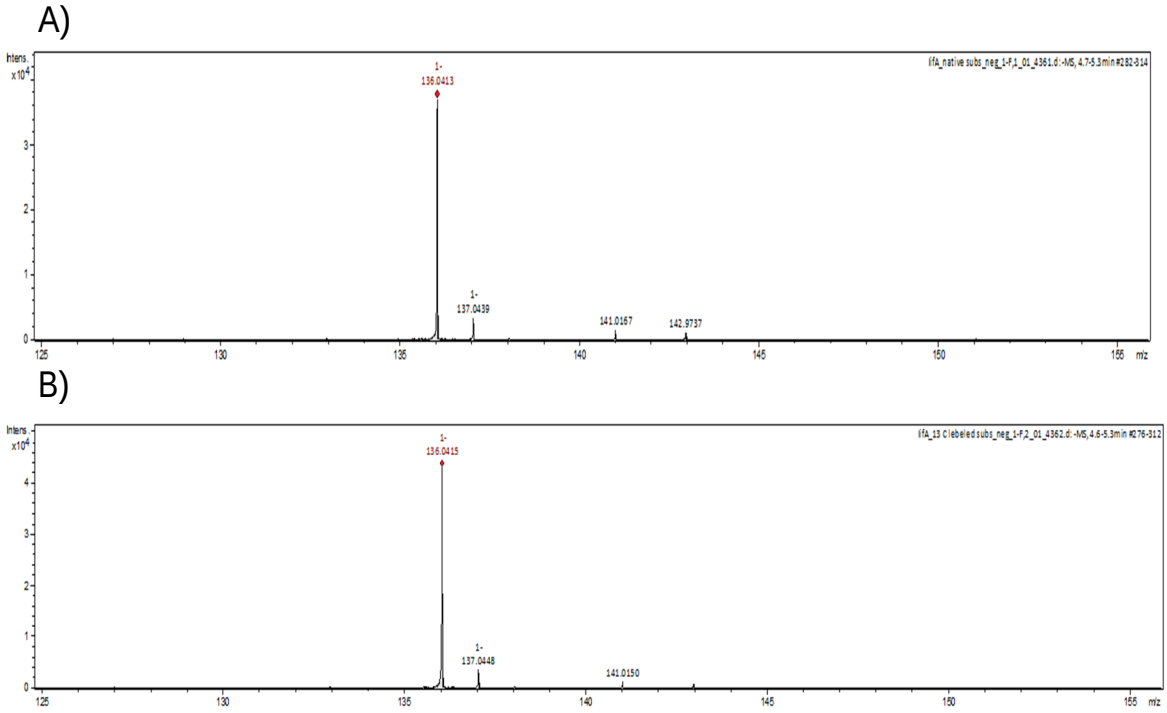

Figure 7.9: LC-MS analysis of IifA catalyzed reaction product using unlabeled (panel A) and 13-C2 labeled substrate (panel B).

7.2.8 Detection of bicarbonate in the IifA catalyzed reaction

To figure out the identity of the lost carbon atom 13-C NMR experiment was performed. A clear change in the chemical shift value of the 13-C labeled carbon was observed in the full reaction compared with no enzyme control. (chemical shift of the 13-C labeled carbon atom is 162 ppm in the full reaction compared with the 182 ppm in the no enzyme control).

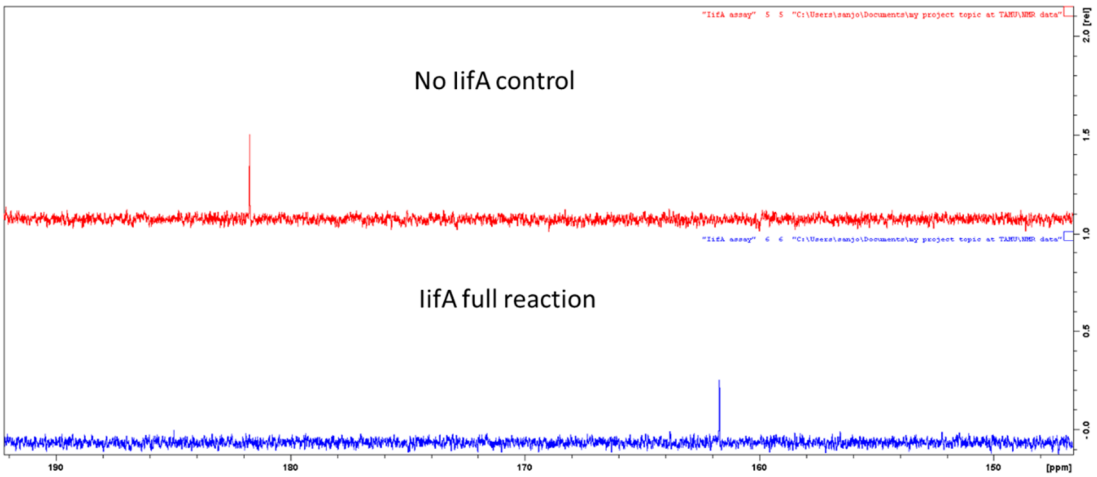

Figure 7.10: 13-C NMR of IifA catalyzed reaction using 13C labeled substrate.

Since the chemical shift value of the unknown carbon fragment is very similar to that of reported chemical shift value of bicarbonate, we ran an NMR sample where IifA reaction mixture is mixed with standard bicarbonate. Under this condition we could see only one peak at 162 ppm thus confirming bicarbonate to be the product in the IifA catalyzed reaction.

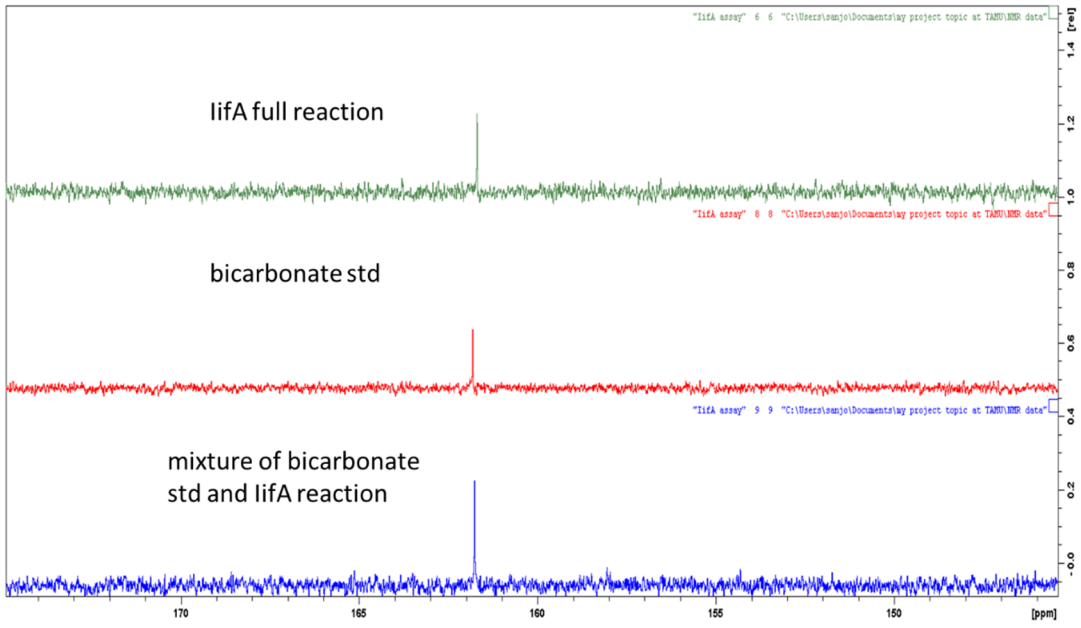

Figure 7.11: 13-C NMR of IifA catalyzed reaction using 13C2 labeled substrate.

7.2.9 Evidence for isatoic anhydride as the intermediate in the IifA catalyzed reaction

To test our proposal of isatoic anhydride being the intermediate in the IifA catalyzed reaction isatoic anhydride was incubated with IifA and the reaction mixture was analyzed by HPLC. As shown in figure 7.12, there was complete consumption of isatoic anhydride in the full reaction and formation a new peak having similar retention time as that of anthranilic acid. The identity of the new peak as anthranilic acid was confirmed by LC-MS and coelution experiment.

A)

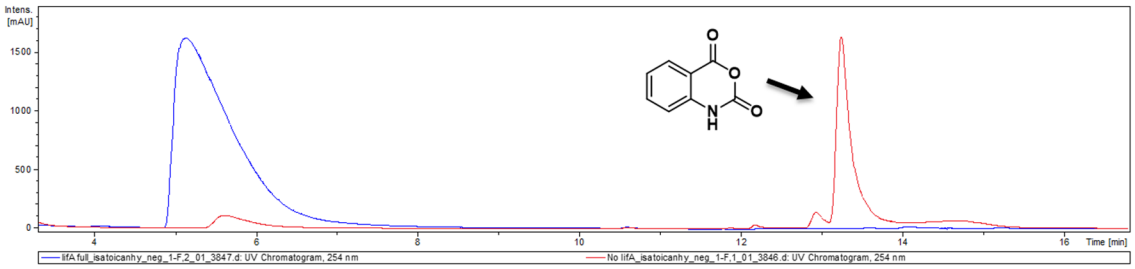

B)

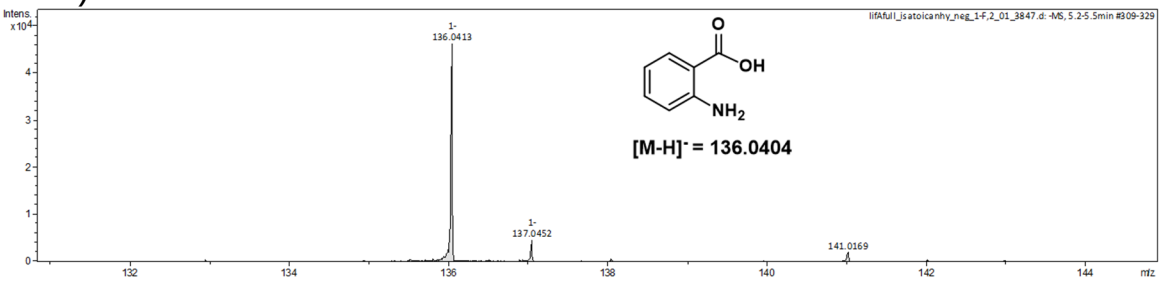

C)

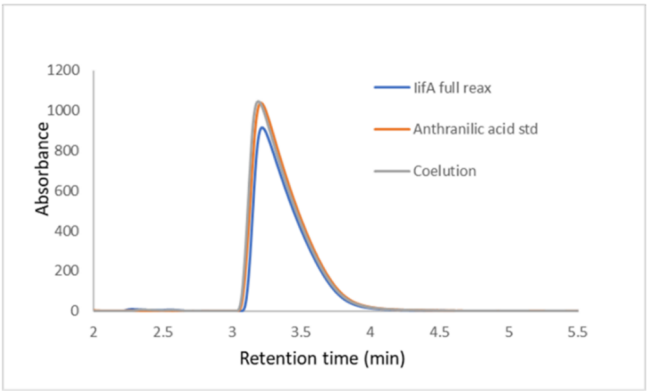

Figure 7.12: Isatoic anhydride as chemically competent intermediate of IifA catalyzed reaction. A) LC chromatogram showing the conversion of isatoic anhydride to anthranilic acid B) Mass of the reaction product matches with the mass of anthranilic acid C) coelution with a standard anthranilic acid

7.2.10 Evidence for incorporation of oxygen atom from molecular oxygen to bicarbonate

According to our mechanistic proposal, one oxygen atom from molecular oxygen gets incorporated into bicarbonate. To test this proposal bicarbonate generated in the IifA catalyzed reaction was derivatized with phosphoenolpyruvate in the presence phosphoenolpyruvate carboxylase.[95] Oxaloacetate **163** thus formed is further derivatized by PFBHA to give oxime **164**. Thus, by running the IifA catalyzed reaction using 13-C labeled substrate under $^{18}O_2$ atmosphere and monitoring the mass of the final PFBHA adduct we can confirm whether oxygen atom from molecular oxygen gets incorporated to bicarbonate. Indeed, the mass corresponding to single 18O label incorporation in the final adduct was observed.

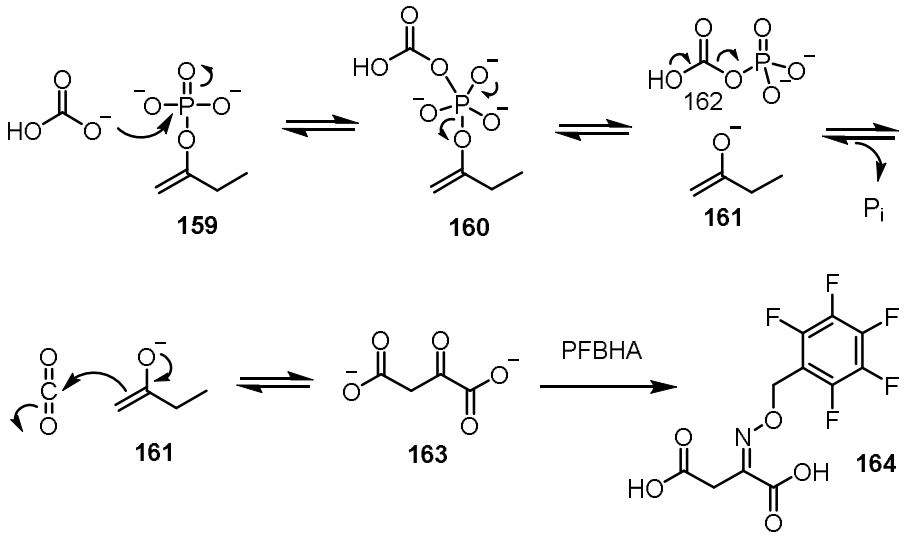

Figure 7.13: PEP carboxylase catalyzed reaction was used to trap bicarbonate generated in the IifA catalyzed reaction

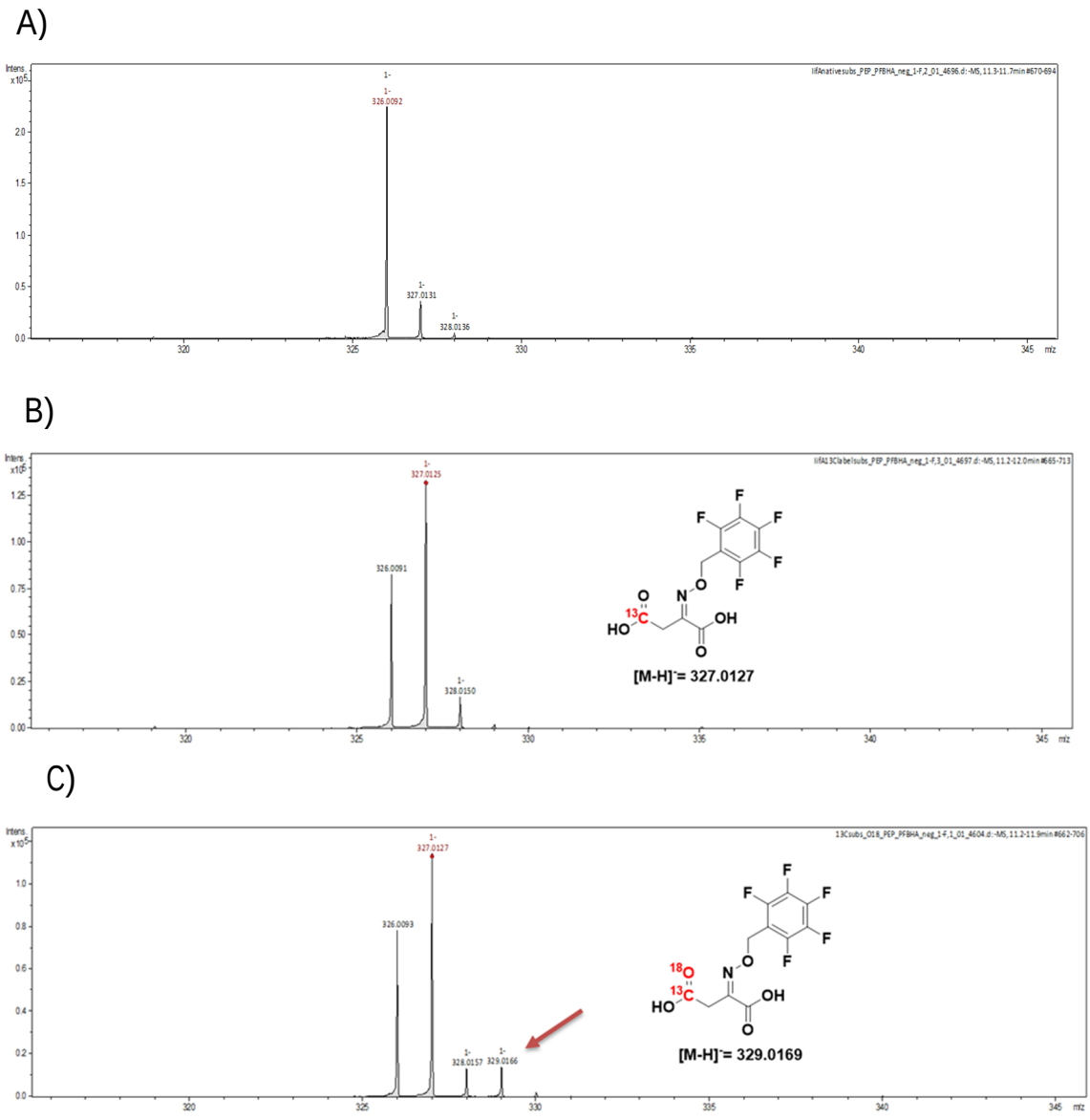

Figure 7.14: LC-MS analysis of oxaloacetate-PFBHA adduct. A) Mass of the oxaloacetate-PFBHA adduct when the IifA catalyzed reaction was carried out using unlabeled substrate in $^{16}O_2$ atmosphere. B) Mass of the oxaloacetate-PEFHA adduct when the IifA catalyzed reaction was carried out using 13-C substrate in $^{16}O_2$ atmosphere C) Mass of the oxaloacetate-PEFHA adduct when the IifA catalyzed reaction was carried out using 13-C labeled substrate in $^{18}O_2$ atmosphere.

7.2.11 Evidence for no involvement of metals in the IifA catalyzed reaction.

Although the amino acid sequence predicts IifA to be a cofactor-independent oxygenase to provide experimental evidence in support of the claim IifA catalyzed reaction was carried out in the presence of chelating agent EDTA and D-(-)-penicillamine. Indeed, no inhibition of activity was observed when the chelating agents were present in the reaction mixture, thus suggesting the absence of metal ions. This was further confirmed by ICP-MS analysis.

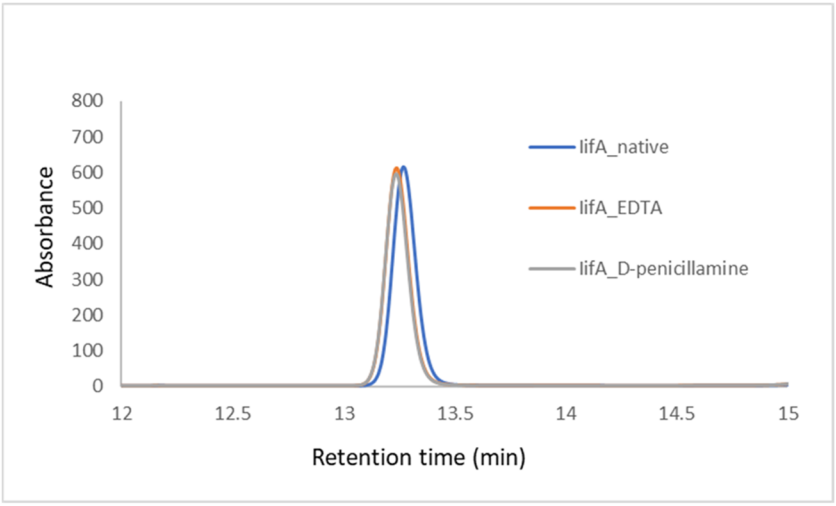

Figure 7.15: HPLC analysis of the IifA catalyzed reaction in the presence of chelating agents: EDTA and D-(-)-penicillamine.

7.3 Conclusion

Our mechanistic studies on the IifA catalyzed reaction support a Baeyer-Villiger type rearrangement, first of its kind, in a cofactor-independent enzyme. We have shown that the reaction goes via the isatoic anhydride intermediate; identified bicarbonate as the reaction product; labeling experiments with $H_2{}^{18}O$ and $^{18}O_2$ showed that the oxygen atom from water was incorporated into the anthranilic acid product while an oxygen atom from molecular oxygen incorporated into carbon dioxide. Till now reported enzymatic Baeyer-Villiger reactions are carried out either in the presence of flavin or metals ions. Cyclohexane monooxygenase is the prototype of flavin dependent Baeyer-Villiger oxygenases (BVMOs). Apart from Cyclohexane monooxygenase flavin dependent Baeyer-Villiger rearrangements have also been reported in CcsB catalyzed[96] carbonate formation in the biosynthesis of cytochalasins; LgnC catalyzed[97] oxygen insertion reaction during legonmycin biosynthesis. Amongst the metal dependent Baeyer-Villiger oxygenases, TflA[22] uses manganese during toxoflavin degradation while AflN[20, 21] and brassinolide synthase[98] use heme-Fe during aflatoxin and brassinolide biosynsthesis. Characterization of IifA as a cofactor independent Baeyer-Villiger oxygenase expands the repertoire of enzyme catalyzed Baeyer-Villiger reactions.

7.4 Experimental Procedure

Materials

All chemicals were purchased from Sigma-Aldrich unless mentioned otherwise. LB broth (Lennox) was purchased from EMB Millipore. kanamycin and IPTG were obtained from Lab Scientific Inc. Amicon Ultra centrifugal filter devices (10,000 MWCO) were obtained from Millipore. Histrap column was obtained from GE Healthcare. Econo-Pack 10DG desalting columns were purchased from Bio-Rad. 2.5 L baffled ultra yield flasks for protein overexpression were obtained from Thomson Instrument Company. HPLC and LC-MS solvents were purchased from EMD and were used without further purification. ZORBAX Eclipse XDB-C18 column (15 cm x 4.6 mm, 5 μm particles) was purchased from Agilent Technologies.

Over-expression and purification of IifA

The *iifA* gene containing overexpression plasmid (pTHT-IifA) was transformed into *Escherichia coli* BL21 (DE3). For the overexpression of the protein, a starter culture was grown overnight in 15 ml of LB medium containing 40 μg/ml of kanamycin at 37 °C. 1.5 liter of LB medium (20 g/L) containing 40 μg/ml of kanamycin, was inoculated with this starter culture. The cells were grown at 37 °C with shaking (220 rpm) until the culture reached an OD_{600} of 0.6. The culture was then incubated at 4°C for ~45min without shaking. Then the culture was induced by adding IPTG to a final concentration of 0.5 mM, the temperature was lowered to 15 °C and the cells were grown with shaking (180 rpm)

for a further 15 hours. The cells were then harvested by centrifugation at 10,000g for 10 min at 4 °C and store at -80 ˚C.

The cell pellet was re-suspended in 30 ml of lysis buffer (50 mM KH_2PO_4, 150 mM NaCl, 10 mM imidazole, pH 8.0). Lysozyme (5 mg) was added and the cells were lysed by sonication on ice (Misonix Sonicator 3000, six cycles of 30 s duration during which 1.5 s sonicator pulses at output level 0.8 were followed by 1.5 s pauses). The resulting suspension was centrifuged (18,000 rpm, 30 min) and the supernatant was filtered through a sterile syringe filter (pore size 0.45 μm). The clarified supernatant was loaded onto a 5 mL Ni-NTA-affinity column pre-equilibrated with lysis buffer kept at 4°C. The Ni-NTA-affinity column was then washed with 50 ml wash buffer (50 mM KH_2PO_4, 150 mM NaCl, 20 mM imidazole, pH 8.0). The protein was eluted from the column with elution buffer (50 mM KH_2PO_4, 150 mM NaCl, 200 mM imidazole, pH 8.0) at 4°C. The fractions containing protein were pooled and concentrated using YM-10 Amicon ultracentrifugal filters at 5000g to a final volume of 3 mL. The concentrated sample was buffer exchanged, using an Econo-Pac 10DG desalting column, into 100 mM phosphate buffer at pH 7.5 containing 100 mM NaCl and glycerol to a final concentration of 15%.

HPLC parameters LC-MS parameters

Same as mentioned in Chapter V.

Activity assay of IifA catalyzed reaction

The IifA catalyzed reaction was performed in 100 mM phosphate buffer, pH 7.5. The final concentrations of all the reaction components were as follows: IifA (50 μM), 3-hydroxyindolin-2-one **147** (500 μM). The protein was heat-denatured and removed by

centrifugal ultrafiltration through a 10 kDa MWCO membrane (Pall Life Sciences). The samples were analyzed by HPLC and LC-MS.

IifA catalyzed reaction in the presence of $H_2{}^{18}O$ and $^{18}O_2$

Two identical reactions were set up; each 200 µL solution contained 500 µM hydroxyindolin-2-one **147**, and IifA (50 µM). One of the samples had a final concentration of 80% $H_2{}^{18}O$. The other sample was used as a 'control' and contained 100% $H_2{}^{16}O$. The reaction mixture was incubated at room temperature for 4 hours after which both the samples were analysed by LC-MS.

Two identical reaction mixtures were made in a glove box; each 200 µL solution contained 500 µM hydroxyindolin-2-one **147**, and IifA (50 µM). One of the reaction mixtures was exposed to $^{18}O_2$ while the other reaction mixture was used as a 'control' and exposed to $^{16}O_2$. The reaction mixture was incubated at room temperature for 4 hours and then analyzed by LC-MS.

Synthesis of 13-C2 labeled 147

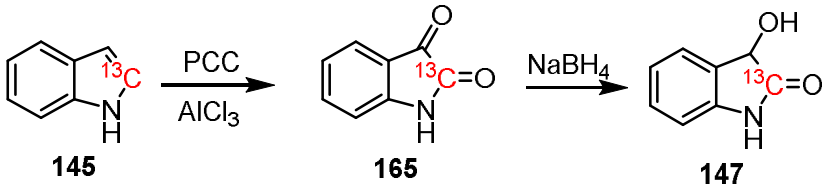

145 165 147

Figure 7.16: Synthetic scheme for 13-C2 labeled **147**.

A solution of indole **145** (100 mg, 0.85 mmol, 1 eq) in 1,2-dichloroethane (DCE) (10 mL) was added to a solution of pyridinium chlorochromate (PCC) (1.5 g, 6.8 mmol, 8 eq) in DCE (10 mL) followed by aluminum chloride (34 mg, 0.25 mmol, 0.3 eq). The reaction mixture was heated at 80 C for 2 h and was concentrated to dryness. Silica gel column chromatography (EtOAc-hexane,1:1) yielded compound **165** as a yellow powder (50% yield). The spectroscopic data were identical to those previously reported.

Sodium borohydride (8 mg, 0.22 mmol, 1.1 eq) was added portion wise to a solution of isatin **165** (30 mg, 0.20 mmol, 1 eq) in EtOH (95%, 4 mL) at 0 ºC and the reaction mixture was stirred at 0 ºC for 20 min. The resulting suspension was poured into cold water (10 mL), acidified (pH 5) using HCl and extracted with EtOAc. The combined extracts were concentrated and the residue was subjected to silica gel column chromatography (EtOAc-hexane, 1:1) to yield compound **147** as light yellow solid (60% yield). The spectroscopic data matched with those previously reported.

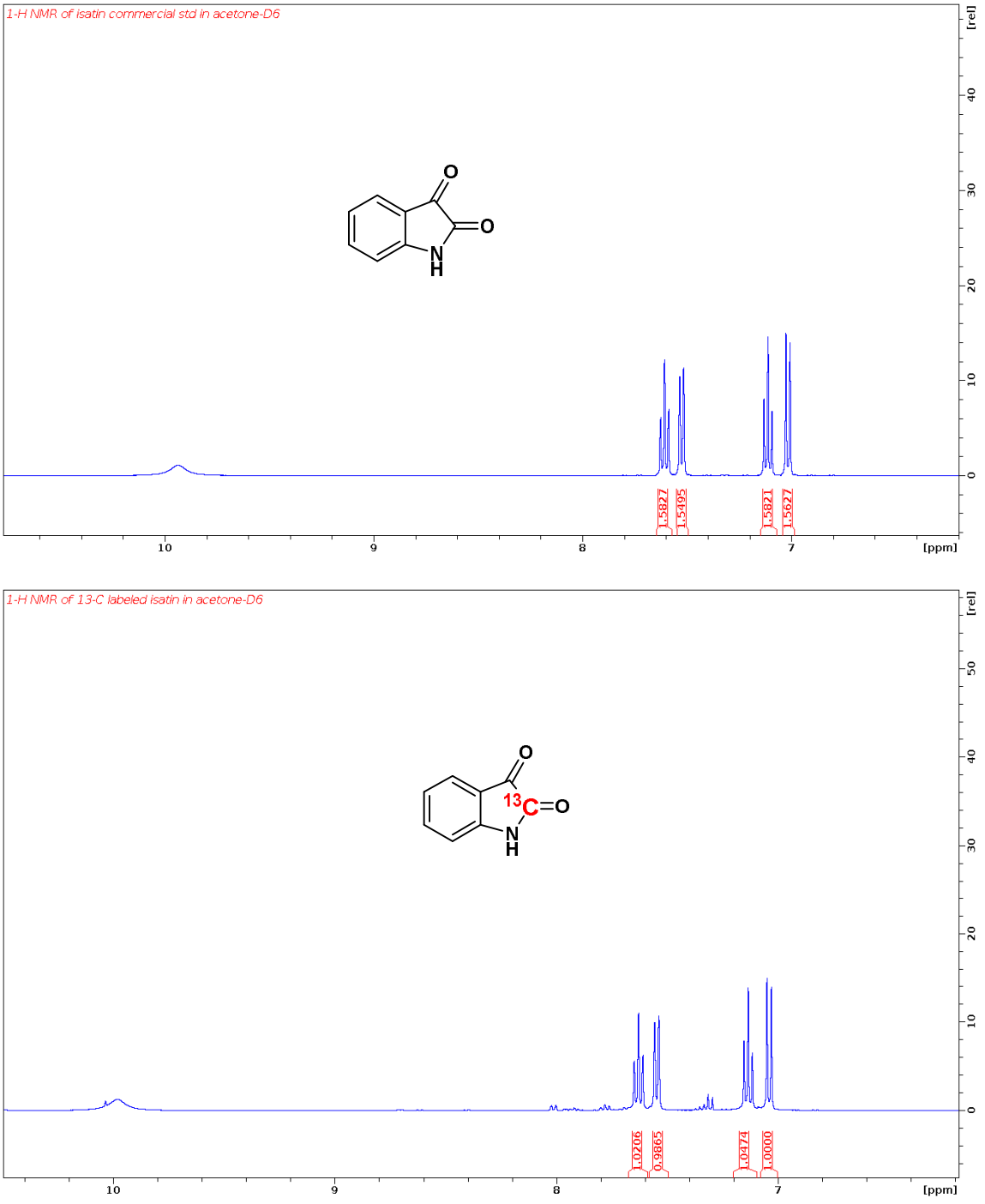

Figure 7.17: 1-H NMR of unlabeled and 13-C2 labeled isatin **165**

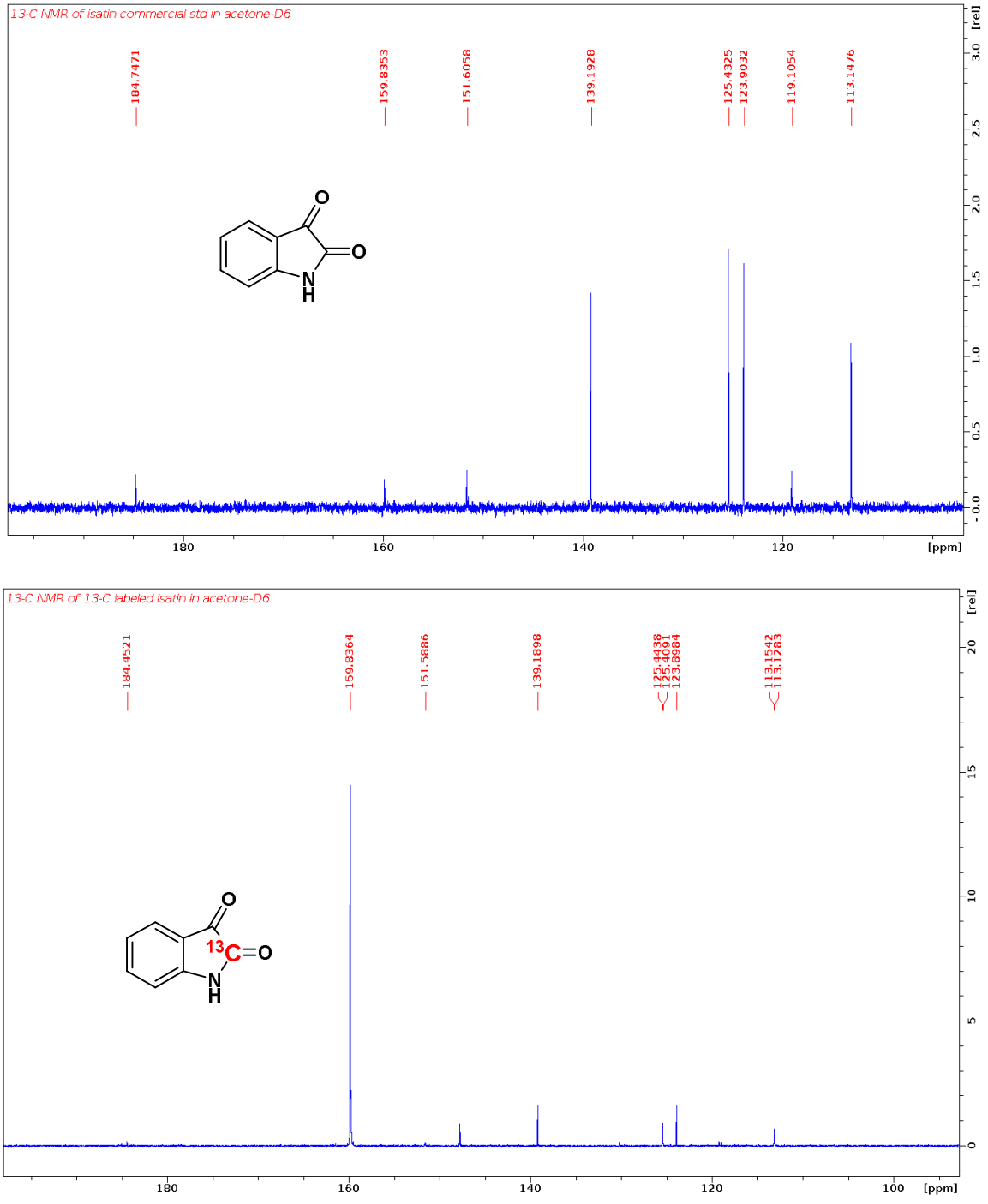

Figure 7.18: 13-C NMR of unlabeled and 13-C2 labeled isatin **165**

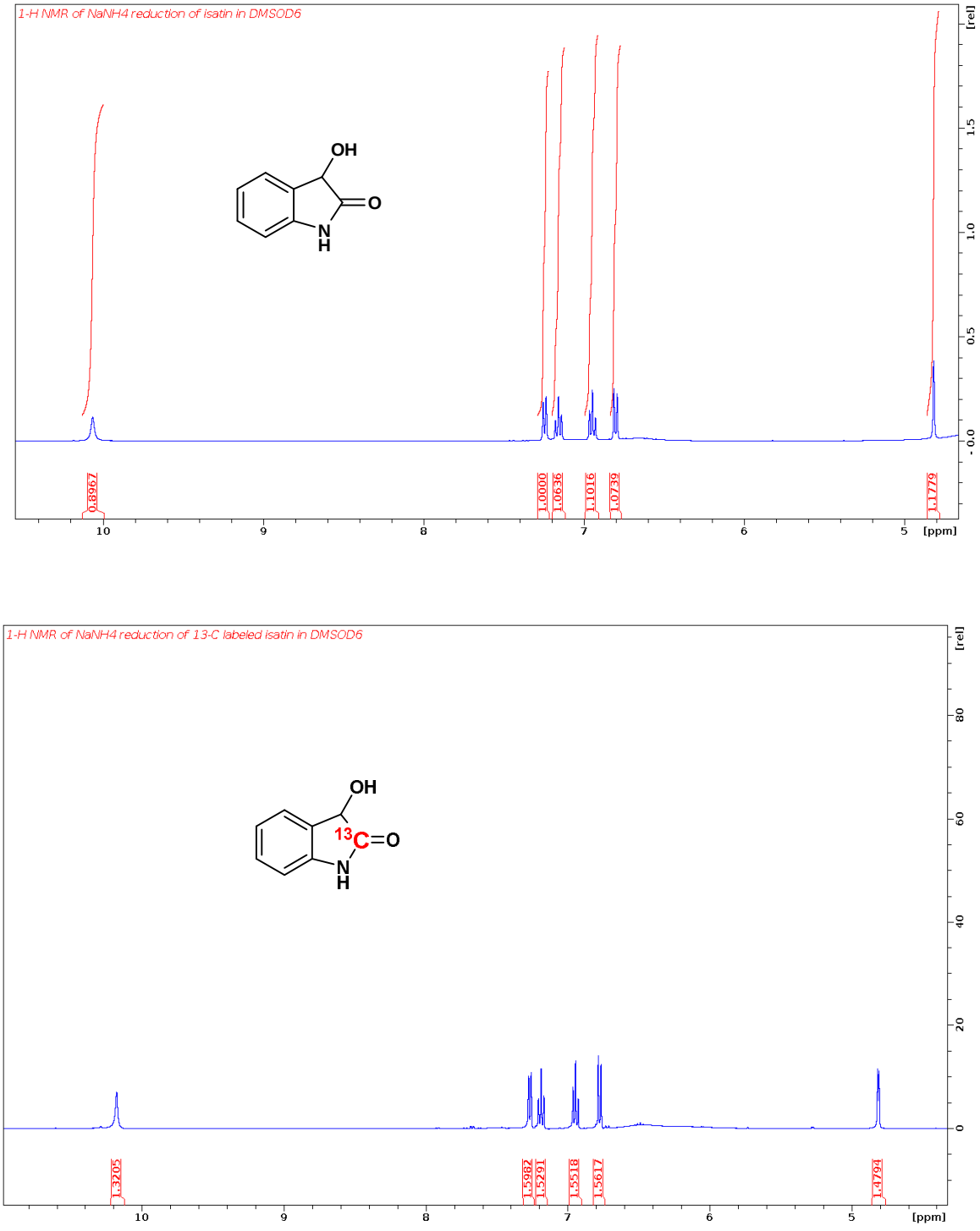

Figure 7.19: 1-H NMR of unlabeled and 13-C2 labeled **147**

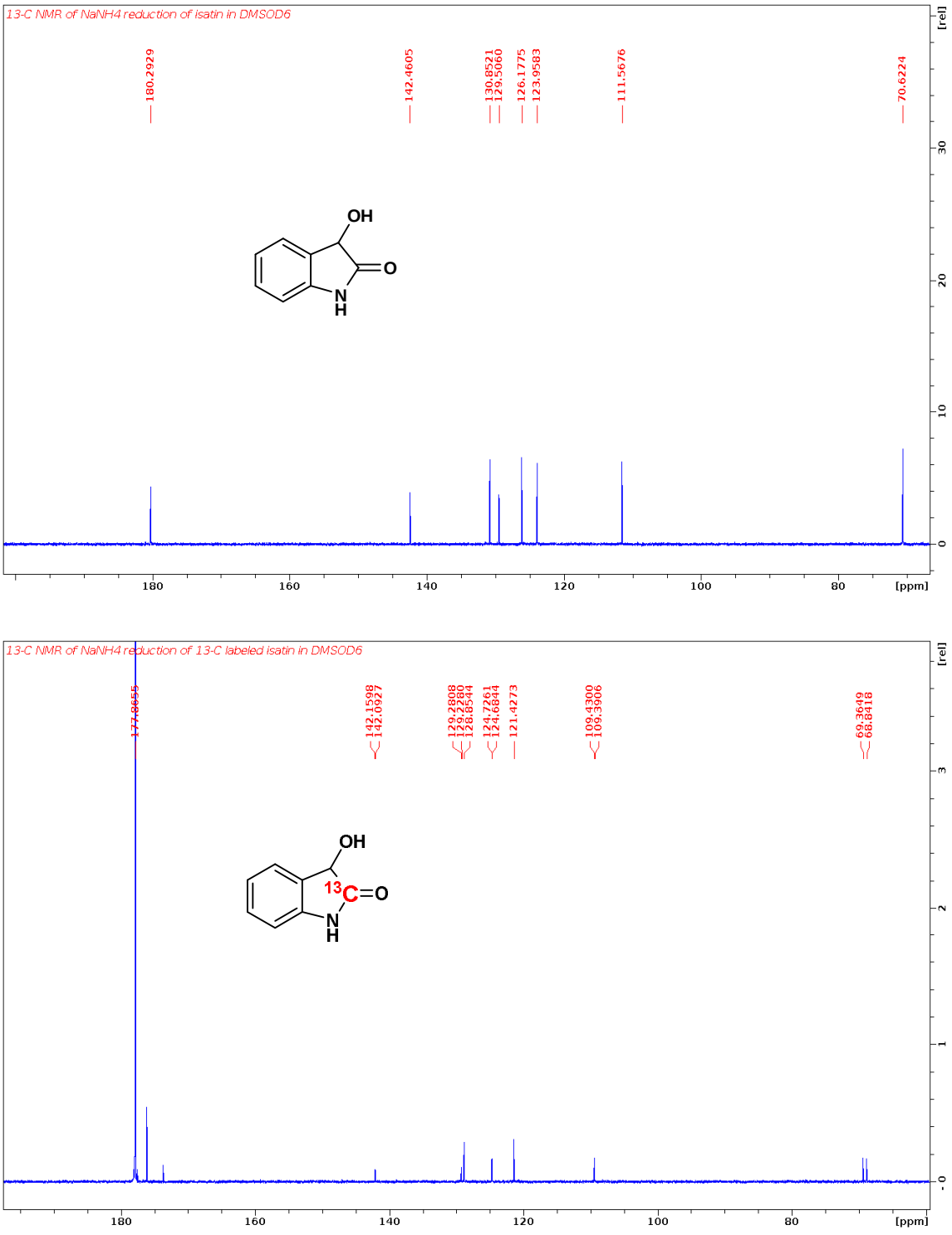

Figure 7.20: 13-C NMR of unlabeled and 13-C2 labeled **147**

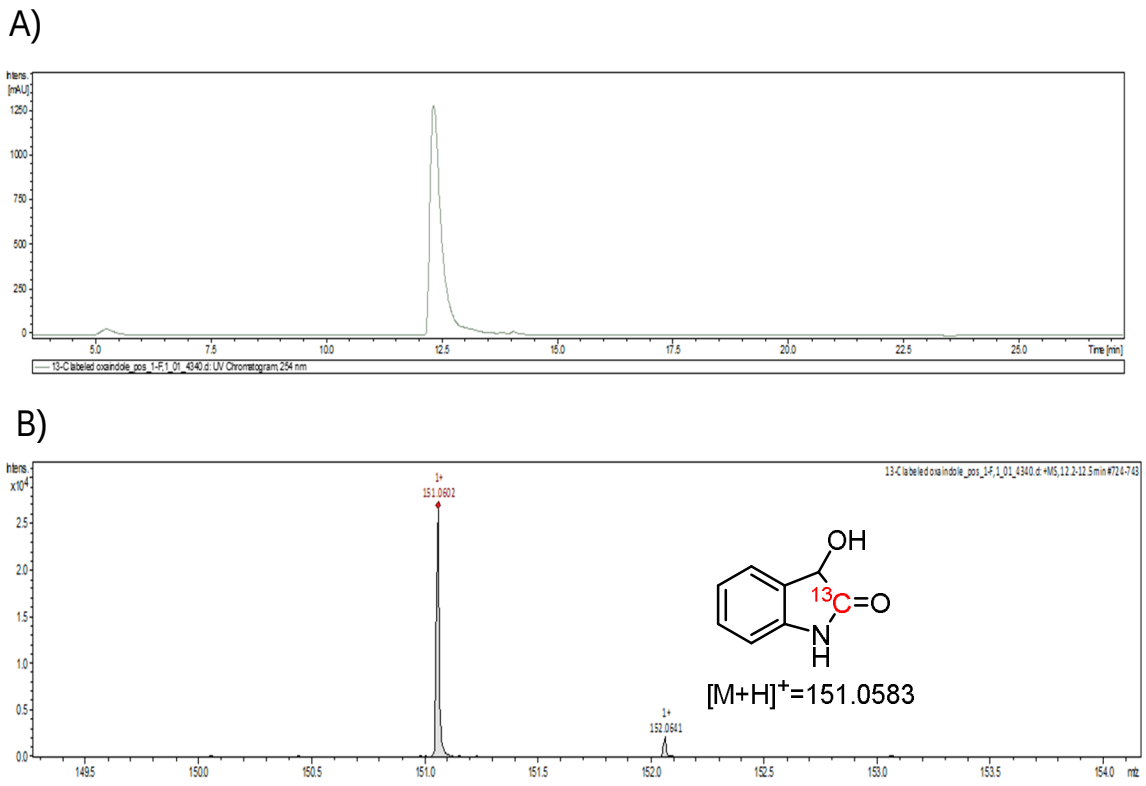

Figure 7.21: LC-MS analysis of synthesized 13-C2 labeled **147**. A) Extracted ion chromatogram (EIC) for $[M+H]^+$= 151.0583 Da indicating formation of **147**. B) Exact mass is consistent with the expected mass of compound **147** ($[M+H]^+$= 151.0583 Da).

CHAPTER VIII

IDENTIFICATION OF A LUMICHROME CATABOLIC PATHWAY IN *PIMELOBACTER SIMPLEX*

8.1 Introduction

Riboflavin is an important vitamin which is converted to FMN and FAD cofactors which carry out plethora of chemical reactions. Over the years there have been extensive studies on the biosynthesis of riboflavin and at present we have an advanced understanding. Unlike the biosynthesis, however, there is not much studies on the catabolic pathway of riboflavin. Previously Foster group in 1944 identified a soil bacterium named *Pseudomonas riboflavina* which degraded riboflavin to lumichrome and ribitol.[99] In 1965, the Stadtman group demonstrated that cell-free enzyme preparations from a *Pseudomanas* RF strain could degrade the isoalloxaxine ring of riboflavin (**166**) to give compound **168** which is converted to compound **169** releasing ribose (**170**) (Figure 8.1).[100] Compound **169** was degraded further to the lactone (**171**) and urea, and CO_2. Some intestinal bacteria are reported to produce **172** from riboflavin under strictly anaerobic condition. Despite these initial studies none of the enzymes responsible for the degradation of lumichrome were characterized. Loss of bacterial strains which were reported to degrade riboflavin hindered future studies.

In a recent breakthrough our lab has identified a bacterial strain (*Microbacterium maritypicum* G10) which can grow on riboflavin using it as a carbon source. The catabolic

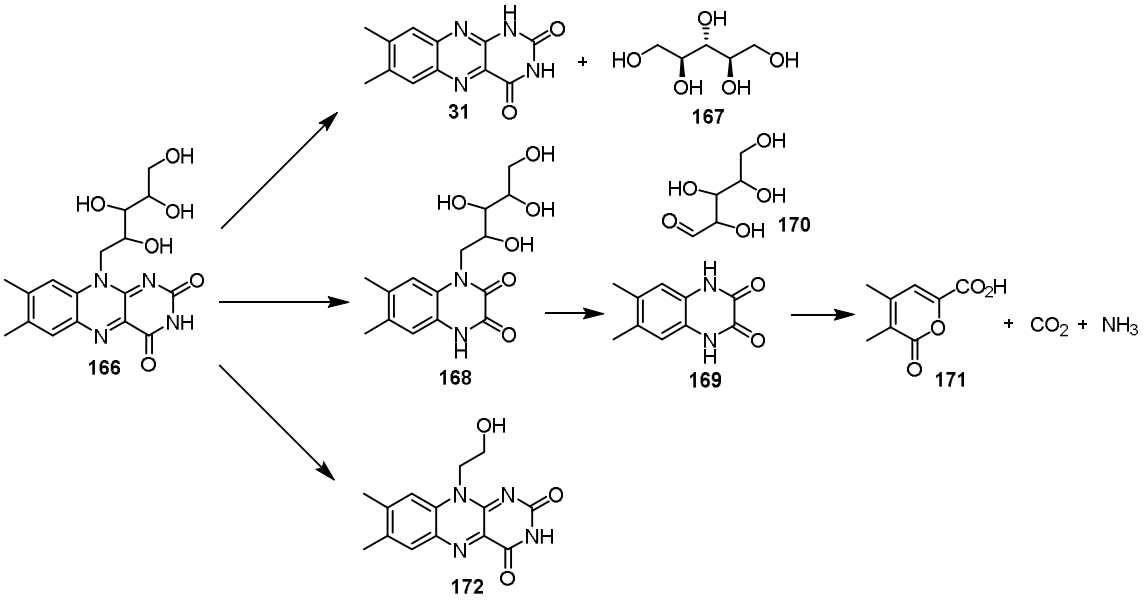

Figure 8.1: Previously reported degradation pathways of riboflavin.

gene cluster was identified based on the screening of cosmid library in *Streptomyces Lividans* and all the enzymes in the pathway were characterized (Figure 8.2).[101] RcaE catalyzes the conversion of riboflavin to lumichrome and ribose and the reaction proceeds via a hydrogen atom abstraction by superoxide radical, the first example of such chemistry in flavoenzymolgy. However, *Microbacterium maritypicum* G10 could not degrade lumichrome further. In this section we describe a) the identification of a bacterial strain that catabolizes lumichrome, b) identification of the gene cluster responsible for the catabolism and c) in vitro reconstitution of the initial three enzymes associated in the pathway.

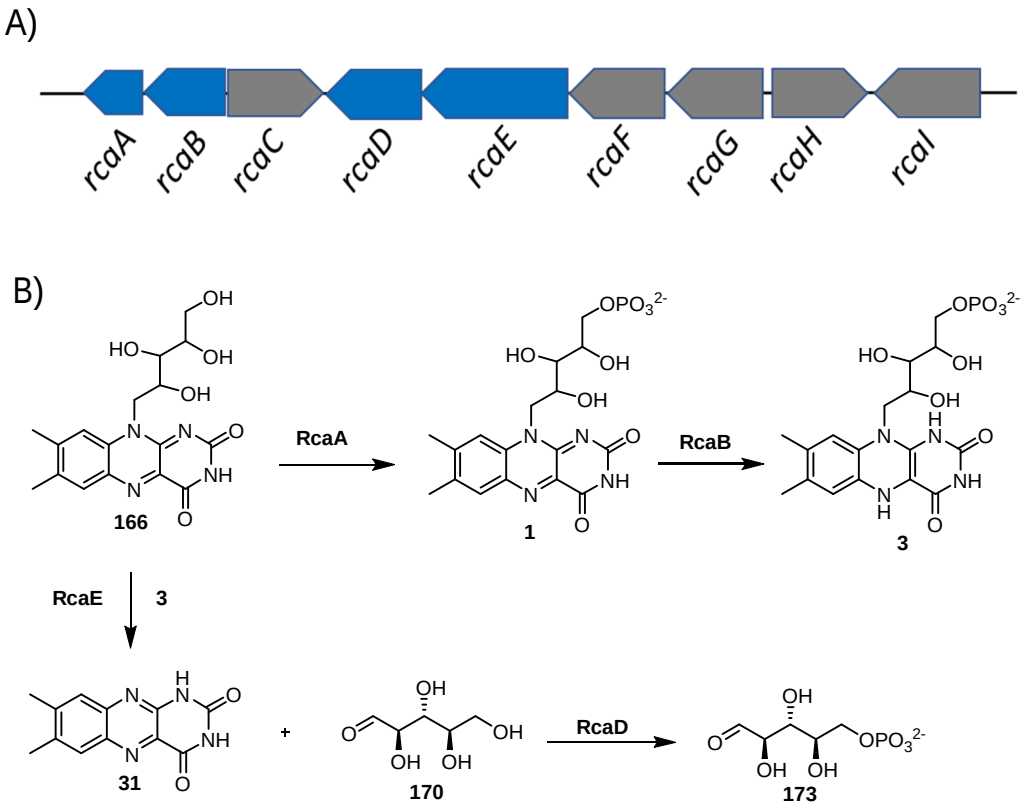

Figure 8.2: Riboflavin catabolism in *Microbacterium maritypicum* G10. A) Riboflavin catabolic gene cluster. B) Proposed degradation pathway.

8.2 Results and discussion

8.2.1 Identification of the lumichrome catabolic strain

In search for a lumichrome catabolic strain we obtained a soil sample from a vitamin factory. Screening of the soil sample by culturing in a defined base metal media with lumichrome as the sole carbon and nitrogen source led to the identification of a lumichrome catabolic strain. The strain was later confirmed as *Pimelobacter simplex* based on 16s rRNA sequencing. *Pimelobacter simplex* ATCC 6946 for which genome sequence is available was also tested for its ability to grow on lumichrome. Indeed,

Pimelobacter simplex ATCC 6946 could grow on lumichrome using it as a carbon and nitrogen source (Figure 8.3).

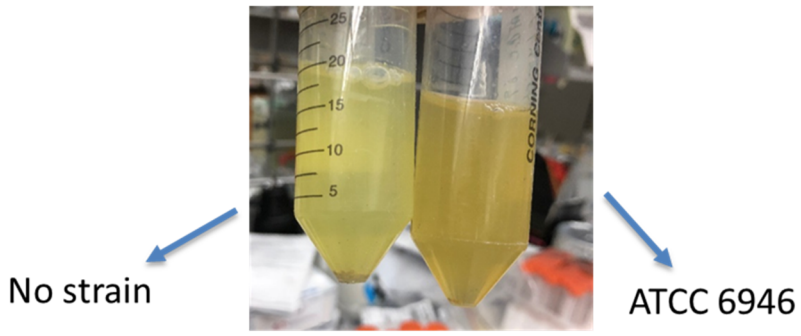

Figure 8.3: Lumichrome degradation by *Pimelobacter simplex* ATCC 6946.

8.2.2 Metabolite analysis and bioinformatics to figure out the catabolic gene cluster

To figure out the identity of degraded metabolites, we analyzed the small molecules from the culture media when *Pimelobacter simplex* was grown in the presence of base metal media and lumichrome. Identification of compound **174** as one of the degraded products (Figure 8.4) gave us a hint that catabolism starts from the alloxan ring of the molecule and probably a hydrolase plays a role in it. To search for the candidate hydrolase, we look for homologous enzymes which carry out cyclic amide bond hydrolysis reactions. These enzymes include dihydropyrimidinase and barbiturase catalyzed reaction during uracil catabolism; HIU hydrolase catalyzed reaction during aerobic purine catabolic pathway; cyanuric acid hydrolase catalyzed reaction in atrazine degradation pathway; hydrolase in NAD catabolic pathway; TflA catalyzed reaction in toxoflavin degradation pathway (Figure 8.5). Based on the exploration of homologous cyclic amidases with the relevant genomic context in *Pimelobacter simplex* we shortlisted two candidate genes which could

potentially catalyzed the initial step in the degradation of lumichrome. These are putative barbiturase (UniProt Id: A0A0A1DH55) and putative hydantoinase (UniProt Id: A0A0C5WZM1)

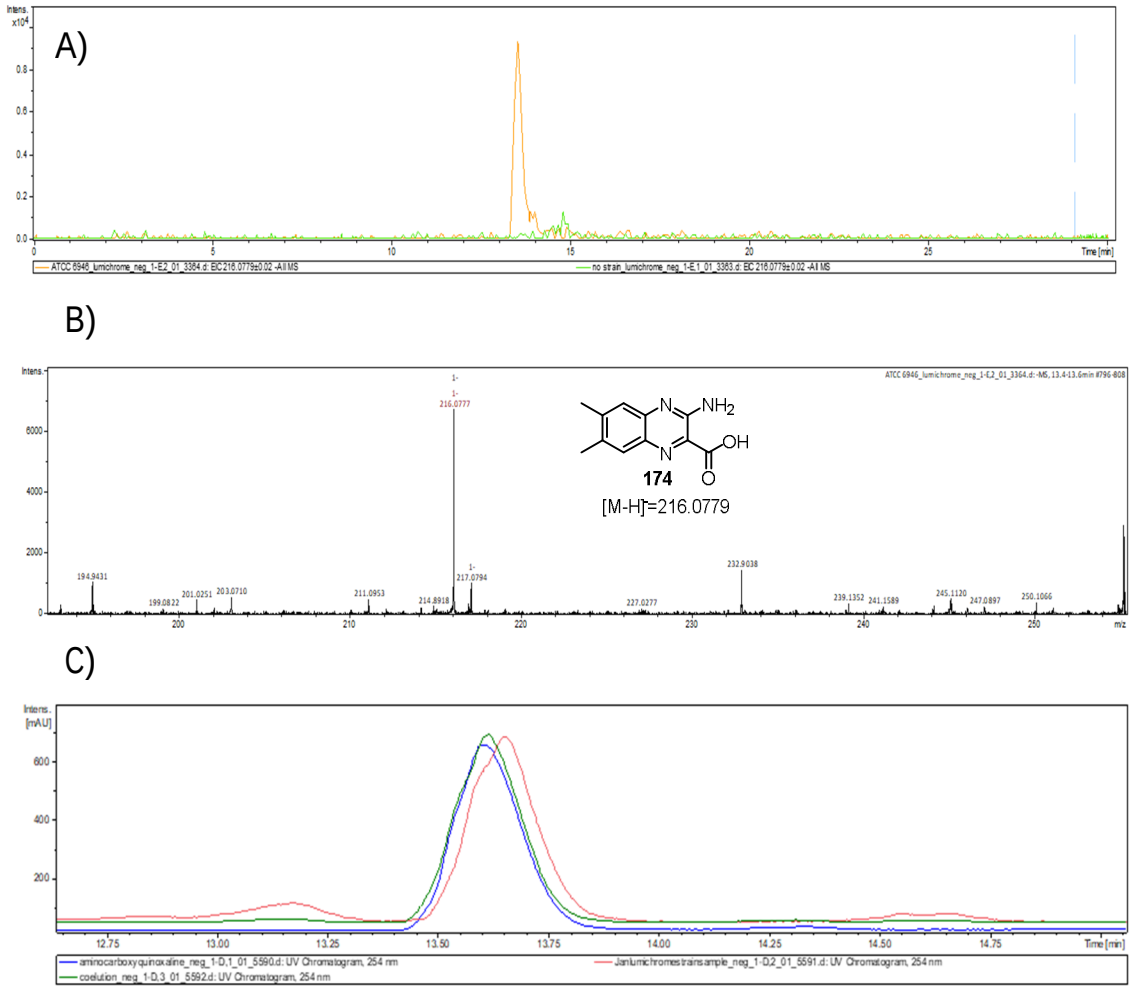

Figure 8.4: Characterization of compound **174** as one of the degradation products of lumichrome by *Pimelobacter simplex* A) Extracted ion chromatogram (EIC) for $[M-H]^-$= 216.0779 Da indicating formation of 174 B) Exact mass is consistent with the expected mass of compound **174** ($[M-H]^-$= 216.079 Da) C) Coelution experiment with a synthetically prepared **174**.

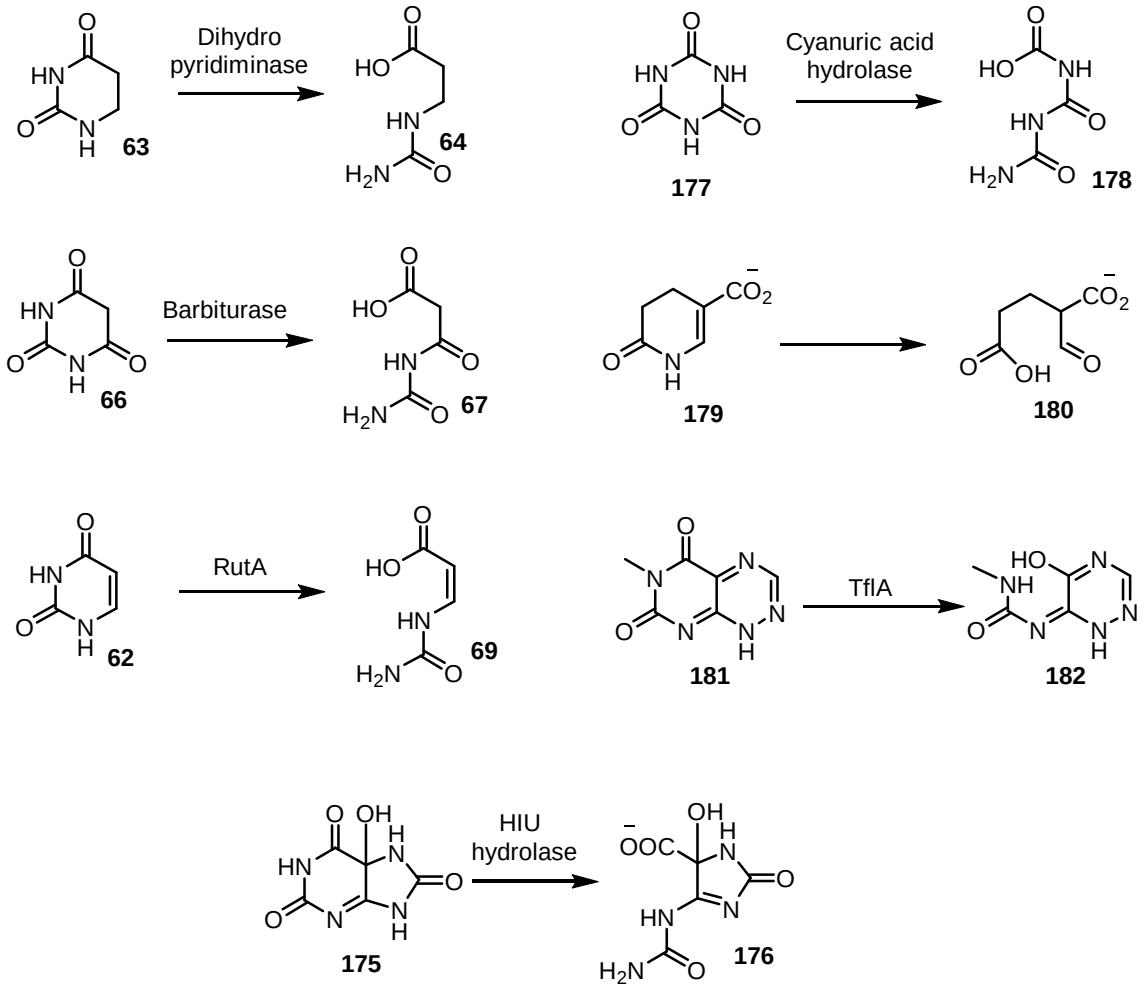

Figure 8.5: List of enzymes which carry out cleavage of cyclic amide bond.

8.2.3 Overexpression and purification of the putative barbiturase and hydantoinase

To check the activity of the putative barbiturase and hydantoinase, codon optimized barbiturase and hydantoinase genes were overexpressed in *E. coli* BL21(DE3) and purified by Ni-affinity chromatography. In both the cases soluble protein could be obtained in high yield.

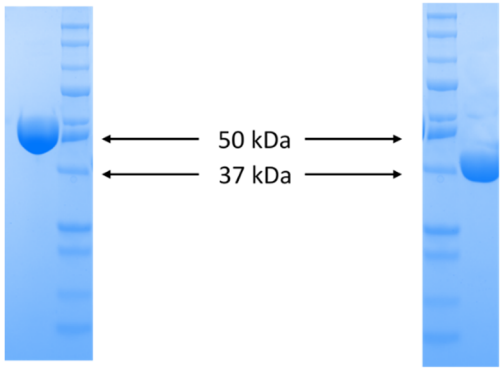

Figure 8.6: SDS-PAGE of purified hydantoinase and barbiturase. The molecular weight of hydantoinase and barbiturase are 50 kDa and 39 kDa.

8.2.4 Activity assay for the putative barbiturase and hydantoinase

Having the purified protein in hand lumichrome degrading activity was tested. When barbiturase was incubated with lumichrome we did not observe any substrate consumption. However, incubation of putative hydantoinase with lumichrome resulted in the consumption of lumichrome and formation of a new peak at 19.5 min under the HPLC condition (Figure 8.7). Riboflavin, FMN and FAD were tested as possible substrates for hydantoianse, however, in none of the cases activity was observed.

A)

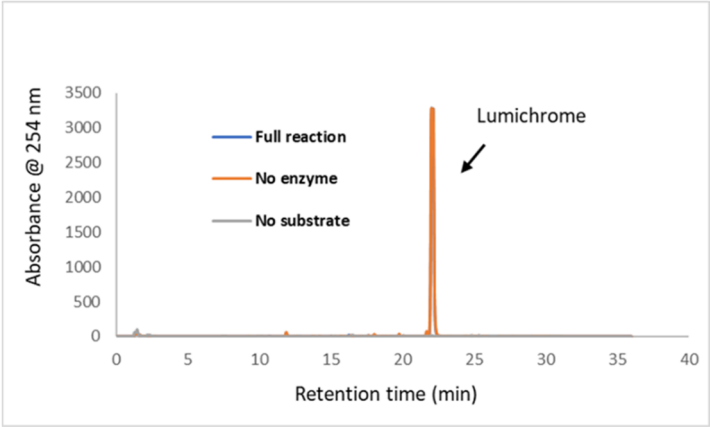

B)

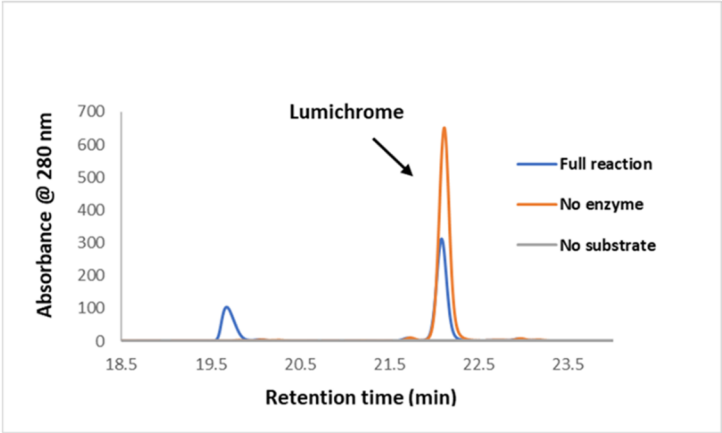

Figure 8.7: HPLC analysis of barbiturase (panel A) and hydantoinase (panel B) catalyzed reaction.

8.2.5 Characterization of the product formed in the hydantoinase catalyzed reaction.

There are two possible amide hydrolysis reaction in lumichrome as shown in figure 8.8. To characterize the product formed in the hydantoinase catalyzed reaction, the reaction mixture was subjected to LC-MS analysis. Mass of the new peak was 261 (in positive mode) and matches with the amide hydrolysis product **184**. The structure of the product

was further validated by the coelution experiment with a chemically synthesized molecule (Figure 8.9).

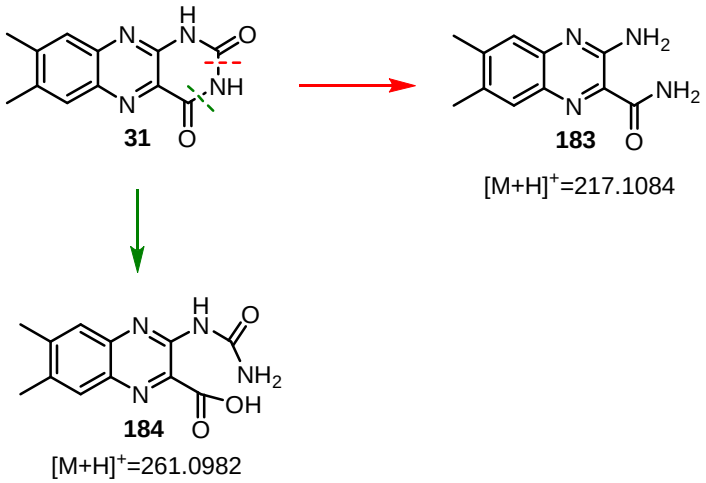

Figure 8.8: Possible products of the hydantoinase catalyzed reaction.

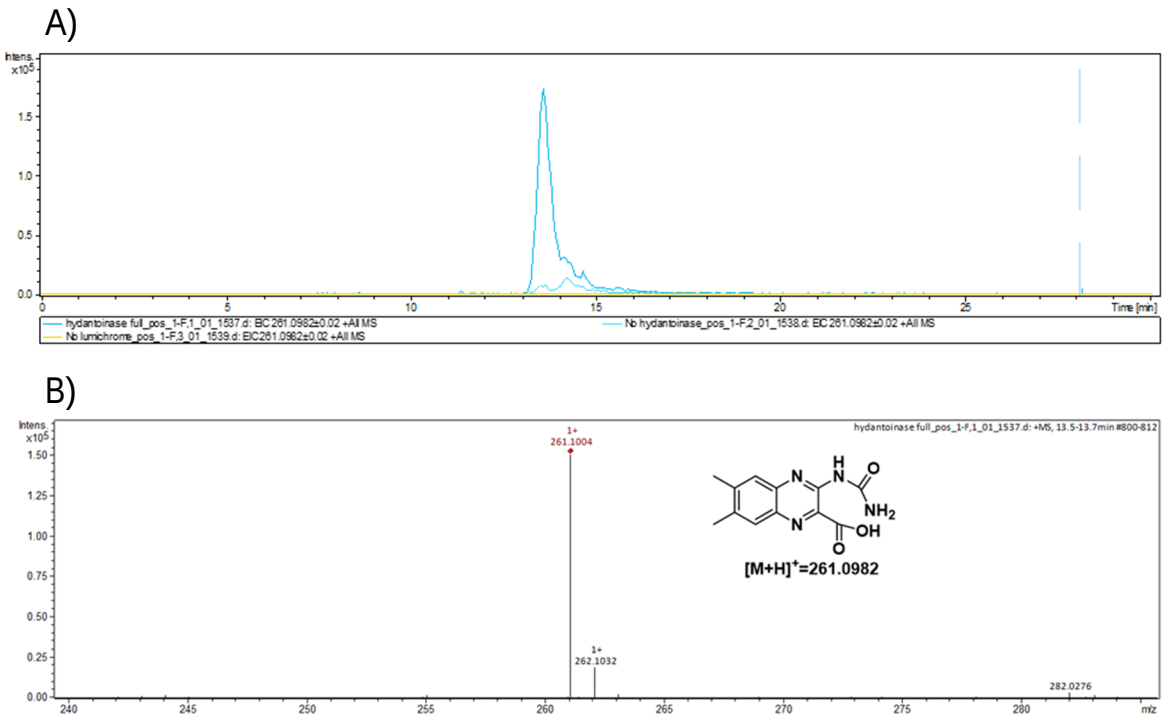

C)

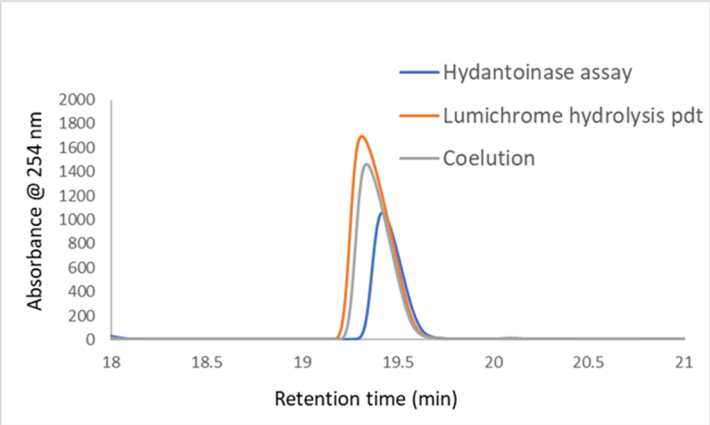

Figure 8.9: Characterization of hydantoinase catalyzed reaction product. A) Extracted ion chromatogram (EIC) for $[M+H]^+$= 261.0982 Da indicating formation of **184**. B) Exact mass is consistent with the expected mass of compound **184** ($[M+H]^+$= 261.0982 Da). C) Coelution experiment with a synthetically prepared **184**.

8.2.6 $H_2{}^{18}O$ labeling experiment for the hydantoinase catalyzed reaction

Since hydantoianse catalyzes amide hydrolysis reaction, the origin of oxygen atom in the product should be from water molecule. To test this, hydantoinse catalyzed reaction was carried out $H_2{}^{18}O$ containing buffer and the reaction mixture was analyzed by LC-MS. Indeed, the mass of the product shows 2 Da increase in mass. However, 4 Da increased mass was also observed (Figure 8.10). This could be rationalized based on the exchange of carbonyl oxygen in the substrate. Indeed, mass of the unreacted lumichrome showed 2 Da increase, implying exchange of one of the oxygen atoms (Figure 8.11).

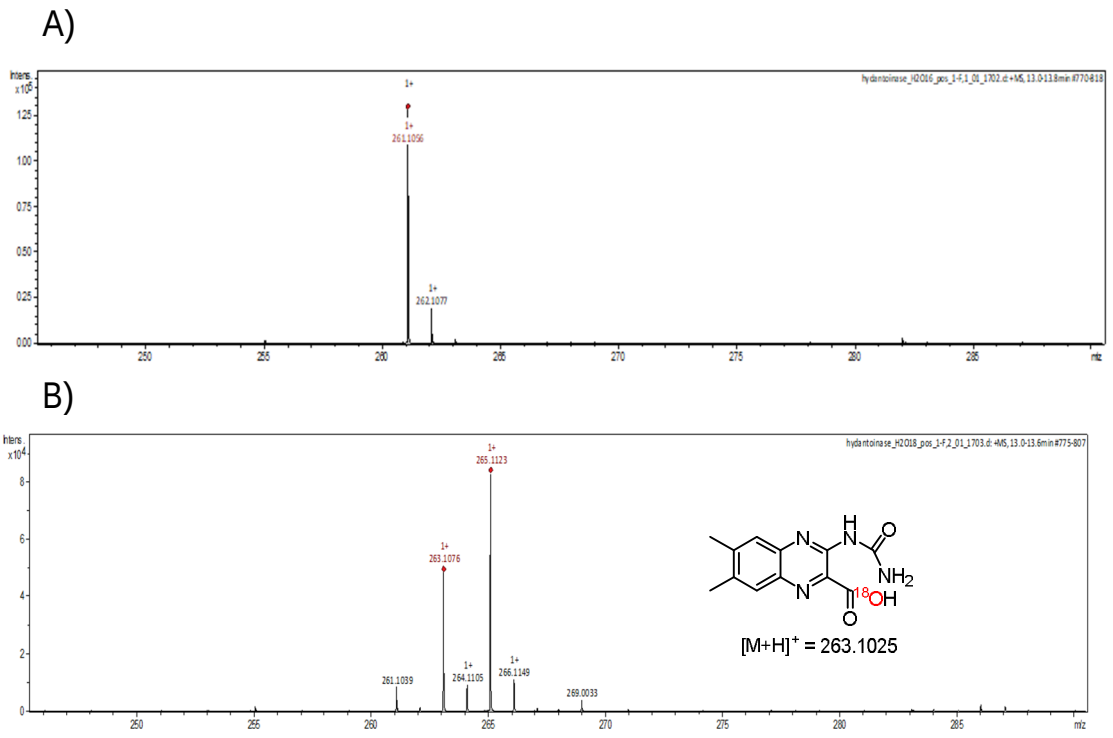

Figure 8.10: LC-MS analysis of the hydantoinase catalyzed reaction product using $H_2{}^{16}O$ (panel A) and 80 % $H_2{}^{18}O$ (panel B) buffer.

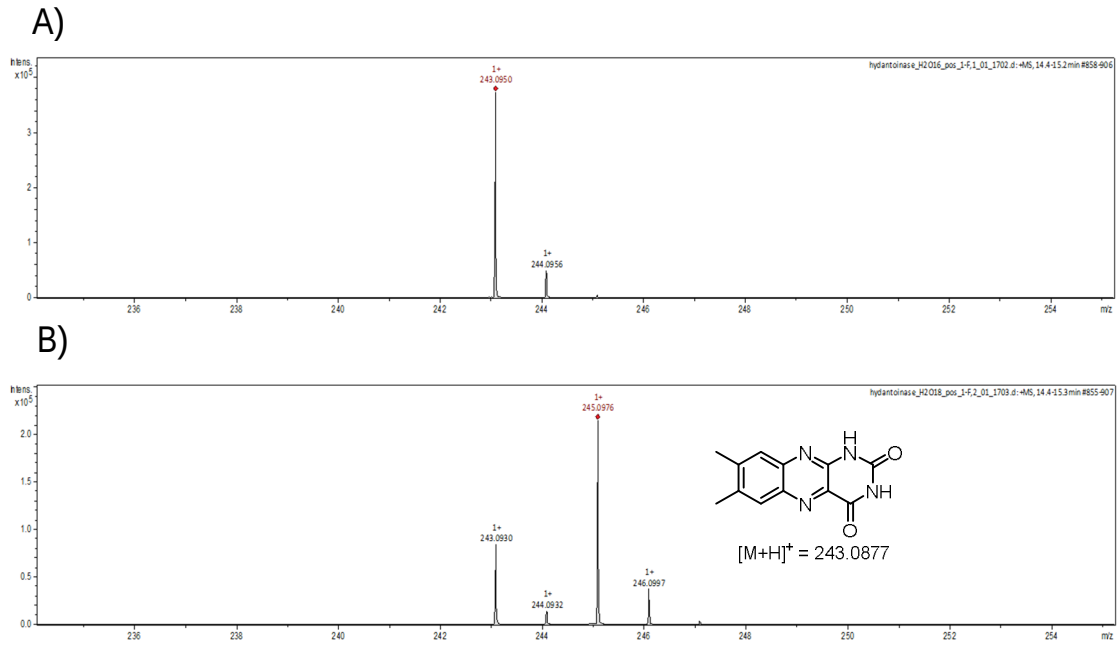

Figure 8.11: LC-MS analysis of unreacted lumichrome in the hydantoinase catalyzed reaction run in $H_2{}^{16}O$ (panel A) and 80 % $H_2{}^{18}O$ (panel B) buffer.

8.2.7 Overexpression and purification of the remaining hydrolase enzymes present in the genome neighborhood of the hydantoinase

Encouraged by the activity shown in the hydantoinase catalyzed reaction, we went for the overexpression and purification of the rest of the hydrolase enzymes present in the genome neighborhood of the hydantoinase (Figure 8.12). Although putative nicotinamidase (UniProt Id A0A0A1DRK3) and deacetylase (UniProt Id A0A0A1DPB8) could be obtained in soluble form with less yield; putative amidohydrolase (UniProt Id A0A0A1DP61) remains in inclusion body. To get the putative amidohydrolase in soluble form it was coexpressed with chaperon protein GroEL-GroES. Under this condition, soluble form of the amidohydrolase could be obtained in less yield (Figure 8.13).

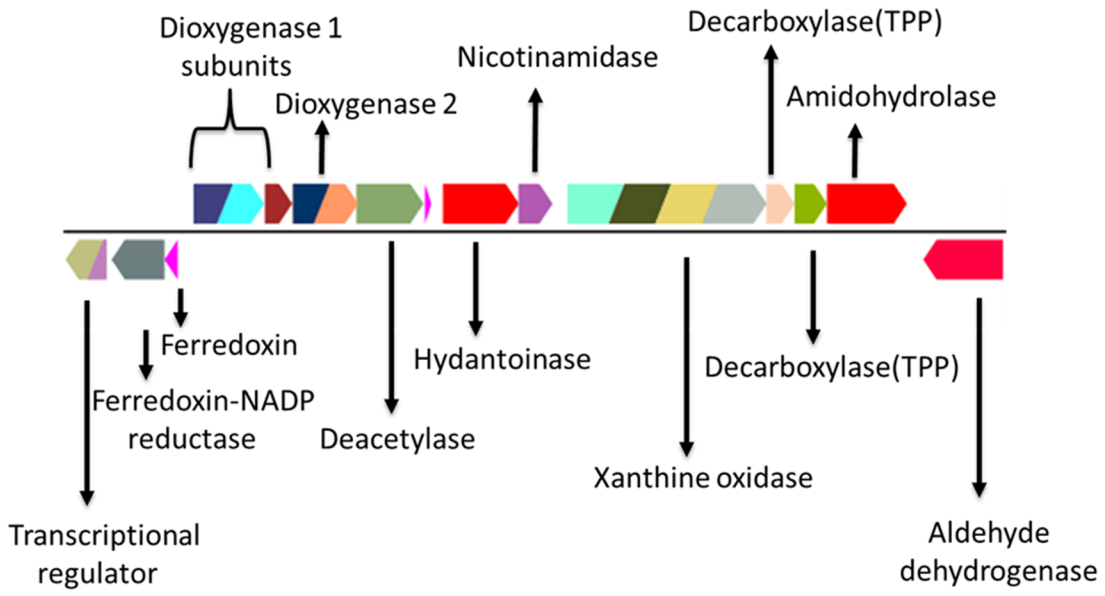

Figure 8.12: Genomic context of the hydantoinase in *Pimelobacter simplex*.

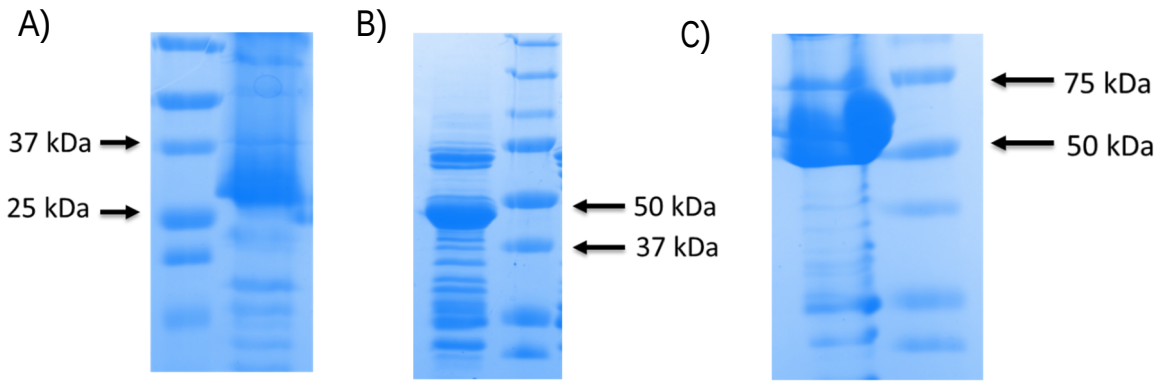

Figure 8.13: SDS-PAGE of partially purified putative niconimadiase, deacetylase and amidohydrolase. Molecular weights are 24 kDa, 43 kDa and 52 kDa respectively.

8.2.8 Activity assay of putative nicotinamidase

Having the three purified hydrolase enzymes in hand we went for testing their activity. Compound **184** was incubated with putative nicotinamidase, putative amidohydrolase and putative deacetylase separately and assay mixtures were analyzed by HPLC. Only nicotinamidase could convert compound **184** to a new compound (no substrate consumption was observed in amidohydrolase and deacetylase catalyzed reaction). The new compound was characterized as compound **174** based on LC-MS data and coelution experiment with a synthetically prepared standard (Figure 8.14).

A)

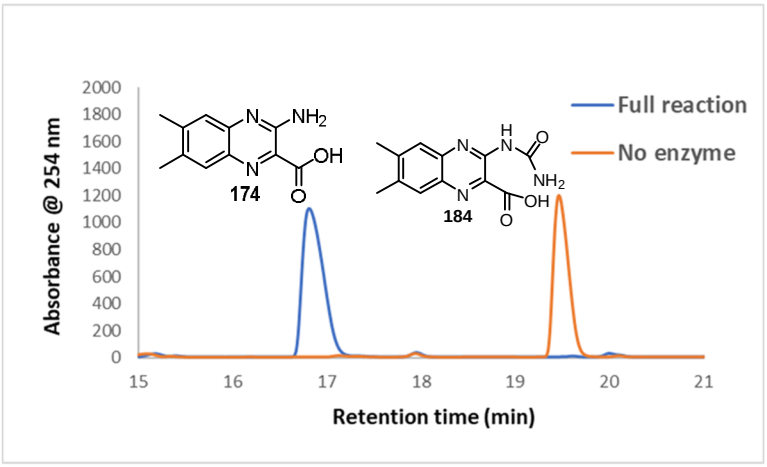

B)

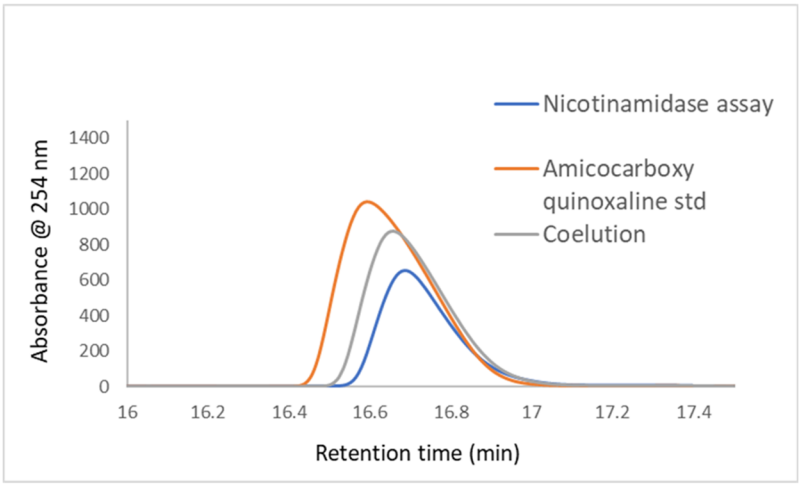

Figure 8.14: Characterization of the nicotinamidase catalyzed reaction product. A) HPLC analysis of nicotinamidase catalyzed reaction mixture. B) Coelution experiment with a synthetically prepared compound **174**.

8.2.9 Detection of ammonia in the nicotinamidase catalyzed reaction.

According to our proposal nicotinamidase catalyzes the conversion of **184** to **174** by release of ammonia and carbon dioxide. To detect ammonia in the nicotinamidase catalyzed reaction we used glutamate dehydrogenase assay. In the glutamate dehydrogenase catalyzed reaction glutamate reacts with ammonia in the presence of reduced nicotinamide to give glutamine and oxidized nicotinamide. Thus, one can monitor the reaction by looking at the decrease of absorbance at 340 nm due to consumption of reduced nicotinamide. Once the nicotinamidase catalyzed reaction was over we added glutamate, glutamate dehydrogenase and NADPH in the reaction mixture and observed the change in absorbance at 340 nm. Indeed, as time passes a decrease in absorbance at 340nm could be observed (Figure 8.15).

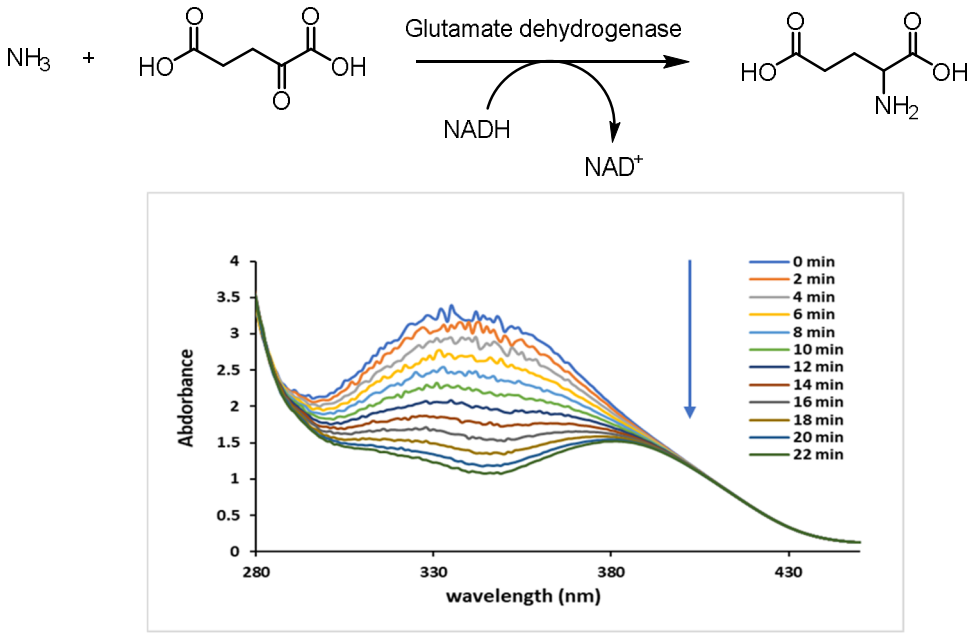

Figure 8.15: Detection of ammonia in the nicotinamidase catalyzed reaction.

8.2.10 Activity assay of putative amidohydrolase

Having identified amino carboxy quinoxaline **174** as the product of nicotinamidase catalyzed reaction we asked the question whether putative amidohydrolase or putative

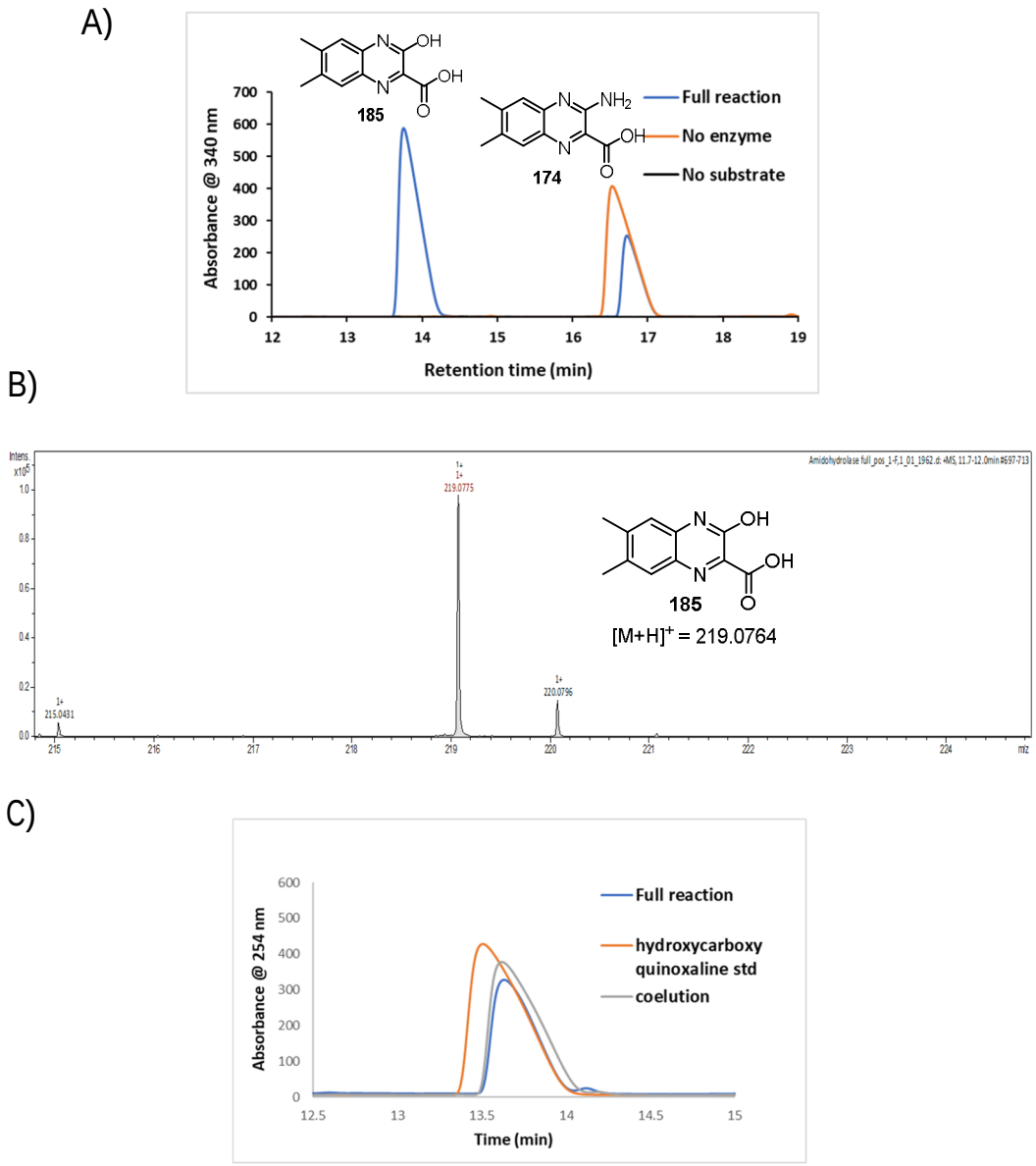

Figure 8.16: Characterization of amidohydrolase catalyzed reaction product. A) HPLC analysis of amidohydrolase catalyzed reaction mixture. B) Mass of the new product formed in the amidohydrolase catalyzed reaction C) Coelution experiment with an authentic compound **185**

deacetylase could convert it to a new compound. To test this proposal, we incubated compound **174** with putative amidohydrolase or putative deacetylase separately and then analyzed the reaction mixture using HPLC. Under this condition amidohydrolase could convert amino carboxy quinoxaline to new compound however putative deacetylase did not show any activity. The product produced in the amidohydrolase catalyzed reaction was identified as hydroxy carboxy quinoxaline based on LC-MS data and a coelution experiment with an authentic standard (Figure 8.16).

8.2.11 $H_2{}^{18}O$ labeling experiment for amidohydrolase catalyzed reaction

Since amidohydrolase catalyzed the deamination reaction of amino carboxy quinoxaline to convert into hydroxy carboxy quinoxaline the source of oxygen the hydroxy moiety has

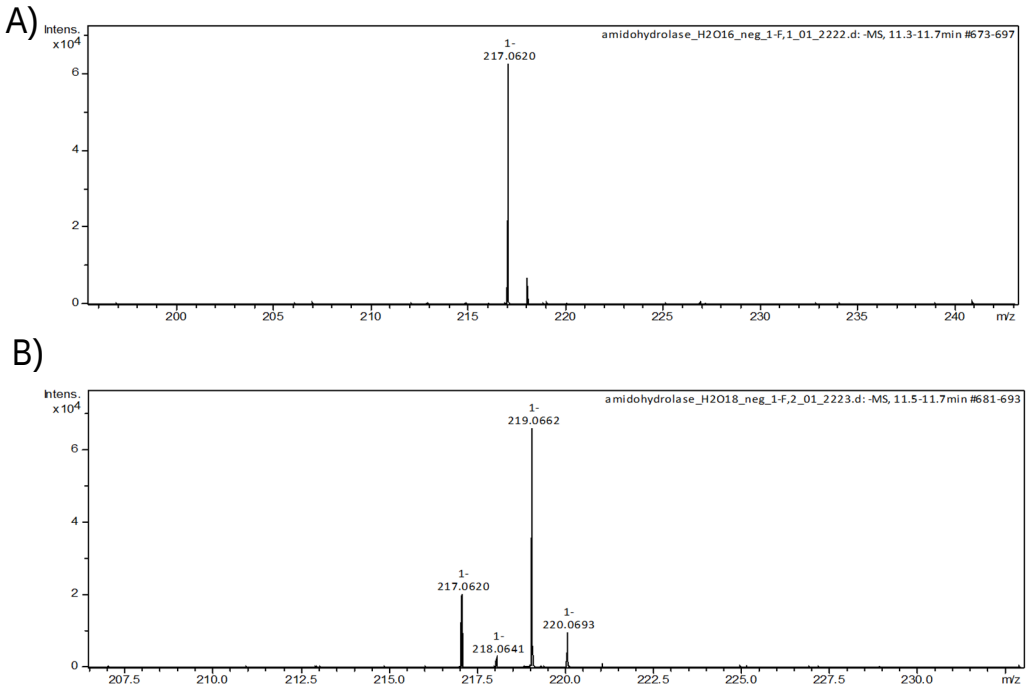

Figure 8.17: LC-MS analysis of amidohydrolase catalyzed reaction run in $H_2{}^{16}O$ (panel A) and 80 % $H_2{}^{18}O$ (panel B) buffer.

to be from water. To test the hypothesis, amidohydrolase catalyzed reaction was performed in $H_2{}^{18}O$ containing buffer and the reaction mixture was analyzed by LC-MS. Indeed, 2 Da increase in mass of the product was observed (Figure 8.17).

8.2.12 Detection of ammonia in the amidohydrolase catalyzed reaction

According to our mechanistic proposal ammonia is the other product in the amidohydrolase catalyzed reaction. This was confirmed by glutamate dehydrogenase assay.

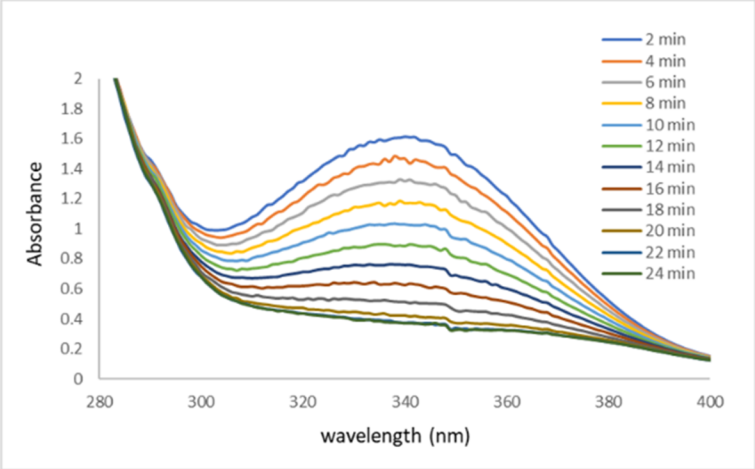

Figure 8.18: Detection of ammonia in the amidohydrolase catalyzed reaction.

8.3 Conclusion

In this section we have identified a bacterial strain named *Pimelobacter simplex* which can grow on lumichrome using it as carbon and nitrogen source. Based on the metabolite analysis and bioinformatics we have identified the catabolic gene cluster. We have also successfully reconstituted the activities of the three enzymes which catalyze the initial steps in lumichorme catabolism.

It will be interesting to see how hydroxy carboxy quinoxaline **185** is further degraded. Rest of the genes in the cluster encode aldehyde dehydrogenase, TPP dependent decarboxylases, xanthine oxidase and dioxygenases. We propose two dioxygenases will play a role in cleaving the benzene ring as dioxygenase mediated aromatic ring degradation reactions are well precedented. However, the roles of xanthine oxidase and TPP dependent decarboxylases are not obvious at this point. Future experiments will give answers to these questions.

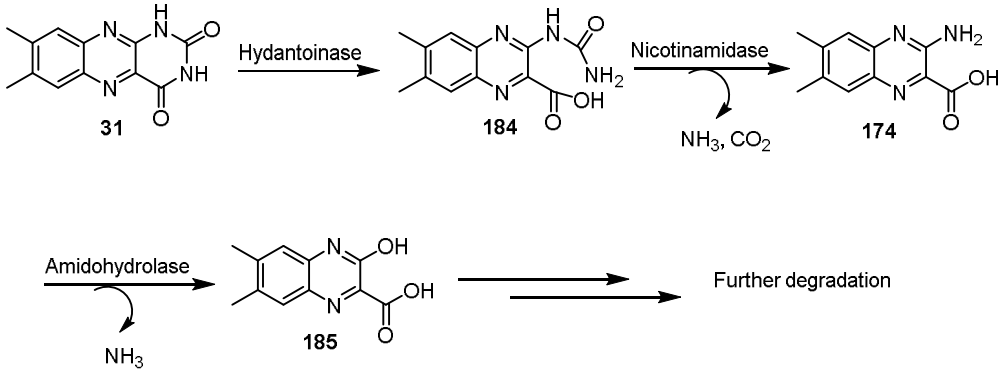

31 **184** **174** **185**

8.4 Experimental Procedure

Materials

All chemicals were purchased from Sigma-Aldrich unless mentioned otherwise. LB broth (Lennox) was purchased from EMB Millipore. kanamycin and IPTG were obtained from Lab Scientific Inc. Amicon Ultra centrifugal filter devices (10,000 MWCO) were obtained from Millipore. Histrap column was obtained from GE Healthcare. Econo-Pack 10DG desalting columns were purchased from Bio-Rad. 2.5 L baffled ultra yield flasks for protein overexpression were obtained from Thomson Instrument Company. HPLC and LC-MS solvents were purchased from EMD and were used without further purification. ZORBAX Eclipse XDB-C18 column (15 cm x 4.6 mm, 5 μm particles) was purchased from Agilent Technologies.

General procedure of over-expression and purification of amidohydrolases.

The amidohydrolase gene containing overexpression plasmid (amidohydrolase-pTHT) was transformed into *E. coli* BL21 (DE3). For the overexpression of the protein, a starter culture was grown overnight in 15 ml of LB medium containing 40 μg/ml of kanamycin at 37 °C. 1.5 liter of LB medium (20 g/L) containing 40 μg/ml of kanamycin, was inoculated with this starter culture. The cells were grown at 37 °C with shaking (220 rpm) until the culture reached an OD_{600} of 0.6. The culture was then incubated at 4°C for ~45min without shaking. Then the culture was induced by adding IPTG to a final concentration of 0.5 mM, the temperature was lowered to 15 °C and the cells were grown with shaking (180 rpm) for a further 15 hours. The cells were then harvested by centrifugation at 10,000g for 10 min at 4 °C and store at -80 ˚C.

The cell pellet was re-suspended in 30 ml of lysis buffer (50 mM KH_2PO4, 150 mM NaCl, 10 mM imidazole, pH 8.0). Lysozyme (5 mg) was added and the cells were lysed by sonication on ice (Misonix Sonicator 3000, six cycles of 30 s duration during which 1.5 s sonicator pulses at output level 0.8 were followed by 1.5 s pauses). The resulting suspension was centrifuged (18,000 rpm, 30 min) and the supernatant was filtered through a sterile syringe filter (pore size 0.45 μm). The clarified supernatant was loaded onto a 5 mL Ni-NTA-affinity column pre-equilibrated with lysis buffer kept at 4°C. The Ni-NTA-affinity column was then washed with 50 ml wash buffer (50 mM KH_2PO_4, 150 mM NaCl, 20 mM imidazole, pH 8.0). The protein was eluted from the column with elution buffer (50 mM KH_2PO_4, 150 mM NaCl, 200 mM imidazole, pH 8.0) at 4°C. The fractions containing protein were pooled and concentrated using YM-10 Amicon ultracentrifugal filters at 5000g to a final volume of 3 ml. The concentrated sample was buffer exchanged, using an Econo-Pac 10DG desalting column, into 100 mM phosphate buffer at pH 7.5 containing 100 mM NaCl and glycerol to a final concentration of 15%.

For the overexpression of the amidohydrolase (UniProt Id A0A0A1DP61), pTHT overexpression plasmid containing the amidohydrolase gene and pGro7 plasmid containing GroEL-GroES encoding gene were transformed into *E. coli* BL21 (DE3). For the overexpression of the protein, a starter culture was grown overnight in 15 ml of LB medium containing 40 μg/ml of kanamycin and 30 μg/ml of chloramphenicol at 37 °C. 1.5 liter of LB medium (20 g/L) containing 40 μg/ml of kanamycin, 30 μg/ml of chloramphenicol and 2 mg/ml L-arabinose, was inoculated with this starter culture. The cells were grown at 37 °C with shaking (220 rpm) until the culture reached an OD_{600} of

0.6. The culture was then incubated at 4°C for ~45min without shaking. Then the culture was induced by adding IPTG to a final concentration of 0.5 mM. The rest of the overexpression and purification protocol is the same as discussed above.

HPLC and LC-MS parameters

An Agilent 1260 HPLC equipped with a quaternary pump was used. The system included a diode array UV-Vis detector and products were detected using absorbance at 254 nm, and 450 nm. Analysis was performed either on a ZORBAX Eclipse XDB-C18 column (15 cm x 4.6 mm, 5 μm particles, Agilent Technologies) or PFP column (150 x 4.6 mm, 2.6 μm particles, Kinetex).

HPLC conditions (for C18 column):

A-Water

B-10mM ammonium acetate buffer, pH 6.6

C-Methanol

HPLC method:

0 min-90% A 10% B, 2 min- 90% A 10% B, 22 min-20%A 10%B 70% C, 27 min-20%A 10%B 70% C, 28 min-90% A 10% B, 36 min-90% A 10% B

LC-MS parameters

LC-ESI-TOF-MS was performed using an Agilent 1260 HPLC system which is equipped with a binary pump and a 1200 series diode array detector followed by a MicroToF-Q II mass spectrometer (Bruker Daltonics) using an ESI source either in negative mode or positive mode. Analysis was performed on an LC-18-T column (15 cm x 3 mm, 3 μm particles, Supelco).

LC conditions:

A-5 mM Ammonium acetate buffer, pH 6.6

B-75% Methanol and 25 % Water.

LC method: (for positive and negative mode on MS) 0 min-100% A, 2 min-100% A, 12 min-30% A 70% B, 17 min-30% A 70% B, 18 min-100% A, 30 min-100%A

General protocol of amidohydrolase catalyzed reaction

All the amidohydrolase catalyzed reaction was carried out in 100 mM phosphate buffer, pH 7.5. The final concentrations of all the reaction components were as follows: enzyme (50 μM), substrate (500 μM). The protein was heat-denatured and removed by centrifugal ultrafiltration through a 10 kDa MWCO membrane (Pall Life Sciences). The samples were analyzed by HPLC and LC-MS.

Synthesis of compound 184

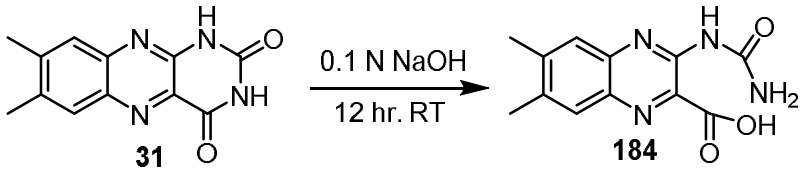

Figure 8.19: Synthetic scheme for compound **184**.

120 mg of lumichrome was suspended in 50 mL aqueous 0.1 N NaOH and heated to 60 ºC to complete dissolution. Then 50 mL water is added and stirred at room temperature for 12 hr. After that the pH of the reaction mixture was set to 8.5 with 2 N HCl followed by addition of 25 ml 0.2 N borate buffer of same pH. The solution was extracted with chloroform to get rid of unreacted lumichrome. The aqueous portion was acidified with 2

N HCl to pH 2 at 0 ºC and the resulting precipitate was filtered. After washing the precipitate with acetone and ether pure compound **184** was obtained.

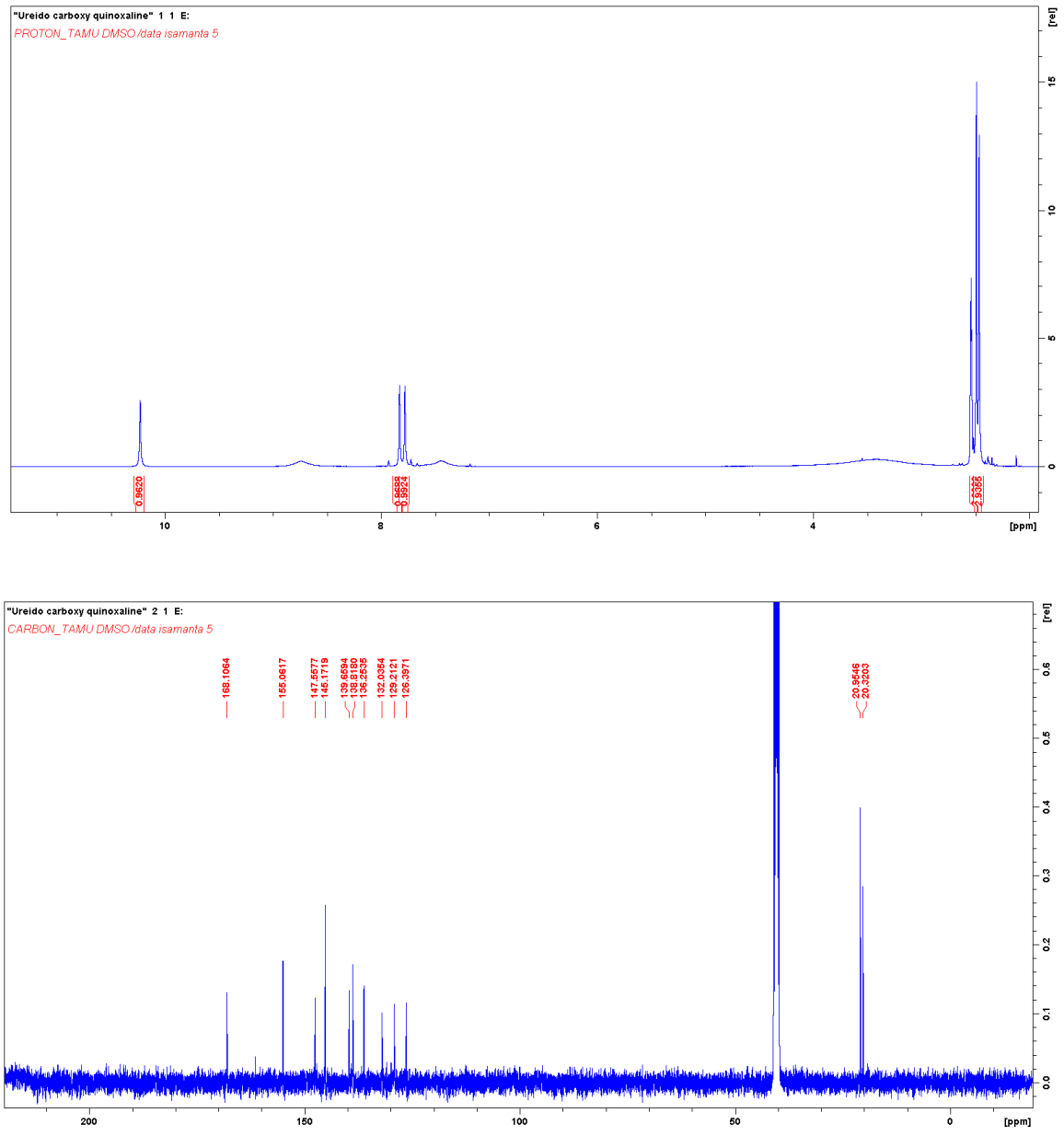

Figure 8.20: 1-H and 13-C NMR of compound **184**

Synthesis of compound 174

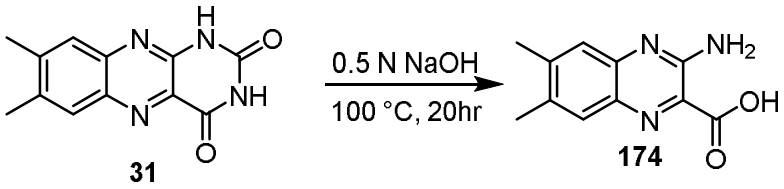

Figure 8.21: Synthetic scheme for compound **174**.

Compound **174** was prepared by heating 150 mg of lumichrome in 100 ml of 0.5 N NaOH for 20 hours at 100 ºC. Upon cooling, the pale-yellow sodium salt of the quinoxaline carboxylic acid separated. The precipitated solid was washed with cold dilute NaOH and taken up in hot water. The acid was precipitated with dilute HCl, washed with water to give pure compound **174** (Figure 8.22).

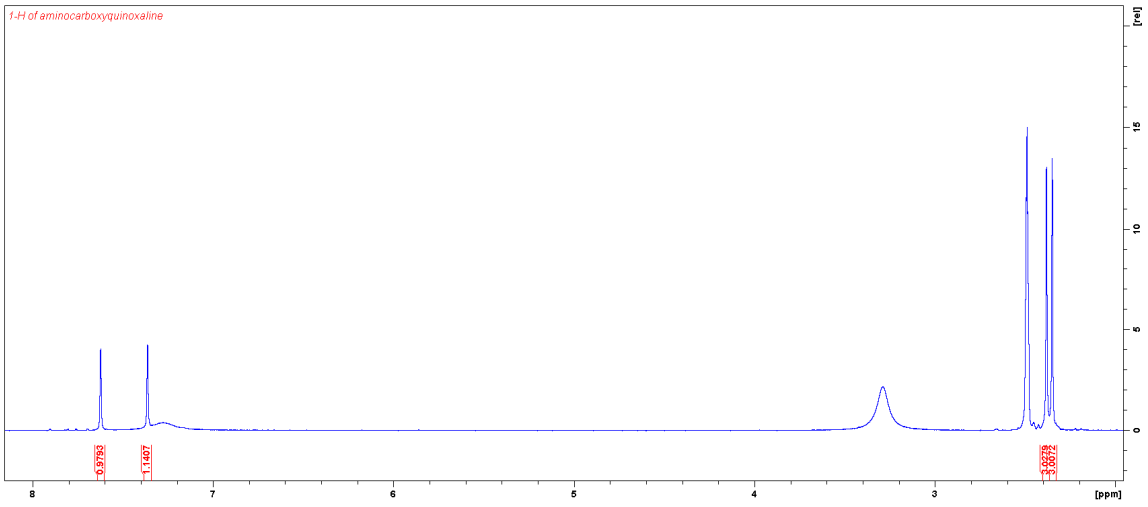

Figure 8.22: 1-H and 13-C NMR of compound **174**

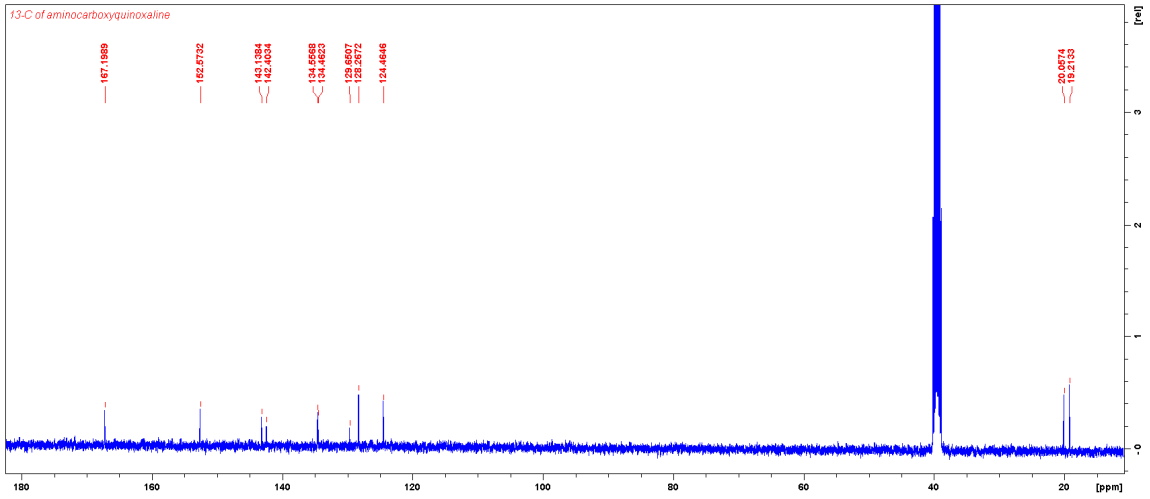

Figure 8.22: continued.

CHAPTER IX

SUMMARY AND OUTLOOK

9.1 Flavin-N5-oxide

In the majority of flavin-dependent oxygenases, the reaction of dihydroflavin with molecular oxygen leads to the formation of flavin-4a-OOH species which then acts as the oxygenating agent and carries out a diverse range of oxygen transfer chemistry. We have identified a new oxidation state of flavin namely flavin-N5-oxide while investigating the mechanism of DszA catalyzed reaction in dibenzothiophene catabolic pathway. The intermediacy of the flavin-N5-oxide was confirmed by LC-MS analysis, a coelution experiment with chemically synthesized FMN-N5-oxide and $^{18}O_2$ labeling studies. Guided by our mechanistic hypothesis, we were able to discover flavin-N5-oxide in the RutA-catalyzed oxidative amide bond cleavage reaction in the uracil catabolic pathway reaction and HcbA1-catalyzed dehalogenation reaction in the hexachlorobenzene catabolic pathway (Figure 1).

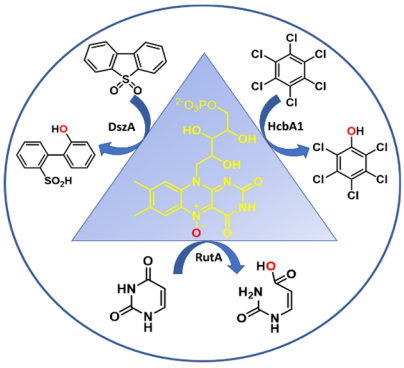

Figure 9.1: Flavin-N5-oxide formation in bacterial catabolic pathways.

9.1.1 General guidelines for the detection of flavin-N5-oxide intermediates

1. Flavin-N5-oxide is readily reduced to flavin. It is therefore essential to exclude reducing agents such as DTT, TCEP and reduced nicotinamide from the reaction mixture. Reduced

flavin is prepared by photoreduction in the presence of EDTA rather than by enzymatic reduction using NAD(P)H as the reducing agent.

2. Although the UV–Visible spectra of oxidized flavin and flavin-N5-oxide are similar, there is a clear distinction between the two species in the 450 nm region (λ_{max} of flavin is 447 nm whereas λ_{max} of flavin-N5-oxide is 462 nm). This can be used as an initial indicator of the formation of a flavin-N5-oxide intermediate.

3. Flavin-N5-oxide can be detected by HPLC analysis of the enzymatic reaction mixture (single turnover) using synthesized FMN-N5-oxide as an authentic standard.

4. As of yet, protein amino acid sequence analysis has not generated a characteristic sequence motif that enables the identification of flavin-N5-oxide-forming enzymes. However, mechanistic analysis has proven useful in the identification of such enzymes. The analysis of the DszA reaction mechanism suggested that flavin-N5-oxides are likely intermediates in any flavoenzyme involving substrate hydroperoxide formation in the absence of an active site cysteine. This model led to the identification of RutA and HcbA1 as possible FMN-N5-oxide generating enzymes, but does not include the catalytic motif shown in the EncM-catalyzed reaction. It is highly likely that many additional examples of flavin-N5-oxide-utilizing-flavoenzymes remain to be discovered.

9.2 Folate catabolism

We have identified a folate catabolic gene cluster in *Mesorhizobium loti* MAFF303099 by bio-informatics analysis. Based on in vitro experiments we have identified the catabolic pathway which consists of a deaminase, a flavin oxygenase, and an amidohydrolase. Detailed biochemical and structural studies suggest a unique flavoenzyme mediated

Baeyer-Villiger type rearrangement of an imine. We have discovered a similar Baeyer-Villiger type rearrangement in the bacterial tetramethylpyrazine catabolic pathway. Blast analysis revealed that the gene cluster responsible for the folate catabolism is widespread amongst several bacteria. In future we will examine the presence of folate catabolic gene cluster in the human gut microbiome and its connection to folate deficiency diseases like neural tube defects.

9.3 Cofactor independent oxygenase

Oxygenases generally require cofactors (either metal or organic) to activate molecular oxygen. Iron and copper are the most widely used metal cofactors to activate molecular oxygen while flavin, pterin, and PLP are known organic cofactors for the activation of di oxygen. In contrast to these ubiquitous cofactor dependent oxygenases there is only a handful of enzymes which are known to activate molecular oxygen without employing any cofactors and the mechanism by which these reactions are catalyzed are not well understood. In an attempt to fill this gap, we have studied the mechanism of a cofactor-independent oxygenase (IifA) involved in the bacterial indole catabolic pathway. IifA catalyzes the transformation of 3-hydroxy-oxindole to anthranilic acid. Our mechanistic studies on the IifA catalyzed reaction support a Baeyer-Villiger type rearrangement, first of its kind, in a cofactor-independent enzyme. We have shown that the reaction goes via the isatoic anhydride intermediate, identified bicarbonate as the reaction product, labeling experiments with O-18 labeled water and molecular oxygen showed that the oxygen atom from water molecule incorporated into anthranilic acid product while oxygen atom from molecular oxygen incorporated into carbon dioxide.

9.4 Lumichrome catabolism

We have successfully isolated a lumichrome catabolizing strain from a soil sample.16s rRNA sequencing revealed the strain to be a relative of *Pimelobacter simplex*. The strain grows in base metal medium with lumichrome serving as both carbon and nitrogen sources. Based on metabolite analysis and bioinformatics we have identified the gene cluster associated with lumichrome catabolism and the initial three steps of degradation pathway have been established by in vitro studies. Future studies will be directed towards the identification of the functions the rest of the proteins encoded by the gene cluster.

REFERENCES

1. Walsh, C. T.; Wencewicz, T. A., Flavoenzymes: versatile catalysts in biosynthetic pathways. *Nat Prod Rep* **2013,** *30* (1), 175-200.

2. Leys, D.; Scrutton, N. S., Sweating the assets of flavin cofactors: new insight of chemical versatility from knowledge of structure and mechanism. *Curr Opin Struct Biol* **2016,** *41*, 19-26.

3. Piano, V.; Palfey, B. A.; Mattevi, A., Flavins as Covalent Catalysts: New Mechanisms Emerge. *Trends Biochem Sci* **2017,** *42* (6), 457-469.

4. Palfey, B. A.; Ballou, D. P.; Massey, V., Oxygen Activation by Flavins and Pterins. In *Active Oxygen in Biochemistry*, Valentine, J. S.; Foote, C. S.; Greenberg, A.; Liebman, J. F., Eds. Springer US: Boston, MA, 1995; pp 37-83.

5. van Berkel, W. J.; Kamerbeek, N. M.; Fraaije, M. W., Flavoprotein monooxygenases, a diverse class of oxidative biocatalysts. *J Biotechnol* **2006,** *124* (4), 670-89.

6. Marshall, S. A.; Payne, K. A. P.; Leys, D., The UbiX-UbiD system: The biosynthesis and use of prenylated flavin (prFMN). *Arch Biochem Biophys* **2017,** *632*, 209-221.

7. Payne, K. A.; White, M. D.; Fisher, K.; Khara, B.; Bailey, S. S.; Parker, D.; Rattray, N. J.; Trivedi, D. K.; Goodacre, R.; Beveridge, R.; Barran, P.; Rigby, S. E.; Scrutton, N. S.; Hay, S.; Leys, D., New cofactor supports alpha,beta-unsaturated acid decarboxylation via 1,3-dipolar cycloaddition. *Nature* **2015,** *522* (7557), 497-501.

8. White, M. D.; Payne, K. A.; Fisher, K.; Marshall, S. A.; Parker, D.; Rattray, N. J.; Trivedi, D. K.; Goodacre, R.; Rigby, S. E.; Scrutton, N. S.; Hay, S.; Leys, D., UbiX is a flavin prenyltransferase required for bacterial ubiquinone biosynthesis. *Nature* **2015,** *522* (7557), 502-6.

9. Teufel, R.; Miyanaga, A.; Michaudel, Q.; Stull, F.; Louie, G.; Noel, J. P.; Baran, P. S.; Palfey, B.; Moore, B. S., Flavin-mediated dual oxidation controls an enzymatic Favorskii-type rearrangement. *Nature* **2013,** *503* (7477), 552-556.

10. Teufel, R.; Stull, F.; Meehan, M. J.; Michaudel, Q.; Dorrestein, P. C.; Palfey, B.; Moore, B. S., Biochemical Establishment and Characterization of EncM's Flavin-N5-oxide Cofactor. *J Am Chem Soc* **2015,** *137* (25), 8078-85.

11. Burg, R. W.; Rodwell, V. W.; Snell, E. E., Bacterial oxidation of vitamin B6. II. Metabolites of pyridoxamine. *J Biol Chem* **1960,** *235*, 1164-9.

12. Ikawa, M.; Rodwell, V. W.; Snell, E. E., Bacterial oxidation of vitamin B6. II. Structure of 260 compound. *J Biol Chem* **1958,** *233* (6), 1555-9.

13. Rodwell, V. W.; Volcani, B. E.; Ikawa, M.; Snell, E. E., Bacterial oxidation of vitamin B6. I. Isopyridoxal and 5-pyridoxic acid. *J Biol Chem* **1958,** *233* (6), 1548-54.

14. Mukherjee, T.; Hanes, J.; Tews, I.; Ealick, S. E.; Begley, T. P., Pyridoxal phosphate: biosynthesis and catabolism. *Biochim Biophys Acta* **2011,** *1814* (11), 1585-96.

15. Baeyer, A.; Villiger, V., Einwirkung des caro'schen reagens auf ketone. *Ber. Dtsch. Chem. Ges.* **1899,** *32* (3), 3625-3633.

16. Criegee, R., Die Umlagerung der Dekalin-peroxydester als Folge von kationischem Sauerstoff. *Justus Liebigs Ann. Chem.* **1948,** *560* (1), 127-135.

17. Leisch, H.; Morley, K.; Lau, P. C., Baeyer− Villiger monooxygenases: more than just green chemistry. *Chem. Rev.* **2011,** *111* (7), 4165-4222.

18. Turfitt, G., The microbiological degradation of steroids: 4. Fission of the steroid molecule. *Biochem J.* **1948,** *42* (3), 376.

19. Donoghue, N. A.; Norris, D. B.; Trudgill, P. W., The purification and properties of cyclohexanone oxygenase from Nocardia globerula CL1 and Acinetobacter NCIB 9871. *Eur. J. Biochem* **1976,** *63* (1), 175-192.

20. Henry, K. M.; Townsend, C. A., Ordering the Reductive and Cytochrome P450 Oxidative Steps in Demethylsterigmatocystin Formation Yields General Insights into the Biosynthesis of Aflatoxin and Related Fungal Metabolites. *J. Am. Chem. Soc.* **2005,** *127* (11), 3724-3733.

21. Henry, K. M.; Townsend, C. A., Synthesis and Fate of o-Carboxybenzophenones in the Biosynthesis of Aflatoxin. *J. Am. Chem. Soc.* **2005,** *127* (10), 3300-3309.

22. Philmus, B.; Abdelwahed, S.; Williams, H. J.; Fenwick, M. K.; Ealick, S. E.; Begley, T. P., Identification of the product of toxoflavin lyase: degradation via a Baeyer-Villiger oxidation. *J Am Chem Soc* **2012,** *134* (11), 5326-30.

23. Soleimani, M.; Bassi, A.; Margaritis, A., Biodesulfurization of refractory organic sulfur compounds in fossil fuels. *Biotechnol. Adv.* **2007,** *25* (6), 570-596.

24. Gray, K. A.; Pogrebinsky, O. S.; Mrachko, G. T.; Xi, L.; Monticello, D. J.; Squires, C. H., Molecular mechanisms of biocatalytic desulfurization of fossil fuels. *Nat. Biotechnol.* **1996,** *14* (13), 1705-1709.

25. Ryerson, C. C.; Ballou, D. P.; Walsh, C., Mechanistic studies on cyclohexanone oxygenase. *Biochemistry* **1982,** *21* (11), 2644-55.

26. Lee, W. C.; Ohshiro, T.; Matsubara, T.; Izumi, Y.; Tanokura, M., Crystal Structure and Desulfurization Mechanism of 2'-Hydroxybiphenyl-2-sulfinic Acid Desulfinase. *J. Biol. Chem.* **2006,** *281* (43), 32534-32539.

27. Eichhorn, E.; Davey, C. A.; Sargent, D. F.; Leisinger, T.; Richmond, T. J., Crystal structure of Escherichia coli alkanesulfonate monooxygenase SsuD. *J Mol Biol* **2002,** *324* (3), 457-68.

28. Aida, T.; Squires, T. G.; Venier, C. G., Reaction of dibenzothiophene sulfone with alkoxides. *Tetrahedron Lett.* **1983,** *24* (34), 3543-6.

29. Rossi, R. A.; Pierini, A. B.; Peñéñory, A. B., Nucleophilic Substitution Reactions by Electron Transfer. *Chemical Reviews* **2003,** *103* (1), 71-168.

30. Walsh, C. T.; Chen, Y. C. J., Enzymic Baeyer-Villiger oxidations with flavin-dependent monooxygenases. *Angew. Chem.* **1988,** *100* (3), 342-52.

31. Mukherjee, T.; Zhang, Y.; Abdelwahed, S.; Ealick, S. E.; Begley, T. P., Catalysis of a Flavoenzyme-Mediated Amide Hydrolysis. *J. Am. Chem. Soc.* **2010,** *132* (16), 5550-5551.

32. Hall, A.; Karplus, P. A.; Poole, L. B., Typical 2-Cys peroxiredoxins - structures, mechanisms and functions. *FEBS J.* **2009,** *276* (9), 2469-2477.

33. Teufel, R.; Agarwal, V.; Moore, B. S., Unusual flavoenzyme catalysis in marine bacteria. *Curr Opin Chem Biol* **2016,** *31*, 31-9.

34. Litvak, Z. I.; Berezovskii, V. M., Study of allo- and isoalloxazines. LIV. Direct oxidation of riboflavin esters into their 5-N-oxides. *Zh. Obshch. Khim.* **1981,** *51* (2), 464-6.

35. Yoneda, F.; Sakuma, Y.; Ichiba, M.; Shinomura, K., Syntheses of isoalloxazines and isoalloxazine 5-oxides. A new synthesis of riboflavin. *J. Am. Chem. Soc.* **1976,** *98* (3), 830-835.

36. Lavilla, R.; Barón, X.; Coll, O.; Gullón, F.; Masdeu, C.; Bosch, J., "Nonbiomimetic" Oxidations of Dihydropyridines. *J. Org. Chem* **1998,** *63* (26), 10001-10005.

37. Vogels, G. D.; Van der Drift, C., Degradation of purines and pyrimidines by microorganisms. *Bacteriol Rev* **1976,** *40* (2), 403-68.

38. Soong, C. L.; Ogawa, J.; Sakuradani, E.; Shimizu, S., Barbiturase, a novel zinc-containing amidohydrolase involved in oxidative pyrimidine metabolism. *J Biol Chem* **2002,** *277* (9), 7051-8.

39. Loh, K. D.; Gyaneshwar, P.; Papadimitriou, E. M.; Fong, R.; Kim, K.-S.; Parales, R.; Zhou, Z.; Inwood, W.; Kustu, S., A previously undescribed pathway for pyrimidine catabolism. *Proc. Natl. Acad. Sci. U. S. A.* **2006,** *103* (13), 5114-5119.

40. Adak, S.; Begley, T. P., Dibenzothiophene Catabolism Proceeds via a Flavin-N5-oxide Intermediate. *J Am Chem Soc* **2016,** *138* (20), 6424-6.

41. Xun, L.; Sandvik, E. R., Characterization of 4-hydroxyphenylacetate 3-hydroxylase (HpaB) of Escherichia coli as a reduced flavin adenine dinucleotide-utilizing monooxygenase. *Appl. Environ. Microbiol.***2000,** *66* (2), 481-486.

42. Chakraborty, S.; Massey, V., Reaction of reduced flavins and flavoproteins with diphenyliodonium chloride. *J Biol Chem* **2002,** *277* (44), 41507-16.

43. Bobbitt, J. M.; Bartelson, A. L.; Bailey, W. F.; Hamlin, T. A.; Kelly, C. B., Oxoammonium Salt Oxidations of Alcohols in the Presence of Pyridine Bases. *J. Org. Chem* **2014,** *79* (3), 1055-1067.

44. Golubev, V. A.; Miklyush, R. V., New preparative method for the oxidation of an activated methylene group to a carbonyl one. *Zh. Org. Khim.* **1972,** *8* (7), 1356-7.

45. Ren, T.; Liu, Y.-C.; Guo, Q.-X., Selective oxyfunctionalization of ketones using 1-oxopiperidinium salt. *Bull. Chem. Soc. Jpn.* **1996,** *69* (10), 2935-2941.

46. Barber, J. L.; Sweetman, A. J.; van Wijk, D.; Jones, K. C., Hexachlorobenzene in the global environment: Emissions, levels, distribution, trends and processes. *Sci. Total Environ.* **2005,** *349* (1-3), 1-44.

47. Ito, K.; Takagi, K.; Iwasaki, A.; Tanaka, N.; Kanesaki, Y.; Martin-Laurent, F.; Igimi, S., Identification of the hcb gene operon involved in catalyzing aerobic hexachlorobenzene dechlorination in Nocardioides sp. strain PD653. *Appl. Environ. Microbiol.* **2017,** *83* (19), e00824-17/1-e00824-17/17.

48. Ito, K.; Takagi, K.; Matsushima, Y.; Igimi, S.; Ito, K.; Takagi, K.; Iwasaki, A.; Tanaka, N.; Kanesaki, Y.; Martin-Laurent, M.-L. F. F., Identification of the novel hcbB operon catalyzing the dechlorination of pentachlorophenol in the Gram-positive bacterium Nocardioides sp. strain PD653. *J Pestic Sci* **2018,** *43* (2), 124-131.

49. Adak, S.; Begley, T. P., Flavin-N5-oxide: A new, catalytic motif in flavoenzymology. *Arch Biochem Biophys* **2017,** *632*, 4-10.

50. Adak, S.; Begley, T. P., RutA-Catalyzed Oxidative Cleavage of the Uracil Amide Involves Formation of a Flavin-N5-oxide. *Biochemistry* **2017,** *56* (29), 3708-3709.

51. Agarwal, V.; Miles, Z. D.; Winter, J. M.; Eustaquio, A. S.; El Gamal, A. A.; Moore, B. S., Enzymatic Halogenation and Dehalogenation Reactions: Pervasive and Mechanistically Diverse. *Chem. Rev. (Washington, DC, U. S.)* **2017,** *117* (8), 5619-5674.

52. de Jong, R. M.; Dijkstra, B. W., Structure and mechanism of bacterial dehalogenases: different ways to cleave a carbon-halogen bond. *Curr. Opin. Struct. Biol.* **2003,** *13* (6), 722-730.

53. Fetzner, S., Bacterial dehalogenation. *Appl. Microbiol. Biotechnol.* **1998,** *50* (6), 633-657.

54. Benning, M. M.; Taylor, K. L.; Liu, R.-Q.; Yang, G.; Xiang, H.; Wesenberg, G.; Dunaway-Mariano, D.; Holden, H. M., Structure of 4-chlorobenzoyl coenzyme A dehalogenase determined to 1.8 Å resolution: An enzyme catalyst generated via adaptive mutation. *Biochemistry* **1996,** *35* (25), 8103-8109.

55. Dong, J.; Carey, P. R.; Wei, Y.; Luo, L.; Lu, X.; Liu, R.-Q.; Dunaway-Mariano, D., Raman Evidence for Meisenheimer Complex Formation in the Hydrolysis Reactions of 4-Fluorobenzoyl- and 4-Nitrobenzoyl-Coenzyme A Catalyzed by 4-Chlorobenzoyl-Coenzyme A Dehalogenase. *Biochemistry* **2002,** *41* (23), 7453-7463.

56. Lau, E. Y.; Bruice, T. C., The active site dynamics of 4-chlorobenzoyl-CoA dehalogenase. *Proc. Natl. Acad. Sci. U. S. A.* **2001,** *98* (17), 9527-9532.

57. Luo, L.; Taylor, K. L.; Xiang, H.; Wei, Y.; Zhang, W.; Dunaway-Mariano, D., Role of Active Site Binding Interactions in 4-Chlorobenzoyl-Coenzyme A Dehalogenase Catalysis. *Biochemistry* **2001,** *40* (51), 15684-15692.

58. Zhang, W.; Wei, Y.; Luo, L.; Taylor, K. L.; Yang, G.; Dunaway-Mariano, D.; Benning, M. M.; Holden, H. M., Histidine 90 Function in 4-Chlorobenzoyl-Coenzyme A Dehalogenase Catalysis. *Biochemistry* **2001,** *40* (45), 13474-13482.

59. Crawford, R. L.; Jung, C. M.; Strap, J. L., The recent evolution of pentachlorophenol (PCP)-4-monooxygenase (PcpB) and associated pathways for bacterial degradation of PCP. *Biodegradation* **2007,** *18* (5), 525-539.

60. Hlouchova, K.; Rudolph, J.; Pietari, J. M. H.; Behlen, L. S.; Copley, S. D., Pentachlorophenol Hydroxylase, a Poorly Functioning Enzyme Required for Degradation of Pentachlorophenol by Sphingobium chlorophenolicum. *Biochemistry* **2012,** *51* (18), 3848-3860.

61. Yadid, I.; Rudolph, J.; Hlouchova, K.; Copley, S. D., Sequestration of a highly reactive intermediate in an evolving pathway for degradation of pentachlorophenol. *Proc Natl Acad Sci U S A* **2013,** *110* (24), E2182-90.

62. Jiménez, J. I.; Canales, Á.; Jiménez-Barbero, J.; Ginalski, K.; Rychlewski, L.; García, J. L.; Díaz, E., Deciphering the genetic determinants for aerobic nicotinic acid degradation: the nic cluster from Pseudomonas putida KT2440. *Proc Natl Acad Sci U S A* **2008,** *105* (32), 11329-11334.

63. Suh, J. R.; Herbig, A. K.; Stover, P. J., New perspectives on folate catabolism. *Annu Rev Nutr* **2001,** *21*, 255-82.

64. Scott, J. M., Evidence of folic acid and folate in the prevention of neural tube defects. *Bibl Nutr Dieta* **2001,** (55), 192-5.

65. McCullough, J. L.; Chabner, B. A.; Bertino, J. R., Purification and properties of carboxypeptidase G 1. *J Biol Chem* **1971,** *246* (23), 7207-13.

66. Levy, C. C.; Goldman, P., The enzymatic hydrolysis of methotrexate and folic acid. *J Biol Chem* **1967,** *242* (12), 2933-8.

67. Fan, H.; Hitchcock, D. S.; Seidel, R. D.; Hillerich, B.; Lin, H.; Almo, S. C.; Sali, A.; Shoichet, B. K.; Raushel, F. M., Assignment of Pterin Deaminase Activity to an Enzyme of Unknown Function Guided by Homology Modeling and Docking. *J. Am. Chem. Soc.* **2013,** *135* (2), 795-803.

68. Warui, D. M.; Li, N.; Norgaard, H.; Krebs, C.; Bollinger, J. M., Jr.; Booker, S. J., Detection of formate, rather than carbon monoxide, as the stoichiometric coproduct in conversion of fatty aldehydes to alkanes by a cyanobacterial aldehyde decarbonylase. *J Am Chem Soc* **2011,** *133* (10), 3316-9.

69. Lu, K.; Li, H.; Ding, M., Analysis of tetramethylpyrazine in Ephedrae herba by gas chromatography-mass spectrometry and high-performance liquid chromatography. *J. Chromatogr. A* **2000,** *878* (1), 147-152.

70. Kosuge, T.; Adachi, T.; Kamiya, H., Isolation of Tetramethylpyrazine from Culture of Bacillus natto, and Biosynthetic Pathways of Tetramethylpyrazine. *Nature* **1962,** *195* (4846), 1103-1103.

71. Rajini, K. S.; Aparna, P.; Sasikala, C.; Ramana Ch, V., Microbial metabolism of pyrazines. *Crit Rev Microbiol* **2011,** *37* (2), 99-112.

72. Kutanovas, S.; Stankeviciute, J.; Urbelis, G.; Tauraite, D.; Rutkiene, R.; Meskys, R., Identification and characterization of a tetramethylpyrazine catabolic pathway in Rhodococcus jostii TMP1. *Appl. Environ. Microbiol.* **2013,** *79* (12), 3649-3657.

73. Chaiyen, P., Flavoenzymes catalyzing oxidative aromatic ring-cleavage reactions. *Arch Biochem Biophys* **2010,** *493* (1), 62-70.

74. Chaiyen, P.; Ballou, D. P.; Massey, V., Gene cloning, sequence analysis, and expression of 2-methyl-3-hydroxypyridine-5-carboxylic acid oxygenase. *Proc. Natl. Acad. Sci. U. S. A.* **1997,** *94* (14), 7233-7238.

75. McCulloch, K. M.; Mukherjee, T.; Begley, T. P.; Ealick, S. E., Structure of the PLP Degradative Enzyme 2-Methyl-3-hydroxypyridine-5-carboxylic Acid Oxygenase from Mesorhizobium loti MAFF303099 and Its Mechanistic Implications. *Biochemistry* **2009,** *48* (19), 4139-4149.

76. Feng, L.; Wang, W.; Cheng, J.; Ren, Y.; Zhao, G.; Gao, C.; Tang, Y.; Liu, X.; Han, W.; Peng, X.; Liu, R.; Wang, L., Genome and proteome of long-chain alkane degrading Geobacillus thermodenitrificans NG80-2 isolated from a deep-subsurface oil reservoir. *Proc Natl Acad Sci U S A* **2007,** *104* (13), 5602-7.

77. Spence, G. G.; Taylor, E. C.; Buchardt, O., Photochemical reactions of azoxy compounds, nitrones, and aromatic amine N-oxides. *Chemical Reviews* **1970,** *70* (2), 231-265.

78. Gunsior, M.; Ravel, J.; Challis, G. L.; Townsend, C. A., Engineering p-hydroxyphenylpyruvate dioxygenase to a p-hydroxymandelate synthase and evidence for the proposed benzene oxide intermediate in homogentisate formation. *Biochemistry* **2004,** *43* (3), 663-74.

79. Teufel, R.; Mascaraque, V.; Ismail, W.; Voss, M.; Perera, J.; Eisenreich, W.; Haehnel, W.; Fuchs, G., Bacterial phenylalanine and phenylacetate catabolic pathway revealed. *Proc Natl Acad Sci U S A* **2010,** *107* (32), 14390-5.

80. Fetzner, S.; Steiner, R. A., Cofactor-independent oxidases and oxygenases. *Appl Microbiol Biotechnol* **2010,** *86* (3), 791-804.

81. Fetzner, S., Oxygenases without requirement for cofactors or metal ions. *Appl Microbiol Biotechnol* **2002,** *60* (3), 243-57.

82. Du, Y. L.; Ryan, K. S., Pyridoxal phosphate-dependent reactions in the biosynthesis of natural products. *Nat Prod Rep* **2019,** *36* (3), 430-457.

83. Sciara, G.; Kendrew, S. G.; Miele, A. E.; Marsh, N. G.; Federici, L.; Malatesta, F.; Schimperna, G.; Savino, C.; Vallone, B., The structure of ActVA-Orf6, a novel type of monooxygenase involved in actinorhodin biosynthesis. *Embo j* **2003,** *22* (2), 205-15.

84. Widboom, P. F.; Fielding, E. N.; Liu, Y.; Bruner, S. D., Structural basis for cofactor-independent dioxygenation in vancomycin biosynthesis. *Nature* **2007,** *447* (7142), 342-5.

85. Hart, R. C.; Stempel, K. E.; Boyer, P. D.; Cormier, M. J., Mechanism of the enzyme-catalyzed bioluminescent oxidation of coelenterate-type luciferin. *Biochem Biophys Res Commun* **1978,** *81* (3), 980-6.

86. Steiner, R. A.; Janssen, H. J.; Roversi, P.; Oakley, A. J.; Fetzner, S., Structural basis for cofactor-independent dioxygenation of N-heteroaromatic compounds at the alpha/beta-hydrolase fold. *Proc Natl Acad Sci U S A* **2010,** *107* (2), 657-62.

87. Sadauskas, M.; Vaitekunas, J.; Gasparaviciute, R.; Meskys, R., Indole Biodegradation in Acinetobacter sp. Strain O153: Genetic and Biochemical Characterization. *Appl Environ Microbiol* **2017,** *83* (19).

88. Deeley, M. C.; Yanofsky, C., Nucleotide sequence of the structural gene for tryptophanase of Escherichia coli K-12. *J Bacteriol* **1981,** *147* (3), 787-96.

89. Ochiai, M.; Wakabayashi, K.; Sugimura, T.; Nagao, M., Mutagenicities of indole and 30 derivatives after nitrite treatment. *Mutat Res* **1986,** *172* (3), 189-97.

90. Mueller, R. S.; Beyhan, S.; Saini, S. G.; Yildiz, F. H.; Bartlett, D. H., Indole acts as an extracellular cue regulating gene expression in Vibrio cholerae. *J Bacteriol* **2009,** *191* (11), 3504-16.

91. Martino, P. D.; Fursy, R.; Bret, L.; Sundararaju, B.; Phillips, R. S., Indole can act as an extracellular signal to regulate biofilm formation of Escherichia coli and other indole-producing bacteria. *Can J Microbiol* **2003,** *49* (7), 443-9.

92. Lee, J. H.; Kim, Y. G.; Kim, M.; Kim, E.; Choi, H.; Kim, Y.; Lee, J., Indole-associated predator-prey interactions between the nematode Caenorhabditis elegans and bacteria. *Environ Microbiol* **2017,** *19* (5), 1776-1790.

93. Kishimoto, S.; Hara, K.; Hashimoto, H.; Hirayama, Y.; Champagne, P. A.; Houk, K. N.; Tang, Y.; Watanabe, K., Enzymatic one-step ring contraction for quinolone biosynthesis. *Nat Commun* **2018,** *9* (1), 2826.

94. Ye, Y.; Muller, J. G.; Luo, W.; Mayne, C. L.; Shallop, A. J.; Jones, R. A.; Burrows, C. J., Formation of 13C-, 15N-, and 18O-labeled guanidinohydantoin from guanosine

oxidation with singlet oxygen. Implications for structure and mechanism. *J Am Chem Soc* **2003,** *125* (46), 13926-7.

95. O'Leary, M. H., Phosphoenolpyruvate Carboxylase: An Enzymologist's View. *Annu Rev Plant Physiol* **1982,** *33* (1), 297-315.

96. Hu, Y.; Dietrich, D.; Xu, W.; Patel, A.; Thuss, J. A.; Wang, J.; Yin, W. B.; Qiao, K.; Houk, K. N.; Vederas, J. C.; Tang, Y., A carbonate-forming Baeyer-Villiger monooxygenase. *Nat Chem Biol* **2014,** *10* (7), 552-4.

97. Huang, S.; Tabudravu, J.; Elsayed, S. S.; Travert, J.; Peace, D.; Tong, M. H.; Kyeremeh, K.; Kelly, S. M.; Trembleau, L.; Ebel, R.; Jaspars, M.; Yu, Y.; Deng, H., Discovery of a Single Monooxygenase that Catalyzes Carbamate Formation and Ring Contraction in the Biosynthesis of the Legonmycins. *Angew Chem Int Ed Engl* **2015,** *54* (43), 12697-701.

98. Nomura, T.; Kushiro, T.; Yokota, T.; Kamiya, Y.; Bishop, G. J.; Yamaguchi, S. J., The last reaction producing brassinolide is catalyzed by cytochrome P-450s, CYP85A3 in tomato and CYP85A2 in Arabidopsis. *J Biol Chem* **2005,** *280* (18), 17873-17879.

99. Foster, J. W., Microbiological Aspects of Riboflavin: I. Introduction. II. Bacterial Oxidation of Riboflavin to Lumichrome. *J Bacteriol* **1944,** *47* (1), 27-41.

100. Harkness, D. R.; Stadtman, E. R., Bacterial degradation of riboflavin. VI. Enzymatic conversion of riboflavin to 1-ribityl-2,3-diketo-1,2,3,4-tetrahydro-6, 7-dimethylquinoxaline, urea, and carbon dioxide. *J Biol Chem* **1965,** *240* (10), 4089-96.

101. Xu, H.; Chakrabarty, Y.; Philmus, B.; Mehta, A. P.; Bhandari, D.; Hohmann, H. P.; Begley, T. P., Identification of the First Riboflavin Catabolic Gene Cluster Isolated from Microbacterium maritypicum G10. *J Biol Chem* **2016,** *291* (45), 23506-23515.